# Chapter 1. General Introduction

## 1-1 Over all outline

In this study, we established the novel methods to prepare homo and hetero dye-clusters in DNA or RNA duplexes and applied the clusters to systematically investigate their properties and develop new fluorescent probes.

Because dye molecules or pigments have some properties such as color, fluorescence and phosphorescence, they have been utilized as tools for colorant, coating and photographic materials since early time, while they have been also used for one of the recording materials and display elements recently.[1] In this way, they have wide range of applications. In addition to color, fluorescence and phosphorescence as monomer properties, when they are assembled each other, novel properties such as narrowing the spectra, spectral shift and nonlinear optical effects are induced.[2] Accordingly, many new methodologies and property of dye-clustering have been studied and developed because of these significances. These properties strongly depend on the orientation, order and size of the cluster, and as a result, controlling these factors is very important to prepare the clusters with high capacity.[3] In the case of homo dye-clusters with identical dyes, their optical properties have been revealed at theoretical and experimental sides because the clusters can be easily prepared.[2] In addition, their behaviors are determined only by the cluster size and orientation. Accordingly, rough controlling the number and orientation of dyes is enough to investigate the properties if the structure can be determined. On the other hand, the reports about hetero dye-clusters with different dyes were limited because the preparation of the clusters was quite difficult. Especially, the

sequence of the dyes is very important as factors to determine the properties of hetero dye-clusters in addition to the number and orientation of the dyes. Consequently, this problem had been a large barrier to develop novel clusters and verify theoretical prediction of these properties by systematic experiment.

On the other hand, to focus on an application side of hetero clusters, hetero dimers with a fluorophore and quencher have been utilized as a very common tool for fluorescent probes to detect biomolecules such as protein, DNA or RNA, because these probes provide high detection sensitivity due to use of fluorescence and simplify detection procedures.[4] Efficient quenching of the fluorophore is significant to design highly sensitive probes because their detection sensitivities are determined by the quenching associated with clustering. However, only a few effective guidelines to design a highly sensitive probe had been proposed because many optical properties of hetero dye-clusters were not revealed due to difficulty of their preparation.[5] Therefore, if the preparation method of the clusters with the pre-determined orientation, order and number of the dyes is developed, the simple and effective guideline can be proposed by systematical investigation of their unclear properties.

DNA and RNA are the kinds of anionic polymers, monomers of which are composed of a base and D-ribose and are linearly connected each other through a phosphodiester bond.[6] They has a fascinating supramolecular property that one strand of them recognize the other strand which has the complementary base sequences and form the duplex with the other one. Especially, this hybridization ability is a very important role in the sense of that they can recognize complementary sequences. However, it is quite difficult to discriminate the difference between an existence and non-existence of

complementary strands by only a use of native DNA and RNA, because they cannot transmit clear signals for us such as color and fluorescence.

On the other hand, to focus on their structures, they have hydrophobic space which is formed by π-π stacking interaction of the bases.[6] As a result, planer dyes can intercalate among their bases.[7] Additionally, each base vertically and regularly stacks along axis of the helix. In other words, I can mention that DNA and RNA are kinds of dye-clusters, which are compose of bases as a dye monomer. Thus, if the bases can be exchanged for dyes, the clusters of a predetermined size, orientation and sequence can be prepared easily and novel properties can be also provided by combination of DNA or RNA functions.

In present study, we developed dye-clusters, which the orientation, sequence and size are controlled, with novel properties by use of DNA or RNA duplexes as a scaffold. In particular, we conducted a) preparation of novel homo- and hetero-dye clusters with identical or different dyes based on DNA duplexes, respectively, b) verification of exciton theory and highly sensitive probes for detecting target DNAs by hetero-clustering between different dyes and c) development of another dye-clusters based on RNA duplexes for monitoring RISC functions.

In part a), we developed dye-clusters with various properties by the use of structural properties of the duplexes and hybridization ability. It was difficult for conventional methods using self association between dyes to control the orientation, sequence and size of the clusters. In this design, we designed that each dye residue paired each other as “a pseudo base-pair” at center of DNA duplex instead of a native nucleotide for

clustering. Consequently, controlling the sequence and number of the dyes can be easy in this cluster design. In addition, we investigated structure at around dye residues and effect of clustering among base-pairs on DNA backbone in detail in order to establish the preparation method of the clusters.

Next, in the part of b), we first evaluated accuracy of exciton model in the theory by comparison between the absorption spectra of the various hetero-clusters and the predicted behavior based on the model.[8] At the same time, relationship between absorption maxima of the clusters and these exciton couplings was also investigated systematically. From these investigations, we expected that one of the important factors determined strength of excitonic interaction. On the other hand, at the other part, novel probes for detecting target DNA were developed by the use of quenching associated with hetero-clustering between a fluorophore and quencher. Then, we clarified the relationship between the quenching efficiency of a fluorophore and the exciton coupling, and designed the highly-sensitive probes based on the relationship. Moreover, we next prepared hetero-clusters with a fluorophore and multiple quenchers for improvement of the probe sensitivity because of further enhancement of excitonic interaction. These probes for highly sensitive detection of the target DNAs can be utilized for the probe immobilized DNA microarray.[9] Additionally, these probes can be also used for gene expression analysis by detection of mRNA in *vivo*.[10]

At the last part c), we developed different type of dye-clusters based on RNA duplexes in order to add RNA specific function to the clusters. In general, structure of RNA duplex is completely different from that of DNA duplex and RNA duplexes hardly

receive any intercalators among their base-pairs due to tightness of the helix and π-π stacking interaction.[11] Here, to focus on structural differences between the clusters based on RNA and DNA duplexes, we revealed RNA specific properties by exploring the common and different points. Besides, we also prepared hetero-dimer with a fluorophore and quencher in RNA duplex for development of system to distinguish single strands from double strands. If incorporating this system into siRNA is acceptable in the view point of RNAi function, the system can be one of the effective tools to monitor RISC functions.[12]

This thesis is composed of six chapters. In chapter 1, we clarify position of each chapter in nucleic acid and dye clusters related chemistry. In chapter 2, we mentioned establishment of preparation methods for dye-clustering based on DNA duplexes. In chapter 3, to focus on the structure-determined hetero-dimer of different dyes, we wrote our systematic investigation of their absorption spectra to verify accuracy of exciton model. In addition, we explain development of a highly-sensitive DNA probe by coherent quenching of a fluorophore in chapter 4. Here, we revealed the relationship between quenching efficiency and excitonic interaction of the clusters by the use of another relationship between absorption maxima and excitonic interaction of the clusters. Moreover, in chapter 5, we wrote further improvement of the probe sensitivity by asymmetric dye-clustering with single fluorophore and multiple quenchers in DNA duplexes. At the same time, we investigated the spectroscopic aggregation number of the clusters by systematic analysis of exciton coupling between a dye and the other multiple dyes. In the last chapter, we mentioned preparation of the dye-clusters based on RNA duplexes and compared the clusters with them based on DNA. And as a

demonstration for monitoring RISC function, we tested the quenching efficiency of hetero-dimer in short RNA duplex. In following this chapter, we mentioned study background and significance of each chapter.

## 1-2 General introduction in Chapter 2

(Stable interstrand clustering in DNA duplexes by use of threoninol-nucleotides)

### 1-2-1 Properties of dye clusters

**Introduction**

Dye and pigment have some properties such as color, fluorescence and phosphorescence. As a result, they have been used for colorant and paint since early time and various studies about them have been performed in order to develop new functions. Furthermore, recently, they have been also utilized for memory materials and display elements and significance of studies about them increase gradually.[1]

In general, dye clustering induces large change of optical properties, and for example, spectral shift, narrowing spectral band, quenching of emission and non-linear optical effects are main properties associated with clustering.[2] These properties largely depend on the orientation, the order and size of the clusters. Therefore, controlling these factors is essential to prepare dye-clusters with the high performance. In the past, the large size clusters have been mainly studied because the clusters have been utilized as photographic materials, memory materials and display elements. Because of this, most studies were focused on macro properties of the clusters prepared by rough controlling the size of the clusters. Therefore, there were only a few preparation methods to precisely control the orientation, the sequence and size of the clusters.

**Effect of orientation on the property**

Various studies about the orientation of the dye-clusters had been reported by many researchers. According to these studies, homo dye-clusters with identical dyes form two kinds of the clusters such as H-aggregates and J-aggregates. In the case of H-aggregates,

dyes stack face-to-face, or vertically stack each other, and hypsochromicity, narrowing the bands and quenching of fluorophores are induced when dyes form H-aggregates.[2a] Especially, change of absorption spectra is explained by exciton theory.[3] As shown in Fig. 1-1, this blue shift occurs because only a higher energy transition in the two associated with clustering is allowed. While in the case of J-aggregates, dyes stack head-to-tail, or stack stair-like orientation, and bathochromicity, narrowing the bands, increase in fluorescent intensity and stokes' shift of fluorophores are induced when dyes form J-aggregates. According to molecular exciton theory, red shift of J-aggregates occurs because only a lower energy transition in the two associated with clustering is allowed. In this way, in the case of home dye-clusters, effect of the orientation on spectroscopic behaviors in detail had been investigated by many studies. However, the properties of hetero dye-clusters with different dyes have not been investigated due to difficulty of their preparation. Therefore, hetero clusters had many unclear properties to investigate in detail.

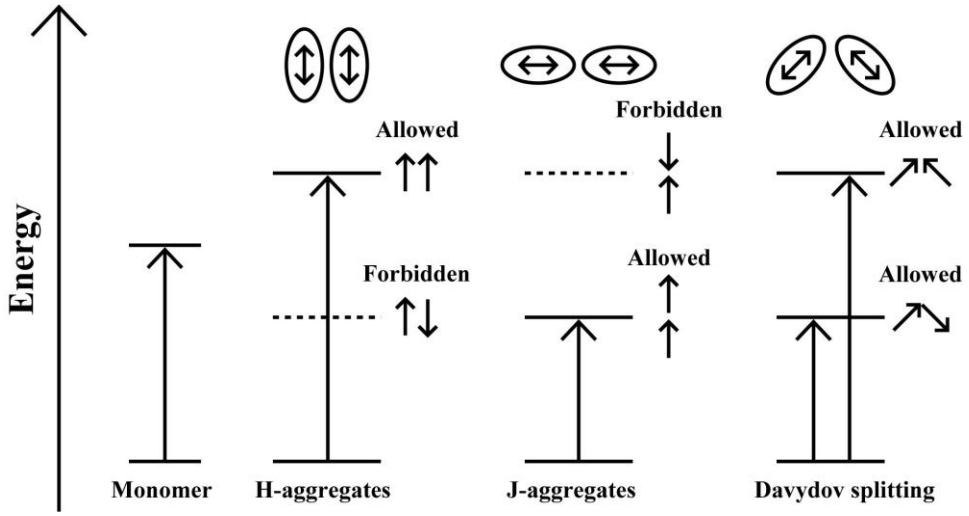


Figure 1-1. Schematic representation of the electronic transition in a monomer, H-aggregates, J-aggregates and Davydov splitting on the basis of the interaction between molecular excitons in aggregates. Arrows represent the transition dipole moment of the dye.

**Relationship between the properties and the number of the dyes**

As previously mentioned, various studies about homo dye-clusters had been conducted in detail. Thus, in the case of homo clusters, the relationship between the properties and the number of the dyes has been revealed comparatively by these studies.[13] According to the studies, whether H-aggregates or J-aggregates, increase in the cluster size facilitate to enhance the change with clustering. On the other hand, the change per the number of the dyes decreases as increase in the size of clusters. In addition, several papers reported the change is saturated from 100-10 dyes on theory or experiments.[14] The number is called in "spectroscopic aggregation number (coherence length)" and it means the number of the dyes which really interact with each other. Therefore, the limit number of dyes for functionalization with clusters is defined from 10 to 20 numbers and the further increase does not affect on their properties.

**Effect of sequence**

Because home dye-clusters are composed of identical dyes, order of each dye does not show any differences and the factor of sequence can be ignored for the clustering. On the other hand, in the case of when the dye A and dye B assemble, the properties of the hetero clusters between the sequences "AAAABBBB" and "ABABABAB" can be different.[15] However, the difference of properties cannot be verified because the each cluster cannot be prepared with clear discrimination by conventional methods.

Therefore, novel preparation methods of the clusters to control the orientation, order and size of the clusters have been needed for both basic and application studies.

1-2-2 Preparation methods of dye clusters

As mentioned in the previous part, various preparation methods of dye-clusters have been proposed because the clusters can be used for various usages. Then, we will explain these methods in following sections.

**Methods with interactions with non-covalent bonds**

1. A use of self-association between dyes

Clustering by self-association between dyes is widely known as the oldest method of clustering. In this method, the clusters are mainly formed by molecular interaction between dyes such as π-π stacking interaction and electrostatic interaction.[16] In addition, basic handling for the preparation is just to dissolve dyes in appropriate solvent and leave it for a while. Accordingly, it is very easy to prepare the dye-clusters by the method. On the other hand, the variety of dyes is limited because dyes do not form clusters if molecular interaction of the dyes is weak. Additionally, the orientation and size of the clusters largely depend on interaction between the dyes, concentration of the dyes and the kind of dyes. Therefore, controlling these factors is almost impossible. In this way, the preparation method using self-association of the dyes has many difficulties.

2. A use of metal surface as a scaffold.

This method has been used for dye-clustering as a photosensitizer of photographs. In general, silver halide is widely utilized as a scaffold of metal surface to prepare dye clusters.[13, 17] In this method, the clustering is based not only on interaction between the dyes, but also on interaction between the metal and dyes. Accordingly, the stability and

variety of the clusters by this method are larger than that of self-association. In addition, this method enables rough control of the orientation by changing the kind of silver halides. Moreover, the method has been widely used due to simpleness of the handling for the preparation. However, because exact control of the orientation and size of the clusters is impossible by this method, hetero-clustering by the method has not been reported.

3. A use of LB (Langmuir-Blodgett) film

LB films are one of the mono-layers which form on the surface of solvent and assemble by intermolecular interactions, and each molecule has a hydrophobic and hydrophilic part.[18] In this method, the film provides the scaffold in which the introduced dyes to the hydrophobic part are assembled orderly (Fig. 1-2).[15, 19] As one of the advantages with this method, the size of the clusters can be easily controlled by controlling the length of the films. Additionally, the dyes, which cannot assemble by only self-association for clustering, can be also used by assistance of the film, and as a result, the various dyes are available for clustering. Furthermore, hetero-clusters of different dyes can be prepared by combining building blocks with different dyes. However, because the order of the dyes in hetero-clusters is determined by only an interaction between different dyes, controlling the order is quite difficult. Although the orientation of the dyes can be roughly controlled, it is difficult to control it exactly.

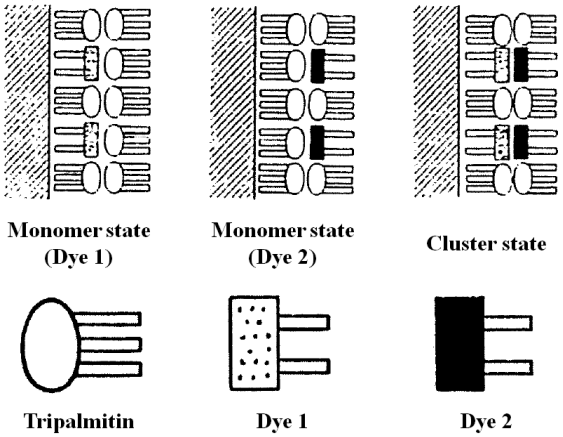

Figure 1-2. Illustration of the dye-clusters based on LB films.

Moreover, strict control of the cluster size is difficult since the strictness of the control largely depends on controlling the length of the LB film on macro scale. Therefore, a novel method for strict controlling of the orientation, order and size of the clusters has been needed, though the preparation method using LB film is effective tools to prepare large size clusters.

4. A use of some templates

A template method is known as preparation methods of the clusters by a use of scaffold molecules. As some of these methods, we introduced two methods using cationic polymers or DNA as a template.[20] In the case of the former, electrostatic interaction between the polymer and dyes is used for dye-clustering (Fig. 1-3).[20e] Accordingly, the orientation and size of the clusters are determined by the size or kind of the polymers and these factors can be controlled by what kinds of the polymers you choose. However, because varieties of templates are poor, the kind of clusters based on this method is severely limited. On the other hand, in the case of the latter, hydrophobic interaction and hydrogen bonds between the dyes and grooves of template DNAs are used for dye-clustering (Fig. 1-4).[20a-d] In this method, the orientation and size of the clusters can be controlled by choosing the length of DNA or the kind of the dyes. Especially, because the size of the clusters depends on the size of dyes and the length of the groove of DNAs, controlling that is relatively easier than previous other methods.

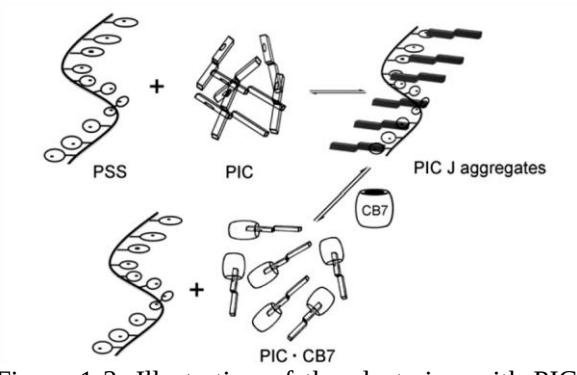

Figure 1-3. Illustration of the clustering with PIC (pseudoisocyanine) based on PSS (poly-styrenesulfonate).

However, modification to the dyes is necessary for clustering because the clustering is mainly based on interaction between DNA groove and dyes. As a result, the available dyes are highly-restricted. In addition, controlling the order of the dyes with hetero-clusters is quite difficult as well as using LB films.

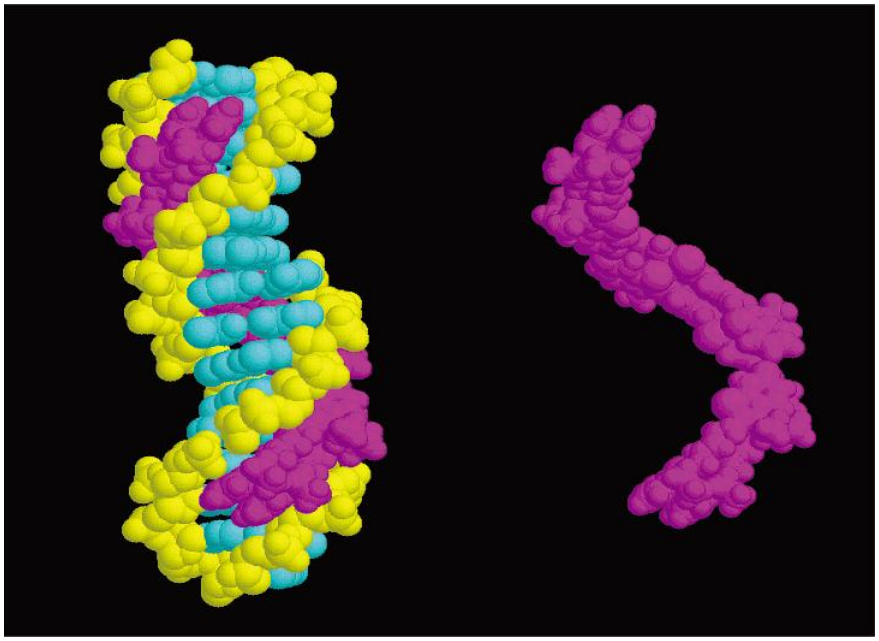

Figure 1-4. Molecular model showing three dimers of the dye aligned end-to-end within the minor groove of a DNA template (left). The DNA is removed in the figure on the right to better visualize the helical structure of the dye aggregate. DNA backbone, yellow; DNA base pairs, cyan; dyes, magenta.

In this way, in the case of methods using intermolecular interaction without covalent bonds, although the handling for preparation is very simple, a strict control of the orientation, order and size of the clusters is quite difficult.

**Methods using covalent bonds**

*Directly introduction of the dyes to polymers as a part of the monomer*

Preparation method of the clusters by a use of polymers has been widely used for materials such as organic EL and conductive polymers.[21] In this method, there are two

types of the methods; introduction of the dyes to main chain or to side chain of the polymer. Because the dye-clusters are grown by polymerization reaction, long and stable dye-clusters can be prepared. In addition, useful dyes are hardly limited due to directly introduction of the dyes by covalent bonds. Moreover, the orientation of the clusters can be controlled by changing how to connect the dyes to the monomer unit. However, strictly controlling the size of the cluster and order of the dyes is quite difficult because polymerization reactions are used.

### 1-2-3 Dye clusters based on DNA or RNA through covalent bonds

In previous section, we have mentioned the several preparation methods of the clusters. However, they have some limitations and difficulties to control the size, orientation and sequence of the clusters. In this section, we explain the preparation methods based on covalent bonds for introducing dyes into DNA or RNA duplex. DNA and RNA can be regarded as kinds of dye-clusters, which are compose of bases as a dye monomer. Because of this, each method in this section has a capacity to design the clusters with the pre-determined size and order of the dyes. Then, we explain these methods in following parts, which are deeply related with our methods.

**Using D-ribose as a scaffold**

1. Exchanging nucleobases for dyes

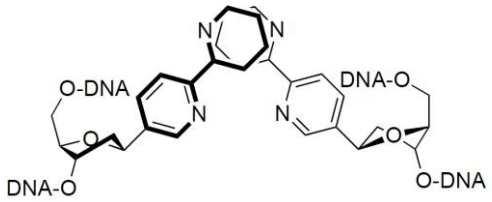

Figure 1-5. Illustration of the clusters by exchanging nucleobases for dyes based on D-ribose.

Preparation methods of dye-clusters by exchanging nucleobases for dyes have been reported as one of the methods based on D-ribose.[22] One of the most characteristic points is that introduced dyes stack with each other between nucleobases.

Because of this, the orientation of the dyes can be roughly controlled by design of the sequence. In addition, the dyes, which can act as an artificial base with hydrogen bonding, have been also reported because this method had been developed for expansion of genetic alphabets.[22d, 22e] However, the method includes difficulty in synthesis because selective reaction to β position on D-ribose is necessary to introduce the dyes. Most dyes have been introduced to bond long axis of the dyes to 1' position of D-ribose. In the most case of introducing the dyes as a pair, stacking area between the dyes is smaller than the area of dyes (see Fig. 1-5). As a result, the duplex was not stabilized by introduction of dyes because destabilization by steric hindrance almost canceled stabilization by stacking interaction between dyes. Furthermore, in the case of introducing a fluorophore, fluorophores prone to receive quenching by electron or hole transfer from nucleobases.[23] Therefore, developments of the dye-clustering which induce stabilization of duplex have been desired.

2. Dye clustering in major groove of DNA or RNA

Clustering in major groove of duplex is mainly performed by introduction of a dye to specific position of a nucleobase such as 5-position of uracil, cytosine, 8-position of guanine and adenine (Fig. 1-6).[24] Main advantages of this method are those introduction of large dyes

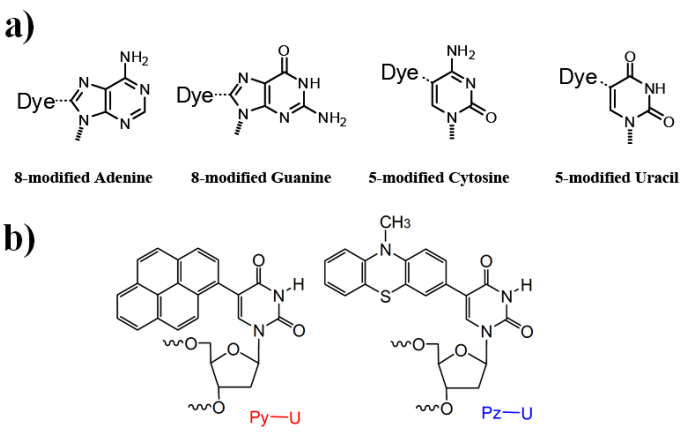


Figure 1-6. a) Modification positions of the bases for introduction of the dyes into major groove. b) One of the designs to dye-clustering in major groove of DNA or RNA duplex.

such as porphyrin is possible without large destabilization of duplex and fluorophores do not prone to receive quenching by an electron or hole transfer from nucleobases. On the other hand, this method has problems associated with direct introduction of dyes to nucleobases. First, it takes much time and effort to prepare modified bases because four kinds of modified bases need to be prepared. As a result, the usable dyes and sequences are limited depending on the dyes. Second, modified bases may not take anti-orientation, which enable to form hydrogen bonds to the counter base, but may take syn-orientation which is inert to the hydrogen bonds. Accordingly, design of dye-clustering with this method is difficult and you always have to give attention which orientation prone to take syn or anti.

3. Dye clustering in minor groove of DNA or RNA

Dye-clustering in minor groove of duplex is performed by introduction of dyes to 2'-position of hydroxyl group or 2'-N-position of 2'-amino-LNA (Fig. 1-7).[24-25] One of the big advantages is that fluorophores do not prone to suffer from quenching by electron or hole transfer from nucleobases because fluorophores do not directly contact with nucleobases. In addition, introduced dyes are fixed at around minor groove and do not flip like previous method. However, it takes much time and effort to prepare modified nucleotides because four kinds of the nucleotides need to be prepared.

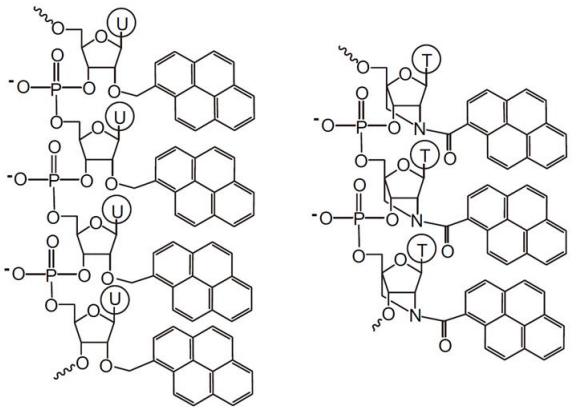

Figure 1-7. Methods of dye-introduction for clustering in minor groove of DNA or RNA duplex.

In this way, D-ribose has been utilized as a scaffold for constructing dye-clusters of pre-determined size and number. One of the reasons for utilizing D-ribose is that functional molecules such as dyes can be incorporated into natural ODNs without distorting their natural B-type structure. Furthermore, functional molecules on natural nucleotides can be substrates of DNA or RNA polymerase and in some cases can be enzymatically incorporated into ODNs. This latter purpose inevitably requires the natural D-ribose backbone. However, there is no limitation on the structure of a scaffold when the ODNs are designed for use as supramolecular material scaffolds and are not enzymatically but chemically synthesized. Non-natural scaffolds should extend the variety of ODNs and their helical structure, and will lead to new functional supramolecular helices without the assistance (and limitations) of natural nucleotides.

**Using artificial linker as a scaffold instead of D-ribose**

As mentioned in the previous part, there is no limitation on the structure of a linker for tethering dyes in DNA when the DNAs are used for material applications such as dye-clusters. Then, we introduced a few examples of the non-natural linkers as a scaffold for dye-clustering in this part.

1. Using a dye as a linker

In this method, dyes themselves are used as a linker and added to two alkyl-hydroxyl groups to introduce DNA or RNA (as shown in Fig. 1-8).[24, 26] One of the main advantages with this method is synthetic simplicity such

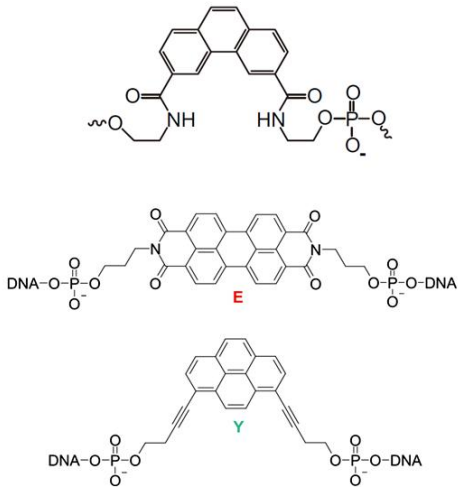

Figure 1-8. Designs of dye-linkers for dye-clustering in DNA or RNA duplex.

as introducing the two alkyl-hydroxyl groups to the dyes. Although the number and kinds of the linkers between a hydroxyl group and a dye slightly affect on orientation between the dyes, restraint of dyes by linker groups is relatively small and the orientation largely depends on interaction between the dyes. Because of this, this method is effective in the case of using interaction between dyes for dye-clustering. However, at the same time, controlling orientation between dyes by design of linker groups is difficult due to high degree of freedom with this method.

2. Using aromatic parts as a linker

In this method, aromatic moiety is used as a linker for dye-clustering as shown in Fig. 1-9.[27] Accordingly, degree of freedom with linker parts is low and the size of the linker is also large. Thus, this method is easier to control the orientation of dyes than the method with dye-linker. However, introduction of large dyes is difficult because the space to introduce the dyes between base-pairs is narrow due to large aromatic linkers. Therefore, the preparation methods, which realize the clusters with large dyes, strong interaction between dyes and the pre-determined orientation of the dyes, have been desired.

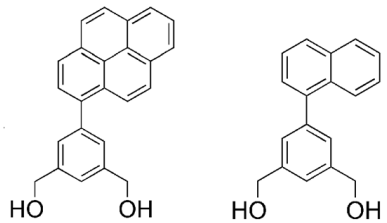

Figure 1-9. Designs of aromatic-linkers for dye-clustering in DNA or RNA duplex.

3. Using an acyclic linker for dye-clustering

In this method, acyclic linkers such as D-threoninol linker, (S)-3-amino -1,2-propanediol linker and glycerol linker are used for dye-clustering (Fig.s 1-10 and 1-11).[28] The linkers have two hydroxyl groups and a functional group, which is needed for introduction of the dyes, such as amino group, carboxyl group and another

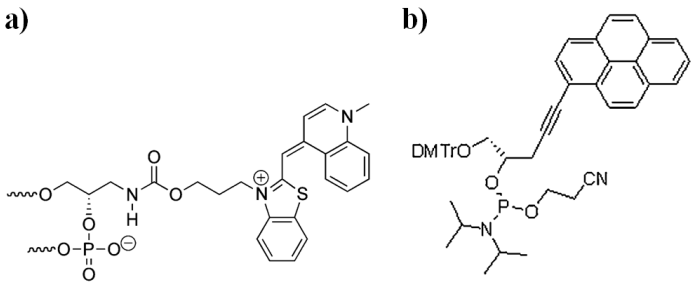


Figure 1-10. Designs of acyclic-linkers: a) (S)-3-Amino-1,2-propanediol linker, b) glycerol linker.

hydroxyl group. Accordingly, procedures are very simple for synthesis of a dye residue because couplings between the dye and linker are performed through amide, urethane or ether bonds. Additionally, various types of the dyes can be introduced with these linkers. Moreover, unfitness between length of the linker and distance per a base-pair hardly contributes destabilization of the duplex because of high degree of freedom with these linkers. In this way, using acyclic linkers can be one of the effective ways to prepare dye-clusters with high duplex stability, strong interaction between dyes and the pre-determined orientation of the dyes.

1-2-4 Present study (Stable interstrand clustering in DNA duplexes by use of threoninol-nucleotides)

As we mentioned at previous section, D-threoninol have been used as an acyclic linker for dye-clustering in our laboratory.

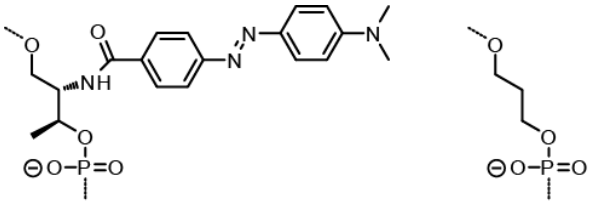


Figure 1-11. Chemical structures of D-threoninol linker and 1,3-propanediol spacer.

As shown in Fig. 1-11, D-threoninol has three carbon atoms between 3'- and 5'-hydroxyl groups as well as D-ribose and also has chirality. In addition, the dyes can be easily inserted through an amido bond because it has an amino group. As compared with other linker using covalent bonds, we have directly attached the dyes to

D-threoninol through an amido bond without any alkyl spacers in most cases. Because of this, the introduced dyes are strongly fixed in the duplex and orientation of the dyes is also fixed.

Previously, Dr. Kashida et al. reported that dye-clusters, which had multiple pairs of a dye residue and spacer (1,3-propanediol), were prepared by hybridization of two single-stranded DNA-dye conjugates (see Fig. 1-11).[29-30] In that study, they revealed that the dyes of these clusters intercalated into DNA duplex and stacked with adjacent dye-moieties at angle of about $35^{o}$ as well as native base-pairs. However, the duplexes were not largely stabilized by weak stacking interaction due to this large angle between adjacent dyes. Accordingly, design to prepare more stable dye-clusters has been desired.

In present study, we developed a new design for dye-clustering based on D-threoninol linkers. In this design, dye residues are introduced as pseudo base-pairs in the center of DNA duplex. Introduction of dyes as a pair can induce increase in the interaction between the dyes because of reducing the angle between adjacent dyes, and as a result, stabilization of the duplex by increase in stacking interaction can be expected. At the same time, the sequence length in dye region can be reduced by this cluster design because the number of the dyes per sequence length increases. Accordingly, a lot of dye residues can be introduced into DNA duplex. In this way, if we can establish the preparation method of dye-clusters, the clusters, which have various properties, with a predetermined size, orientation and sequence, can be developed. Moreover, controlling the orientation of the dyes can be expected because introduced dyes should take nearly fixed states. Therefore, if controlling the orientation, size and order of dyes can be performed by our preparation method, novel dye-clusters can be developed and utilized for excellent biological tools or optical materials by uses of their properties.

In chapter 2, we showed establishment of preparation method for novel dye-clusters based on DNA duplex and investigation of their properties. In addition, this method in chapter 2 is fundamental to other chapters from 3 to 6 because it was used for dye-clustering in all chapters. Therefore, chapter 2 is quite important for this study.

## 1-3 General introduction in Chapter 3

(Analysis of Coherent Heteroclustering of Different Dyes by Use of Threoninol Nucleotides for Comparison with the Molecular Exciton Theory)

### 1-3-1 Hetero dye-clusters

**Introduction**

In general, dye-clustering induces large spectral change, which is not observed in monomer states as mentioned before. Homo dye-clusters, which are composed of identical dyes, and hetero dye-clusters, which are composed of different dyes, are known as typical clusters. In the case of homo dye-clusters, their optical properties have been revealed at theoretical and experimental sides because the clusters can be easily prepared. In addition, their behaviors are determined only by the cluster size and orientation. Accordingly, just rough controlling the number and orientation of dyes is enough to investigate the properties if the structure can be determined. On the other hand, the reports about hetero dye-clusters were limited because the preparation of the clusters was quite difficult. Especially, the sequence of the dyes is very important as factors to determine the properties of hetero dye-clusters in addition to the number and orientation of the dyes. As a result, the order of dyes with the clusters needs to be controlled strictly for spectral investigation of the clusters. However, the number of studies, which achieved strict control of the factor, was limited. Particularly, systematical investigation of spectroscopic behaviors had been hardy performed. Therefore, to investigate the properties of hetero dye-clusters systematically, preparation methods of the clusters with the pre-determined size, sequence and orientation have been desired.

In following sentences, we introduced studies of other groups about hetero

dye-clusters.

**Works by Kuhn et al.**

In 1963, Kuhn et al. successfully developed hetero H-aggregates with cyanine dyes by a use of Langmuir-Blodgett films and reported the spectral change of hetero H-aggregates by experiments coincided with prediction by exciton theory.[8] However, the preparation methods by LB films are quite difficult to control alignment of two different dyes. In addition, because their clusters had the large cluster size, they could not reveal the sequence of the dyes. Therefore, the observed spectral changes were regarded as macroscopic behaviors.

**Works by Yonezawa group and Kuroda group**

Both Yonezawa et al. and Kuroda et al. individually reported mixed (hetero) J-aggregates of merocyanine dyes were developed by a use of LB films as well as Kuhn group.[15, 19] Especially, Yonezawa et al. predicted the alignment of two different dyes in the clusters by systematic investigation of the spectroscopic behaviors. However, this prediction just was based on the spectral changes without any information of the dye sequence. Therefore, the relationship between the spectral changes and alignment of the dyes could not been clarified in those studies based on LB films.

**Works by Armitage et al.**

As mentioned before section, Armitage et al. reported development of various dye clusters by a use of DNA minor groove as a template.[20a-d] They also prepared hetero H-aggregates of cyanine dyes in DNA minor groove.[20c] In that study, they observed the

behaviors of hetero dimers and clusters by controlling the length of template DNA, though these behaviors originated from hetero dimers, homo dimers and each monomer. In this way, preparation methods of the clusters by weak intermolecular interaction might not have large possibility to control the dye sequence strictly, though the procedures of dye-clustering are very simple.

**Works by Tyagi et al.**

In 1996, Tyagi et al. successfully developed a novel probe for DNA detection such as "Molecular Beacon", which have been already recognized as a very common tool for biology and biotechnology (Fig. 1-12).[4a] They utilized hetero dimerization of a fluorophore and quencher dyes at DNA terminals for quenching of the fluorophore. In this case, two different dyes stack with each other without any difficulties to control the dye order. Therefore, their method was regarded as a new effective method for dye-clustering. However, they did not investigate behaviors of UV/Vis spectra in detail because they focused on development of a highly sensitive probe, though they did quenching of the fluorophore.[5b]

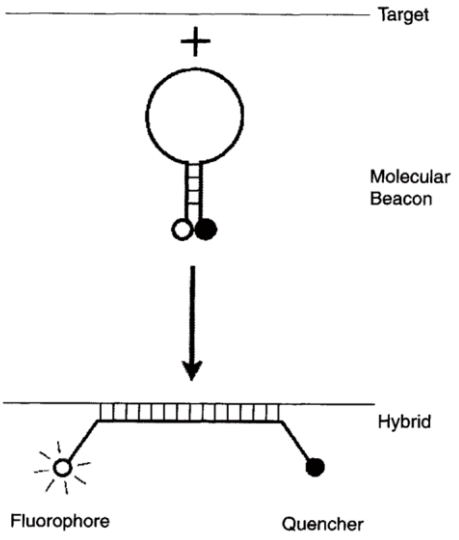

Figure 1-12. Detection mechanism of molecular beacon.

**Works by Mély et al.**

To be motivated by Tyagi works, Mély et al. compared the spectral changes of hetero dimers based on the beacon system with explanation by exciton theory and reported their coincidence.[31] In these studies, they investigated the behaviors with only a few

kinds of the clusters. Accordingly, some questions remained such as what factors determine the strength of excitonic interaction and how much the number of the dyes effect on their properties. However, increase in the number of the dyes induces difficulties on synthesis in the case of using conventional molecular beacon system because additional modification to a DNA terminal is necessary for further introduction of dyes.

In this way, a lot of unclear properties with hetero dye-clusters remained and a novel preparation method of hetero dye-clusters with pre-determined the size, orientation and sequence had been strongly desired. If these kinds of methods are developed, the clusters with high-performance can be designed based on more precise prediction.

### 1-3-2 Exciton theory

**Introduction**

Change of absorption spectra associated with dye-clustering has been investigated by many experiments. On the other hand, the reasons why the spectra are changed by dye-clustering have been also investigated by a lot of theoretical researches. Through these studies, exciton theory was proposed to explain and predict the spectral changes associated with dye-clustering as the simplest theory.[3] Exciton theory can be applicable in the case of dyes with strong interaction between other dyes such as dye-clusters and solid crystals. In the theory, spectroscopic behaviors are explained by stabilization or destabilization of “exciton”, which represents a produced pair of an excited electron and remaining hole associated with excitation.[32] In following parts, we mentioned basic concepts of exciton theory and explanation of the spectral changes with homo and

hetero dye-clusters based on the theory.

**Basic concepts of exciton theory**

As mentioned at the previous part, exciton theory focuses on stabilization or destabilization of exciton to explain the spectral changes. The stabilization or destabilization are performed by delocalization of exciton in the clusters and exciton must be independent each other as precondition in the theory. Excitonic interaction is one of the static interactions which induce energy change of excited states by delocalization of exciton. In the case of homo dimer, excitonic interaction is expressed by following the equation.[2a, 3, 33]

$$E = \frac{|\mu|^2}{r^3}(1 - 3\,cos^2\,\theta) \qquad (1)$$

$\mu$ : Transition dipole moment

$r$ : distance between dyes

$\theta$ : angle between transition dipole moments of dyes

As shown in equation (1), excitonic interaction largely depends not only on distance and angle between dyes, but also on strength of transition dipole moment with monomer dyes. Especially, excitonic interaction tends to be observed in the case of dye-clustering with large absorption coefficient, because the square of transition dipole moment is proportional to absorption coefficient of the monomer. In exciton theory, a dye is regarded as a vector of transition dipole moment without the size of the molecule in order to simplify a system. Consequently, the largeness of dyes and orbit-orbit interaction are not considered in exciton theory.

In following parts, we showed the explanation of spectral changes with dye-clusters based on above concepts.

**Predicted absorption spectra of dye-clusters by exciton theory**

Homo dye-clusters have mainly three kinds of clusters such as H-aggregates, J-aggregates and oblique types. Figure 1-1 shows energy diagrams of the clusters.[2a, 3, 33] In addition, ellipse boxes with an arrow also show transition dipole moments and two arrows beside the energy level represent the positional relationship between transition dipole moments. To regard the arrows as vectors, an energy level with the sum of vectors, each of which direction is opposite, corresponds to forbidden transition because the sum vector is canceled while the level with the sum of vectors remained corresponds to allowed transition. In the case of H-aggregates, exciton theory explains hypsochromicity associated with dye-clustering derives from only an allowance of higher energy level. In contrast, in the case of J-aggregates, exciton theory also explains bathochromicity associated with dye-clustering derives from only an allowance of lower energy level. On the other hand, when dyes form oblique arrangement, the theory explains that band splitting is observed because both energy states are allowed (Davydov splitting). In this way, the behaviors in the case of homo dye-clusters can be explained by exciton theory and tended to coincide with the prediction according to previous reports.

In the case of hetero H-aggregates, the energy diagram is depicted in Fig. 1-13.[8, 34] In this case, transition dipole moments between different dyes take different strength. Because of this, a

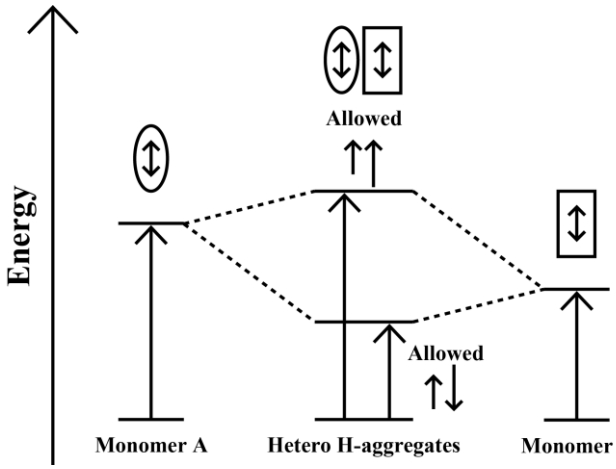


Figure 1-13. Schematic energy diagram of the heterodimer depicted on the basis of the exciton model. Each arrow designated the transition dipole moment.

lower energy level, which is forbidden in the case of homo H-aggregates, is allowed because the sum of vectors is not completely canceled, though a higher energy level is allowed obviously. Accordingly, exciton theory predicts that hypsochromicity and hyperchromicity of a band at shorter wavelength and bathochromicity and hypochromicity of a band at longer wavelength will be observed. In the case of the hetero dye-clusters as shown in previous parts, the behaviors coincided with the prediction, but the other important factors to determine the behaviors such as distance and angle between the dyes were not clarified. Therefore, they just used the theory for calculation of these factors and they have never verified validity of prediction based on exciton theory. In this way, systematic investigation of optical properties with hetero dye-clusters is quite important to reveal unclear points of their behaviors and verify the prediction based on exciton theory.

1-3-3 Present study (Analysis of Coherent Heteroclustering of Different Dyes by Use of Threoninol Nucleotides for Comparison with the Molecular Exciton Theory)

As mentioned at 1-3-1 and 1-3-2, behaviors of absorption spectra with hetero dye-clusters have not been investigated systematically because preparation method of the cluster with the pre-determined size, orientation and sequence had not been developed before. Thus, it was difficult to verify exciton theory by experimental results. However, these problems have been gradually solved by new preparation methods of the clusters to introduce dye residues into DNA or RNA duplex. For example, as hetero dye-clusters with the pre-determined sequence of the dyes,

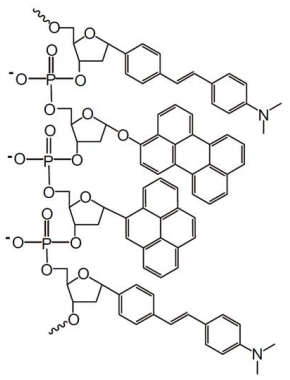

Figure 1-14. Illustration of "oligofluorosides".

Kool et al. reported “oligofluorosides” whose monomers were composed of an artificial nucleotide with a dye instead of a native base (Fig. 1-14).[22g, 35] They prepared one dimensional hereto dye-clusters with various fluorophores without any native nucleobases and successfully extracted the clusters with excellent properties by making libraries of random oligomers like combinatorial chemistry.[35] Their results indicate that the kinds and sequence of the dyes largely contribute their optical properties. Therefore, investigation of the effect, which is induced by these factors, on their properties is significant for development of novel dye-clusters.

In present study, we prepared hetero dye-clusters by the preparation method as shown in part 1-2 and chapter 2, and revealed their behaviors of absorption spectra. Furthermore, we also verified exciton theory of hetero aggregates by systematic analysis of their spectroscopic behaviors. This method provides easy preparation of various hetero dye-clusters by changing the kinds or sequence of dyes. Accordingly, we can systematically analyze properties of hetero dye-clusters because the method does not have any problems which previous conventional methods have. If spectroscopic behaviors of hetero dye-clusters become much clearer, exact prediction of their behaviors can be realized. Moreover, these results can provide novel guideline to design appropriate dye for development of DNA probes. Especially, in chapter 4, we explained how much excitonic interaction between a fluorophore and quencher dyes affected on properties of the probes with hetero dye-clustering.

## 1-4 General introduction in Chapter 4

(Development of a Highly Sensitive In-Stem Molecular Beacon

by Coherent Quenching of a Fluorophore)

### 1-4-1 Significance of development of DNA probes

Recently, various life phenomena have been rapidly revealed since all DNA sequence of human gene had been determined by Human Gene Project. For its part, specific gene expressions associated with some diseases were reported by a lot of papers.[36] Accordingly, diagnosis of diseases by detection of gene expression has been tried by many researchers. One of the procedures of the diagnosis is shown in Fig. 1-15.[37] When you get some disease inducing specific gene expression, mRNAs are produced by transcription from DNA. After that, proteins are also produced by translation from the mRNAs. Here, for disease diagnosis, existence of the proteins or mRNAs needs to be detected. In the case of the mRNA detection, we showed the procedure as in Fig. 1-15. According to that, first step is to extract all mRNAs in the cell and transform the mRNA into DNAs by reverse transcription. Next step is to amplify the DNAs by polymerase chain reaction (PCR). Final step is to detect a target DNA in all mixture DNAs. This

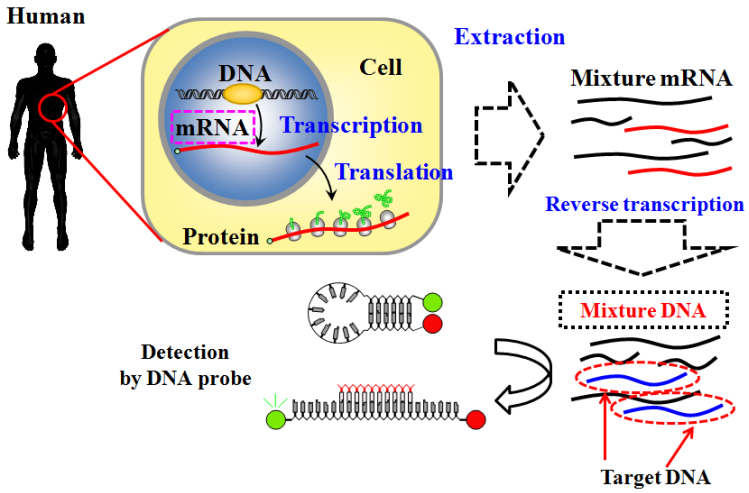


Figure 1-15. A general diagnosis procedure of some diseases by DNA probes.

DNA detection has been performed by gel shift assay or DNA sequencing. However, it takes much time to detect the target DNA by these methods and the detection sensitivities are low. Then, DNA probes have attracted attention as an excellent tool which can easily detect target DNA. The DNA probes with various detection methods were reported: detection by electrochemical methods[38], nano particles[39], fluorescence[4a, 40] and so on. Actually, the detection by fluorescence is regarded as one of the major strategies because the detection sensitivity is quite high as compared with other methods. This probe can detect target DNA in amplified mixture DNAs by addition of the probe to the DNAs. Because of that, you can simplify the procedure and reduce much time to diagnose the diseases. However, the probe does not go far enough to be put to practical use because the probe sensitivity has not been enough for practical application. Therefore, development of a highly sensitive probe for DNA detection has been desired.

### 1-4-2 Molecular Beacon

Many kinds of probes for DNA detection have been reported among recently. In these probes, molecular beacons (MBs) are one of the most common probes which can detect target DNA by fluorescence.[4a, 4b, 10, 28b, 41] we showed the basic detection mechanism of MBs in Fig. 1-16. As shown in Fig. 1-16, MB is hair-pin DNA which has a fluorophore

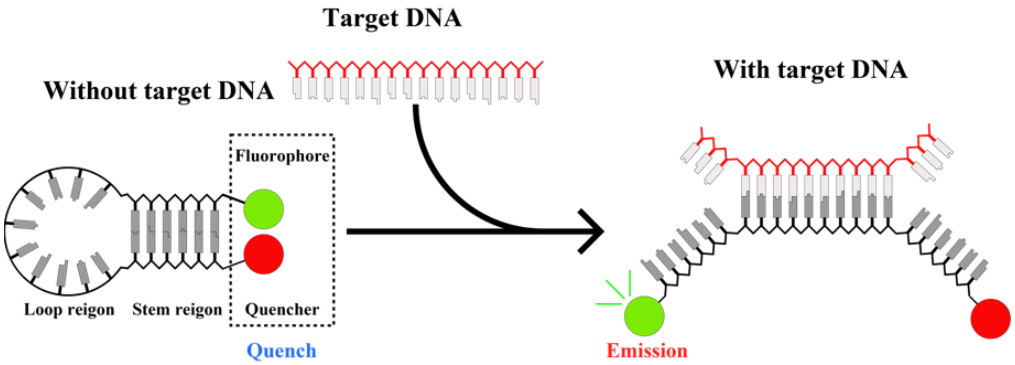


Figure 1-16. Schematic illustration of detection mechanism with molecular beacons.

and quencher at each terminal. A loop of MB recognizes target DNA and the dyes introduced at both termini of the stem transmit signal as fluorescence. In the case of without target DNA, the fluorophore is quenched by contact with quencher because the MB takes close states of stem region. On the other hand, in the case of with target DNA, the stem of MB is opened by recognition of target DNA and fluorescence recovers by dissociation of these dyes. In this way, MB detects target DNA by fluorescence and quenching. Thus, to improve probe sensitivity, two following things are important: strengthening brightness at only open states and reducing background emission at close states. Especially, reducing background emission is quite important because background emission directly determines the probe sensitivity. However, in the case of conventional MB, there are some problems derived from introduction of the dyes at termini of MB. For example, the background emission is relative high for the highly sensitive detection because stacking between dyes is weakened by terminal breathing of MB. As mentioned before, although conventional MB was developed by Tyagi et al. in 1996, only a few highly sensitive MBs have been reported in spite of development of various improved MBs[4b, 41b, 42] except probes with ratio-metric detection such as using FRET (fluorescent resonance energy transfer), excimer and exciplex emission.[28b, 41c]

Consequently, efficient quenching of a fluorophore is very important in the case of MBs which detect target DNA by the quenching associated with hetero dye-clustering between the fluorophore and quencher. Because of this, many researchers have tried to improve the quenching efficiency by various approaches. In next section, we mentioned quenching mechanisms which have been reported before and guide lines for proper design of dyes based on the mechanisms.

1-4-3 Quenching of a fluorophore by hetero dye-clustering

In previous section, we mentioned the importance of the efficient quenching to develop a highly sensitive DNA probe. Then, we explained quenching by electron transfer and energy transfer as some of effective methods for efficient quenching.

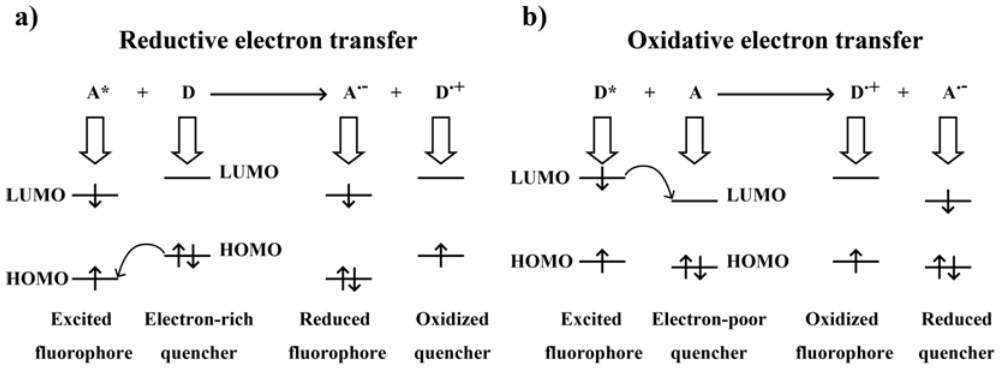


Figure 1-17. Schematic illustration of quenching mechanism by PET. a) Reductive and b) Oxidative electron transfer are shown.

Quenching by PET (photo-induced electron transfer)

Photo-induced electron transfer is known as one of the quenching mechanisms between different dyes.[43] This quenching largely depends on distance between dyes and their combination. Thus, quenching by PET is one of the important factors in the case of hetero dye-clustering. As shown in Fig. 1-17, the mechanisms take two procedures through reductive electron transfer or oxidative electron transfer. In the case of reductive electron transfer, HOMO and LUMO energy levels of two dyes take following relationship.

$$^{f}\boldsymbol{E}_{HOMO} < {}^{q}\boldsymbol{E}_{HOMO} < {}^{f}\boldsymbol{E}_{LUMO} < {}^{q}\boldsymbol{E}_{LUMO}$$

According to this relationship, when the fluorophore is excited, an electron of HOMO energy level with the quencher transfers to HOMO of the fluorophore. As a result, the fluorophore becomes a radical anion which does not have any fluorescence. This type quenching is observed in the case of electron-rich quenchers.

On the other hand, in the case of oxidative electron transfer, HOMO and LUMO energy levels of two dyes take following relationship.

$$^{q}E_{HOMO} < {}^{f}E_{HOMO} < {}^{q}E_{LUMO} < {}^{f}E_{LUMO}$$

According to this relationship, when the fluorophore is excited, the excited electron of the fluorophore transfers to LUMO of the quencher. As a result, the fluorophore becomes a radical cation which does not have any fluorescence. This type quenching is observed in the case of using electron-poor quenchers in contrast to the reductive quenching.

Previously, Nagano and Urano et al. have successfully developed probes to detect various small molecules and enzyme reactions in *vivo* by uses of intramolecular PET.[44] However, highly sensitive probes by use of PET have hardly reported in the case of hetero dye-clustering such as DNA probes. Because quenching by the PET is assumed that distance between the dyes is close but dyes do not stack with each other. In this way, if the dyes do not interact each other electrostatically (non-excitonic interaction), design of the dyes based on this diagram work well for efficient quenching. However, if the dyes strongly stack and interact, design of the dyes based on this diagram may not work properly because energy levels of the dyes are changed by dye-clustering. Accordingly, pre-selection of the dye combination is difficult for efficient quenching. Moreover, to develop more practical probes, the fluorophores with longer emission at more than 500 nm should be desirable. Because of this, effect of excitonic interaction between dyes on quenching becomes stronger because absorption coefficient of the fluorophore is inevitably large. Therefore, the effect of the excitonic interaction on quenching of a fluorophore has needed to be revealed to design a highly sensitive probe.

Quenching by FRET (fluorescence resonance energy transfer)

Quenching by energy transfer is also important for quenching of a fluorophore as well as quenching by PET. In general, FRET occurs in the case of relatively short distance between dyes (for example, less than 10 nm)[43a]. FRET is classified into two mechanisms such as Förster mechanism and Dexter mechanism as shown in Fig. 1-18. In the case of Förster mechanism, an accepter dye (quencher) receives energy of the excited donor dye (fluorophore) and the excited fluorophores are relaxed to ground states without any fluorescence. Because of this, overlap area between a fluorescent spectrum of the fluorophore and an absorption spectrum of the quencher is very important for efficient quenching (Fig. 1-19). The largeness of the area determines how much quencher can resonate to the provided energy from the fluorophores.

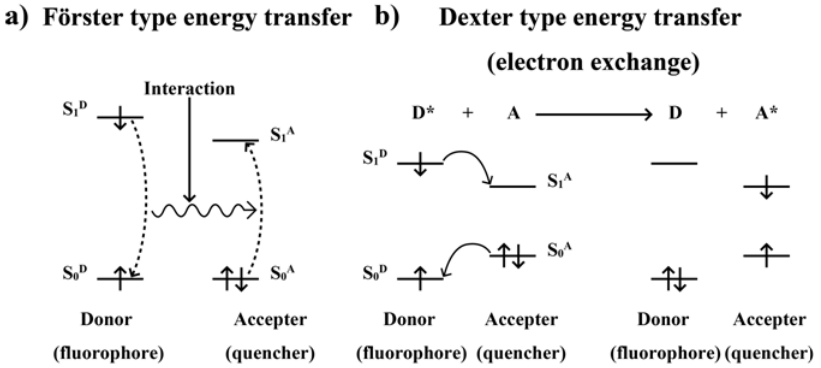


Figure 1-18. Schematic illustration of quenching mechanism by FRET. Energy transfer by a) Förster and b) Dexter mechanisms are shown.

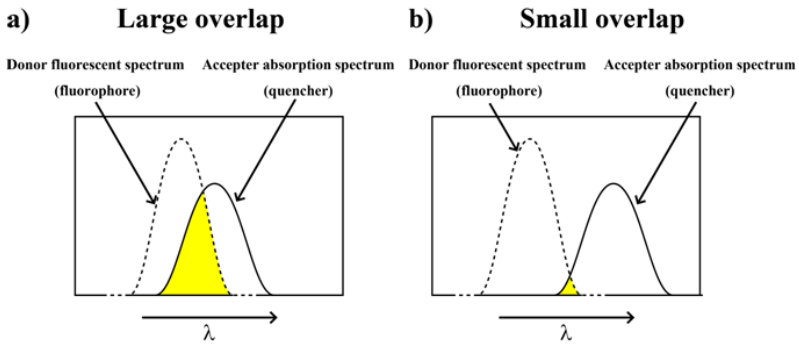


Figure 1-19. Illustration of the overlap between donor fluorescent spectrum and accepter absorption spectrum: a) in the case of large overlap and b) in the case of small overlap.

On the other hand, FRET through Dexter mechanism occurs when distance between dyes is closer than in the case of Förster mechanism. Electron exchange reaction between a donor and accepter is a main procedure in Dexter mechanism. In this case, HOMO and LUMO energy levels of two dyes take following relationship.

$$^{f}E_{HOMO} < {}^{q}E_{HOMO} < {}^{q}E_{LUMO} < {}^{f}E_{LUMO}$$

According to this relationship, when the fluorophore is excited, the excited electron of the fluorophore transfers to LUMO of the quencher while the other electron of HOMO state with the quencher transfers to HOMO of the fluorophore at the same time. As a result, the fluorophores become ground states without any radiation because of this electron exchange reaction while the quenchers become excited states.

FRET has been used for ratio-metric detection by clustering between identical or different fluorophores in many studies.[45] However, in the case of clustering between a fluorophore and quencher, reports about efficient quenching of the fluorophore by FRET has been limited. Because quenching by Förster mechanism or Dexter mechanism do not involved change of energy levels associated with dye-clustering. Accordingly, pre-designing combination of the dyes was quite difficult. In general, to increase in overlap area between a fluorescent spectrum of the fluorophore and an absorption spectrum of the quencher, the fluorophore with shorter absorption wavelength and the quencher with longer absorption wavelength are chosen for the efficient quenching. However, when the efficient quenching was performed based on this strategy, only a few clear evidences, which show that the efficient quenching is mainly performed by FRET, have been reported.[46]

In this way, although quenching of a fluorophore by PET and FRET act very

important roles in the case of hetero dye-clustering, simple guidelines for designing the dyes have not been proposed in order to force these mechanisms to work efficiently. Because of this, it is urgent to establish the guideline for improvement of the quenching efficiency by hetero dye-clustering.

### 1-4-4 Present study (Development of a Highly Sensitive In-Stem Molecular Beacon by Coherent Quenching of a Fluorophore)

As mentioned in section 1-4-2 and 1-4-3, efficient quenching of a fluorophore is necessary to develop a highly sensitive DNA probe. Because of this, development of effective guideline to design dyes has been desired. In contrast, we have systematically investigated the excitonic interaction between different dyes with hetero dye-clusters as shown in section 1-3. Moreover, we thought excitonic interaction between the dyes was an important factor for efficient quenching because of following two reasons.

1. Quenching by PET and FRET are not considered effects of interaction between dyes such as orbit-orbit interaction and excitonic interaction.
2. Dyes which are used for practical applications absorb light at longer wavelength (more than 500 nm) and have strong excitonic interaction between each other due to large absorption coefficient.

In present study, we investigated relationship between excitonic interaction and quenching efficiency of a fluorophore and proposed a novel guideline to design an optimal fluorophore-quencher pair for efficient quenching. Furthermore, we also developed a highly sensitive DNA probe based on this guideline. If the guideline is effective for efficient quenching of a fluorophore, it can be expected that the guideline

gives big impact to probe detection technology because the guideline can be applied to not only DNA probes, but also all probes which fluorophore-quencher pairs are used to. In addition, because highly sensitive detection by DNA probes can realize early diagnosis of some diseases, the development of this probe is very important.

In this way, we explain a highly sensitive DNA probe by an effective use of excitonic interaction in chapter 4. Additionally, the knowledge is important for further improvement of probe sensitivity by asymmetric dye-clustering in chapter 5.

## 1-5 General introduction in Chapter 5

(Maximizing Excitonic Interaction by Bulge Like Asymmetric Dye-clustering for Efficient Quenching of Background Emission)

### 1-5-1 Relationship between excitonic interaction and the number of the dyes

As mentioned in before section, we revealed that excitonic interaction of hetero dye-clusters was quite important for quenching of a fluorophore. On the other hand, in general, excitonic interaction between dyes is enhanced by increase in the size of the clusters. However, the change per the number of the dyes decreases as increase in the size of clusters. In the case of homo dye-clusters with identical dyes, several papers reported the change is saturated from 10-100 dyes on theory or experiments.[14] This number is called in "spectroscopic aggregation number (coherence length)" and it means the number of the dyes which really interact with each other. The coherent length of homo dye-clusters has been investigated by many papers while only a few reports about the length of hetero dye-clusters has been informed. Especially, most studies had hardly focused on excitonic interaction which a "dye-A" receives by "dye-Bs" and no reports have showed relationship between the interaction and the number of "dye-Bs". As the related reports, Kuhn et al. reported the relationship between absorption spectra of hetero dye-clusters based on LB films and the size of the clusters.[8] They investigated spectral change associated with controlling ratio between two dyes on the condition that the sum of concentration between two dyes was a constant. Accordingly, they could not observe excitonic interaction which "dye-A" receives by "dye-Bs" from these spectroscopic behaviors because concentration of "dye-A" was not a constant. Therefore, if the excitonic interaction can be systematically investigated, the coherent length of hetero dye-clusters can be revealed.

### 1-5-2 Present study (Maximizing Excitonic Interaction by Bulge Like Asymmetric Dye-clustering for Efficient Quenching of Background Emission)

As mentioned before, development of a highly sensitive DNA probe is significant to put DNA probe, which is expected to diagnose some diseases earlier, to practical use. To develop a highly sensitive DNA probe, efficient quenching of a fluorophore is quite important. Because of this, many methodologies have been reported for realization of the efficient quenching. On the other hand, we have systematically investigated a relationship between excitonic interaction and quenching efficiency of a fluorophore by the preparation of various hetero dye-clusters. As we explain these results in chapter 4, we revealed that efficient quenching of a fluorophore was performed by large excitonic interaction between the fluorophore and quencher. Excitonic interaction also depends on the number of the quencher dyes, though the interaction depends on the combination between dyes as we mentioned before. In present study, we tried to further enhance the excitonic interaction between dyes for improvement of the probe sensitivity by increase in the number of the quenchers. At the same time, we tried to reveal the number of the quenchers which actually interacted with a fluorophore. If we achieve these purposes, a highly sensitive DNA probe which has enough sensitivity for practical use can be developed and the cluster size dependence of excitonic interaction between different dyes can be revealed.

In this way, we explain asymmetric dye-clustering for further enhancement of quenching efficiency and the cluster size dependence of excitonic interaction between different dyes.

## 1-6 General introduction in Chapter 6

(Dye-clustering in RNA duplexes to apply for a fluorophore-quencher system)

### 1-6-1 Structural difference between DNA and RNA duplex

A major difference between RNA and DNA, other than their biological roles, is the presence of the 2'-hydroxyl group in the ribose scaffold, which induces different 3D structures of the duplex (Fig. 1-20)[47]. RNA and DNA duplexes adopt A- and B-form structures by taking C3'-*endo* and C2'-*endo* conformations of the (deoxy)ribose ring puckering, respectively.[48] Base-pairs in A-formed RNA duplexes, which are tighter than B-formed DNA duplexes, are wound aslope around the helix axis, while base-pairs are almost axially stacked in DNA duplexes.[49] These structural differences also significantly affect the binding behavior of intercalators in the duplexes. It is well-known that DNA duplexes readily accept some planar dyes intercalated between the base-pairs, and thus the duplexes are fairly stabilized. However, unlike DNA duplexes, dyes do not readily

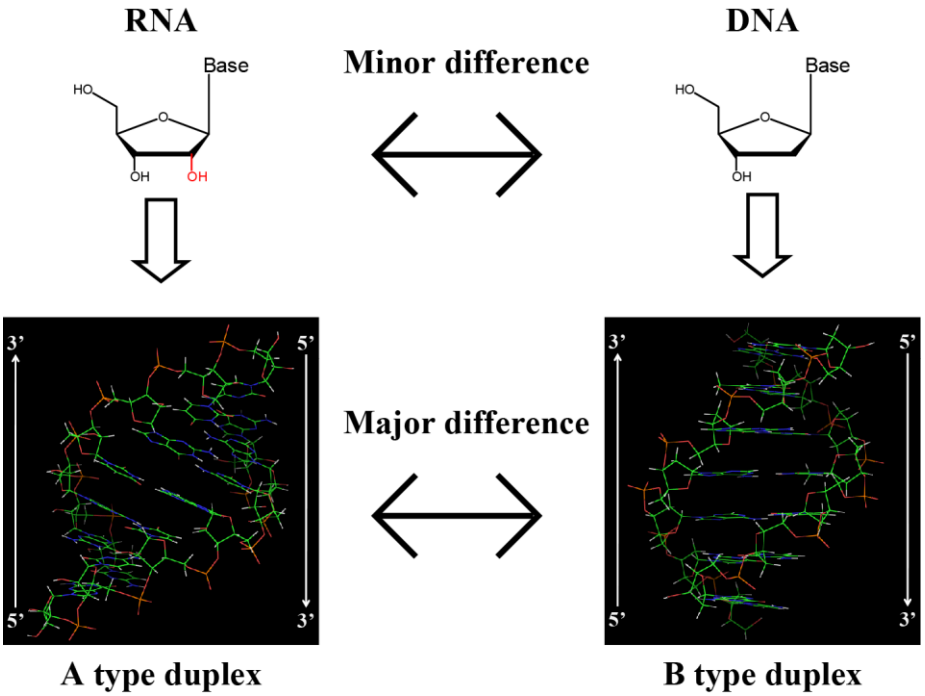


Figure 1-20. Illustration of structural differences between RNA and DNA duplex.

intercalate into tightly wound A-formed RNA duplexes.[11, 50] Similarly, covalently introduced functional molecules interact differently with DNA or RNA duplexes.[25a-e, 25g, 25h, 51] For example, pyrenes introduced at the 2'-position of ribose are flipped out from the duplex to the minor groove when they are involved in an RNA duplex. But pyrenes tethered at the same position intercalate between the base-pairs in a DNA duplex. Because of this, functional molecules in RNA duplexes do not necessarily behave similar to those in DNA duplexes, although DNA and RNA have similar nucleotide structures.

1-6-2 Biological significance of hetero dye-clustering in RNA duplex

Recently, various functions of RNA except messenger of gene information have been reported while DNA acts a record medium of the information. Especially, functional short RNAs such as ribozyme[52], RNA aptamer[50, 53] and siRNA[12a, 12b] were discovered in non-coding RNAs and significance of RNA studies has been drastically increasing. In these functional RNAs, siRNA has attracted much attention as one of the nucleic acid medicines because siRNA directly and efficiently suppresses specific gene expression by translation inhibition. Moreover, siRNA can work efficiently and stably compared with antisense[54], antigene[55], ribozyme and DNAzyme[56] because the suppression by siRNA was performed through endogenous system. Therefore, siRNA has been used as a promising tool to suppress gene expression in biological field. Figure 1-21 shows RNAi mechanism which has been revealed so far.[12c, 57] When siRNA is introduced into mammalian cells, 2 or 3 nucleotides at both 5'-ends with introduced siRNA into cell are cut by Dicer. Next, it is recognized by the RNA-induced silencing complex (RISC), a multiprotein complex containing the endonuclease Argonaute2 (Ago2). One strand of

the duplex (the so-called passenger or sense strand) is removed, while the other remains (the so-called guide or antisense strand) associated with RISC and guides it to complementary mRNA. After that, RISC recognize and cut the target mRNA efficiently. Accordingly, hybridization of RNA duplex is one of the most important procedures in RNAi process. If each state of siRNA can be visualized without losing RNAi activity, time scale of each process can be revealed. The labeling with a fluorophore and quencher is known as effective way to distinguish between single- and double-stranded states. However, this strategy has not succeeded for visualization of these states.[58] Because dye residues labeled at the terminal of siRNA are removed by Dicer processing and discrimination between single- and double-stranded states is impossible for terminal labeling. Therefore, hetero dye-clustering in RNA duplex (not at terminal) without losing RNAi activity is significant to visualize siRNA states.

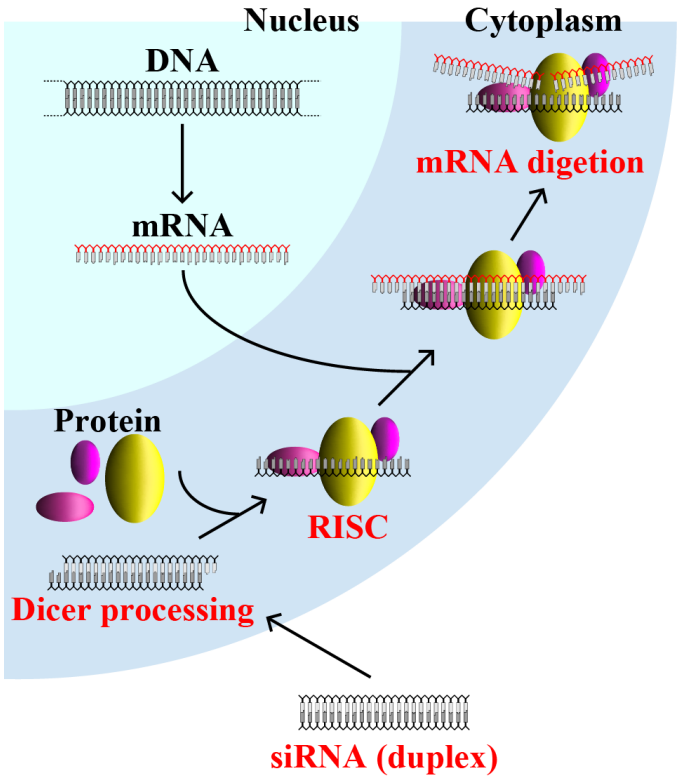


Figure 1-21. Schematic illustration of RNAi machinery which has been revealed since now.

1-6-3 Present study (Dye-clustering in RNA duplexes to apply for a fluorophore-quencher system)

As mentioned in section 1-6-1 and 1-6-2, dye-clustering in RNA duplex is important to prepare the clusters with novel orientation and biological tool for investigation of RNAi mechanism. In present study, we developed the novel dye-clusters in RNA duplex by a use of the cluster design in DNA duplex and established the fluorophore-quencher system in RNA duplex. This hetero dye-cluster with a fluorophore and quencher can be one of the effective ways to visualize the RISC states.

In this way, we explain the dye clustering based on RNA duplex in Chapter 6.

## 1-7 Note and reference


1. 詫間啓輔、藤井志朗, *わかりやすい機能性色素材料: 「光」の時代のキーマテリアル*, 工業調査会, 1999.
2. (a) T. Kobayashi, *J-aggregates*, World Scientific, Singapore, 1996; (b) A. Mishra, R. K. Behera, P. K. Behera, B. K. Mishra and G. B. Behera, *Chem. Rev.*, 2000, **100**, 1973.
3. M. Kasha, *Radiat. Res.*, 1963, **20**, 55.
4. (a) S. Tyagi and F. R. Kramer, *Nat. Biotechnol.*, 1996, **14**, 303; (b) W. Tan, K. Wang and T. J. Drake, *Curr. Opin. Chem. Biol.*, 2004, **8**, 547; (c) C. Sun, J. Yang, L. Li, X. Wu, Y. Liu and S. Liu, *J.Chromatogr.B*, 2004, **803**, 173; (d) A. A. Martí, S. Jockusch, N. Stevens, J. Ju and N. J. Turro, *Acc. Chem. Res.*, 2007, **40**, 402; (e) A. Herland and O. Inganäs, *Macromol. Rapid Commun.*, 2007, **28**, 1703.
5. (a) T. Förster, *Ann. Phys.*, 1948, **2**, 55; (b) S. A. E. Marras, F. R. Kramer and S. Tyagi, *Nucleic Acids Res.*, 2002, **30**, e122; (c) M. K. Johansson and R. M. Cook, *Chem. Eur. J.*, 2003, **9**, 3466.
6. N. Stephen, *Principles of nucleic acid structure*, Elsevier, London, 2008.
7. W. C. Tse and D. L. Boger, *Acc. Chem. Res.*, 2003, **37**, 61.
8. Czikkely V., Dreizler G., Försterling H. D., Kuhn H., Sondermann J., Tillmann P. and Wiegand J. Z., *Z. Naturforsch.*, 1969, **24a**, 1821.
9. (a) P. O. Brown and D. Botstein, *Nat. Genet.*, 1999, 33; (b) M. B. Eisen and P. O. Brown, *Meth. Enzymol.*, 1999, **Volume 303**, 179; (c) J. R. Epstein, I. Biran and D. R. Walt, *Anal. Chim. Acta*, 2002, **469**, 3.
10. S. Tyagi, *Nat. Meth.*, 2009, **6**, 331.
11. (a) R. Sinha, M. M. Islam, K. Bhadra, G. S. Kumar, A. Banerjee and M. Maiti, *Bioorg. Med. Chem.*, 2006, **14**, 800; (b) M. M. Islam and G. Suresh Kumar, *DNA Cell Biol.*, 2009, **28**, 637.
12. (a) A. Fire, S. Xu, M. K. Montgomery, S. A. Kostas, S. E. Driver and C. C. Mello, *Nature*, 1998, **391**, 806; (b) M. K. Montgomery and A. Fire, *Trends Genet.*, 1998, **14**, 255; (c) T. Kawamata and Y. Tomari, *Trends Biochem. Sci.*, 2010, **35**, 368.
13. A. H. Herz, *Adv. Colloid Interface Sci.*, 1977, **8**, 237.
14. (a) E. W. Knapp, *Chem. Phys.*, 1984, **85**, 73; (b) A. S. R. Koti and N. Periasamy, *J. Mater. Chem.*, 2002, **12**, 2312; (c) A. S. R. Koti, J. Taneja and N. Periasamy, *Chem. Phys. Lett.*, 2003, **375**, 171; (d) J. R. Durrant, J. Knoester and D. A. Wiersma, *Chem. Phys. Lett.*, 1994, **222**, 450.
15. A. Yamaguchi, N. Kometani and Y. Yonezawa, *Thin Solid Films*, 2006, **513**, 125.

16. (a) S. C. Doan, S. Shanmugham, D. E. Aston and J. L. McHale, *J. Am. Chem. Soc.*, 2005, **127**, 5885; (b) L. P. F. Aggarwal and I. E. Borissevitch, *Spectrochim. Acta Part A*, 2006, **63**, 227.
17. H. Asanuma and T. Tani, *J. Phys. Chem. B*, 1997, **101**, 2149.
18. G. G. Roberts, *Contempt. Phys.*, 1984, **25**, 109.
19. K. Murata, H.-K. Shin, K. Saito and S.-i. Kuroda, *Thin Solid Films*, 1998, **327-329**, 446.
20. (a) J. L. Seifert, R. E. Connor, S. A. Kushon, M. Wang and B. A. Armitage, *J. Am. Chem. Soc.*, 1999, **121**, 2987; (b) M. Wang, G. L. Silva and B. A. Armitage, *J. Am. Chem. Soc.*, 2000, **122**, 9977; (c) R. A. Garoff, E. A. Litzinger, R. E. Connor, I. Fishman and B. A. Armitage, *Langmuir*, 2002, **18**, 6330; (d) A. L. Stadler, B. R. Renikuntla, D. Yaron, A. S. Fang and B. A. Armitage, *Langmuir*, 2010, **27**, 1472; (e) S. Gadde, E. K. Batchelor and A. E. Kaifer, *Chem. Eur. J.*, 2009, **15**, 6025; (f) R. Iwaura, M. Ohnishi-Kameyama and T. Iizawa, *Chem. Eur. J.*, 2009, **15**, 3729.
21. (a) C. Samyn, T. Verbiest and A. Persoons, *Macromol. Rapid Commun.*, 2000, **21**, 1; (b) T. Klingstedt and K. P. R. Nilsson, *Biochim. Biophys. Acta*, 2011, **1810**, 286.
22. (a) T. J. Matray and E. T. Kool, *J. Am. Chem. Soc.*, 1998, **120**, 6191; (b) C. Brotschi and C. J. Leumann, *Angew. Chem. Int. Ed*, 2003, **42**, 1655; (c) C. Brotschi, G. Mathis and C. J. Leumann, *Chem. Eur. J.*, 2005, **11**, 1911; (d) I. Hirao, M. Kimoto, T. Mitsui, T. Fujiwara, R. Kawai, A. Sato, Y. Harada and S. Yokoyama, *Nat Meth*, 2006, **3**, 729; (e) Y. Kim, A. M. Leconte, Y. Hari and F. E. Romesberg, *Angew. Chem. Int. Ed*, 2006, **45**, 7809; (f) T. Mitsui, M. Kimoto, R. Kawai, S. Yokoyama and I. Hirao, *Tetrahedron*, 2007, **63**, 3528; (g) J. N. Wilson, J. Gao and E. T. Kool, *Tetrahedron*, 2007, **63**, 3427; (h) S. K. Jarchow-Choy, A. T. Krueger, H. Liu, J. Gao and E. T. Kool, *Nucleic Acids Res.*, 2010; (i) L. M. Wilhelmsson, *Q. Rev. Biophys.*, 2010, **43**, 159.
23. H.-A. Wagenknecht, *Ann. N. Y. Acad. Sci.*, 2008, **1130**, 122.
24. E. Mayer-Enthart, C. Wagner, J. Barbaric and H.-A. Wagenknecht, *Tetrahedron*, 2007, **63**, 3434.
25. (a) K. Yamana, R. Iwase, S. Furutani, H. Tsuchida, H. Zako, T. Yamaoka and A. Murakami, *Nucleic Acids Res.*, 1999, **27**, 2387; (b) K. Yamana, H. Zako, K. Asazuma, R. Iwase, H. Nakano and A. Murakami, *Angew. Chem. Int. Ed*, 2001, **40**, 1104; (c) A. Mahara, R. Iwase, T. Sakamoto, K. Yamana, T. Yamaoka and A. Murakami, *Angew. Chem. Int. Ed*, 2002, **41**, 3648; (d) A. Mahara, R. Iwase, T.

Sakamoto, T. Yamaoka, K. Yamana and A. Murakami, *Bioorg. Med. Chem.*, 2003, **11**, 2783; (e) M. Nakamura, Y. Shimomura, Y. Ohtoshi, K. Sasa, H. Hayashi, H. Nakano and K. Yamana, *Org. Biomol. Chem.*, 2007, **5**, 1945; (f) I. V. Astakhova, V. A. Korshun and J. Wengel, *Chem. Eur. J.*, 2008, **14**, 11010; (g) M. Nakamura, Y. Murakami, K. Sasa, H. Hayashi and K. Yamana, *J. Am. Chem. Soc.*, 2008, **130**, 6904; (h) M. Fukuda, M. Nakamura, T. Takada and K. Yamana, *Tetrahedron Lett.*, 2010, **51**, 1732.

26. (a) V. L. Malinovskii, F. Samain and R. Häner, *Angew. Chem. Int. Ed*, 2007, **46**, 4464; (b) H. Bittermann, D. Siegemund, V. L. Malinovskii and R. Häner, *J. Am. Chem. Soc.*, 2008, **130**, 15285; (c) T. M. Wilson, T. A. Zeidan, M. Hariharan, F. D. Lewis and M. R. Wasielewski, *Angew. Chem. Int. Ed*, 2010, **49**, 2385.
27. Y. Ueno, S. Komatsuzaki, K. Takasu, S. Kawai, Y. Kitamura and Y. Kitade, *Eur. J. Org. Chem.*, 2009, **2009**, 4763.
28. (a) H. Zhou, X. Ma, J. Wang and L. Zhang, *Org. Biomol. Chem.*, 2009, **7**, 2297; (b) C. Holzhauser and H.-A. Wagenknecht, *Angew. Chem. Int. Ed*, 2011, **50**, 7268.
29. H. Kashida, M. Tanaka, S. Baba, T. Sakamoto, G. Kawai, H. Asanuma and M. Komiyama, *Chem. Eur. J.*, 2006, **12**, 777.
30. 樫田啓　平成 18 年度博士（工学）学位論文　東京大学大学院工学研究科化学生命光学専攻　「色素とのコンジュゲーションによる DNA の機能化に関する研究」
31. (a) S. Bernacchi and Y. Mély, *Nucleic Acids Res.*, 2001, **29**, e62; (b) S. Bernacchi, E. Piémont, N. Potier, A. v. Dorsselaer and Y. Mély, *Biophys. J.*, 2003, **84**, 643.
32. 久保淳一　2009 年度修士学位論文　名古屋大学大学院工学研究科物質制御工学専攻　「会合体形成で誘起された軌道間相互作用による色素の励起エネルギー変化」
33. J. Mizuguchi, *Journal of The Society of Photographic Science and Technology of Japan*, 2007, **70**, 268.
34. B. Z. Packard, D. D. Toptygin, A. Komoriya and L. Brand, *J. Phys. Chem. B*, 1998, **102**, 752.
35. (a) J. Gao, C. Strässler, D. Tahmassebi and E. T. Kool, *J. Am. Chem. Soc.*, 2002, **124**, 11590; (b) S. S. Tan, S. J. Kim and E. T. Kool, *J. Am. Chem. Soc.*, 2011, **133**, 2664.
36. (a) X.-H. Peng, Z.-H. Cao, J.-T. Xia, G. W. Carlson, M. M. Lewis, W. C. Wood and L. Yang, *Cancer Res.*, 2005, **65**, 1909; (b) H. Döhner, S. Stilgenbauer, K.

Fischer, M. Schröder, M. Bentz and P. Lichter, *Stem Cells*, 1995, **13**, 76; (c) C. Preudhomme, F. Révillion, A. Merlat, L. Hornez, C. Roumier, N. Duflos-Grardel, J. P. Jouet, A. Cosson, J. P. Peyrat and P. Fenaux, *Leukemia.*, 1999, **13**, 957; (d) C. L. Sawyers, *N. Engl. J. Med.*, 1999, **340**, 1330; (e) P. Bolufer, G. F. Sanz, E. Barragan, M. A. Sanz, J. Cervera, E. Lerma, L. Senent, I. Moreno and M. D. Planelles, *Haematologica*, 2000, **85**, 1248.

37. J. J. M. van Dongen, E. A. Macintyre, J. A. Gabert, E. Delabesse, V. Rossi, G. Saglio, E. Gottardi, A. Rambaldi, G. Dotti, F. Griesinger, A. Parreira, P. Gameiro, M. G. Diáz, M. Malec, A. W. Langerak, J. F. San Miguel and A. Biondi, *Leukemia.*, 1999, **13**, 1901.
38. T. G. Drummond, M. G. Hill and J. K. Barton, *Nat. Biotechnol.*, 2003, **21**, 1192.
39. N. L. Rosi and C. A. Mirkin, *Chem. Rev.*, 2005, **105**, 1547.
40. (a) Q. Li, G. Luan, Q. Guo and J. Liang, *Nucleic Acids Res.*, 2002, **30**, e5; (b) E. Ergen, M. Weber, J. Jacob, A. Herrmann and K. Müllen, *Chem. Eur. J.*, 2006, **12**, 3707.
41. (a) C. Crey-Desbiolles, D.-R. Ahn and C. J. Leumann, *Nucleic Acids Res.*, **2005**, **33**, e77; (b) E. Socher, L. Bethge, A. Knoll, N. Jungnick, A. Herrmann and O. Seitz, *Angew. Chem. Int. Ed*, 2008, **47**, 9555; (c) N. Venkatesan, Y. Jun Seo and B. Hyean Kim, *Chem. Soc. Rev.*, 2008, **37**, 648.
42. L. Wang, C. J. Yang, C. D. Medley, S. A. Benner and W. Tan, *J. Am. Chem. Soc.*, 2005, **127**, 15664.
43. (a) B. Valeur, *Molecular Fluorescence: Principles and Applications*, Wiley-VHC, Weinheim, 2002; (b) 山崎巖, *有機量子化学と光化学*, 一麦出版社, 札幌, 2003.
44. Y. Urano, M. Kamiya, K. Kanda, T. Ueno, K. Hirose and T. Nagano, *J. Am. Chem. Soc.*, 2005, **127**, 4888.
45. (a) A. Dietrich, V. Buschmann, C. Müller and M. Sauer, *Rev. Mol. Biotechnol.* 2002, **82**, 211; (b) K. Börjesson, S. Preus, A. H. El-Sagheer, T. Brown, B. Albinsson and L. M. Wilhelmsson, *J. Am. Chem. Soc.*, 2009, **131**, 4288.
46. P. Crisalli and E. T. Kool, *Bioconjugate Chem.*, 2011, **22**, 2345.
47. J. Fohrer, U. Reinscheid, M. Hennig and T. Carlomagno, *Angew. Chem. Int. Ed*, 2006, **45**, 7033.
48. G. Mayer, *The Chemical Biology of Nucleic Acids*, Wiley, Chichester, UK 2010.
49. E. Lescrinier, M. Froeyen and P. Herdewijn, *Nucleic Acids Res.*, 2003, **31**, 2975.
50. R. Pei, J. Rothman, Y. Xie and M. N. Stojanovic, *Nucleic Acids Res.*, 2009, **37**, e59.

51. (a) H. Ito, X. Liang, H. Nishioka and H. Asanuma, *Org. Biomol. Chem.*, 2010, **8**, 5519; (b) H. Nishioka, X. Liang and H. Asanuma, *Chem. Eur. J.*, 2010, **16**, 2054.
52. (a) K. Kruger, P. J. Grabowski, A. J. Zaug, J. Sands, D. E. Gottschling and T. R. Cech, *Cell*, 1982, **31**, 147; (b) C. Guerrier-Takada, K. Gardiner, T. Marsh, N. Pace and S. Altman, *Cell*, 1983, **35**, 849; (c) T. R. Cech and B. L. Bass, *Annu. Rev. Biochem.*, 1986, **55**, 599; (d) J. A. Doudna and T. R. Cech, *Nature*, 2002, **418**, 222.
53. (a) A. D. Ellington and J. W. Szostak, *Nature*, 1990, **346**, 818; (b) D. S. Wilson and J. W. Szostak, *Annu. Rev. Biochem.*, 1999, **68**, 611; (c) S. M. Nimjee, C. P. Rusconi and B. A. Sullenger, *Annu. Rev. of Med.*, 2005, **56**, 555; (d) J. F. Lee, G. M. Stovall and A. D. Ellington, *Curr. Opin. Chem. Biol.*, 2006, **10**, 282; (e) E. J. Cho, J.-W. Lee and A. D. Ellington, *Annu. Rev. Anal. Chem.*, 2009, **2**, 241.
54. E. Uhlmann and A. Peyman, *Chem. Rev.*, 1990, **90**, 543.
55. D. Praseuth, A. L. Guieysse and C. Hélène, *Biochim. Biophys. Acta*, 1999, **1489**, 181.
56. G. F. Joyce, *Nature*, 1989, **338**, 217.
57. (a) L. Aagaard and J. J. Rossi, *Adv. Drug Deliv. Rev.*, 2007, **59**, 75; (b) M. Sano, M. Sierant, M. Miyagishi, M. Nakanishi, Y. Takagi and S. Sutou, *Nucleic Acids Res.*, 2008, **36**, 5812; (c) J. K. Watts, G. F. Deleavey and M. J. Damha, *Drug Discov. Today*, 2008, **13**, 842; (d) R. W. Carthew and E. J. Sontheimer, *Cell*, 2009, **136**, 642; (e) A. Jagannath and M. J. A. Wood, *Mol. Biol. Cell*, 2009, **20**, 521; (f) M. Gaglioneg and A. Messere, *Mini-Rev. Med. Chem.*, 2010, **10**, 578; (g) Y. Dang, Q. Yang, Z. Xue and Y. Liu, *Eukaryot. Cell*, 2011, **10**, 1148.
58. A. Järve, J. Müller, I.-H. Kim, K. Rohr, C. MacLean, G. Fricker, U. Massing, F. Eberle, A. Dalpke, R. Fischer, M. F. Trendelenburg and M. Helm, *Nucleic Acids Res.*, 2007, **35**, e124.

# Chapter 2. Stable interstrand clustering in DNA duplexes by use of threoninol-nucleotides

## 2-1 Abstract

Functional molecules such as dyes (Methyl Red, azobenzene, and Naphthyl Red) were tethered on D-threoninol as base surrogates (threoninol-nucleotide), which were consecutively incorporated at the center of natural oligodeoxyribonucleotides (ODNs). Hybridization of two ODNs involving threoninol-nucleotides allowed interstrand clustering of the dyes on D-threoninol and greatly stabilized the duplex. When two complementary ODNs, both of which had tethered Methyl Reds on consecutive D-threoninols, were hybridized, the melting temperature increased proportionally to the number of Methyl Reds, due to stacking interactions. Clustering of Methyl Reds induced both hypsochromicity and narrowing of the band, demonstrating that Methyl Reds were axially stacked relative to each other (H-aggregation). Since hybridization lowered the intensity of circular dichroism peaks at the $\pi$-$\pi^*$ transition region of Methyl Red (300-500 nm), clustered Methyl Reds were scarcely wound in the duplex. Alternate hetero dye clusters could also be prepared only by hybridization of two ODNs with different threoninol-nucleotides, such as Methyl Red-azobenzene and Methyl Red-Naphthyl Red combinations. A combination of Methyl Red and azobenzene induced bathochromic shift and broadening of the band at the Methyl Red region due to the disturbance of exciton interaction among Methyl Reds. But interestingly, the Methyl Red and Naphthyl Red combination induced merging of each absorption band to give a single sharp band, indicating that exciton interaction occurred among the different dyes.

Thus, D-threoninol can be a versatile scaffold for introducing functional molecules into DNA for their ordered clustering.

## 2-2 Introduction

Modification of nucleotides is one of the most active research fields in chemical biology. A wide variety of modified oligodeoxyribonucleotides (ODNs) have been synthesized for reasons such as expansion of the genetic alphabet,[1] antigene or antisense therapy,[2] and fluorescent labeling.[3] Moreover, ODNs have been also utilized as a scaffold for preparing supramolecular arrays.[4] For example, Tanaka and Shionoya *et al*. reported on metal arrays of copper(II) ions in an ODN double helix by introducing metal ligands into the base positions.[4a] Kool *et al.* reported on arrays of fluorescence dyes, made by consecutively introducing dyes into a single strand.[4b, 4c] They succeeded in constructing arrays of functional molecules of pre-determined size and number. Therefore, ODNs are a promised tool to line up functional molecules such as dyes.

As mentioned in general introduction, D-ribose has been utilized as a scaffold for constructing dye-clusters of pre-determined size and number. However, there is no limitation on the structure of a linker for tethering dyes in DNA when the DNAs are used for dye-clustering. Previously, our laboratory have synthesized modified ODNs incorporating D-threoninol (not the L-form) as a linker,[5] and found that even non-natural molecules on this linker intercalated between base pairs without destabilizing the duplex. Here, we propose D-threoninol as a useful scaffold (threoninol-nucleotide) of various non-natural functional molecules for incorporating them into ODNs and tethering various dyes on to it, without disturbing hybridization to a complementary ODN. In our design, non-natural functional molecules on D-threoninol (threoninol-nucleosides) are

introduced at the counterpart of each strand to form a pseudo “base-pair”. Larger molecules than natural bases can be introduced and pseudo “base-pairs” stabilize the duplex by intermolecular stacking interactions as depicted in Scheme 2-1. By this design, highly organized molecular clusters can be easily constructed without disturbing the duplex. Such molecular clusters are applicable to nonlinear optical materials and molecular wire as well as detection of single nucleotide polymorphisms and so on.

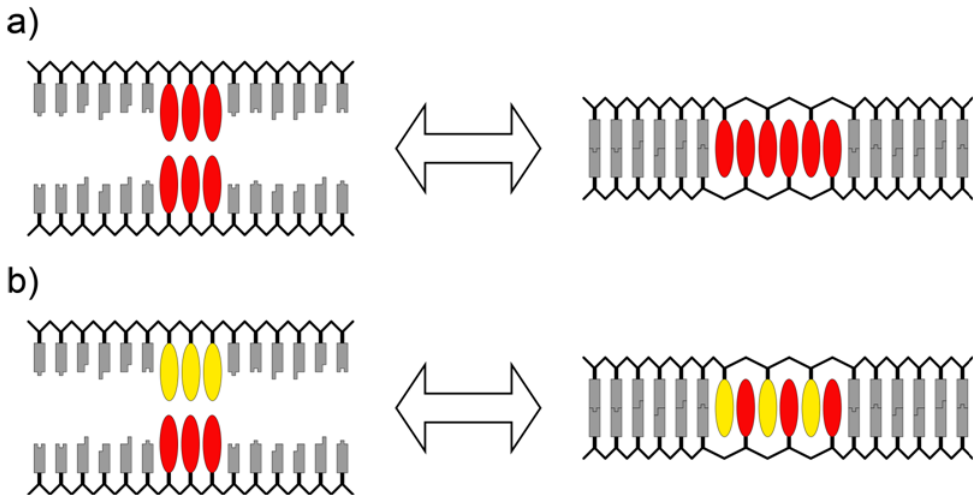


Scheme 2-1. Schematic illustration of stabilization by insertion of threoninol-nucleotides of a) homo and b) hetero pairs.

In this chapter, three threoninol-nucleotides tethering Methyl Red (**M**), Naphthyl Red (**N**) and azobenzene (**Z**) were prepared and incorporated into ODNs (Scheme 2-1). Interstrand stacking of these dyes was investigated from UV/Vis and CD spectra as well as the melting profiles of the resulting duplexes. We found that D-threoninol could be a useful scaffold of non-natural molecules, for their clustering in the duplex and stabilization of the duplex. By these threoninol-nucleotides, homo- and alternate hetero-clusters can be easily designed and synthesized.

**M*n*a** : 5'-GGT-ATC-**M**$_n$-GCA-ATC-3' ***n*** = 1-6
**M*n*b** : 3'-CCA-TAG-**M**$_n$-CGT-TAG-5'

**Z*n*a** : 5'-GGT-ATC-**Z**$_n$-GCA-ATC-3' ***n*** = 1,2,3,6
**Z*n*b** : 3'-CCA-TAG-**Z**$_n$-CGT-TAG-5'

**MP3a** : 5'-GGT-ATC-**MPMPMP**-GCA-ATC-3'
**MP3b** : 3'-CCA-TAG-**MPMPMP**-CGT-TAG-5'

**N3a** : 5'-GGT-ATC-**N**$_3$-GCA-ATC-3'
**A*n*a** : 5'-GGT-ATC-A$_n$-GCA-ATC-3' ***n*** = 1-6
**T5a** : 5'-GGT-ATC-T$_5$-GCA-ATC-3'
**C5a** : 5'-GGT-ATC-C$_5$-GCA-ATC-3'
**G5a** : 5'-GGT-ATC-G$_5$-GCA-ATC-3'

**N** :5'-GGT-ATC-GCA-ATC-3'
**C** : 3'-CCA-TAG-CGT-TAG-5'

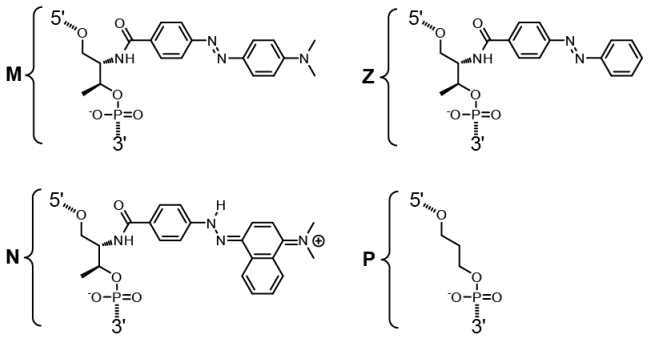


Scheme 2-2. Sequences of ODNs synthesized in this chapter.

## 2-3 Results

### 2-3-1 Effect of the pairing of threoninol-nucleotides on the melting temperature

**Homo-combination.**

The sequences of the ODNs involving threoninol-nucleotides are shown in Scheme 2-2: threoninol-nucleotides (**M**, **N**, and **Z** in Scheme 2-2) were introduced consecutively into the middle of ODNs. Here, they are located at the counterpart of each strand to form a pseudo "base-pair" with an anti-parallel orientation (see Scheme 2-1). First, the effect of pairing of threoninol-nucleotides on the stability of the duplex (melting

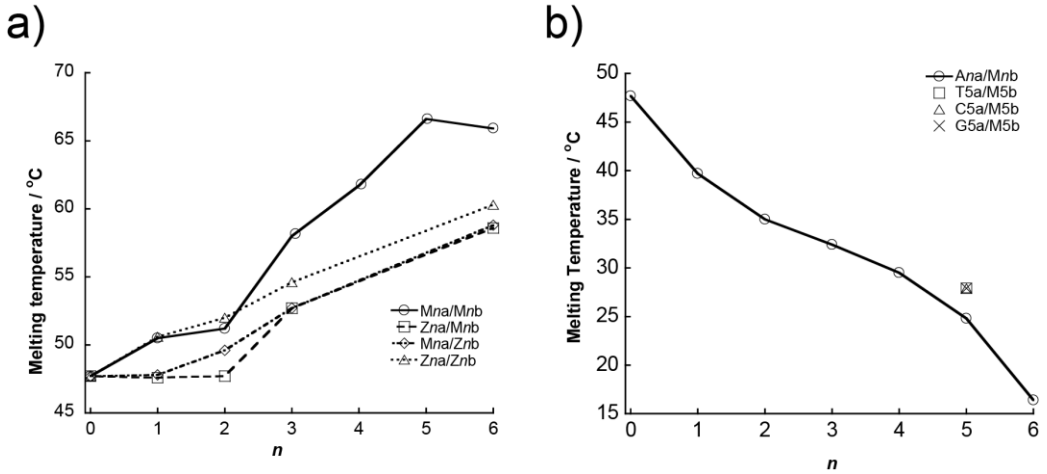


Figure 2-1. Melting temperatures of a) threoninol-nucleotide pairs of **M*n*a**/**M*n*b** and **Z*n*a**/**Z*n*b** involving Methyl Red and azobenzene homo clusters, respectively, and **Z*n*a**/**M*n*b** and **M*n*a**/**Z*n*b** involving an azobenzene-Methyl Red hetero cluster, b) a natural and threoninol-nucleotide pair, **A*n*a**/**M*n*b**, involving adenosine and Methyl Red. Melting temperatures of **T5a**/**M5b**, **C5a**/**M5b**, and **G5a**/**M5b** are also shown. Melting temperatures of each duplex are listed in appendix Table 2-1. Solution conditions are as follows: [ODN] = 5 μM, [NaCl] = 100 mM, pH 7.0 (10 mM phosphate buffer).

Table 2-1. Effects of the number of Methyl Red on the melting temperature ($T_m$) and absorption maximum and half-line-width of π-π* transition of Methyl Red[a]

| Sequences | $T_m$ / °C | $\lambda_{max}$ / nm[b] | Half-line width[b] / $cm^{-1}$ |
|---|---|---|---|
| **N/C** | 47.7 | - | - |
| **M1a/M1b** | 50.5 | 471 | 2283 |
| **M2a/M2b** | 51.2 | 446 | 3113 |
| **M3a/M3b** | 58.0 | 437 | 3112 |
| **M4a/M4b** | 61.7 | 429 | 3389 |
| **M5a/M5b** | 66.6 | 409 | 3228 |
| **M6a/M6b** | 65.9 | 404 | 2639 |
| **MP3a/MP3b** | 50.9 | 444 | 4543 |

[a] Solution conditions: [ODN] = 5 μM, [NaCl] = 100 mM, pH 7.0 (10 mM phosphate buffer). [b] UV/Vis spectrum was measured at 0 °C.

temperature, $T_m$) was examined. Figure 2-1a shows $T_m$s of **M*n*a/M*n*b** (circles), **Z*n*a/Z*n*b** (triangles), **M*n*a/Z*n*b** (diamonds) and **Z*n*a/M*n*b** (squares) determined from the change of absorbance at 260 nm. When **M1a** and **M1b**, both of which involve single threoninol-nucleotide of Methyl Red (**M** residue), were hybridized, its $T_m$ was determined as 50.5 °C as listed in Table 2-1 (and also plotted in Fig. 2-1a), which was 2.8 °C higher than that of the native **N**/**C** duplex (47.7 °C). The $T_m$ increased almost linearly as the number of **M** residues ($n$) increased from 1 to 5 and reached a plateau above $n \geq 5$ (see circles in Fig. 2-1a). Up to $n = 5$, the rate of $T_m$ increase was 3.6-3.7 °C per **M**-**M** pair. Thus, pairing of threoninol-nucleotides significantly stabilized the duplex. Similarly, the **Z*n*a**/**Z*n*b** combination involving azobenzene instead of Methyl Red also raised the $T_m$ almost linearly as the dye number increased to $n = 6$ (see Table 2-2 and triangles in Fig. 2-1a), although the $T_m$ increase was smaller (around 2.0 °C per **Z**-**Z** pair) than that of the **M**-**M** pair.

**Hetero-combinations of Z*n*a/M*n*b and M*n*a/Z*n*b.**

Hetero clusters were also easily prepared from the two ODNs, each of which had different threoninol-nucleotides. However, the hetero-combination **Z*n*a**/**M*n*b** and **M*n*a**/**Z*n*b** were less stable in the duplex than the homo-combination (**M**-**M** or **Z**-**Z**). As summarized in Table 2-2, the $T_m$s of **Z1a**/**M1b**, **Z2a**/**M2b** and **M1a/Z1b** were 47.6, 47.7 and 47.8 $^oC$, respectively, which were almost the same as that of the native **N**/**C** duplex, and were even lower than the $T_m$s of corresponding homo-combinations. In the cases of **Z3a**/**M3b**, **Z6a**/**M6b**, **M3a**/**Z3b** and **M6a**/**Z6b** the $T_m$s were fairly high, although they were still lower than those of homo-combinations. The order of stability was **M**-**M** > **Z**-**Z** > **M**-**Z** ≈ **Z**-**M**, indicating that threoninol-nucleotides recognized themselves.

Table 2-2. Melting temperatures of azobenzene-Methyl Red hetero- and azobenzene homo-cluster[a]

| | $T_m$ / $^oC$ | | |
|---|---|---|---|
| *n* | **Z*n*a/M*n*b** | **M*n*a/Z*n*b** | **Z*n*a/Z*n*b** |
| 1 | 47.6 | 47.8 | 50.6 |
| 2 | 47.7 | 49.6 | 52.0 |
| 3 | 52.7 | 52.7 | 54.5 |
| 6 | 58.6 | 58.8 | 60.3 |

[a] Solution conditions: [ODN] = 5 μM, [NaCl] = 100 mM, pH 7.0 (10 mM phosphate buffer).

**Hetero-combinations of natural nucleotides and M*n*b.**

In order to examine the possibility of clustering of threoninol-nucleotides with natural ones (A, T, G, and C), **M*n*b** was hybridized with natural ODN **A*n*a** involving an adenosine oligomer at its center. But unlike the threoninol-nucleotide pairs, the **A*n*a**/**M*n*b** combination uniformly decreased in $T_m$ with an increase in the number of adenosines (*n*), and the $T_m$ of the **A5a**/**M5b** duplex became as low as 24.8 $^oC$, which

was 23 °C lower than the native **N**/**C**, as shown in Fig. 2-1b.[6] Similarly, a combination of threoninol-nucleotide with other natural ones, thymidine, cytidine, and guanosine (**T5a**/**M5b**, **C5a**/**M5b**, and **G5a**/**M5b**) also drastically lowered the $T_m$. Thus, threoninol-nucleotides did not recognize natural nucleotides.

2-3-2 Spectroscopic behavior of the clustering of Methyl Reds

Most of the dyes exhibit distinct spectral changes upon clustering. Figure 2-2a shows the effect of the temperature on the absorption spectrum of the **M3a**/**M3b** duplex. When the temperature was higher than 60 °C, where the duplex was dissociated, the solution gave an absorption maximum at 432 nm with a relatively broad peak (both $\lambda_{max}$ and half-line width of **M*n*a**/**M*n*b** duplex are summarized in Table 2-1). However, the spectrum became much narrower upon lowering the temperature below 40 °C (compare dotted line with solid line in Fig. 2-2a). As shown in Fig. 2-3, the melting profiles of **M3a**/**M3b** monitored at 260 nm (solid line) and 420 nm (broken line), which were derived from the π-π* transition of Methyl Red moieties, were fairly synchronized. The $T_m$ determined from 260 nm was 58.0 °C, which almost coincided with that at 420 nm

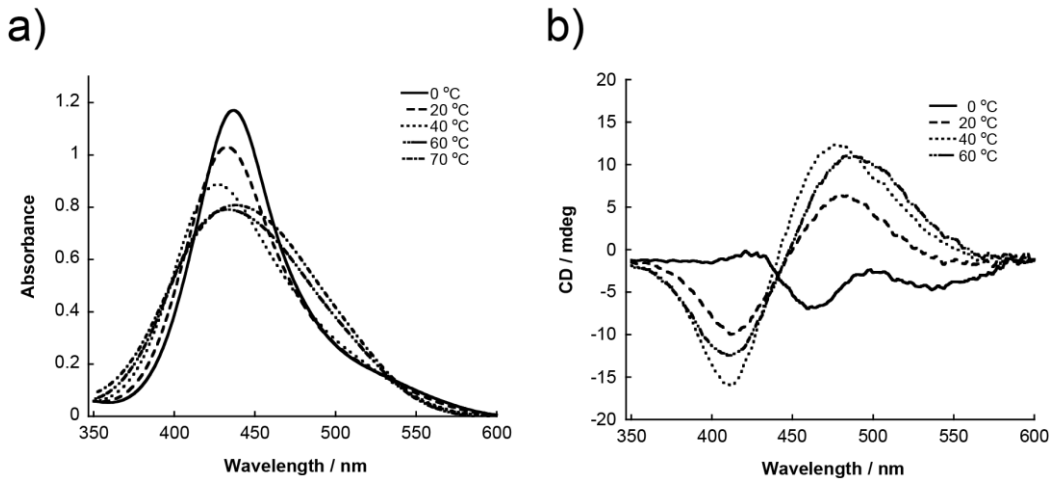


Figure 2-2. a) UV/Vis and b) CD spectra of **M3a**/**M3b** at various temperatures. Solution conditions are as follows: [ODN] = 5 μM, [NaCl] = 100 mM, pH 7.0 (10 mM phosphate buffer).

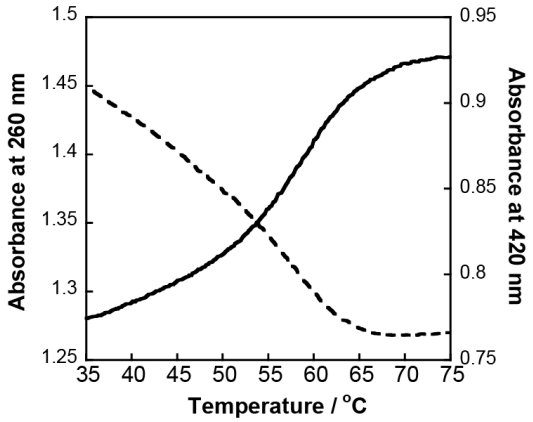


Figure 2-3. Melting curves of **M3a**/**M3b** monitored at 260 nm (solid line) and 420 nm (broken line). Solution conditions are as follows: [ODN] = 5 μM, [NaCl] = 100 mM, pH 7.0 (10 mM phosphate buffer).

(56.6 °C). Furthermore, a simple sum of the absorption spectra of single-stranded **M3a** and **M3b** at 0 °C was obviously different from the spectrum of the **M3a**/**M3b** duplex as shown in Fig. 2-4: the **M3a**/**M3b** duplex (solid line in Fig. 2-4) showed narrowing as well as hypsochromicity in its absorption spectrum compared with their simple sum (broken line). Thus, we could conclude that narrowing of the band was mostly attributed to the clustering of **M** residues, not to the simple temperature effect.

Clustering also affected circular dichroism (CD) spectra as depicted in Fig. 2-2b. At 60 °C, the solution of **M3a**/**M3b** displayed a relatively strong positive-negative Cotton effect at the π-π* transition region of Methyl Red, due to intrastrand exciton coupling of

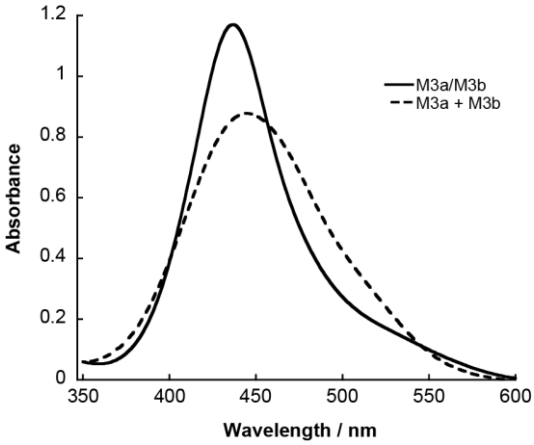


Figure 2-4. UV/Vis spectra of **M3a**/**M3b** duplex (solid line) and simple sum of the spectra of their single strands (broken line) at 0 °C. Solution conditions are as follows: [ODN] = 5 μM, [NaCl] = 100 mM, pH 7.0 (10 mM phosphate buffer).

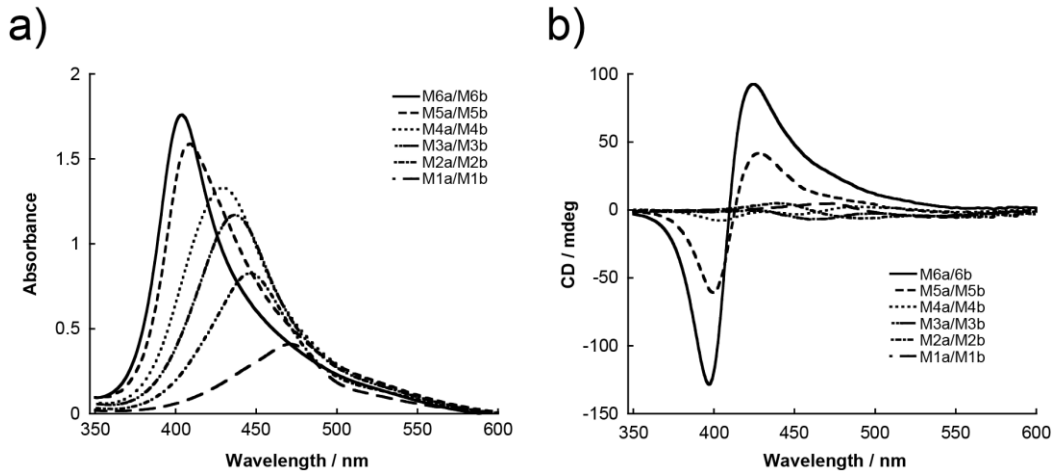


Figure 2-5. a) UV/Vis and b) CD spectra of the **M*n*a/M*n*b** ($1 \leq n \leq 6$) duplex at 0 °C. Solution conditions are as follows: [ODN] = 5 μM, [NaCl] = 100 mM, pH 7.0 (10 mM phosphate buffer).

the chromophore in the single-stranded state (note that single-stranded **M3a** and **M3b** are chiral). However, CD was not enhanced at all by lowering the temperature. Rather, it became smaller at 0 °C where the cluster was firmly formed.

The number of pairs greatly affected the UV/Vis and CD spectra as shown in Fig. 2-5. The absorption maximum of the **M1a**/**M1b** duplex involving two Methyl Reds appeared at 471 nm at 0 °C, and an increase in the number of dyes induced continuous hypsochromic shift: $\lambda_{max}$ of **M2a**/**M2b**, **M3a**/**M3b**, and **M4a**/**M4b** were observed at 446, 437, and 429 nm, respectively (see Table 2-1). This hypsochromicity is characteristic of the so-called H-aggregates (H*-aggregates) in which chromophores are vertically stacked, and increases with the number of chromophores due to the extended exciton interaction.[7] The absorption maximum tended to converge at around 420 nm as deduced from the hypsochromic shift from **M3a**/**M3b** to **M4a**/**M4b**, which was only 8 nm. However, there was a small gap between **M4a**/**M4b** and **M5a**/**M5b**. **M5a**/**M5b** gave $\lambda_{max}$ at 409 nm, which was 20 nm shorter than that of **M4a**/**M4b**. In addition, significant narrowing of the band was induced with this increment (3228 and 2639 $cm^{-1}$ for **M5a**/**M5b** and **M6a**/**M6b**, respectively). Such a gap was also observed in the CD

spectra. As shown in Fig. 2-5b, induced CD (ICD) was rather small in spite of the clustering of Methyl Reds when *n* in **M*n*a**/**M*n*b** was four and below. But a fairly strong ICD was observed for both **M5a**/**M5b** and **M6a**/**M6b** duplexes. These spectroscopic differences indicate that the stacked structures in **M5a**/**M5b** and **M6a**/**M6b** were different from other **M*n*a**/**M*n*b** ($n \leq 4$).

2-3-3 Insertion of spacer at the counterpart of threoninol-nucleotide

Previously, our laboratory has reported another type of pairing:[8] threoninol-nucleotide (**M** residue) and 1,3-propanediol (**P** in Scheme 2-2) were alternately incorporated, and **P** was located as the counterpart of **M** to form a tentative **M**-**P** pair, such as **MP3a**/**MP3b** in Scheme 2-2. In this **MP3a**/**MP3b** duplex, threoninol-nucleotides and spacer residues were introduced alternately into DNA and formed tentative **M**-**P** "base pairs". Although this design also allowed Methyl Reds to stack in an anti-parallel orientation, both the stability of the duplex and spectroscopic behavior were different. As listed in Table 2-1, the $T_m$ of **MP3a**/**MP3b** was 50.9 $^oC$,[8a] which was about 3 $^oC$ higher than the native **N**/**C** duplex, but 7 $^oC$ lower than **M3a**/**M3b**.

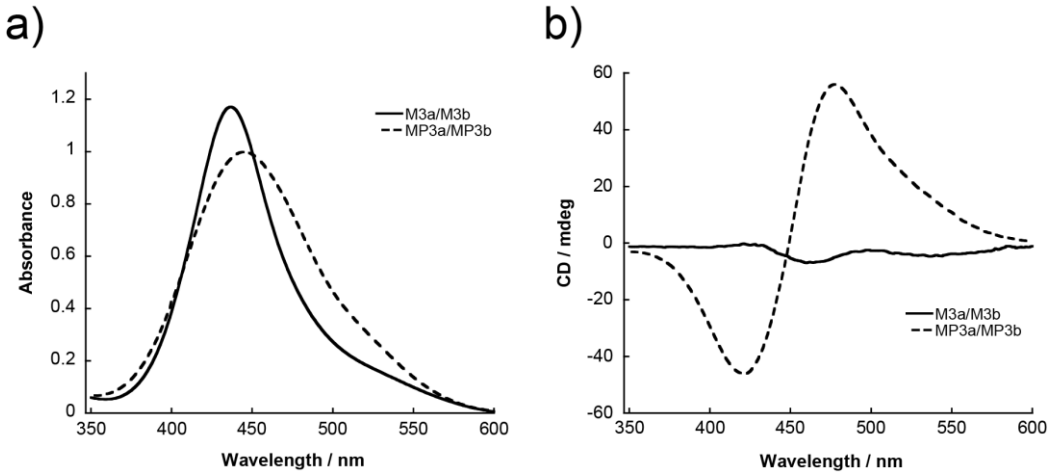


Figure 2-6. a) UV/Vis and b) CD spectra of **M3a**/**M3b** (solid line) and **MS3a**/**MS3b** (broken line) at 0 $^oC$. Solution conditions are as follows: [ODN] = 5 μM, [NaCl] = 100 mM, pH 7.0 (10 mM phosphate buffer).

UV/Vis spectra of **M3a**/**M3b** and **MP3a**/**MP3b** are depicted in Fig. 2-6a. Although both duplexes contained six **M** residues, **M3a**/**M3b** exhibited a larger hypsochromic shift than **MP3a**/**MP3b** (compare **M3a**/**M3b** with **MP3a**/**MP3b** in Table 2-1). Furthermore, the spectrum of **M3a**/**M3b** was much narrower. These facts indicate stronger exciton interactions among the chromophores in **M3a**/**M3b** than in **MP3a**/**MP3b**. However, the CD signal of **MP3a**/**MP3b** showed a much stronger positive and negative Cotton effect than that of **M3a**/**M3b** in spite of weaker exciton interaction (compare broken line with solid line Fig. 2-6b).

2-3-4 Effect of hetero-combinations on the spectroscopic behavior

**Z6a/M6b combination.**

As described above, hetero-combinations such as **Z*n*a**/**M*n*b** could also form relatively stable duplexes. In the case of a **M*n*a**/**M*n*b** homo-combination, clustering induced both narrowing and hypsochromicity due to the extended exciton interaction. In contrast, the **Z*n*a**/**M*n*b** combination induced bathochromic shift as well as broadening of the band at the π-π* region of Methyl Red. Figure 2-7 shows the UV/Vis spectrum of

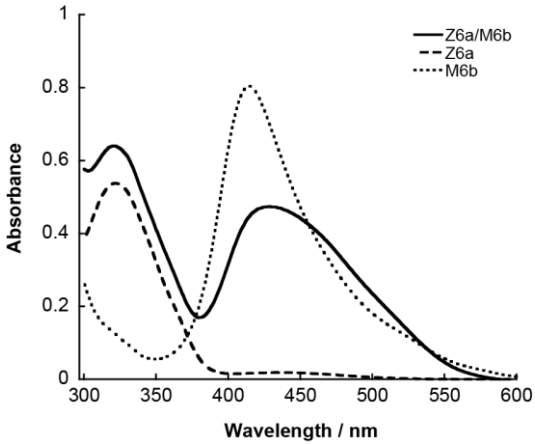


Figure 2-7. UV/Vis spectra of a hetero-cluster of Methyl Red and azobenzene (**Z6a**/**M6b**; solid line), single-stranded **Z6a** (broken line) and **M6b** (dotted line) at 0 $^{o}$C. Solution conditions are as follows: [ODN] = 5 μM, [NaCl] = 100 mM, pH 7.0 (10 mM phosphate buffer).

the **Z6a**/**M6b** duplex as well as single-stranded **Z6a** and **M6b** under the same buffer conditions. **M6b** in the absence of **Z6a** gave $\lambda_{max}$ at 415 nm with a half-line width of 3662 $cm^{-1}$ as shown by the broken line in Fig. 2-7. Since **M1b** involving a single Methyl Red had $\lambda_{max}$ at 481 nm (see Appendix Fig. 2-1), Methyl Red chromophores in **M6b** excitonically interacted in the single-stranded state.[9] By hybridization with **Z6a**, however, $\lambda_{max}$ shifted to 429 nm with a half-line width of 4169 $cm^{-1}$. This bathochromicity and peak broadening demonstrated that Methyl Red and azobenzene moieties stacked alternately and intramolecular stacking among Methyl Reds in the single strand was weakened by azobenzene moieties. Similar broadening was also observed with **Z3a**/**M3b** (see Appendix Fig. 2-2).

**N3a/M3b combination.**

Single-stranded **N3a** showed a broad peak at 506 nm, whereas the $\lambda_{max}$ of **M3b** appeared at 441 nm at 0 °C, as depicted by dotted and dashed-dotted lines in Fig. 2-8a, respectively.[10] Interestingly, unlike the **Z6a**/**M6b** or **Z3a**/**M3b** case, a sharp peak appeared at 466 nm by hybridization of **N3a** with **M3b**. This peak was completely

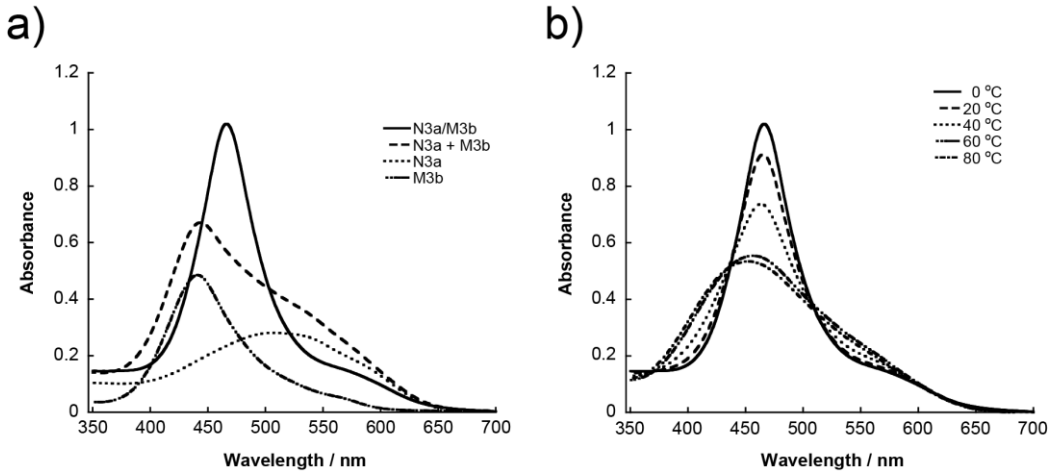


Figure 2-8. a) UV/Vis spectra of the **N3a**/**M3b** duplex (solid line), single-stranded **N3a** (dotted line), **M3b** (dashed-dotted line), and a simple sum of their spectra (broken line) at 0 °C. b) UV/Vis spectra of **N3a**/**M3b** at various temperatures. Solution conditions are as follows: [DNA] = 5 mM, [NaCl] = 100 mM, pH 5.0 (10 mM MES buffer).

different from the sum of the spectra of single strands that showed broad peaks with a shoulder (compare solid and broken lines). This sharp peak reversibly broadened above 60 $^{o}$C where the duplex was dissociated as shown in Fig. 2-8b. Previously, our laboratory has demonstrated that alternate hetero-stacking of Methyl Red and Naphthyl Red allowed merging of each band to a give single peak for the **NP3a**/**MP3b** duplex in which three **N**-**P** and **P**-**M** pairs were introduced alternately.[11] Here, removal of the spacer residue (**P**) from **NP3a**/**MP3b** also induced further hypsochromic shift and narrowing of the band as observed for **MP3a**/**MP3b** and **M3a**/**M3b** (see Appendix Fig. 2-3).

**A5a/M5b combination.**

Figure 2-9 shows the UV/Vis spectra of the **A5a**/**M5b** duplex when changing the temperature from 40 to 0 $^{o}$C. When the temperature was above 40 $^{o}$C, a relatively sharp band corresponding to the single-stranded **M5b** was observed. But, a large bathochromic shift as well as broadening of the band was induced at 0 $^{o}$C where the duplex was formed (note that the $T_m$ of **A5a**/**M5b** was 24.8 $^{o}$C). Hyperchromicity was

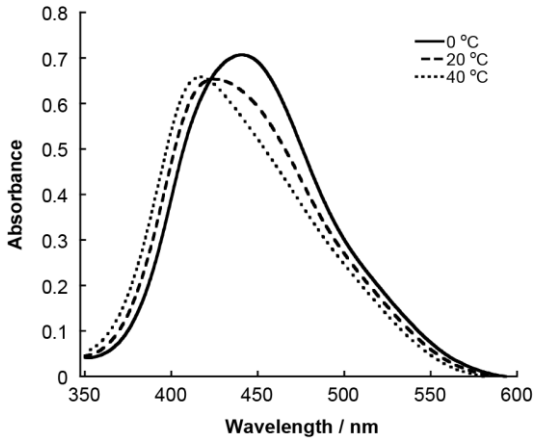


Figure 2-9. UV/Vis spectra of the **A5a**/**M5b** duplex at various temperatures. Solution conditions are as follows: [DNA] = 5 μM, [NaCl] = 100 mM, pH 7.0 (10 mM phosphate buffer).

also observed concurrently.

## 2-4 Discussion

### 2-4-1 Stable "base-pairing" of homo threoninol-nucleotides in the duplex

In the present design, "threoninol-nucleotides", in which functional molecules are tethered on D-threoninols, are introduced at the counterpart of each strand to form a pseudo "base-pair". Such sequence design allowed significant stabilization of the duplex in cases of homo-combination (see Fig. 2-1a and Table 2-1).The increase in $T_m$ is derived from the interstrand stacking interaction among the chromophores. But the Methyl Red combination (**M*n*a**/**M*n*b**) showed an even higher $T_m$ than the azobenzene combination (**Z*n*a**/**Z*n*b)**. This is probably attributed to the stronger dipole-dipole interaction of Methyl Reds because of the push (-$N(CH_3)_2$) and pull (-CONH-) substituents. Such alternate stacking also affected the spectroscopic behavior of the dyes: hybridization of **M3a** and **M3b** induced hypsochromic shift and narrowing of the band with respect to the simple sum of their spectra (Fig. 2-4). Furthermore, increases in the number of **M** residues caused continuous hypsochromic shift (see Fig. 2-5a). These shifts are characteristic features of molecular clusters where the molecules are stacked in a face-to-face manner (H-aggregates).[7]

### 2-4-2 Stacked structure of the **M*n*a**/**M*n*b** duplex

Previously, our laboratory has reported that threoninol-nucleotide tethering Methyl Red and 1,3-propanediol (**P** in Scheme 2-2) were alternately introduced at the center of the DNA sequence, such as **MP3a** and **MP3b**, and the dyes from both strands were stacked with each other. By this sequence design, a molecular cluster was also

successfully prepared in the duplex. However, these stacked structures were different from each other as estimated from the UV/Vis and CD spectra. In our previous design involving **P** residues (**MP3a**/**MP3b**), positive and negative CD was strongly induced by hybridization, whereas the present **M3a**/**M3b** duplex did not show such ICD (compare solid line with broken one in Fig. 2-6b). Similarly, ICD was rather small up to four **M**-**M** pairs (see Fig. 2-5b). These ICD demonstrate that Methyl Reds in **MP3a**/**MP3b** formed a right-handed helix resembling natural B type DNA, and removal of **P** residue (**M3a**/**M3b**) made the helix rewind. In **MP3a**/**MP3b**, winding made the Methyl Reds stack as shown in Fig. 2-10a because each **M** residue was separated by a **P** residue. But in the absence of **P**, Methyl Reds did not need winding in order to form a firmly stacked structure (Fig. 2-10b). The threoninol scaffold would allow such a ladder-like structure due to its flexibility.[12,13] Consequently, the stacking area in **M3a**/**M3b** became larger than that in **MP3a**/**MP3b** and thus **M3a**/**M3b** duplex exhibited a larger hypsochromic shift and narrower band than **MP3a**/**MP3b** due to the stronger exciton coupling (compare solid line with broken one in Fig. 2-6a).

However, the UV/Vis and CD spectra of **M5a**/**M5b** and **M6a**/**M6b** were different from other **M*n*a**/**M*n*b** spectra. In particular, **M6a**/**M6b** had stronger ICD with a narrower half-line width (see Fig. 2-5b and Table 2-1). Furthermore, the $T_m$ did not increase above $n$ = 5, indicating that **M5a**/**M5b** and **M6a**/**M6b** (especially **M6a**/**M6b**)

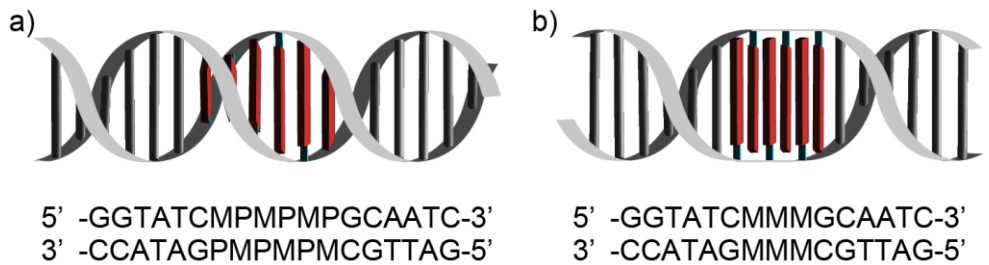


Figure 2-10. Illustration of the possible structure of a) **MS3a**/**MS3b** duplex involving spacer residue **S** and b) **M3a**/**M3b** duplex as elucidated from CD spectra.

adopted different stacked structures. Since multiplication of dyes caused fairly stable *intramolecular* stacking even in the single-stranded DNA,[14] distal benzene rings of the Methyl Reds from both strands would be partially stacked with each other. Accordingly, the reduced stacked area diminished *intermolecular* stacking and suppressed further stabilization of the duplex.

2-4-3 Effect of hetero-combinations on the melting temperature and spectroscopic behavior

Hetero combinations such as **Z*n*a/M*n*b** did not destabilize the duplex but raised the $T_m$ with an increase in the number of threoninol-nucleotides, although the $T_m$ was smaller than that of the corresponding homo combinations. Such an increase in the $T_m$ was associated with the alternate interstrand stacking of the dyes, which also affected the spectroscopic behavior of the Methyl Reds: when **Z6a** was hybridized with **M6b**, broadening and bathochromic shift of the band were observed (Fig. 2-7). Since the overlapping region of the UV/Vis spectrum between Methyl Red and azobenzene was very small, alternate stacking of Methyl Red and azobenzene disturbed excitonic interaction among the Methyl Red chromophores by the intervening azobenzenes. In contrast, hetero combinations with much wider overlapping absorption (**N3a**/**M3b** combination, see Fig. 2-8) showed merging of two bands into a single sharp one due to strong exciton coupling among the alternate stacked dyes.[11, 15]

Unlike this threoninol-nucleotide combination, hybridization of threoninol -nucleotides with natural ones such as in **A*n*a/M*n*b**, significantly destabilized the duplex as shown in Fig. 2-1b. This result indicates that dyes on D-threoninol are difficult to stack with molecules on D-ribose.[16] Spectroscopic behavior also reflected a

non-stacked structure of Methyl Reds: both bathochromicity and broadening by hybridization of **A5a**/**M5b** were attributable to the disordering of the intrastrand Methyl Reds cluster. In addition, hyperchromism was clearly observed following hybridization. Similar bathochromicity and broadening were also observed for **Z6a**/**M6b**. However, hyperchromicity was not seen because azobenzene and Methyl Reds were firmly stacked. In contrast, hybridization of **A5a** with **M5b** untied the ordered stacking of Methyl Red in the single-stranded **M5b**. Although the number of carbons between the phosphodiester linkages was the same in both cases, the rigid ribose scaffold would be incompatible with flexible D-threoninol.

## 2-5 Conclusions

(1) Threoninol-nucleotides tethering non-natural functional molecules such as dyes on D-threoninols were consecutively incorporated at the center of an ODN, and an interstrand molecular cluster was successfully prepared by hybridizing them. Clustering of dyes evenly raised the melting temperature due to the stacking interactions.

(2) Interstrand homo-clustering of the dyes (Methyl Reds) exhibited both hypsochromic shift and narrowing of the band, which were characteristic of H-aggregates (H*-aggregates) in which chromophores were vertically stacked. The cluster formed in the duplex was unwound as elucidated from CD spectra.

(3) An alternate hetero cluster was easily prepared by hybridizing two strands involving different threoninol-nucleotides. With a Methyl Red and azobenzene combination (**Z*n*a**/**M*n*b**), both bathochromicity and broadening of the band were observed due to the disturbance of exciton interactions among Methyl Reds. In contrast, merging of the bands was observed with the Naphthyl Red-Methyl Red combination

(**N3a**/**M3b**).

Thus, D-threoninol can be a versatile linker for introducing functional molecules into DNA and stabilizing duplexes. Threoninol-nucleotides facilitate clustering of various functional molecules. With this method, the preparation of highly organized molecular clusters for use as molecular wires or non-linear optical effects is promising.[17]

## 2-6 Experimental section

### 2-6-1 Materials

All the conventional phosphoramidite monomers, CPG columns, reagents for DNA synthesis and Poly-Pak II cartridges were purchased from Glen Research. Other reagents for the synthesis of phosphoramidite monomer were purchased from Tokyo Kasei Co., Ltd, Kishida Chemical Co., Ltd., Wako Pure Chemical Industries, Ltd. and Sigma-Aldrich.

### 2-6-2 Synthesis of the modified DNA involving **M**, **N** and **Z**

All the modified DNAs were synthesized on an automated DNA synthesizer (ABI-3400 DNA synthesizer, Applied Biosystems) by using phosphoramidite monomers bearing dye molecules synthesized according to previous reports,[5a, 8a, 18] and other conventional ones. Coupling efficiency of the monomers corresponding to modified residues was as high as the conventional ones as judged from the coloration of released trityl cation. After the recommended work-up, they were purified by reversed-phase HPLC and characterized by MALDI-TOFMS (Autoflex II, BRUKER DALTONICS).

MALDI-TOFMS for:

**M1a**: Obsd. 4062 (Calcd. for [**M1a** + $H^+$]: 4063). **M1b**: Obsd. 4065 (Calcd. for [**M1b** + $H^+$]: 4063). **M2a**: Obsd. 4481 (Calcd. for [**M2a** + $H^+$]: 4481). **M2b**: Obsd. 4481 (Calcd. for [**M2b** + $H^+$]: 4481).**M3a**: Obsd. 4899 (Calcd. for [**M3a** + $H^+$]: 4899).**M3b**: Obsd. 4899 (Calcd. for [**M3b** + $H^+$]: 4899). **M4a**: Obsd. 5318 (Calcd. for [**M4a** + $H^+$]: 5317). **M4b**: Obsd. 5317 (Calcd. for [**M4b** + $H^+$]: 5317).**M5a**: Obsd. 5735 (Calcd. for [**M5a** + $H^+$]: 5735).**M5b**: Obsd. 5736 (Calcd. for [**M5b** + $H^+$]: 5735). **M6a**: Obsd. 6155 (Calcd. for [**M6a** + $H^+$]: 6154). **M6b**: Obsd. 6154 (Calcd. for [**M6b** + $H^+$]: 6154). **Z1a**: Obsd. 4020 (Calcd. for [**Z1a** + $H^+$]: 4020). **Z1b**: Obsd. 4019 (Calcd. for [**Z1b** + $H^+$]: 4020). **Z2a**: Obsd. 4395 (Calcd. for [**Z2a** + $H^+$]: 4395). **Z2b**: Obsd. 4396 (Calcd. for [**Z2b** + $H^+$]: 4395). **Z3a**: Obsd. 4770 (Calcd. for [**Z3a** + $H^+$]: 4770). **Z3b**: Obsd. 4771 (Calcd. for [**Z3b** + $H^+$]: 4770). **Z6a**: Obsd. 5898 (Calcd. for [**Z6a** + $H^+$]: 5895). **Z6b**: Obsd. 5898 (Calcd. for [**Z6b** + $H^+$]: 5895). **N3a**: Obsd. 5050 (Calcd. for [**N3a** + $H^+$]: 5049).

2-6-3 Spectroscopic measurements

The UV/Vis and CD spectra were measured on a JASCO model V-550 spectrophotometer and a JASCO model J-820 spectropolarimeter, respectively, with a 10 mm quartz cell. Both models were equipped with programmable temperature controllers. The conditions of the sample solutions were as follows (unless otherwise noted): [NaCl] = 100 mM, pH 7.0 (10 mM phosphate buffer), [DNA] = 5 μM. For measurements at pH 5.0, 10 mM MES buffer was used. All samples of DNA-dye conjugates were heated at 80 $^oC$ for 5 min in the dark, to thermally isomerize the cis form, which might be photoisomerized by the ambient light, to trans form before spectroscopic measurement.[5c]

2-6-4 Measurement of melting temperature

The melting curve of duplex DNA was obtained by measurement of the change in absorbance at 260 nm versus temperature (unless otherwise noted), using a spectrophotometer as described above. The melting temperature ($T_m$) was determined from the maximum of the first derivative of the melting curve. Both the heating and the cooling curves were measured, and the obtained $T_m$ values agreed to within 2.0 $^oC$. The temperature ramp was 1.0 $^oCmin^{-1}$. The conditions of the sample solutions were the same as those described for the above spectroscopic measurements.

## 2-7 Notes and References


1. I. Hirao, *Curr. Opin. Chem. Biol.*, 2006, **10**, 622.
2. (a) J. Kurreck, *Eur. J. Biochem.*, 2003, **270**, 1628; (b) C. Wilson and A. D. Keefe, *Curr. Opin. Chem. Biol.*, 2006, **10**, 607.
3. C. Wojczewski, K. Stolze and J. W. Engels, *Synlett*, 1999, **1999**, 1667.
4. (a) K. Tanaka, A. Tengeiji, T. Kato, N. Toyama and M. Shionoya, *Science*, 2003, **299**, 1212; (b) J. Gao, C. Strässler, D. Tahmassebi and E. T. Kool, *J. Am. Chem. Soc.*, 2002, **124**, 11590; (c) J. N. Wilson, J. Gao and E. T. Kool, *Tetrahedron*, 2007, **63**, 3427; (d) M. Kosuge, M. Kubota and A. Ono, *Tetrahedron Lett.*, 2004, **45**, 3945; (e) M. Nakamura, Y. Shimomura, Y. Ohtoshi, K. Sasa, H. Hayashi, H. Nakano and K. Yamana, *Org. Biomol. Chem.*, 2007, **5**, 1945; (f) E. Mayer-Enthart and H.-A. Wagenknecht, *Angew. Chem. Int. Ed*, 2006, **45**, 3372; (g) V. L. Malinovskii, F. Samain and R. Häner, *Angew. Chem. Int. Ed*, 2007, **46**, 4464; (h) J. Chiba, S. Takeshima, K. Mishima, H. Maeda, Y. Nanai, K. Mizuno and M. Inouye, *Chem. Eur. J.*, 2007, **13**, 8124.
5. (a) H. Asanuma, T. Takarada, T. Yoshida, D. Tamaru, X. Liang and M. Komiyama, *Angew. Chem. Int. Ed*, 2001, **40**, 2671; (b) X. Liang, H. Asanuma, H. Kashida, A. Takasu, T. Sakamoto, G. Kawai and M. Komiyama, *J. Am. Chem. Soc.*, 2003, **125**, 16408; (c) H. Nishioka, X. Liang, H. Kashida and H. Asanuma, *Chem. Commun.*, 2007, 4354.
6. Melting temperatures of **A*n*a/M*n*b**, **T5a/M5b**, **C5a/M5b**, and **G5a/M5b** are listed in Appendix Table 2-1 in the Appendix. Absorption maxima and halfline widths of the band of Methyl Red in these duplexes are also shown.
7. M. Kasha, *Radiat. Res.*, 1963, **20**, 55.
8. (a) H. Asanuma, K. Shirasuka and M. Komiyama, *Chem. Lett.*, 2002, **31**, 490; (b) H. Kashida, M. Tanaka, S. Baba, T. Sakamoto, G. Kawai, H. Asanuma and M. Komiyama, *Chem. Eur. J.*, 2006, **12**, 777.
9. Note that **Z6a** did not show either narrowing or hypsochromicity, indicating that azobenzenes were not excitonically interacting.
10. Spectra were measured at pH 5.0 because Naphthyl Red did not show distinct exciton coupling in its deprotonated form. The pKa of naphthyl red was 6.5 in duplex. Thus, UV/Vis spectra of Naphthyl Red-Methyl Red hetero aggregates were measured at pH 5.0, where Naphthyl Red moieties were protonated. See ref. 11 for effects of pH on the spectroscopic behavior of Naphthyl Red.
11. H. Kashida, H. Asanuma and M. Komiyama, *Angew. Chem. Int. Ed*, 2004, **43**, 6522.

12. (a) C. Brotschi and C. J. Leumann, *Angew. Chem. Int. Ed*, 2003, **42**, 1655; (b) C. Brotschi, G. Mathis and C. J. Leumann, *Chem. Eur. J.*, 2005, **11**, 1911.
13. According to Leumann et al. (see ref. 12), Bph moieties on D-ribosewere partially stacked with each other and adopted a B-DNA conformation from CD measurements, suggesting that multiple Bphs adopted a helical structure. ButMethyl Reds on D-threoninol did not adopt such a wound structure as estimated from the small ICD. We think that the flexibility of the threoninol scaffold also contributed to the non-helical structure.
14. The strong CD, especially for **M6a/M6b**, would be derived from the single-stranded **M6a** or **M6b**, in which Methyl Reds adopted a helical structure in the single strand.
15. (a) R. A. Garoff, E. A. Litzinger, R. E. Connor, I. Fishman and B. A. Armitage, *Langmuir*, 2002, **18**, 6330; (b) A. Yamaguchi, N. Kometani and Y. Yonezawa, *Thin Solid Films,* 2006, **513**, 125.
16. The difference in hydrophilicity between the dyes and natural nucleobases may also induce the destabilization of the duplex.
17. (a) W. Lin, W. Lin, G. K. Wong and T. J. Marks, *J. Am. Chem. Soc.*, 1996, **118**, 8034; (b) O. R. Evans and W. Lin, *Acc. Chem. Res.*, 2002, **35**, 511; (c) E. L. Botvinick and J. V. Shah, *Methods Cell Biol.*, 2007, **82**, 81.
18. H. Asanuma, H. Kashida, X. Liang and M. Komiyama, *Chem. Commun.*, 2003, 1536.

## 2-8 Appendixes

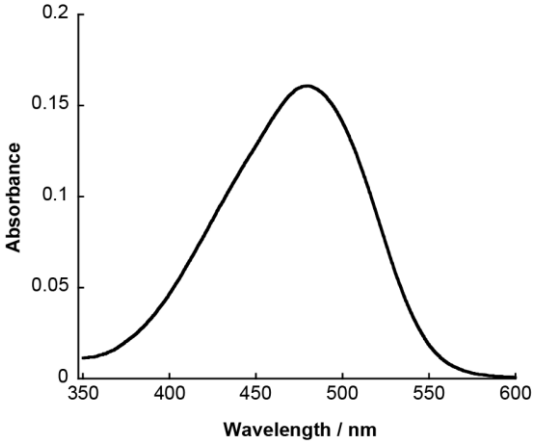


Appendix Figure 2-1. UV/Vis spectra of **M1b** at pH 7.0 (10 mM phosphate buffer), 0 $^{o}$C, in the presence of 100 mM NaCl.

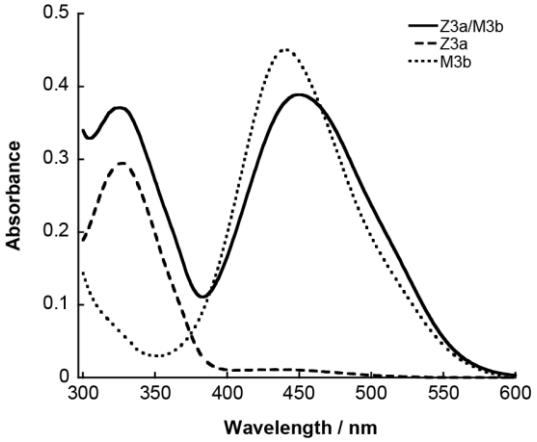


Appendix Figure 2-2. UV/Vis spectra of hetero cluster of Methyl Red and azobenzene (**Z3a**/**M3b;** solid line), single-stranded **Z3a** (broken line) and **M3b** (dotted line) at 0 $^{o}$C, pH 7.0 (10 mM phosphate buffer) in the presence of 100 mM NaCl.

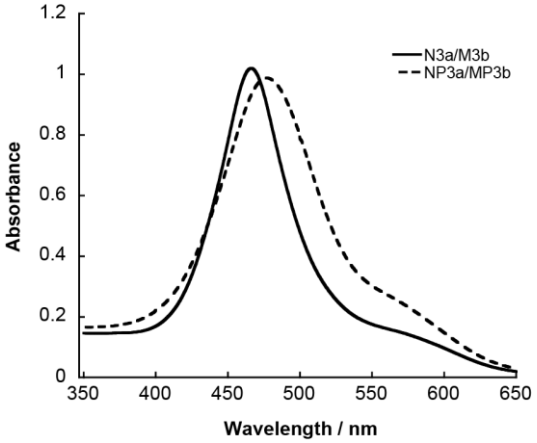


Appendix Figure 2-3. UV/Vis spectra of **N3a**/**M3b** and **NP3a**/**MP3b** at 0 $^{o}$C. Solution conditions are as follows: [ODN] = 5 μM, [NaCl] = 100 mM, pH 5.0 (10mM MES buffer)

Appendix Table 2-1. Effects of the number of Methyl Red/adenine pairs on the melting temperature ($T_m$) and absorption maximum and half-line-width of π-π* transition of Methyl Red.[a)]

| Sequences | $T_m$ / °C | $\lambda_{max}$ / nm [b)] | Half-line width [b)] / $cm^{-1}$ |
|---|---|---|---|
| **A1a/M1b** | 39.7 | 485 | 3946 |
| **A2a/M2b** | 35.0 | 462 | 4452 |
| **A3a/M3b** | 32.4 | 456 | 4381 |
| **A4a/M4b** | 29.5 | 442 | 4487 |
| **A5a/M5b** | 24.8 | 441 | 4751 |
| **A6a/M6b** | 16.4 | 422 | 4890 |
| **T5a/M5b** | 27.9 | 441 | 4852 |
| **C5a/M5b** | 27.9 | 442 | 4845 |
| **G5a/M5b** | 27.9 | 437 | 4891 |

a) Solution conditions: [ODN] = 5 μM, [NaCl] = 100 mM, pH 7.0 (10 mM phosphate buffer)
b) UV/Vis spectrum was measured at 0 °C.

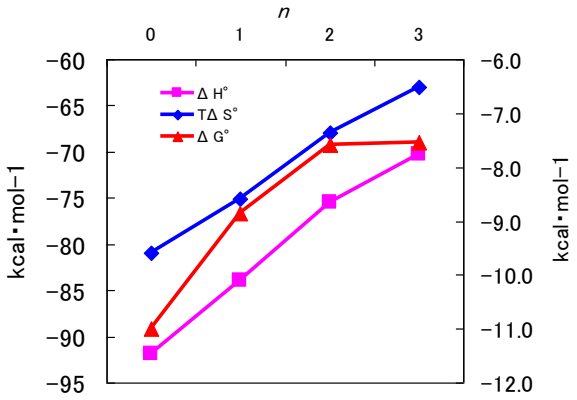


Appendix Figure 2-4. Plots of $\Delta H^o$, $T\Delta S^o$ and $\Delta G^o_{37}$ in **A*n*a/M*n*b**. T = 315.15 K (37 °C). *n* = 0 indicates **N/C**.

Appendix Table 2-2. Thermodynamic parameters of hetero clusters with combinations of Native base and dye residue.

| Sequence | Wavelength | $\Delta H^o$ / kcal・$mol^{-1}$ | $\Delta S^o$ / cal・K・$mol^{-1}$ | $\Delta G^o_{37}$ [a)] / kcal・$mol^{-1}$ | $\Delta\Delta G^o_{37}$(kcal・$mol^{-1}$) |
|---|---|---|---|---|---|
| **N/C** | 260 nm | -91.9 | -261 | -11.0 | — |
| **A1a/M1b** | | -84.0 | -242 | -8.9 | 2.1 |
| **A2a/M2b** | | -75.5 | -219 | -7.6 | 3.4 |
| **A3a/M3b** | | -70.3 | -203 | -7.5 | 3.5 |
| | | | | | |
| **A1a/M1b** | 420 nm | -82.3 | -237 | -8.8 | — |
| **A2a/M2b** | 410 nm | -78.4 | -228 | -7.5 | 1.3 |
| **A3a/M3b** | 410 nm | -73.1 | -214 | -6.7 | 2.1 |

a) $\Delta G^o_{37}$ is change of Gibbs free energy at 37 °C (310 K).

Appendix Table 2-3. $T_m$ of **A1a/M1b**.[a)]

| Concentration / μM | 260 nm / °C | 420nm / °C |
|---|---|---|
| 1 | 36.6 | 36.8 |
| 2 | 38.1 | 37.9 |
| 4 | 39.8 | 39.8 |
| 6 | 40.8 | 40.8 |
| 16 | 43.1 | 43.1 |
| 24 | 44.2 | 44.5 |
| 32 | 44.9 | 44.9 |
| 64 | 46.0 | 46.2 |

a) [NaCl] = 100 mM, pH 7.0 (10 mM phosphate buffer)

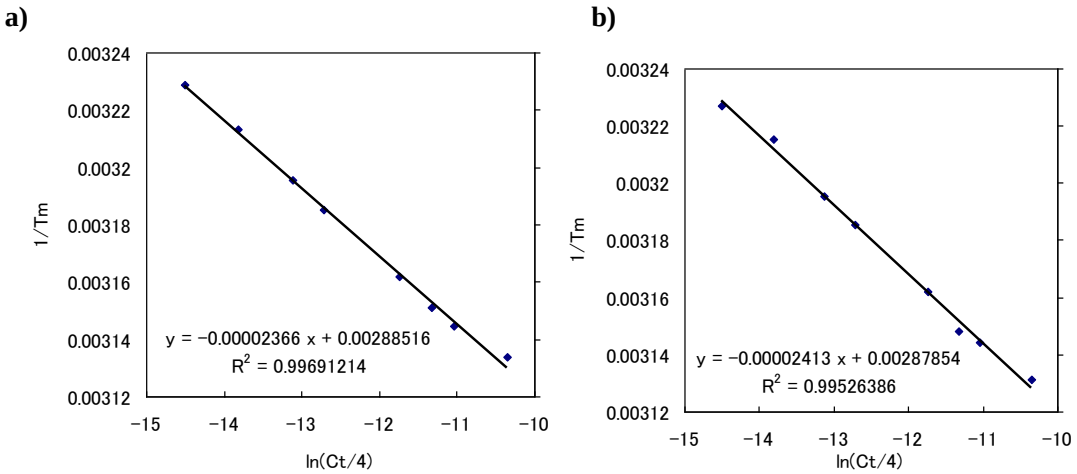


Appendix Figure 2-5. Van't Hoff plot of **A1a/M1b**. a) : 260 nm, b) : 420 nm.

Appndix Table 2-4. $T_m$ of **A2a/M2b**.[a)]

| Concentration /μM | 260 nm / °C | 410 nm/ °C |
|---|---|---|
| 1 | 31.4 | 31.5 |
| 2 | 33.2 | 33.5 |
| 4 | 34.9 | 34.8 |
| 6 | 35.9 | 35.9 |
| 16 | 38.1 | 37.7 |
| 24 | 39.4 | 39.3 |
| 32 | 40.3 | 40.1 |
| 64 | 42.0 | 41.9 |

a) [NaCl] = 100 mM, pH 7.0 (10 mM phosphate buffer)

**a)** **b)**

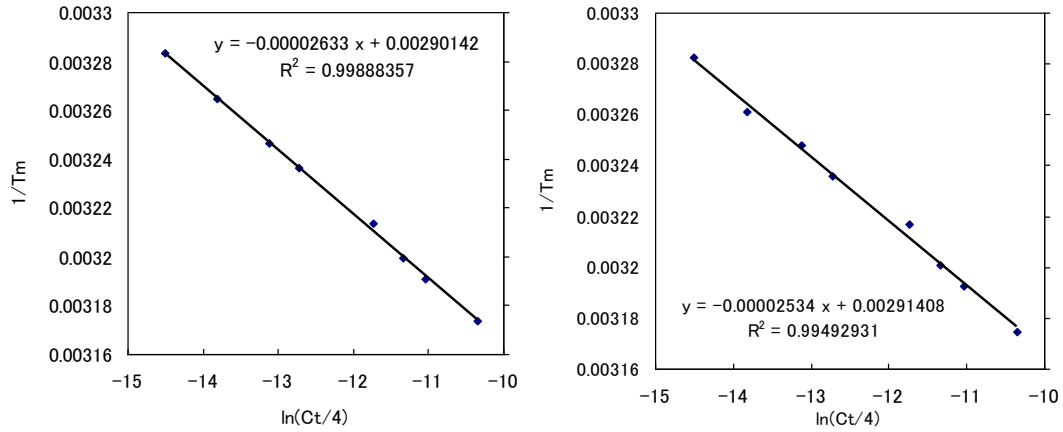


Appendix Figure 2-6**.** Van't Hoff plot of **A2a/M2b**. a) : 260 nm, b) : 410 nm.

Appendix Table 2-5**.** $T_m$ of **A3a/M3b**.[a)]

| Concentration / μM | 260 nm / °C | 410 nm / °C |
|---|---|---|
| 1 | 28.5 | 28.0 |
| 2 | 30.2 | 29.6 |
| 4 | 31.8 | 31.0 |
| 6 | 32.8 | 32.2 |
| 16 | 35.2 | 34.4 |
| 24 | 36.7 | 35.8 |
| 32 | 37.7 | 37.1 |
| 64 | 39.5 | 38.4 |

a) [NaCl] = 100 mM, pH 7.0 (10 mM phosphate buffer)

**a)** **b)**

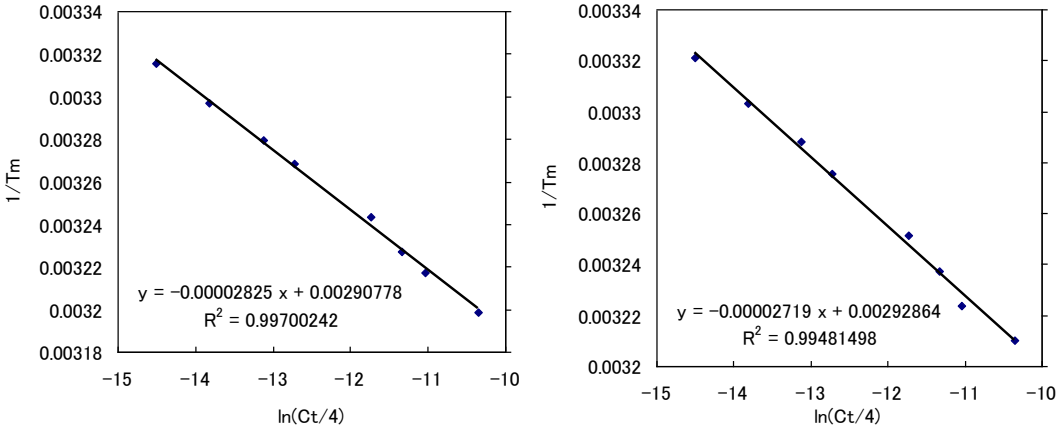


Appendix Figure 2-7. Van't Hoff plot of **A3a/M3b**. a) : 260 nm, b) : 410 nm.

Appendix Table 2-6. $T_m$ of **M3a/M3b**.[a)]

| Concentration / μM | 260 nm / °C | 490 nm / °C |
|---|---|---|
| 1 | 53.0 | 52.5 |
| 2 | 54.6 | 54.1 |
| 4 | 56.3 | 55.8 |
| 6 | 57.2 | 56.8 |
| 16 | 59.8 | 59.6 |
| 24 | 61.6 | 60.9 |
| 32 | 61.5 | 61.3 |
| 64 | 63.7 | 63.4 |

a) [NaCl] = 100 mM, pH 7.0 (10 mM phosphate buffer)

**a)** **b)**

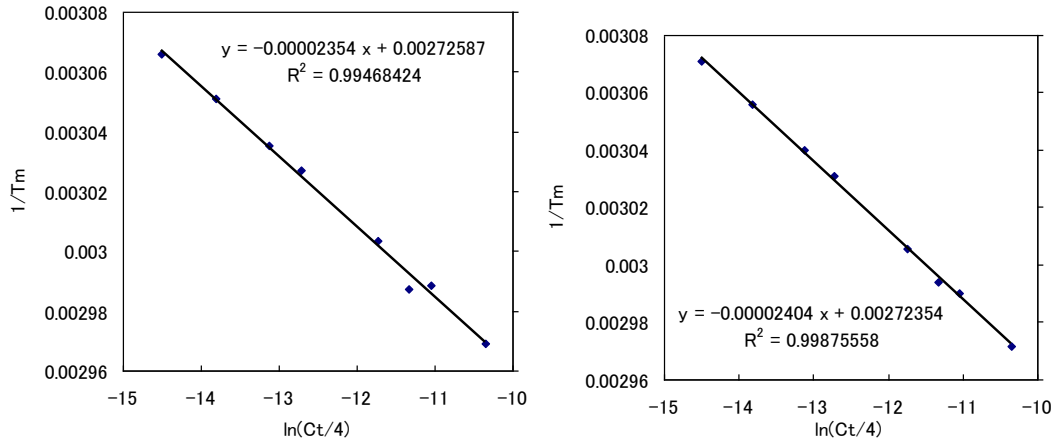


Appendix Figure 2-8. Van't Hoff plot of **M3a/M3b**. a) : 260 nm, b) : 490 nm.

# Chapter 3. Analysis of Coherent Heteroclustering of Different Dyes by Use of Threoninol Nucleotides for Comparison with the Molecular Exciton Theory

## 3-1 Abstract

To test the molecular exciton theory for heterodimeric chromophores, various heterodimers and clusters, in which two different dyes were stacked alternately, were prepared by hybridizing two oligodeoxyribonucleotides (ODNs), each of which tethered a different dye on D-threoninol at the center of the strand. NMR analyses revealed that two different dyes from each strand were stacked antiparallel to each other in the duplex, and were located adjacent to the 5'-side of a natural nucleobase. The spectroscopic behavior of these heterodimers was systematically examined as a function of the difference in the wavelength of the dye absorption maxima ($\Delta\lambda_{max}$). We found that the absorption spectrum of the heterodimer was significantly different from that of the simple sum of each monomeric dye in the single strand. When azobenzene and Methyl Red, which have $\lambda_{max}$ at 336 and 480 nm, respectively, in the single strand ($\Delta\lambda_{max}$ = 144 nm), were assembled on ODNs, the band derived from azobenzene exhibited a small hyperchromism, whereas the band from Methyl Red showed hypochromism and both bands shifted to a longer wavelength (bathochromism). These hyper- and hypochromisms were further enhanced in a heterodimer derived from 4'-methylthioazobenzene and Methyl Red, which had a much smaller $\Delta\lambda_{max}$ (82 nm; $\lambda_{max}$ = 398 and 480 nm in the single-strand, respectively). With a combination of 4'-dimethylamino-2-nitroazobenzene and Methyl Red, which had an even smaller $\Delta\lambda_{max}$

(33 nm), a single sharp absorption band that was apparently different from the sum of the single-stranded spectra was observed. These changes in the intensity of the absorption band could be explained by the molecular exciton theory, which has been mainly applied to the spectral behavior of H- and/or J-aggregates composed of homo dyes. However, the bathochromic band shifts observed at shorter wavelengths did not agree with the hypsochromism predicted by the theory. Thus, these data experimentally verify the molecular exciton theory of heterodimerization. This coherent coupling among the heterodimers could also partly explain the bathochromicity and hypochromicity that were observed when the dyes were intercalated into the duplex.

## 3-2 Introduction

Assembly of a dye induces characteristic spectroscopic behavior, such as band narrowing and band shifts, that cannot be achieved with a monomeric dye.[1] Furthermore, since dye assemblies have the potential to contribute to the production of nonlinear optical materials[2] and light-harvesting systems,[3] the preparation of ordered dye assemblies and their characterization is very important both from a scientific and a practical point of view. To date, various methodologies for the preparation of homo-assemblies composed of identical dyes have been proposed, and their spectroscopic behaviors, such as J- and H-bands, have been examined theoretically on the basis of molecular exciton theory.[1, 4] However, due to the difficulty of their preparation, there have only been a limited number of reports on the characterization of hetero-assemblies, especially those of a predetermined size and orientation.[5-7] Hence, theoretical investigation of the spectroscopic behavior and potential applications of hetero-assemblies is less advanced than that of homo-assemblies, at least in part because

theoretical calculations concerning their spectroscopic behavior cannot be experimentally verified. As far as we know, there are only a few examples that demonstrate a relationship between the experimental observation of the spectroscopic behavior of hetero-aggregation (dimerization) and its theoretical prediction. The first report of this type was by Kuhn et al. on the spectroscopic behavior of a heterodimer of cyanine dyes spread on the water/air interface using the Langmuir-Blodgett method.[6] Furthermore, a change in the absorption spectra of a fluorescence resonance energy transfer (FRET) donor-acceptor pair and/or an fluorescein isothiocyanate/dimethyl aminophenylazo benzoic acid (FITC/Dabcyl; Methyl Red) pair tethered at both the 3'- and 5'-termini of a molecular beacon has been demonstrated.[7,8]However, since mutual orientation of these heterodimers was not well-defined and was difficult to control, they were not appropriate models to verify the exciton theory experimentally. Furthermore, these investigations lacked the viewpoint of the difference of $\lambda_{max}$, which should significantly affect the coherency of the dimers. Verification of the exciton theory will lead to the design of new hetero-assemblies having special optical properties that cannot be realized by homo-assemblies.

In chapter 2, we proposed a unique method for the preparation of a dye assembly by hybridization of two single-stranded oligodeoxyribonucleotides (ODNs), each of which tethered dyes to D-threoninols (threoninol nucleotides) at the center of the strand.[9] The use of threoninol as a dye scaffold allows easy programming of various dye assemblies that are difficult to design based on the conventional self-association of dyes. Alternating heteroclusters of a predetermined size and orientation can be easily prepared by hybridization of two complementary DNA-dye conjugates, each of which is conjugated to a different dye. In this chapter, we prepared various heterodimers of

Methyl Red with other dyes using threoninol nucleotides. The dyes chosen for heterodimerization with Methyl Red were chosen with a focus on the difference in $\lambda_{max}$ between Methyl Red and the second dye ($\Delta\lambda_{max}$), as shown in Schemes 3-1 and 3-2. Such a systematic investigation of the relationship between $\Delta\lambda_{max}$ and coherency in a firmly stacked heterodimer of predetermined orientation has not yet been reported. The stacked structure of the heterodimer in the duplex was first determined by NMR analysis,[10] and the spectroscopic behavior of the dyes was then investigated in detail in order to verify qualitatively the predictions of the molecular exciton theory. We used azo compounds as model dyes because: 1) the molecular sizes of these dyes are very similar; 2) the π-π* transition (light absorption) of these dyes occurs in a similar manner; 3) they have a single and fairly symmetrical absorption band; and 4) the absorption spectra reflect the exciton coupling (coherency) of the dyes rather than fluorescence. Five threoninol nucleotides with azobenzene (**Z**), 4'-methylthio -azobenzene (**S**), Methyl Red (**M**), 4'-dimethylamino-2-nitroazobenzene (**R**), or Naphthyl Red (**N**) tethers were incorporated into ODNs (see Scheme 3-2 for the structures), and various heterodimers were prepared to investigate their spectroscopic behavior from both experimental and theoretical viewpoints. These insights into

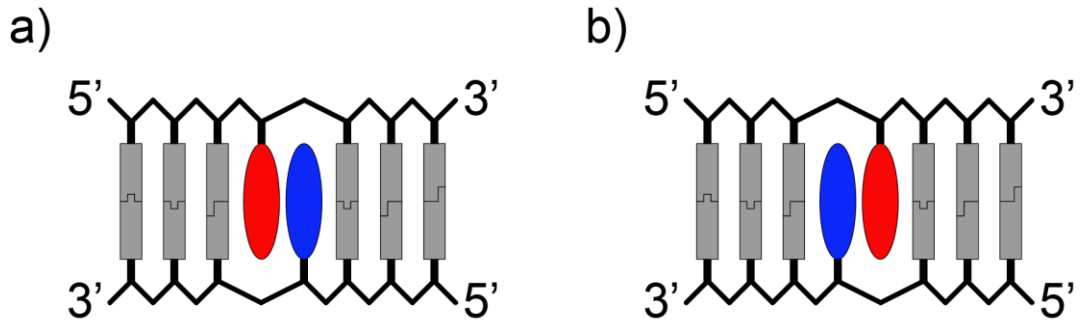


Scheme 3-1. Schematic illustration of the design of the heterodimer using threoninol nucleotides as dye tethers. There are two possible dye locations: the dyes are located adjacent to a) the 5'-side (corresponding to **M**/**Z** orientation in NMR-**Ma**/NMR-**Zb**) or b) the 3'-side of a natural nucleobase (corresponding to **Z**/**M** orientation).

heterodimerization leaded to the design of more sensitive fluorophore-quencher pairs of molecular beacons (In Stem Molecular Beracon in Chapter 4).

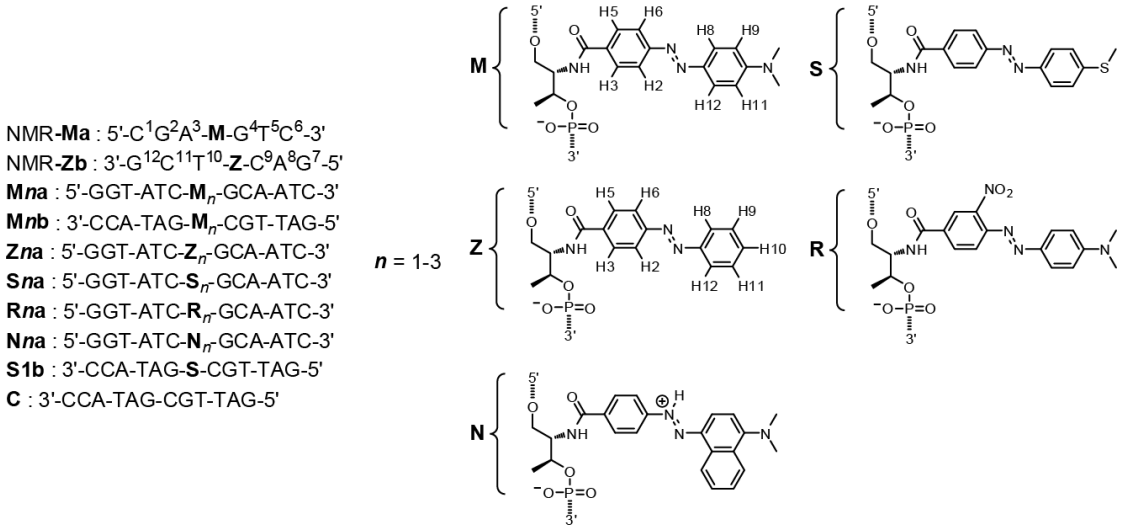


Scheme 3-2. Sequences of ODNs synthesized in this chapter.

## 3-3 Results

### 3-3-1 Structural determination of the heterodimers by NMR spectroscopy

As illustrated in Scheme 3-1, heterodimer formation is based on the tentative base-pairing of threoninol nucleotides at the center of paired ODNs. A dye residue is located at the counterpart of the other dye residue in the complementary ODN sequence,[11] and these dye residues from the two strands stack with each other, in an antiparallel orientation, by pseudo "base-pairing". The ODNs synthesized for this chapter are outlined in Scheme 3-2. We first conducted an NMR analysis of a heteroduplex of ODNs conjugated with Methyl Red and azobenzene (NMR-**Ma**/NMR-**Zb**, respectively), in order to determine the location of the stacked **M** and **Z** in the duplex. There are two possible locations of the dyes: adjacent to the 5'-side (Scheme 3-1a, **M**/**Z**) or to the 3'-side (Scheme 3-1b, **Z**/**M**) of the natural nucleobase.

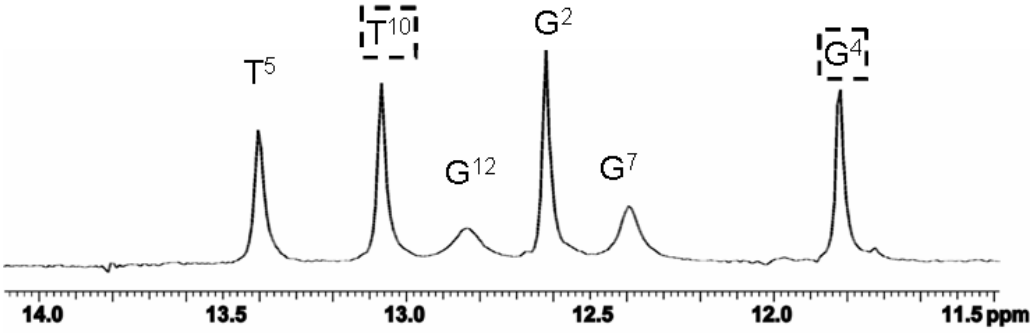


Figure 3-1. One-dimensional NMR spectrum of the NMR-**Ma**/NMR-**Zb** duplex at the imino region in $H_2O/D_2O$ 9:1 at 278 K (mixing time = 150 ms), pH 7.0 (20 mM phosphate buffer), in the presence of 200 mM NaCl. The concentration of NMR-**Ma**/NMR-**Zb** was 1.0 mM. Assignments of the imino-protons and the residue number are denoted at the top of the peak.

Because the melting temperature of the NMR-**Ma**/NMR-**Zb** duplex was determined to be 22.1 $^{o}$C,[12] NMR measurements were performed at 5 $^{o}$C (278 K), a temperature at which a stable duplex exists. In order to monitor imino protons, which are exchangeable with water molecules, NMR was measured in $H_2O$ ($H_2O/D_2O$, 9:1) with a 3-9-19 WATERGATE pulse sequence for $H_2O$ suppression.[13] When these data were

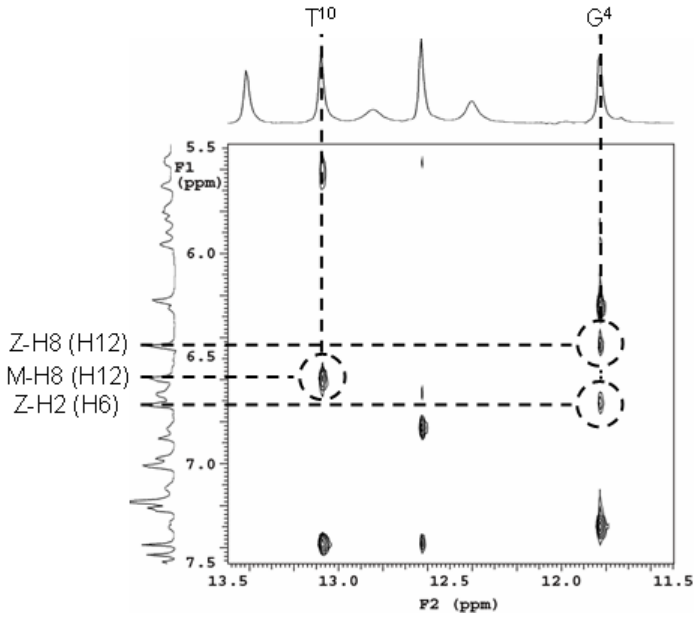


Figure 3-2. 2D NOESY spectrum (mixing time = 150 ms) between the imino-proton signal (11-14 ppm) and the aromatic-proton signal regions (5.5-7.5 ppm) for the NMR-**Ma**/NMR-**Zb** duplex in $H_2O/D_2O$ 9:1 at 278 K, pH 7.0 (20 mM phosphate buffer), in the presence of 200 mM NaCl. Assignments of the Methyl Red and azobenzene protons are denoted on the one-dimensional spectra (*F1* axis) using the numbers designated in Scheme 2. The NOE signals surrounded by broken circles demonstrate intercalation of the Methyl Red and azobenzene.

combined with the NOESY, DQFCOSY, and TOCSY spectra obtained in $H_2O$, most of the signals of the duplex could be assigned. The one-dimensional NMR spectrum measured in $H_2O$ at the region of imino protons (11–14 ppm) is depicted in Fig. 3-1. The NMR-**Ma**/NMR-**Zb** duplex allowed six natural base-pairs ($C^1$-$G^{12}$, $G^2$-$C^{11}$, $A^3$-$T^{10}$, $G^4$-$C^9$, $T^5$-$A^8$, and $C^6$-$G^7$), and one tentative **M**-**Z** pair (Scheme 3-2). As expected, there were six individual signals that could be assigned on the basis of the NOESY and chemical shift of each signal, indicating that the non-natural **M** and **Z** did not interrupt the base-pairing. The imino proton signals of the terminal $G^7$ and $G^{12}$ were rather broad, because of the rapid exchange with water, whereas signals from the other residues remained sharp. Figure 3-2 depicts the NOEs between the imino proton signal (11–14 ppm) and the aromatic proton signal (5.5–7.5 ppm) regions. A distinct NOE signal was observed between the imino proton of $T^{10}$ and H8 (H12) of the Methyl Red protons, indicating that the Methyl Red moiety was located at around $T^{10}$. In addition, strong NOE signals were detected between the imino proton of $G^4$ and H2 (H6) and H8 (H12) of the azobenzene protons, indicating that the azobenzene moiety was located in the vicinity of $G^4$. Thus, we could unambiguously conclude that each dye was located adjacent to the 5'-side of the natural nucleobase (**M**/**Z**, corresponding to Scheme 3-1a).

Evidence for antiparallel stacking of **M** and **Z** was given by the NOESY spectrum between the regions of 5.5–7.5 ppm and 1.0–2.6 ppm (Fig. 3-3). Strong NOE signals were observed between N-$CH_3$ of **M** and H2 (H6) of **Z**, as well as between N-$CH_3$ of **M** and H3 (H5) of **Z**, indicating that **M** and **Z** were stacked in an antiparallel manner. The combined NOE signals demonstrate that **M** and **Z** are stacked antiparallel to each other and are located adjacent to the 5'-side of the nucleobase, as depicted in Fig. 3-4a, which validates our design of the heterodimer. Computer modeling of

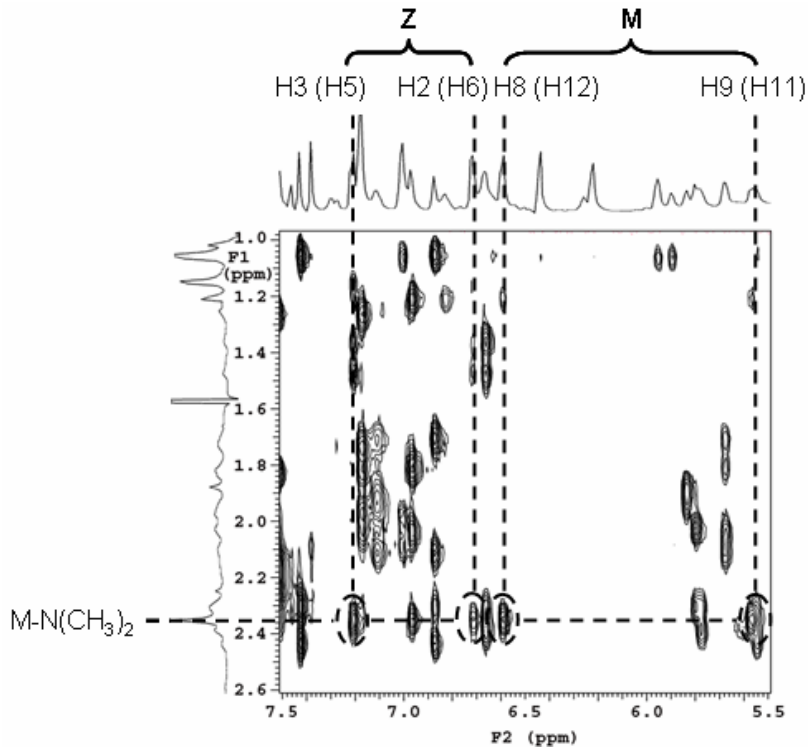


Figure 3-3. 2D NOESY spectrum (mixing time = 150 ms) between the regions of 5.5-7.5 ppm and 1.0-2.6 ppm for the NMR-**Ma**/NMR-**Zb** duplex in $H_2O/D_2O$ 9:1 at 278 K (20 mM phosphate buffer), in the presence of 200 mM NaCl.

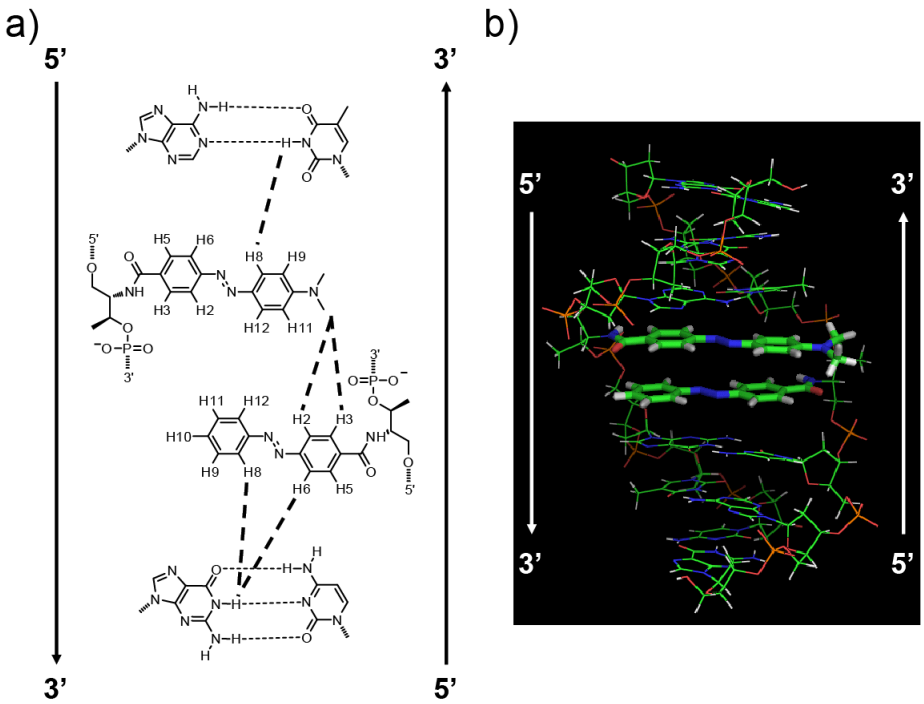


Figure 3-4. Stacking manner and orientation of **Z** and **M** residues in the duplex determined from NOESY a), and an energy-minimized structure of the NMR-**Ma**/NMR-**Zb** duplex b) calculated with InsightII/Discover3 from the initial structure determined by NMR analyses. Broken lines in a) show the observed NOE signals. The sticks in b) depict azobenzene and Methyl Red in the duplex.

NMR-**Ma**/NMR-**Zb**, using the InsightII/discover3 software, was entirely consistent with the NMR analyses (Fig. 3-4b).

### 3-3-2 Spectroscopic behavior of the alternate heterodimers

Having validated our heterodimer design and confirmed its stacked structure, we next investigated spectral changes of heterodimers composed of the various ODN-dye conjugates shown in Scheme 3-2. This analysis focused on the difference of $\lambda_{max}$ between the dyes ($\Delta\lambda_{max}$) in the heterodimer. Figure 3-5 shows the UV/Vis spectra of the single-stranded dye conjugates synthesized in this chapter. These conjugates, **Z1a**,

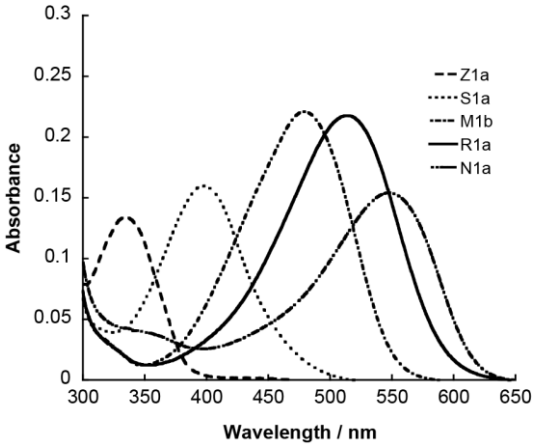


Figure 3-5. UV/Vis spectra of single-stranded **Z1a**, **S1a**, **N1a**, **R1a** and **M1b** at 0 $^{o}$C, which corresponded to a monomeric transition. Solution conditions were as follows: [ODN] = 5 μM, [NaCl] = 100 mM, pH 7.0 (10 mM phosphate buffer). For the measurement of **N1a**, 10 mM MES buffer at pH 5.0 was used.

Table 3-1. Melting temperature ($T_m$) of double-stranded DNA-dye conjugates.

| Sequences | $\lambda_{max}$ / nm$^a$ ($\lambda_{max}$ / cm$^{-1}$) | $\Delta\lambda_{max}$ / nm$^a$ ($\Delta\lambda_{max}$ / cm$^{-1}$) |
|---|---|---|
| **M1b** | 480 ($2.08\times10^4$) | — |
| **Z1a** | 336 ($2.98\times10^4$) | 144 ($8.93\times10^3$) |
| **S1a** | 398 ($2.51\times10^4$) | 82 ($4.29\times10^3$) |
| **R1a** | 513 ($1.95\times10^4$) | 33 ($1.34\times10^3$) |
| **N1a** | 548 ($1.82\times10^4$)$^b$ | 68 ($2.59\times10^3$)$^b$ |

[a] Measurement conditions were pH 7.0 (10 mm phosphate buffer), [ODN] = 5 μM, [NaCl] = 100 mM, at 0 $^{o}$C. [b] Measurement conditions were pH 5.0 (10 mM MES buffer), [ODN] = 5 μM, [NaCl] = 100 mm, at 0 $^{o}$C.

**S1a**, **M1b**, **R1a**, and **N1a**, showed absorption maxima at 336, 398, 480, 513, and 548 nm, respectively. The absorption maxima corresponded to a monomeric transition at 0 $^{o}$C, which is controlled by the introduction of electron-donating and electron-attracting functional groups to the azobenzene scaffold.[14] We then prepared four different kinds of heteroclusters by combining Methyl Red-conjugated ODNs (**M*n*b**) with ODNs conjugated with the other dyes, thus forming **Z*n*a/M*n*b**, **S*n*a/M*n*b**, **R*n*a/M*n*b**, and **N*n*a/M*n*b** heterodimers. A summary of the $\lambda_{max}$ of the single conjugates and the $\Delta\lambda_{max}$ between **M1b** and the other dye conjugates is shown in Table 3-1.

**Z/M** combination ($\Delta\lambda_{max}$ = 144 nm): Figure 3-6 shows the UV/Vis spectra of **Z1a/M1b**, **Z1a**, **M1b**, and a spectrum calculated as the simple sum of the two single strands (sum-spectrum). Both single-stranded **Z1a** and **M1b** exhibited broad bands (peaks) at 336 and 480 nm, respectively. The sum spectrum gave two bands because $\Delta\lambda_{max}$ of **Z1a/M1b** was as high as 144 nm. The absorption spectrum of the **Z1a/M1b** duplex also gave two bands at around 344 and 500 nm, although the pattern was slightly but distinctly different from the pattern for the sum of each spectrum. Dimerization of **Z**

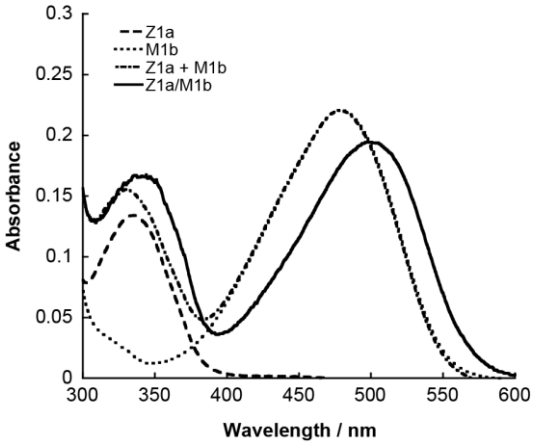


Figure 3-6. UV/Vis spectra of the **Z1a/M1b** duplex (solid line), single-stranded **Z1a** (broken line), **M1b** (dotted line), and a simple sum of their spectra (sum-spectrum, **Z1a + M1b,** dashed-dotted line) at 0 $^{o}$C. Solution conditions were as follows: [ODN] = 5 μM, [NaCl] = 100 mM, pH 7.0 (10 mM phosphate buffer).

and **M** induced a bathochromic shift in the $\lambda_{max}$ of both dyes. In addition, the peak located at a shorter wavelength in **Z1a/M1b** (derived from the single-stranded **Z**) showed hyperchromism. In contrast, hypochromism was observed for the peak derived from the single-stranded **M**.

**S/M** combination ($\Delta\lambda_{max}$ = 82 nm): An **S/M** combination of the dyes gave a $\Delta\lambda_{max}$ of 82 nm, which was half that of the **Z1a** and **M1b** combination. The absorption spectra of **S1a/M1b**, **S1a**, **M1**b, and their sum-spectrum are depicted in Fig. 3-7a. Interestingly, hybridization of these two conjugates displayed an absorption spectrum that was apparently different from that of the sum of their single strands. The UV/Vis spectrum of the **S1a/M1b** duplex gave one main band at 422 nm and a shoulder band at around 480–560 nm, as depicted by the solid line in Fig. 3-7a, whereas the sum-spectrum of **S1a** and **M1b** (dashed-dotted line in Fig. 3-7a) showed two broad bands with almost equal absorbance at 398 and 480 nm. Following hybridization, the absorption band at 398 nm, corresponding to **S1a**, showed both strong bathochromicity and

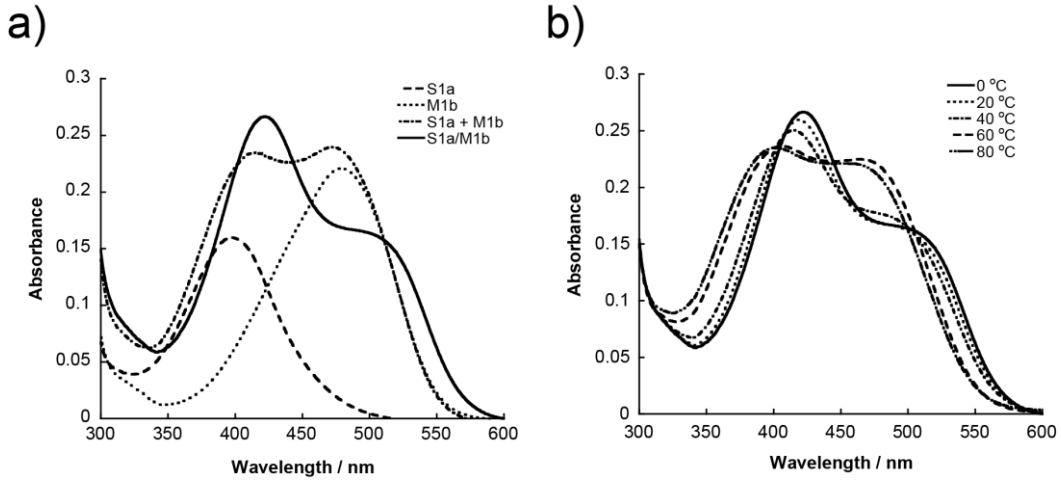


Figure 3-7. UV/Vis spectra of a) **S1a/M1b** duplex (solid line), single-stranded **S1a** (broken line), **M1b** (dotted line), and a simple sum of their spectra (sum-spectrum, **S1a + M1b,** dashed-dotted line) at 0 $^{o}$C, and b) effect of temperature on the absorption spectrum of **S1a/M1b**. Solution conditions were as follows: [ODN] = 5 μM, [NaCl] = 100 mM, pH 7.0 (10 mM phosphate buffer).

hyperchromicity, whereas the band at 480 nm, corresponding to **M1b**, displayed bathochromicity and hypochromicity (Fig. 3-7a). Although this tendency was similar to that observed with the **Z1a** and **M1b** combination, the spectral change induced by hybridization was further amplified with the **S1a** and **M1b** combination, which had a smaller $\Delta\lambda_{max}$. In order to rule out the possibility that these spectral behaviors were due to an unexpected covalent interaction of these dyes, thermal reversibility of the **S1a/M1b** duplex was examined. The absorption spectrum of **S1a/M1b** above 60 $^{o}$C, a temperature at which the duplex was completely dissociated, was similar to the sum-spectrum of **S1a** and **M1b** (compare the dashed-dotted line in Fig. 3-7a with the broken line in Fig. 3-7b). Note that the melting temperature ($T_m$) of **S1a/M1b** was 51.2 $^{o}$C under the conditions employed (see Supporting Information, Table 3-1). In contrast, a reduction in temperature below $T_m$ allowed a large, reversible, spectroscopic change. Thus, the spectral changes observed in the duplex were confirmed to be due to a noncovalent interaction between **S** and **M** in the duplex. Since further reduction in temperature from 40 to 0 $^{o}$C slightly changed their absorption spectra, chromophore motions would also affect the exciton interaction slightly.[15]

**R/M** and **N/M** combination ($\Delta\lambda_{max}$ = 33 and 68 nm): The combination of **R** and **M** had the smallest $\Delta\lambda_{max}$ (33 nm) of all the combinations examined in this chapter. Hence, the sum-spectrum of these two single strands gave not two, but one broad single band, due to the proximity of the absorption maxima. When these two conjugates were hybridized, however, a single sharp absorption band appeared at 483 nm, with a broad, weak shoulder at 550–650 nm, which was entirely different from the pattern of the sum-spectrum, as shown in Fig. 3-8a. Similarly, **N1a/M1b**, which we

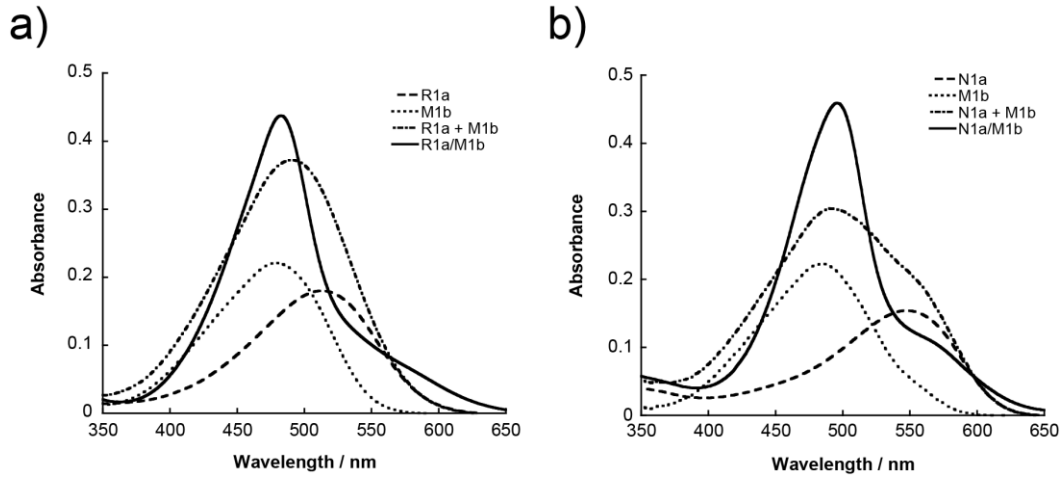


Figure 3-8. a) UV/Vis spectra of the **R1a/M1b** duplex (solid line), single-stranded **R1a** (broken line), **M1b** (dotted line), and a simple sum of their spectra (sum-spectrum, **R1a + M1b,** dashed-dotted line) at 0 $^{o}$C. Solution conditions of a) were as follows: [ODN] = 5 μM, [NaCl] = 100 mM, pH 7.0 (10 mM phosphate buffer). b) UV/Vis spectra of the **N1a/M1b** duplex (solid line), single-stranded **N1a** (broken line), **M1b** (dotted line), and a simple sum of their spectra (sum-spectrum, **N1a + M1b,** dashed-dotted line) at 0 $^{o}$C. Solution conditions of b) were as follows: [ODN] = 5 μM, [NaCl] = 100 mM, pH 5.0 (10 mM MES buffer).

demonstrated in chapter 2 as an alternating heterocluster,[9] also showed a single absorption band at 496 nm with a broad weak shoulder (Fig. 3-8b).

### 3-3-3 Effect of aggregate size on spectroscopic behavior of alternating heteroclusters

We next examined the effect of alternating heteroclustering of **S*n*a/M*n*b** and **R*n*a/M*n*b**, both of which exhibited a large spectral change upon dimerization. As shown in Fig. 3-9a, an increase in dye number in **S*n*a/M*n*b** ($n$ = 1–3) increased the absorbance of the band of shorter wavelength, whereas little increase was observed in the shoulder band of the longer wavelength. Consequently, **S3a/M3b** exhibited almost a single band with a broad shoulder. In addition, prominent hypsochromism was induced as the size of the aggregates increased. In the case of **R*n*a/M*n*a**, the single sharp band that appeared at 483 nm in **R1a/M1b** grew as the number of dyes incorporated per strand increased ($n$ = 1–3) and was accompanied by a distinct hypsochromic shift, as depicted in Fig. 3-9b. The spectroscopic behavior of these ODNs with higher

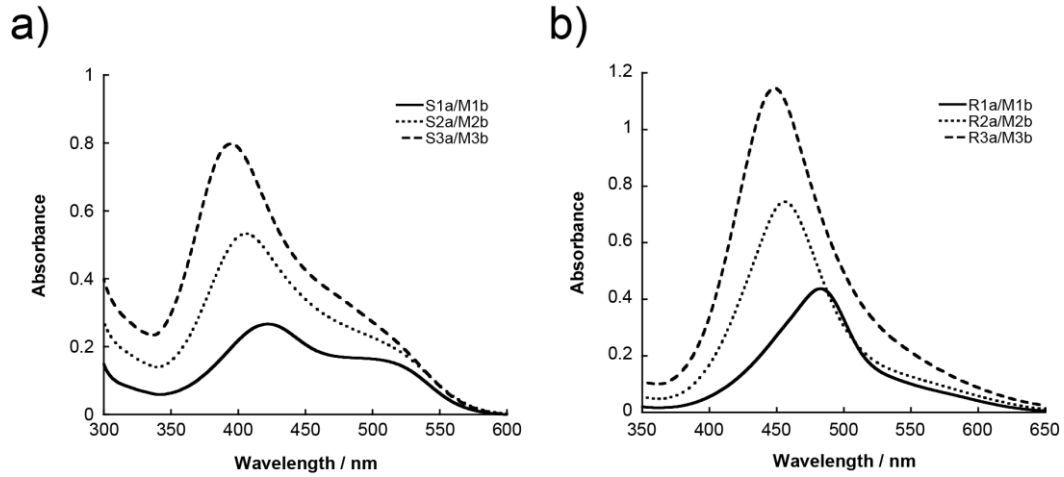


Figure 3-9. Effect of the number of dye pairs on the UV/Vis spectra of a) **S*n*a**/**M*n*b** and b) **R*n*a**/**M*n*b** combinations. Solution conditions were as follows: 0 °C, [ODN] = 5 μM, [NaCl] = 100 mM, pH 7.0 (10 mM phosphate buffer).

numbers of dyes incorporated was similar to that of homo H-aggregates, which exhibit hypsochromic shifts and sharp bands.[16] **N/M** pairs with a $\Delta\lambda_{max}$ of 68 nm also showed a similar spectroscopic behavior to **R/M** pairs with an increase in the cluster size (see Appendix Fig. 3-1 in the Appendix).

The effect of cluster size on circular dichroism (CD) spectra is shown in Fig. 3-10. Although heteroclusters were stably formed below $T_m$ for both **S*n*a**/**M*n*b** and **R*n*a**/**M*n*b**, the induced CD (ICD) at the π-π* transition region was not so strong. A small ICD is interpreted as an unwound structure of a stacked dye assembly on D-threoninol. In a

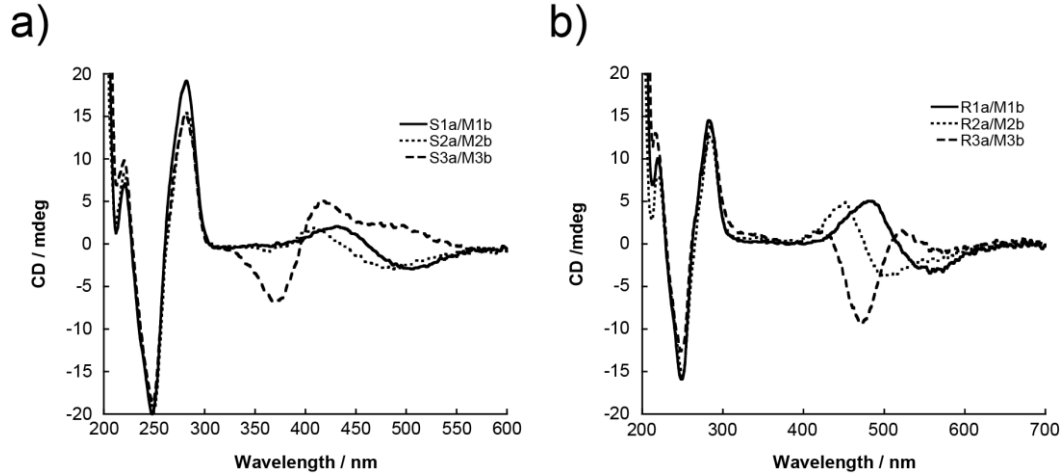


Figure 3-10. Effect of the number of dye pairs on the CD spectra of a) **S*n*a**/**M*n*b** and b) **R*n*a**/**M*n*b** combinations. Solution conditions were as follows: 0 °C, [ODN] = 5 μM, [NaCl] = 100 mM, pH 7.0 (10 mM phosphate buffer).

Methyl Red homocluster, this would result in a ladder-like structure due to its flexibility, as demonstrated in chapter 2.

## 3-4 Discussion

### 3-4-1 Stacked structure of the heteroclusters

Our heterodimer design is based on the pseudo "base-pairing" of threoninol nucleotides incorporated at the center of an ODN. In contrast with natural A-T and/or G-C base-pairs, however, paired threoninol nucleotides stack with each other through hydrophobic stacking interactions. Therefore there are two possible stacked structures in which dyes are located either adjacent to the 5'-side (**M**/**Z**) or the 3'-side (**Z**/**M**) of the natural nucleobase (see Scheme 3-1). NMR analyses of an NMR-**Ma**/NMR-**Zb** duplex clearly revealed that the dyes were located adjacent to the 5'-side (**M**/**Z**), and other minor structures were rarely observed. This stacked structure can be explained by the space between the threoninol and natural nucleotide, in which a dye at the counterstrand is inserted. As shown in Fig. 3-11, the number of atoms from the dye to a rigid

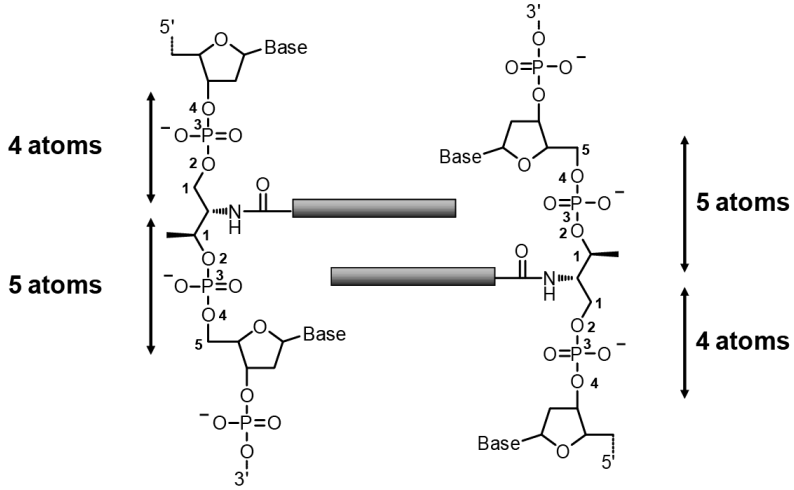


Figure 3-11. Illustration of the stacking manner of the dyes from each strand. The number of atoms from the dye to the rigid five-membered ring is five between the crotches of ribose and threoninol at the 3'-side whereas it is four at the 5'-side. The number labelled in the figure indicates the atoms between the crotches of ribose and threoninol.

five-membered ring is five between the crotches of ribose and threoninol at the 3'-side, whereas it is four at the 5'-side. Thus, the 3'-side is one carbon longer than the 5'-side, due to the 5'-carbon of the natural ribose scaffold, which facilitates the intercalation of the dye from the counterstrand. Computer modeling also supported the 5'-side **M/Z** orientation of the dye in the ODN dimer. In this model, both dyes from each strand fitted well into the space at the 5'-side of each other and were stacked in an antiparallel manner. Furthermore, stacked dyes of the unwound structure, shown in Fig. 3-4b, are also consistent with the small ICDs measured (Fig. 3-10). As reported in chapter 2, dyes conjugated to threoninols do not need winding in order to form a firmly stacked structure, and the flexibility of this structure allows the formation of a ladder-like structure. It is also expected that a heterocluster of two different dyes, such as **Z3a/M3b**, **S3a/M3b**, **R3a/M3b**, or **N3a/M3b**, would be alternately aligned in the same manner as the 5'-side **M/Z** orientation (Appendix Fig. 3-2 in the Appendix).

3-4-2 Comparison of the spectroscopic behavior of the heterodimer with the molecular exciton model

As shown in Fig.s 3-6 to 3-8, all four heterodimers exhibited UV/Vis spectra that were distinctly different from those calculated from the sum-spectrum, and this difference depended on the $\Delta\lambda_{max}$ of the combined dyes. Next is an explanation of these spectroscopic behaviors by the molecular exciton theory.[1, 4a, 5b, 6-7]

*Spectral behavior predicted from the molecular exciton theory:* Figure 3-12 shows a schematic illustration of the energy diagram of two laterally stacked dyes of different $\lambda_{max}$. When monomer A of a higher transition energy is excitonically coupled with a dye

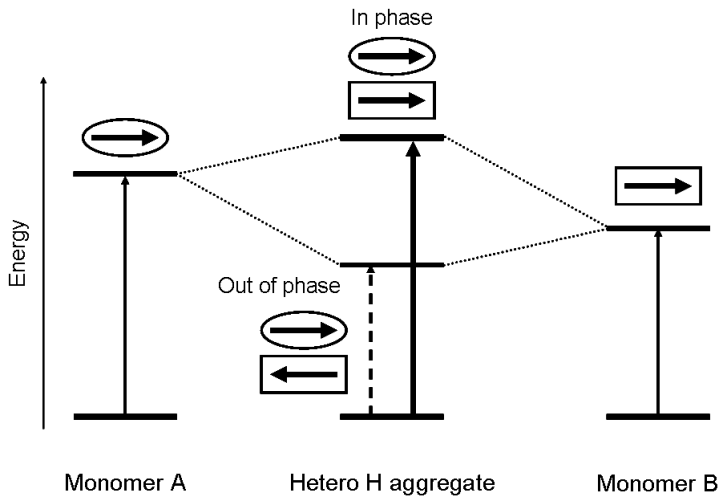


Figure 3-12. Schematic energy diagram of the heterodimer depicted on the basis of the exciton model. Each arrow, outlined by an ellipse or an oblong, designates the transition dipole moment.

of lower transition energy, the excited state splits into two energy levels.[5b, 7, 17] The higher energy level corresponds to the in-phase transition in which the transition dipole moments of the monomers A and B have the same direction. In this case, the energy level becomes higher than that of monomer A due to the repulsive interaction between the two transition dipoles. The absorption coefficient of the in-phase transition is expected to increase due to the sum of the transitions A and B. In contrast, the energy level of the out-of-phase transition becomes lower than that of monomer B, due to the attractive interaction. However, the absorption coefficient of this transition decreases because the transition moment is partially cancelled due to its antiparallel orientation. The above excitonic interaction (namely, coherency) should be enhanced when the gap between the transition energies of monomers A and B, $\Delta\lambda_{max}$, decreases. In the case where the transition moment of A is the same as that of B (i.e., A and B are the same dye), an out-of-phase transition is forbidden due to the complete cancellation of transition moment, whereas the in-phase transition is maximized.[18] Comparison with experimental results: The experimental results almost completely coincide with the above predictions based on the molecular exciton theory, with the exception of the

results obtained for the spectral shift. In the case of **Z1a/M1b**, the band of the shorter wavelength (higher transition energy), derived from the azobenzene transition, displayed hyperchromism, whereas that of the longer wavelength (lower transition energy), derived from Methyl Red, displayed hypochromism. Both hyper- and hypochromism were enhanced in the **S1a** and **M1b** combination, because the $\Delta\lambda_{max}$ of this combination was smaller than that between **Z1a** and **M1b**. These absorbance changes qualitatively coincided with the prediction based on the molecular exciton theory. In the case of **R1a/M1b** and **N1a/M1b**, which displayed a much smaller $\Delta\lambda_{max}$, the out-of-phase transition became much weaker and hence a single sharp band, corresponding to an enhanced in-phase transition, appeared. The broad, weak shoulder observed at the longer wavelength may correspond to a weakened, out-of-phase transition. Thus, the molecular exciton theory of heterodimer formation was qualitatively validated from the viewpoint of transition intensity. However, the spectral shift corresponding to the in-phase transition that we observed did not fit with the theory. According to the theory, an in-phase transition (higher transition energy) induces a hypsochromic shift with respect to the transition of monomer A, whereas an out-of-phase transition (lower transition energy) induces a bathochromic shift with respect to the transition of monomer B. Our experimental results revealed that the out-of-phase transition displayed a bathochromic shift (**Z1a/M1b** and **S1a/M1b**, Fig.s 3-6 and 3-7), in accordance with the theory. However, the in-phase transition also showed a bathochromic shift, which is contrary to the theory. Other combinations that were examined, such as **R1a/S1b** and **Z1a/S1b**, also exhibited bathochromicity of the in-phase transition (Appendix Fig. 3-3 in the Appendix). In order to rule out the possibility that this bathochromicity was induced simply by intercalation with the

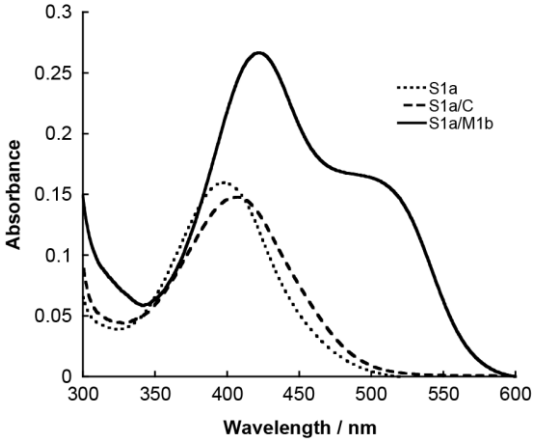


Figure 3-13. UV/Vis spectra of the **S1a/M1b** duplex (solid line), the **S1a/C** duplex (dashed line) and the single-stranded **S1a** (dotted line) at 0 $^{o}$C. Solution conditions were as follows: [ODN] = 5 μM, [NaCl] = 100 mM, pH 7.0 (10 mM phosphate buffer).

base-pairs of the ODN,[19] we analyzed the hybridization of **S1a** with a natural C strand, which does not contain any threoninol nucleotides. Our previous NMR investigations demonstrated that such a sequence design (**S1a/C** duplex) facilitates intercalation of the dye tethered to threoninol between the base pairs.[20] As shown in Fig. 3-13, single-stranded **S1a**, double-stranded **S1a/C**, and double-stranded **S1a/M1b** had $\lambda_{max}$ at 398, 408, and 422 nm, respectively. The bathochromicity induced by hybridization of **S1a** with **C** was only 10 nm (compare the dotted and dashed lines in Fig. 3-13), indicating that the presence of the adjacent bases did not much affect the spectral shift. However, **S1a/M1b** allowed a bathochromic shift as large as 24 nm (compare the solid and dotted lines in Fig. 3-13), which was obviously larger than that induced by the **S1a/C** duplex.[21] Hence, we conclude that the bathochromicity of the in-phase transition cannot be explained by the conventional molecular exciton theory.

Since the conventional molecular exciton theory is based on the point-dipole approximation model, this may cause problems in its application to a firmly stacked heterodimer, because stacked dyes of 10 Å size that are in close proximity (3.5 Å) cannot be approximated as a "point".[1] A further improved model (such as the extended

dipole approximation[1] and/or molecular transition density[22]) will be needed to explain the bathochromic shift of heterodimerization. Sawabe and Kubo et at. revealed this discord derived from the orbital overlap between two dyes firmly stacked close to each other in a duplex by quantum calculation (ab initio calculation) of the heterodimer.[23]

*Heteroclustering of the dyes*: As shown in Fig. 3-9, an increase in the dye number resulted in intensification of the in-phase transition together with a hypsochromic shift, whereas the corresponding out-of-phase transition did not. This spectroscopic behavior is very similar to that of homo H-aggregates in which identical dyes are axially stacked. Although the hypsochromic shift was smaller than that seen for homo H-aggregates, these results clearly demonstrate that strong coherent coupling occurred even among the heteroclusters. Even **S3a/M3b**, which had a $\Delta\lambda_{max}$ of 82 nm, exhibited almost a single band due to the strong coherent coupling within the heterocluster. We can predict from this result that one- or two-dimensional clusters, composed of two different dyes with different absorption maxima, should exhibit essentially a single band when the dyes are assembled in an orderly fashion, and should show strong coherency (exciton coupling). [4]

## 3-5 Conclusions

The NMR study revealed that different dyes incorporated at the center of an ODN through tethering to D-threoninols were stacked antiparallel to each other, and were located adjacent to the 5'-side of a natural nucleobase.

Heterodimerization induced hyperchromism of the band of the shorter wavelength (in-phase transition), but hypochromism of the band of the longer wavelength, and these absorbance changes were enhanced when the $\Delta\lambda_{max}$ of the two dyes was decreased.

Furthermore, both bands exhibited a distinct bathochromic shift. These spectroscopic behaviors were consistent with the shifts predicted from the molecular exciton theory, except for the bathochromic shift of the in-phase transition. This discordance might be due to limitations of the point dipole approximation of the conventional molecular exciton theory.

An increase in dye number dramatically intensified the in-phase transition, which resulted in the spectrum of the heterocluster being almost a single absorption band even though the two dyes had different absorption maxima.

Thus, we have presented, for the first time, a qualitative comparison of the actual spectroscopic behavior of heterodimers with the spectroscopic behavior predicted for such heterodimers by the molecular exciton theory, by systematically changing the $\Delta\lambda_{max}$ of the two dyes.

Our results partly explain the spectroscopic behavior of intercalation. In general, dyes show batho- and hypochromicity when they are intercalated between the base pairs of a duplex. According to Sarkar et al., this bathochromic shift is due to the change in local polarity around the chromophore.[19] However, we demonstrate here that exciton coupling of a natural nucleobase ($\lambda_{max} \approx 260$ nm) with an intercalated dye ($\lambda_{max}$ should be longer than 260 nm) also partly contributes to the weak but distinct bathochromic shift and hypochromicity. Furthermore, the design of a fluorophore and a quencher pair, tethered to D-threoninols, with a smaller $\Delta\lambda_{max}$ should result in a highly sensitive molecular beacon based on a firmly stacked fluorophore-quencher heterodimer with greater coherency. The molecular design of a new heterodimer of a fluorophore -quencher pair as a component of a molecular beacon was shown in chapter 4.

## 3-6 Experimental Section

### 3-6-1 Materials

See 2-6-1 because the contents are the same.

### 3-6-2 Synthesis of DNA modified with **S**, **M**, **N**, **R**, or **Z**

All the modified DNAs were synthesized by using an automated DNA synthesizer (ABI-3400 DNA synthesizer, Applied Biosystems) with conventional and dye-carrying phosphoramidite monomers. Azobenzene, Methyl Red, and Naphthyl Red phosphoramidite monomers were synthesized according to a previous report and Chapter 2.[24] The compounds 4'-methylthioazobenzene and 4'-dimethylamino -2-nitroazobenzene, synthesized according to the literature,[25] were converted to phosphoramidite monomers as described in Scheme 3-3 of 3-6-7. The coupling efficiency of the monomers with modified residues was as high as that of the conventional monomers, as judged from the intensity of the color of the released trityl cation. After the recommended workup, the oligomers were purified by reverse-phase HPLC and characterized by MALDI-TOFMS (Autoflex II, Bruker Daltonics).

The MALDI-TOFMS data, observed (found) versus calculated (calcd.), for the monomers were: **Z1a**: calcd for [**Z1a**+H]$^+$: 4020; found: 4020; **Z2a**: calcd for [**Z2a**+H]$^+$: 4395; found: 4395; **Z3a**: calcd for [**Z3a**+H]$^+$: 4770; found: 4770; **S1a**: calcd for [**S1a**+H]$^+$: 4066; found: 4067; **S2a**: calcd for [**S2a**+H]$^+$: 4487; found: 4488; **S3a**: calcd for [**S3a**+H]$^+$: 4908; found: 4909; **R1a**: calcd for [**R1a**+H]$^+$: 4108; found: 4108; **R2a**: calcd for [**R2a**+H]$^+$: 4571; found: 4572; **R3a**: calcd for [**R3a**+H]$^+$: 5034; found: 5035; **N1a**: calcd for [**N1a**+H]$^+$: 4113; found: 4113; **N2a**: calcd for [**N2a**+H]$^+$: 4581; found: 4581; **N3a**: calcd for [**N3a**+H]$^+$: 5049; found: 5050; **M1b**: calcd for [**M1b**+H]$^+$:

4063; found: 4065; **M2b**: calcd for [**M2b**+H]$^+$: 4481; found: 4481; **M3b**: calcd for [**M3b**+H]$^+$: 4899; found: 4899; NMR-**Ma**: calcd for [MMR-**Ma**+H]$^+$: 2211; found: 2211; NMR-**Zb**: calcd for [MMR-**Zb**+H]$^+$: 2167; found: 2168.

3-6-3 Spectroscopic measurements

See 2-6-3 because basic procedures were the same. The conditions of the sample solutions were as follows (unless otherwise noted): [NaCl] = 100 mM, pH 7.0 (10 mM phosphate buffer), [DNA] = 5 μM. For measurements at pH 5.0, 10 mm MES buffer was used.

3-6-4 Measurement of melting temperature

See 2-6-1 because the procedures are the same. The conditions of the sample solutions were the same as those described for the above spectroscopic measurements.

3-6-5 NMR measurements

NMR samples were prepared by dissolving three-times-lyophilized DNA (modified and complementary DNA) in a $H_2O/D_2O$ 9:1 containing 20 mM sodium phosphate (pH 7.0), to give a duplex concentration of 1.0 mM. NaCl was added to give a final sodium concentration of 200 mM. NMR spectra were measured with a Varian INOVA spectrometer (700 MHz) equipped for triple resonance at a probe temperature of 278 K. Resonances were assigned by standard methods using a combination of 1D, TOCSY (60 ms of mixing time), DQF-COSY, and NOESY (150 ms of mixing time) experiments. All spectra in the $H_2O/D_2O$ 9:1 were recorded using the 3-9-19 WATERGATE pulse sequence for water suppression.

3-6-6 Computer modeling

Molecular modeling by conformational energy minimization was performed with the InsightII/discover3 software (Molecular Simulation, Inc.) on a Silicon Graphics O2+ workstation with the operating system IRIX64 Release 6.5, and the AMBER force field was used for the calculations. The results of the NMR analyses served as a starting point for the modeling. For the analysis, a dimer of Methyl Red and azobenzene was prepared by positioning the two dye molecules in a cofacial orientation and replacing two native base pairs.

3-6-7 Synthesis of the phosphoramidite monomers of 4'-methylthioazobenzene and 4'-dimethylamino-2-nitroazobenzene

**Synthesis of 4'-dimethylamino-2-nitroazobenzene-4-carboxylic acid (Compound 1)**

4-Amino-3-nitrobenzoic acid (1.46 g, 8.0 mmol) was dissolved into a mixture of acetic acid (2.4 mL) and water (9.6 mL). To this solution, aqueous $NaNO_2$ (0.58 g; 8.4 mmol) solution (4 mL) and concentrated HCl (4 mL) was added, followed by stirring for 15 min at 15–20 $^{o}$C. Then, ice-water (80 mL) was further added giving an aqueous diazonium salt solution. The obtained diazonium solution was added dropwise to an aqueous solution (82 mL) of *N*,*N*-dimethylaniline (0.97 g, 8.0 mmol) under acidic (HCl) conditions at 0–5 $^{o}$C to afford 2.50 g (7.95 mmol) of dark red powder of compound **1** (yield 99.4%).

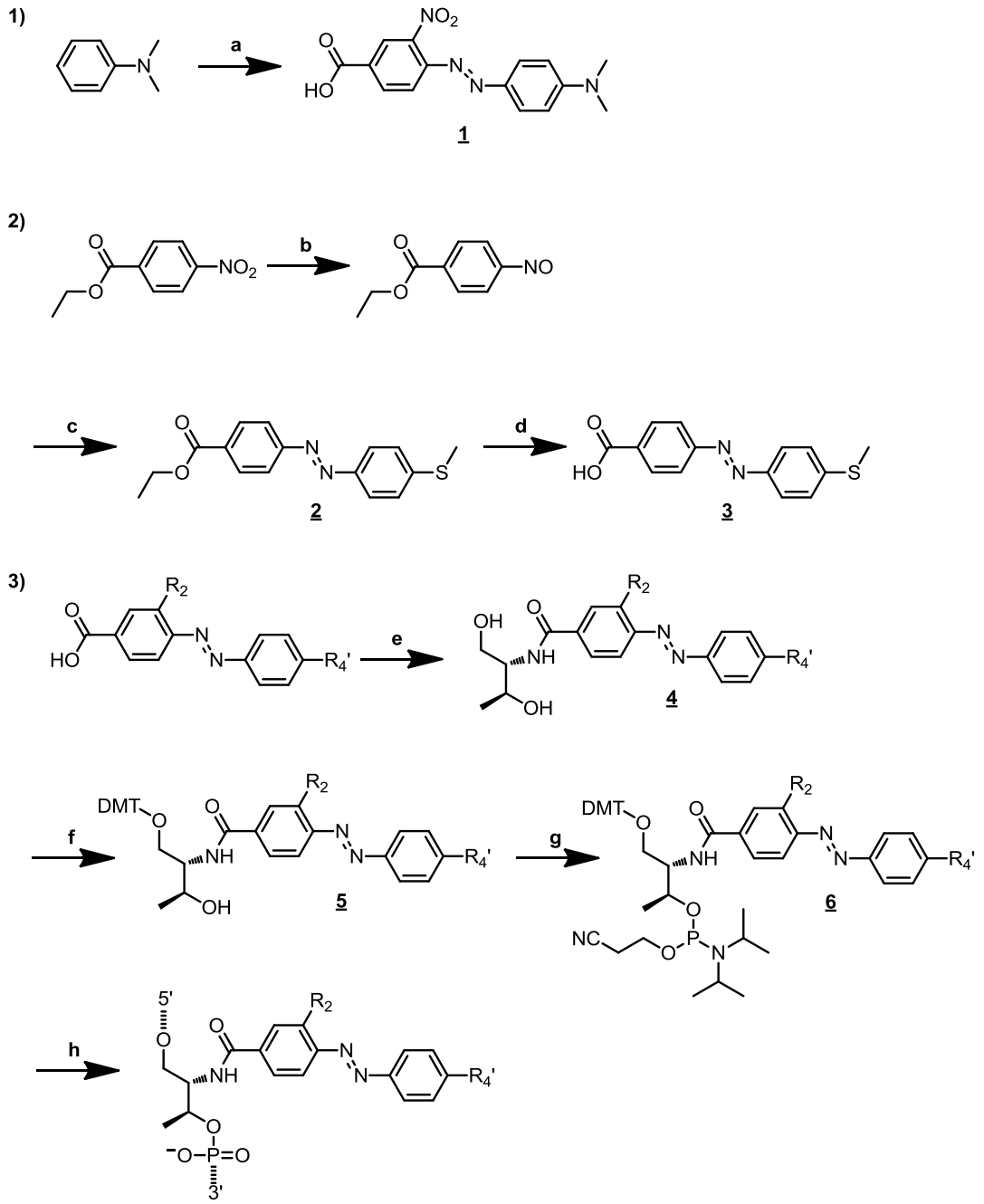


$R_2$ = H, $R_{4'}$ = $SCH_3$: **S** (4'-methylthioazobenzene)
$R_2$ = $NO_2$, $R_{4'}$ = $NMe_2$: **R** (4'-dimethylamino-2- nitroazobenzene)

Scheme 3-3. Synthetic procedures of the azobenzene derivatives and corresponding phosphoramidite monomers. (a) 4-amino-3-nirtobenzoic acid, $NaNO_2$, HCl, AcOH, 0 $^oC$; (b) 1) $NH_4Cl$, Zn, $CH_3OC_2H_5OH$, 20 $^oC$; 2) $FeCl_3$, $CH_3OH$, 0 $^oC$; (c) *p*-methylthioaniline, AcOH; (d) 1) 2 M NaOH, EtOH, 2) HCl; (e) D-threoninol, DCC, HOBt, DMF; (f) DMT-Cl, $CH_2Cl_2$, Pyridine, 0→25 $^oC$; (g) 2-cyanoethyl-*N*,*N*,*N'*,*N'*-tetraisopropylphosphorodiamidite, $CH_3CN$; (h) DNA synthesizer.

**Synthesis of 4'-methylthioazobenzene-4-carboxylic acid (Compound 3)**

Ethyl 4-nitrosobenzoate was synthesized according to the previous report.[26] This compound was used to next reaction without purification.

1.55 g (8.7 mmol) of ethyl 4-nitrosobenzoate and 1.67 g (12.0 mmol) of *p*-methylthioaniline were dissolved in 35 mL of acetic acid. The mixture was stirred at room temperature overnight under dark. Then, the solution was poured into water and extracted with ethyl acetate. The organic layer was washed with distilled water, saturated solution of $NaHCO_3$ and NaCl, and then dried over $MgSO_4$. After the removal the solvent, the crude mixture was subjected to silica gel column chromatography (Hexane : AcOEt = 15 : 1) to afford 1.32 g (4.4 mmol) of compound **2** (yield 50.5%).

1.32 g (4.4 mmol) of compound **2** was dissolved in 225 mL of ethanol. Then 15 mL of aqueous NaOH solution (2 M) was added and the mixture was stirred overnight under dark. After the hydrolysis was completed, aqueous HCl solution (1 M) was added to mixture and pH of the solution was adjusted to around 5.0, followed by the extraction with ethyl acetate. The organic layer was washed with distilled water and saturated solution of NaCl and then dried over $MgSO_4$. After removal solvent, the crude product (compound **3**) was used in the next step without further purification (0.96 g (3.5 mmol) yield 80.3%).

**Synthesis of the phosphoramidite monomer**

0.37 g (3.5 mmol) of D-threoninol was coupled with 0.96 g (3.5 mmol) of compound **3** in the presence of dicyclohexylcarbodiimide (0.87 g, 4.2 mmol) and 1-hydroxybenzotriazole (0.57 g, 4.2 mmol) in 70 mL DMF. After the reaction mixture was stirred at room temperature for 24 h under dark, the solvent was removed and the

remained oil was subjected to silica gel column chromatography (Chloroform : MeOH = 10 : 1) to afford 1.05 g (2.9 mmol) of compound **4** (yield 83.0%)

Dry pyridine (60 mL) and dichloromethane (5 mL) solution containing 1.05 g (2.9 mmol) of compound **4** and 0.57 g (4.4 mmol) of diisopropylethylamine was cooled on ice under nitrogen, and 1.48 g (4.4 mmol) of 4,4'-dimethoxytrityl chloride and 45 mg (0.37 mmol) of 4-dimethylaminopyridine in 15 mL of dichloromethane was added to the above mixture. After 4 h of stirring, the solvent was removed, followed by silica gel column chromatography (Hexane : AcOEt : $Et_3N$= 50 : 50 : 3) to afford 1.69 g (2.6 mmol) of compound **5** (yield 87.5%).

In dry acetonitrile (18 mL) under nitrogen, 0.69 g (1.0 mmol) of compound **5** and 0.38 g (1.3 mmol) of 2-cyanoethyl *N*,*N*,*N'*,*N'*-tetraisopropylphosphorodiamidite were reacted with 95 mg (1.4 mmol) of 1*H*-tetrazole. Prior to the reaction, compound **5** and 1*H*-tetrazole were dried by coevaporation with dry acetonitrile (twice). After 2 h, the solvent was removed by evaporation and the crude mixture was dissolved in ethyl acetate. The solvent was washed with distilled water and saturated solution of $NaHCO_3$ and NaCl and dried over $MgSO_4$. After the removal the solvent, the crude mixture was subjected to silica gel column chromatography (Hexane : AcOEt : $Et_3N$= 60 : 40 : 3) to afford 0.60 g (0.70 mmol) of compound **6** (yield 66.9%).

**NMR and MS assignment**

**Compound 1 (4'-dimethylamino-2-nitroazobenzene-4-carboxylic acid, corresponding to R)**

(yield 99.4%): $^1$H NMR [DMSO-$d_6$, 500 MHz] δ = 8.45 (d, 1H, *J* = 2.0 Hz, aromatic proton), 8.27 (d, 1H, *J* = 8.5 Hz, aromatic proton), 7.84–7.81 (m, 3H, aromatic protons) 6.92 (dd, 2H, *J* = 9.5, *J* = 2.0 Hz, aromatic protons) 3.16 ppm (s, 6H, -N-(C$H_3$)$_2$)

FAB-LRMS: *m/z* calcd for $C_{15}H_{14}N^4O_4^+$: 315 ($M^+$+H); found: 315

**Compound 4 of R**

Silica gel column chromatography (Chloroform : MeOH = 10 : 1) (yield quant): $^1$H NMR [DMSO-$d_6$, 500 MHz] δ = 8.54 (d, 1H, *J* = 1.5 Hz, aromatic proton), 8.25 (m, 2H, aromatic proton and -N*H*-CO-), 7.83-7.81 (m, 3H, aromatic protons) 6.92 (dd, 2H, *J* = 9.5, *J* = 2.0 Hz, aromatic protons) 4.68 (m, 2H, -O*H*) 3.95 (m, 2H, HO-$CH_2$C*H*(NH-)C*H*(OH)$CH_3$) 3.65 and 3.55 (m, 2H, HO-C$H_2$CH(NH-)-) 3.16 (s, 6H, -N-(C$H_3$)$_2$) 1.11 ppm (d, 3H, $^3J$ = 6.5 Hz, -CH(OH)C$H_3$)

FAB-LRMS: *m/z* calcd for $C_{19}H_{23}N_5O_5^+$: 402 ($M^+$+H); found: 402

**Compound 5 of R**

Silica gel column chromatography (Hexane : AcOEt : $Et_3N$= 50 : 50 : 3) (yield 74.2%): $^1$H NMR [DMSO-$d_6$, 500 MHz] δ = 8.57 (d, 1H, *J* = 2.0 Hz, aromatic proton), 8.50 (d, 1H, $^3J$ = 9.0 Hz, -N*H*-CO-) 8.25 (dd, 1H, *J* = 8.5, *J* = 2.0 Hz aromatic proton), 7.86–7.81 (m, 3H, aromatic protons) 7.43 (d, H2, *J* = 7.0, aromatic protons) 7.28 (m, 6H, aromatic protons) 7.23 (m, 1H, aromatic protons) 6.93–6.88 (m, 6H, aromatic protons) 4.68 (m, 1H, -O*H*) 4.19 (m, 1H, DMT-O-$CH_2$C*H*(NH-)-) 4.07 (m, 1H, -C*H*(OH)$CH_3$) 3.76 (s, 6H, Ph-O-C$H_3$) 3.28 and 3.04 (m, 2H, DMT-O-C$H_2$CH(NH-)-) 3.16 (s, 6H, -N-(C$H_3$)$_2$) 1.07 ppm (d, 3H, $^3J$ = 6.5 Hz, -CH(OH)C$H_3$); $^{13}$C NMR [DMSO-$d_6$, 125 MHz] δ = 165.2, 159.0 (2C), 154.6, 147.4, 147.0, 146.1, 143.8, 136.8, 136.7, 135.6, 133.1, 130.6 (4C), 128.7 (4C), 127.5, 127.1 (2C), 123.9, 119.3, 114.0 (4C), 112.6 (2C), 86.1, 66.2, 64.0, 56.6, 55.9 (2C), 21.3 ppm

FAB-HRMS: *m/z* calcd for $C_{40}H_{42}N_5O_7^+$: 704.3006 ($M^+$+H); found: 704.3002

**Compound 6 of R**

$^{31}$P NMR [$CDCl_3$, 121 MHz] δ = 148.9, 148.7 ppm; FAB-HRMS: *m/z* calcd for $C_{49}H_{59}N_7O_8P^+$: 904.4085 ($M^+$+H); found: 904.4072

**Compound 2 (Ethyl 4'-methylthioazobenzene-4-carboxylate)**

Silica gel column chromatography (Hexane : AcOEt = 15 : 1) (yield 50.5%): $^1$H NMR [DMSO-$d_6$, 500 MHz] δ = 8.20 (d, 2H, *J* = 8.5 Hz, aromatic protons), 8.01 (d, 2H, *J* = 8.5 Hz, aromatic protons), 7.94 (d, 2H, *J* = 8.5 Hz, aromatic protons) 7.52 (d, 2H, *J* = 8.5 Hz, aromatic protons) 4.40 (q, 2H, $^3J$ = 7.0 Hz, $CH_3CH_2OCO$-) 2.62 (s, 3H, -S-$CH_3$) 1.40 ppm (t, 3H, $^3J$ = 7.0 Hz, $CH_3CH_2OCO$-)

FAB-LRMS: *m/z* calcd for $C_{16}H_{16}N_2O_2S^+$: 301 ($M^+$+H); found: 301

**Compound 3 (4'-methylthioazobenzene-4-carboxylic acid, corresponding to S)**

(yield 80.3%): $^1$H NMR [DMSO-$d_6$, 500 MHz] δ = 8.17 (d, 2H, *J* = 8.5 Hz, aromatic protons), 7.98 (d, 2H, *J* = 8.5 Hz, aromatic protons), 7.93 (d, 2H, *J* = 8.5 Hz, aromatic protons) 7.51 (d, 2H, *J* = 8.5 Hz, aromatic protons) 2.62 ppm (s, 3H, -S-$CH_3$)

FAB-LRMS: *m/z* calcd for $C_{14}H_{12}N_2O_2S^+$: 273 ($M^+$+H); found: 273

**Compound 4 of S**

Silica gel column chromatography (Chloroform : MeOH = 10 : 1) (yield 83.0%): $^1$H NMR [DMSO-$d_6$, 500 MHz] δ = 8.11 (d, 2H, *J* = 8.5 Hz, aromatic protons), 7.98 (m, 3H, aromatic protons and -N*H*-CO-), 7.93 (d, 2H, *J* = 8.5 Hz, aromatic protons) 7.51 (d, 2H, *J* = 8.5 Hz, aromatic protons) 4.69–4.66 (m, 2H, -O*H*) 3.97 (m, 2H, HO-$CH_2CH$(NH-)$CH$(OH)$CH_3$) 3.65 and 3.56 (m, 2H, HO-$CH_2$CH(NH-)-) 2.62 (s, 3H, -S-$CH_3$) 1.11 ppm (d, 3H, $^3J$ = 6.5 Hz, -CH(OH)$CH_3$)

FAB-LRMS: *m/z* calcd for $C_{18}H_{21}N_3O_3S^+$: 360 ($M^+$+H); found: 360

**Compound 5 of S**

Silica gel column chromatography (Hexane : AcOEt : $Et_3N$= 50 : 50 : 3) (yield 87.5%): $^1$H NMR [DMSO-$d_6$, 500 MHz] δ = 8.27 (d, 1H, $^3J$ = 8.5 Hz, -N*H*-CO-) 8.14 (d, 2H, *J* = 9.0 Hz, aromatic protons), 7.99 (d, 2H, *J* = 9.0 Hz, aromatic protons), 7.93 (d, 2H, *J* = 9.0 Hz, aromatic protons) 7.51 (d, 2H, *J* = 8.5 Hz, aromatic protons) 7.45–6.88 (m, 13H, aromatic protons) 4.66 (d, 1H, $^3J$ = 6.0 Hz, -O*H*) 4.18 (m, 1H, DMT-O-$CH_2$C*H*(NH-)-) 4.07 (m, 1H, -C*H*(OH)$CH_3$) 3.76 (s, 6H, -Ph-O-C$H_3$) 3.28 and 3.02 (m, 2H, DMT-O-C$H_2$CH(NH-)-) 2.62 (s, 3H, -S-C$H_3$) 1.07 ppm (d, 3H, $^3J$ = 6.5 Hz, -CH(OH)C$H_3$) ; $^{13}$C NMR [DMSO-$d_6$, 125 MHz] δ = 166.8, 158.9 (2C), 154.3, 150.0, 147.0, 146.1, 145.1, 137.6, 136.8, 136.7, 130.6 (4C), 129.6 (2C), 128.7 (4C), 127.5, 126.7 (2C), 124.3 (2C), 123.1 (C), 114.0 (4C), 86.1, 66.2, 63.9, 56.3, 55.9 (2C), 21.3, 15.1 ppm

FAB-HRMS: *m/z* calcd for $C_{39}H_{40}N_3O_5S^+$: 662.2610 ($M^+$+H); found: 662.2609

**Compound 6 of S**

$^{31}$P NMR [$CDCl_3$, 121 MHz] δ = 149.1, 148.6 ppm; FAB-HRMS: *m/z* calcd for $C_{48}H_{56}N_5O_6PS^+$: 862.3689 ($M^+$+H); found: 862.3665

## 3-7 Notes and References


1. T. Kobayashi, *J-aggregates*, World Scientific, Singapore, 1996.
2. (a) W. Lin, W. Lin, G. K. Wong and T. J. Marks, *J. Am. Chem. Soc.*, 1996, **118**, 8034; (b) O. R. Evans and W. Lin, *Acc. Chem. Res.*, 2002, **35**, 511; (c) E. L. Botvinick and J. V. Shah, *Methods Cell Biol.*, 2007, **82**, 81.
3. (a) S. Bahatyrova, R. N. Frese, C. A. Siebert, J. D. Olsen, K. O. van der Werf, R. van Grondelle, R. A. Niederman, P. A. Bullough, C. Otto and C. N. Hunter, *Nature*, 2004, **430**, 1058; (b) T. S. Balaban, N. Berova, C. M. Drain, R. Hauschild, X. Huang, H. Kalt, S. Lebedkin, J.-M. Lehn, F. Nifaitis, G. Pescitelli, V. I. Prokhorenko, G. Riedel, G. Smeureanu and J. Zeller, *Chem. Eur. J.*, 2007, **13**, 8411; (c) J. D. Olsen, J. D. Tucker, J. A. Timney, P. Qian, C. Vassilev and C. N. Hunter, *J. Biol. Chem.*, 2008, **283**, 30772.
4. (a) M. Kasha, *Radiat. Res.*, 1963, **20**, 55; (b) J. L. Seifert, R. E. Connor, S. A. Kushon, M. Wang and B. A. Armitage, *J. Am. Chem. Soc.*, 1999, **121**, 2987; (c) M. Wang, G. L. Silva and B. A. Armitage, *J. Am. Chem. Soc.*, 2000, **122**, 9977; (d) N. R. Conley, A. K. Pomerantz, H. Wang, R. J. Twieg and W. E. Moerner, *J. Phys. Chem. B*, 2007, **111**, 7929; (e) S. Ikeda and A. Okamoto, *Chem. Asian J.*, 2008, **3**, 958.
5. (a) K. Murata, S.-i. Kuroda and K. Saito, *Thin Solid Films*, 1997, **295**, 73; (b) B. Z. Packard, D. D. Toptygin, A. Komoriya and L. Brand, *J. Phys. Chem. B*, 1998, **102**, 752; (c) R. A. Garoff, E. A. Litzinger, R. E. Connor, I. Fishman and B. A. Armitage, *Langmuir*, 2002, **18**, 6330; (d) A. Yamaguchi, N. Kometani and Y. Yonezawa, *Thin Solid Films*, 2006, **513**, 125; (e) H. Bittermann, D. Siegemund, V. L. Malinovskii and R. Häner, *J. Am. Chem. Soc.*, 2008, **130**, 15285; (f) I. V. Astakhova, V. A. Korshun and J. Wengel, *Chem. Eur. J.*, 2008, **14**, 11010; (g) Y. N. Teo, J. N. Wilson and E. T. Kool, *J. Am. Chem. Soc.*, 2009, **131**, 3923.
6. Czikkely V., Dreizler G., Försterling H. D., Kuhn H., Sondermann J., Tillmann P. and Wiegand J. Z., *Z. Naturforsch.*, 1969, **24a**, 1821.
7. (a) S. Bernacchi and Y. Mély, *Nucleic Acids Res.*, 2001, **29**, e62; (b) S. Bernacchi, E. Piémont, N. Potier, A. v. Dorsselaer and Y. Mély, *Biophys. J.*, 2003, **84**, 643.
8. (a) S. Tyagi and F. R. Kramer, *Nat. Biotechnol.*, 1996, **14**, 303; (b) M. K. Johansson, H. Fidder, D. Dick and R. M. Cook, *J. Am. Chem. Soc.*, 2002, **124**, 6950; (c) E. Socher, L. Bethge, A. Knoll, N. Jungnick, A. Herrmann and O. Seitz, *Angew. Chem. Int. Ed*, 2008, **47**, 9555.
9. H. Kashida, H. Asanuma and M. Komiyama, *Angew. Chem. Int. Ed*, 2004, **43**,

6522.

10. There are two possible structures for the heterodimer, as shown in Scheme 3-1.
11. (a) C. Brotschi and C. J. Leumann, *Angew. Chem. Int. Ed*, 2003, **42**, 1655; (b) C. Brotschi, G. Mathis and C. J. Leumann, *Chem. Eur. J.*, 2005, **11**, 1911; (c) Z. Johar, A. Zahn, C. J. Leumann and B. Jaun, *Chem. Eur. J.*, 2008, **14**, 1080; (d) A. Zahn and C. J. Leumann, *Chem. Eur. J.*, 2008, **14**, 1087.
12. The melting temperature was measured in the presence of 100 mM NaCl at pH 7.0 (10 mM phosphate buffer). The concentration of NMR-**Ma**/NMR-**Zb** was 5 μM. The melting temperature of the duplex under NMR measurement conditions should be much higher because the concentrations of both NaCl and modified ODNs are higher: a) R. Owczarzy, Y. You, B. G. Moreira, J. A. Manthey, L. Huang, M. A. Behlke, J. A. Walder, *Biochemistry* **2004**, *43*, 3537; b) H. Long, A. Kudlay, G. C. Schatz, *J. Phys. Chem. B* **2006**, *110*, 2918.
13. M. Liu, X.-a. Mao, C. Ye, H. Huang, J. K. Nicholson and J. C. Lindon, *J. Magn. Reson.*, 1998, **132**, 125.
14. (a) E. Sawicki, *J. Org. Chem.*, 1957, **22**, 915; (b) R. K. Burkhard, R. D. Bauer and D. H. Klaassen, *Biochemistry*, 1962, **1**, 819; (c) T. Sueyoshi, N. Nishmura, S. Yamamono and S. Hasegawa, *Chem. Lett.*, 1974, **3**, 1131; (d) P. C. Chen, Y. C. Chieh and J. C. Wu, *J. Mol. Struct.*, 2005, **715**, 183.
15. Since the absorption spectra also slightly depended on the temperature being higher than the $T_m$ at which the duplex was dissociated into two single-strands, chromophore motion also affected the ground-state spectra slightly.
16. A. H. Herz, *Photogr. Sci. Eng.*, 1974, **18**, 323.
17. N. Berova and K. Nakanishi, *Circular Dichroism: Principles and Applications*, Wiley-VCH, New York, 2000.
18. This is what we call the H-band, which displays distinct hypsochromicity.
19. D. Sarkar, P. Das, S. Basak and N. Chattopadhyay, *J. Phys. Chem. B*, 2008, **112**, 9243.
20. X. Liang, H. Asanuma, H. Kashida, A. Takasu, T. Sakamoto, G. Kawai and M. Komiyama, *J. Am. Chem. Soc.*, 2003, **125**, 16408.
21. Since exciton splitting depended on the Dlmax between these dyes and DNA, the effect of natural base on the chromophore–chromophore splitting might be small. Furthermore, since the dye has already been located next to the natural base in the single strand, the adjacent natural base did not greatly affect the spectral change (exciton coupling) of incorporated dyes by hybridization.
22. K. Norland, A. Ames and T. Taylor, *Photogr. Sci. Eng.*, 1970, **14**, 295.

23. 久保淳一　2009 年度修士学位論文　名古屋大学大学院工学研究科物質制御工学専攻　「会合体形成で誘起された軌道間相互作用による色素の励起エネルギー変化」
24. (a) H. Asanuma, H. Kashida, X. Liang and M. Komiyama, *Chem. Commun.*, 2003, 1536; (b) H. Asanuma, K. Shirasuka, T. Takarada, H. Kashida and M. Komiyama, *J. Am. Chem. Soc.*, 2003, **125**, 2217.
25. (a) W. H. Nutting, R. A. Jewell and H. Rapoport, *J. Org. Chem.*, 1970, **35**, 505; (b) K. A. Bello and J. Griffiths, *Dyes Pigm.*, 1989, **11**, 65; (c) M. A. Rahim, P. N. P. Rao and E. E. Knaus, *J. Heterocycl. Chem.*, 2002, **39**, 1309.
26. H. Nishioka, X. Liang, H. Kashida and H. Asanuma, *Chem. Commun.*, 2007, 4354.

## 3-8 Appendixes

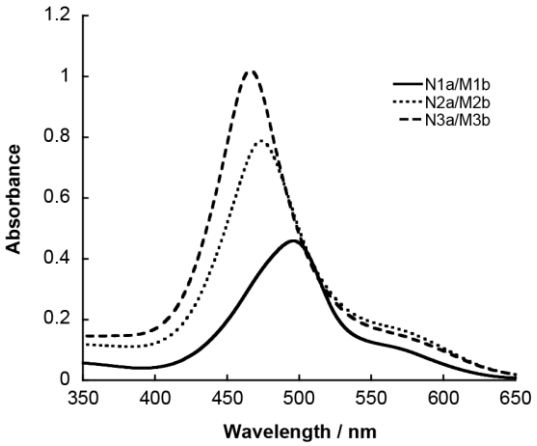


Appendix Figure 3-1. Effects of the size of aggregates on UV/Vis spectra of combinations of **N** and **M**. Solution conditions were as follows: 0 $^{o}$C, [ODN] = 5 μM, [NaCl] = 100 mM, pH 5.0 (10 mM MES buffer).

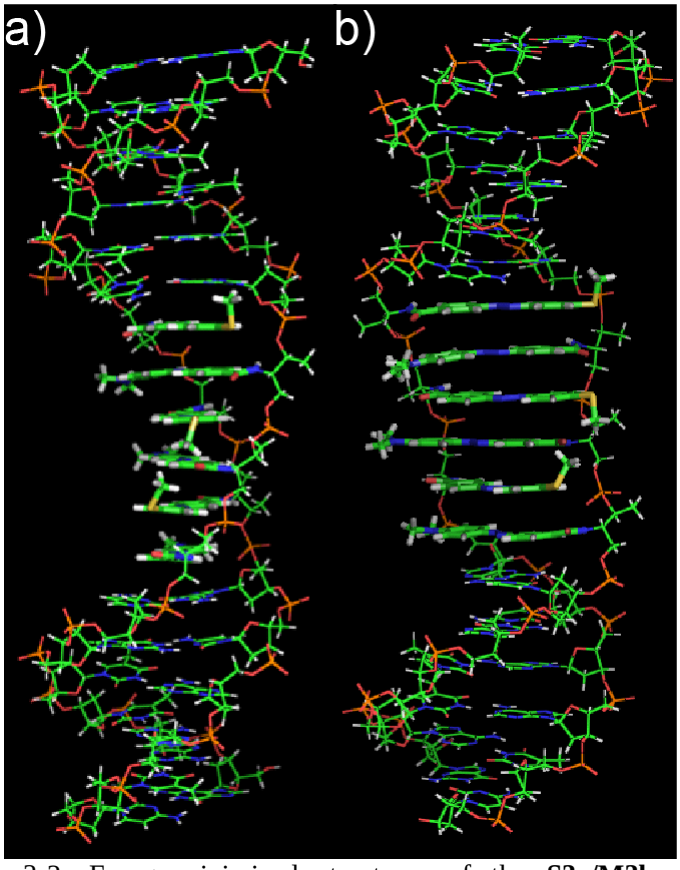


Appendix Figure 3-2. Energy-minimized structures of the **S3a/M3b** duplex involving 4'-methylthioazobenzene and Methyl Red (sticks part) calculated with InsightII/Discover3. a): View from long axis of dye residues, b): View from short axis of dye residues.

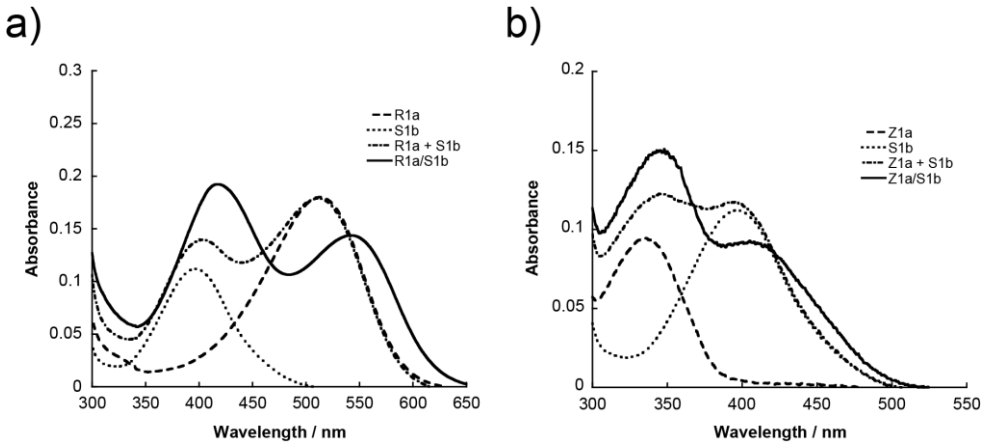


Appendix Figure 3-3. a) UV/Vis spectra of the **R1a/S1b** duplex (solid line), single-stranded **R1a** (broken line), **S1b** (dotted line), and a simple sum of their spectra (sum-spectrum, **R1a + S1b**, dashed-dotted line) at 0 °C. b) UV-Vis spectra of the **Z1a/S1b** duplex (solid line), single-stranded **Z1a** (broken line), **S1b** (dotted line), and a simple sum of their spectra (sum-spectrum, **Z1a + S1b**, dashed-dotted line) at 0 °C. Solution conditions were as follows: [ODN] = 5 μM, [NaCl] = 100 mM, pH 7.0 (10 mM phosphate buffer).

Appendix Table 3-1. Melting temperature ($T_m$) of double-stranded DNA-dye conjugates.

| | $T_m$ / °C [a] | | | | | |
|---|---|---|---|---|---|---|
| ***n*** | **Z*n*a/M*n*b** | **S*n*a/M*n*b** | **R*n*a/M*n*b** | **R*n*a/S*n*b** | **R*n*a/Z*n*b** | **Z*n*a/S*n*b** |
| **0 (N/C)** | | | 47.7 | | | |
| **1** | 47.6 [b] | 51.2 | 49.9 | 51.4 | 49.2 | 49.9 |
| **2** | 47.7 [b] | 52.7 | 51.0 | 54.1 | 50.5 | 51.7 |
| **3** | 52.7 [b] | 58.5 | 56.2 | 58.7 | 53.1 | 54.9 |

a) Measurement conditions were pH 7.0: [ODN] = 5 μM, [NaCl] = 100 mM (10 mM phosphate buffer), at 0 °C.
b) These data were showed in chapter 2.
**N** : 5'-GGT-ATC-GCA-ATC-3'
**C** : 3'-CCA-TAG-CGT-TAG-5'
**X*n*a** : 5'-GGT-ATC-(**X**)$_n$-GCA-ATC-3'
**X*n*b** : 3'-CCA-TAG-(**X**)$_n$-CGT-TAG-5' **X** = **M**, **R**, **S**, **Z**

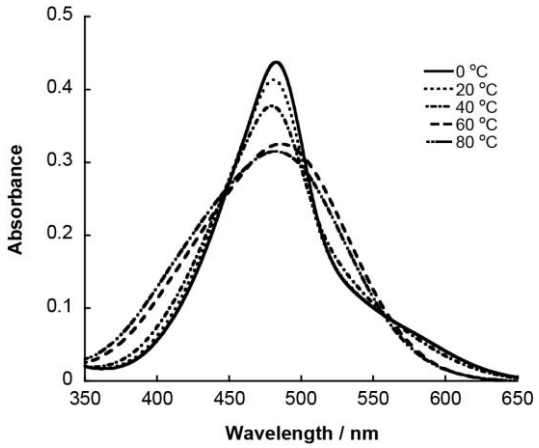


Appendix Figure 3-4. Effect of temperature on the absorption spectrum of **R1a/M1b**. Solution conditions were as follows: [ODN] = 5 μM, [NaCl] = 100 mM, pH 7.0 (10 mM phosphate buffer).

Appendix Table 3-2 $T_m$ of all homo combinations.[a)]

| | $T_m$ [°C] | | | |
|---|---|---|---|---|
| *n* | **Z*n*a/Z*n*b** | **M*n*a/M*n*b** | **S*n*a/S*n*b** | **R*n*a/R*n*b** |
| 0 | | 47.7 | | |
| 1 | 50.5 | 50.5 | 52.4 | 49.2 |
| 2 | 51.2 | 51.7 | 53.8 | 51.6 |
| 3 | 54.5 | 58.0 | 59.2 | 54.7 |

a) Solution conditions: [ODN] = 5 μM, [NaCl] = 100 mM, pH 7.0 (10 mM phosphate buffer)

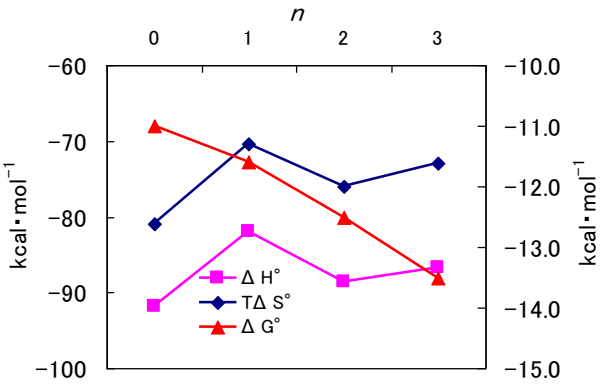


Appendix Figure 3-5. Plots of $\Delta H^o$, $T\Delta S^o$ and $\Delta G^o_{37}$ in **S*n*a/M*n*b**. T = 315.15 K (37 °C). *n* = 0 indicates **N/C**.

Appendix Table 3-3. Thermodynamic parameters of hetero and homo aggregates.

| Sequence | Wavelength | $\Delta H^o$ / kcal・mol$^{-1}$ | $\Delta S^o$ / cal・K・mol$^{-1}$ | $\Delta G^o_{37}$ [a)] / kcal・mol$^{-1}$ | $\Delta\Delta G^o_{37}$ / kcal・mol$^{-1}$ |
|---|---|---|---|---|---|
| **N/C** | | -91.9 | -261 | -11.0 | — |
| **S1a/M1b** | | -82.0 | -227 | -11.6 | -0.6 |
| **S2a/M2b** | 260 nm | -88.6 | -245 | -12.5 | -1.5 |
| **S3a/M3b** | | -86.7 | -235 | -13.5 | -2.5 |
| **M3a/M3b** | | -84.4 | -230 | -13.0 | -2.0 |
| | | | | | |
| **S1a/M1b** | 380 nm | -82.5 | -229 | -11.6 | — |
| **S2a/M2b** | 470 nm | -86.7 | -240 | -12.2 | -0.6 |
| **S3a/M3b** | 460 nm | -83.5 | -227 | -13.2 | -1.6 |
| **M3a/M3b** | 490 nm | -82.7 | -225 | -12.8 | -1.3 |

a) $\Delta G^o_{37}$ is change of Gibbs free energy at 37 $^o$C (310 K).

Appendix Table 3-4. $T_m$ of **S1a/M1b**.[a)]

| Concentration / μM | 260 nm / $^o$C | 380 nm / $^o$C |
|---|---|---|
| 1 | 47.4 | 47.4 |
| 2 | 48.9 | 48.9 |
| 4 | 50.6 | 50.6 |
| 6 | 51.6 | 51.3 |
| 16 | 54.9 | 54.5 |
| 24 | 56.0 | 56.0 |
| 32 | 56.1 | 56.0 |
| 64 | 57.5 | 57.4 |

a) [NaCl] = 100 mM, pH 7.0 (10 mM phosphate buffer)

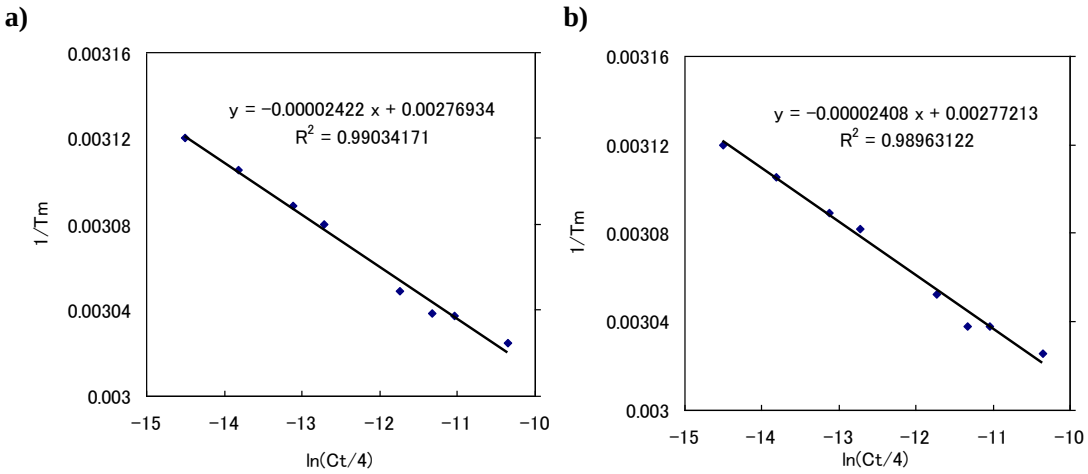


Appendix Figure 3-6. Van't Hoff plot of **S1a/S1b**. a) : 260 nm, b) : 380 nm.

Appendix Table 3-5. $T_m$ of **S2a/M2b**.[a)]

| Concentration / μM | 260 nm / °C | 470 nm / °C |
|---|---|---|
| 1 | 50.2 | 49.4 |
| 2 | 51.6 | 50.8 |
| 4 | 53.3 | 52.5 |
| 6 | 54.4 | 53.6 |
| 16 | 56.7 | 56.0 |
| 24 | 57.8 | 57.0 |
| 32 | 58.2 | 57.6 |
| 64 | 60.2 | 59.6 |

a) [NaCl] = 100 mM, pH 7.0 (10 mM phosphate buffer)

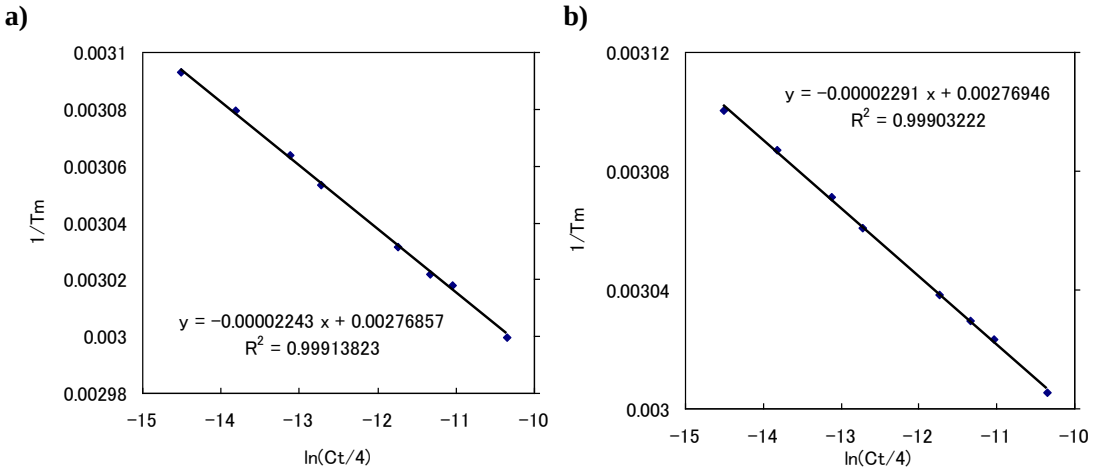


Appendix Figure 3-7. Van't Hoff plot of **S2a/M2b**. a) : 260 nm, b) : 470 nm.

Appendix Table 3-6. $T_m$ of **S3a/M3b**.[a)]

| Concentration / μM | 260 nm / °C | 460 nm / °C |
|---|---|---|
| 1 | 54.5 | 53.8 |
| 2 | 56.2 | 55.4 |
| 4 | 57.9 | 57.1 |
| 6 | 58.7 | 58.1 |
| 16 | 61.3 | 60.6 |
| 24 | 62.6 | 61.8 |
| 32 | 63.4 | 62.7 |
| 64 | 64.9 | 64.8 |

a) [NaCl] = 100 mM, pH 7.0 (10 mM phosphate buffer)

**a)** **b)**

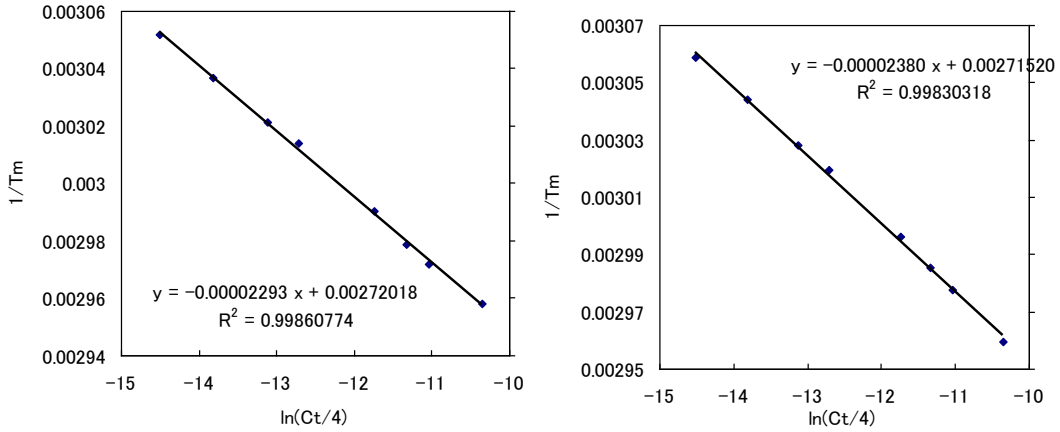


Appendix Figure 3-8. Van't Hoff plot of **S3a/M3b**. a) : 260 nm, b) : 460 nm.

# Chapter 4. Development of a Highly Sensitive In-Stem Molecular Beacon by Coherent Quenching of a Fluorophore

## 4-1 Abstract

To establish novel guideline to design an optimal fluorophore-quencher pair for efficient quenching of a fluorophore, relationship between excitonic interaction and quenching efficiency of a fluorophore was systematically investigated. Various heterodimers, in which a fluorophore and quencher were stacked alternately, were prepared by hybridizing two oligodeoxyribonucleotides (ODNs), each of which tethered a different dye on D-threoninol at the center of the strand. Thiazole orange or pentamethylindocarbocyanine (Cy3) were used as a fluorophore and four kinds of azobenzen derivatives were also used as a quencher. The spectroscopic behaviors of these heterodimers were systematically examined as a function of the difference in the wavelength of the dye absorption maxima ($\Delta\lambda_{max}$). In the case of using each fluorophore, $\Delta\lambda_{max}$ of the dimers negatively correlated with coherency (excitonic interaction) between the fluorophore and quencher as well as chapter 3. On the other hand, the coherency positively correlated with quenching efficiency of the fluorophore. From these spectral analyses, we conclude that minimizing the $\Delta\lambda_{max}$ maximizes quenching efficiency of the fluorophore due to maximization of the coherency. Finally, we introduced the fluorophore-quencher pair based on the design into the stem region of a molecular beacon (In-stem Molecular Beacon) targeting the survivin gene. As the results, we could attain signal/background ratio of as high as 70 by the efficient suppression of background emission due to the enhancement of excitonic interaction.

## 4-2 Introduction

Fluorescence-labeled oligonucleotides provide powerful tools for highly sensitive, sequence-specific detection of target DNA/RNA.[1] A variety of fluorescent probes have been designed for purposes such as genotyping of individuals, identification of pathogens, and real-time monitoring of mRNA within cells.[2] One practical problem with the use of these fluorescent probes is background emission intensity in the absence of the target, because background emission, as well as scattered light of excitation due to a small Stokes shift, critically affects probe sensitivity.[3] Suppression of background emission is particularly important for the design of a highly sensitive molecular beacon (MB); that is, a hairpin oligonucleotide dual-labeled at both 5'- and 3'-termini with a fluorophore and a quencher.[4] Therefore, efforts have been made to efficiently quench a fluorophore in a closed MB.[5]

There are two types of energy transfer that will efficiently quench fluorescence: Förster (dynamic) quenching and contact (static) quenching.[6] The former requires a fluorophore-quencher pair that has sufficient spectral overlap between the emission spectrum of the fluorophore and the absorption spectrum of the quencher, and allows relatively long range (10–100 Å) quenching.[7] The latter is based on the formation of a ground state complex of a fluorophore and a dark quencher by their direct contact,[8] which is favorable for an MB. In this case, a change in their absorption spectra often occurs due to excitonic interaction (coherency). However, Marras also pointed out that any non-fluorescent quencher can be an efficient acceptor for contact quenching.[3] We have already established a novel method for the preparation of a heterodimer or cluster by hybridization of two oligonucleotides, each of which had dyes tethered to D-threoninols (termed threoninol nucleotides) in chapter 2 and 3. The use of

D-threoninol as a scaffold facilitated dimerization or clustering of the dyes in the duplex. Our laboratory have utilized this base surrogate (threoninol nucleotide) to develop a new in-stem molecular beacon (ISMB) in which both fluorophore (perylene) and quencher (anthraquinone) on D-threoninols are incorporated into the stem region as a pseudo base pair (Scheme 4-1a).[9] Direct and strong contact of perylene with the quencher in the stem efficiently removed background emission in the closed ISMB and allowed discrimination of fully matched and one-base deletion mutant pairs. In this case, the absorption spectrum of perylene showed only a slight change with any quencher that we tested, showing that coherency (excitonic interaction) between the perylene and the quenchers was poor. Nevertheless, quenching was very strong, indicating that strong contact by pseudo base-pairing dominated the efficient quenching. However, as Johansson et al. proposed previously,[6, 10] stronger coherency (that is, excitonic interaction or ground-state complexation) should enhance the quenching and further

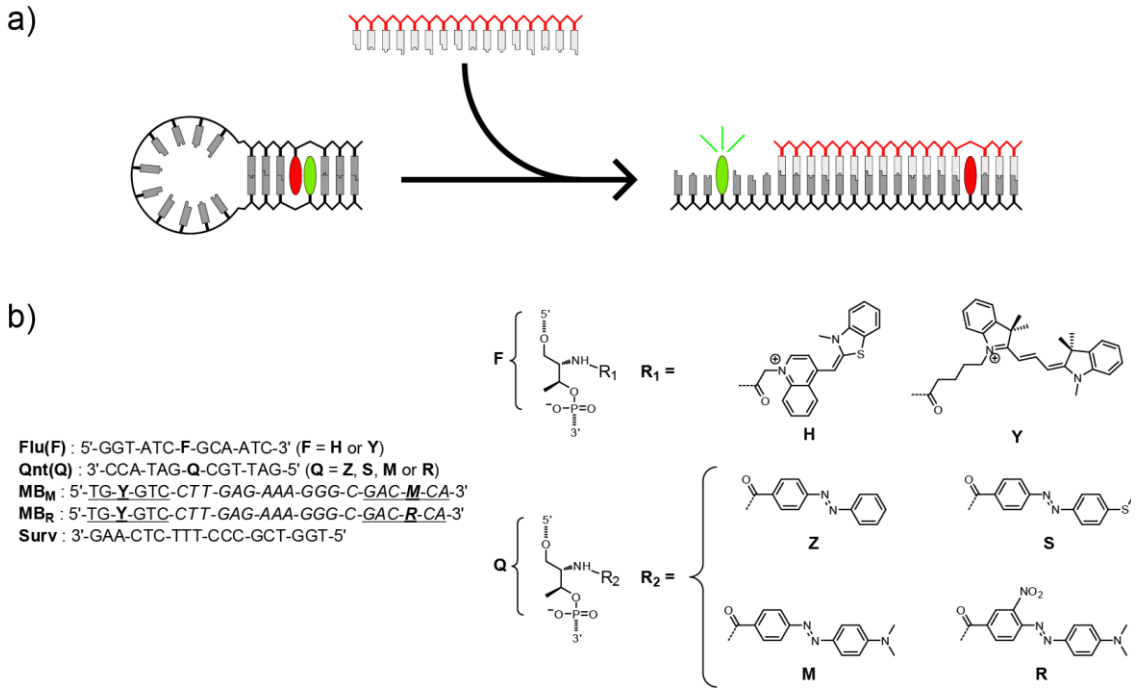


Scheme 4-1. a) An in-stem molecular beacon (ISMB), and b) the chemical structure of the dyes and sequences of the modified DNAs. In the MB sequences, the bases in the stem part are underlined and the complementary bases to the target sequence are italicized.

increase the sensitivity of the probe.

In this chapter, which works towards the design of a highly sensitive ISMB, the effect of coherency (excitonic interaction) on the quenching of a fluorophore was systematically examined using azobenzene derivatives as quenchers. In chapter 3, we have previously experimentally verified the molecular exciton theory using threoninol nucleotides involving azo dyes that have different absorption maxima, and found that heterodimerization induced hyperchromism of the band of shorter wavelength (in-phase transition), but hypochromism of the band of longer wavelength (out-of-phase transition; Scheme 4-2). Herein, we used Thiazole Orange (**H**) and Cy3 (**Y**) as fluorophores (Scheme 4-1b), because these are of known practical use in the labeling of biomolecules,[5b, 11] and are expected to have stronger coherency with azo dyes than perylene due to large absorption coefficient. By systematically varying the absorption maxima of azo dyes with a similar structure as shown in Fig. 4-1 (see Scheme 4-1b for the structures), the quenching efficiency was maximized, resulting in a more sensitive ISMB.

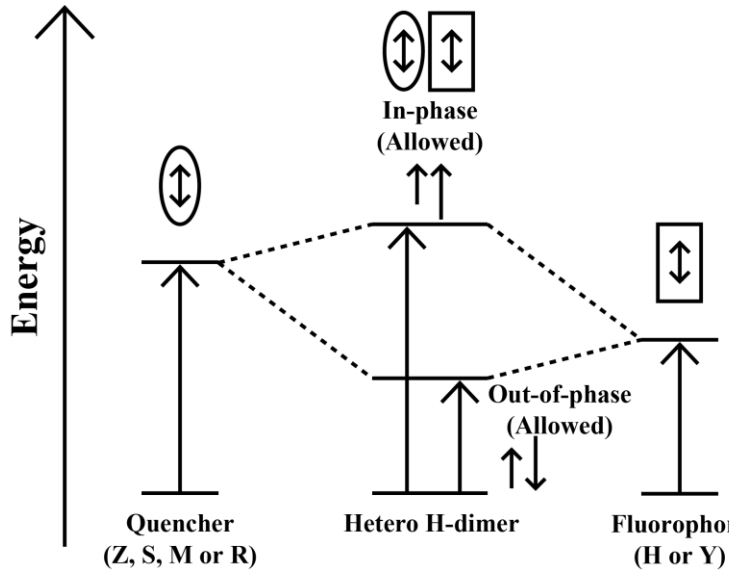


Scheme 4-2. Energy diagram of the heterodimer of fluorophore and quencher depicted on the basis of the exciton model. Each arrow, outlined by an ellipse or an oblong, designates the transition dipole moment.

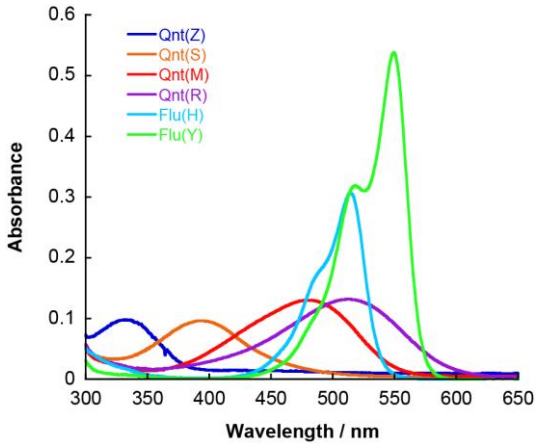


Figure 4-1. UV/Vis spectra of single-stranded **Flu(H)**, **Flu(Y)**, **Qnt(Z)**, **Qnt(S)**, **Qnt(M)**, and **Qnt(R)** at 20 $^{o}$C. Solution conditions were as follows: [DNA] = 4 μM, [NaCl] = 100 mM, pH 7.0 (10 mM phosphate buffer).

## 4-3 Results

### 4-3-1 Duplex stabilities of the heterodimers with the fluorophore and quencher

We used four kinds of quencher (azo) dyes which have different absorption maxima such as azobenzene (**Z**), 4'-methylthioazobenzene (**S**), Methyl Red (**M**) and 4'-dimethylamino-2-nitroazobenzene (**R**), and we also used two kinds of fluorophores such thiazole orange (**H**) and Cy3 (**Y**). First, in order to confirm stable pseudo "base-pairing" (hetero-dimerization) of the fluorophore and quencher in DNA duplex, we measured the duplex stabilities of the dimers. $T_m$s of the dimers are shown in Table 4-1. Compared with $T_m$ of native one, **H-Q** pairing induced a little stabilization to the duplexes while **Y-Q** paring did a little destabilization. This tendency is different

Table 4-1. Effect of pseudo "base-pairing" of a fluorophore and a quencher on the melting temperature of the duplex.

| Quencher | $T_m$ of **Flu(F)/Qnt(Q)** / $^{o}$C | |
|---|---|---|
| (**Qnt(Q)**) | **F = H** | **F = Y** |
| **Q = Z** | 46.3 | 47.2 |
| **S** | 47.7 | 46.9 |
| **M** | 48.5 | 45.2 |
| **R** | 49.7 | 44.6 |

[a] [**Flu(F)**] = [**Qnt(Q)**] = 4 μM, [NaCl] = 100 mM, pH 7.0 (10 mM phosphate buffer).

from the results of the dimers between azo dyes in chapter 2 and 3 due to addition of the alkyl chain between the chromophore and the amido bond.[5o] However, each dimer had enough stability to investigate fluorescent spectra of the duplex and use as a probe in room temperature (20 $^{o}$C).

4-3-2 Spectroscopic behaviors of heterodimer with a fluorophore and quencher

***Investigation of relationship between $\Delta\lambda_{max}$ and coherency***

The used azobenzene derivatives (**Q** = **Z**, **S**, **M**, **R**) in Qnt showed a $\lambda_{max}$ at 334, 394, 480, and 513 nm, respectively, whereas **H** and **Y** in Flu showed a $\lambda_{max}$ at 516 and 550 nm in single-stranded DNAs at 20 $^{o}$C (Fig. 4-1). What we expect for the UV/Vis spectra of Flu/Qnt duplexes based on the molecular exciton theory (Scheme 4-2) is as follows: when the quencher that has a higher transition energy is excitonically coupled with a fluorophore of lower transition energy, the excited state splits into two energy levels. The higher energy level corresponds to the in-phase transition in which the transition

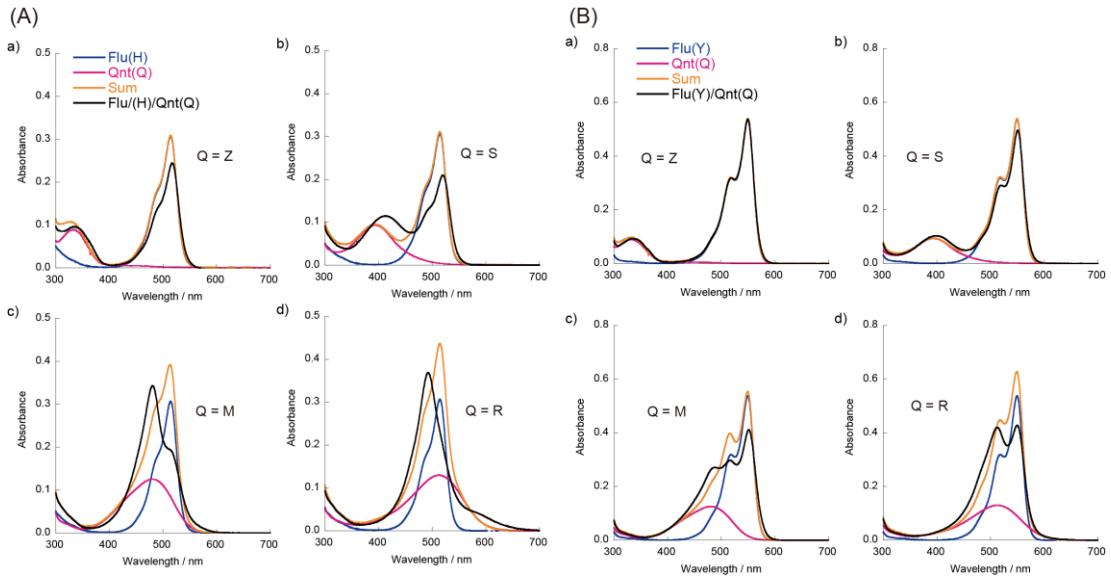


Figure 4-2. UV/Vis spectra of Flu(**F**)/Qnt(**Q**) with A) **F** = **H**, B) **F** = **Y**. Sum: a simple sum of the spectra. Solution conditions: [Flu(**F**)] = 4 μm, [Qnt(**Q**)] = 4 μm, [NaCl]=100 mm, pH 7.0 (10 mm phosphate buffer); 20 $^{o}$C.

dipole moments of the quencher and fluorophore have the same direction. In this case, the energy level becomes higher than that of quencher due to the repulsive interaction between the two transition dipoles. The absorption coefficient of the in-phase transition is expected to increase due to the sum of the transitions quencher and fluorophore. In contrast, the energy level of the out-of-phase transition becomes lower than that of fluorophore due to the attractive interaction. However, the absorption coefficient of this transition decreases because the transition moment is partially cancelled due to its antiparallel orientation. The above excitonic interaction (namely coherency) is enhanced when the gap between the transition energies of quencher and fluorophore, this is, $\Delta\lambda_{max}$, decreases. To evaluate coherency, the absorption spectrum of Flu(X)/Qnt(Y) duplexes was compared to that of the individual single strands. The degree of coherency can be estimated from the hypochromicity (decrease in absorbance) of the absorption band of **H** (516 nm at 20 $^{o}$C) or of **Y** (550 nm), which is at longer wavelengths than that of the quenchers.[12] Figure 4-2A shows the UV/Vis spectra of Flu(**H**)/Qnt(**Q**) duplexes, Flu(**H**) and Qnt(**Q**) single strands, and a spectrum calculated as the simple sum of the two single strands. When **Z** was used as a quencher, the spectral change between the summation spectrum and the Flu(**H**)/Qnt(**Z**) duplex was small (orange and black lines in Fig. 4-2A(a)); that is, hypochromicity induced by hybridization was small. However, hypochromicity increased as the $\Delta\lambda_{max}$ between the **H** and the quencher decreased. In the case of the **H** and **R** combination, the UV/Vis spectrum of the Flu(**H**)/Qnt(**R**) duplex was entirely different from that of the summation spectrum (orange and black lines in Fig. 4-2A(d)): the band of Flu(**H**) at 516 nm and that of Qnt(**R**) at 513 nm almost disappeared in Flu(**H**)/Qnt(**R**), and a new strong band and weak shoulder band appeared at 492 and 590 nm, respectively.[13,14] This large change in the UV/Vis spectrum, namely

the hypochromicity of the **H** band, was attributed to the strong coherency (excitonic interaction or ground-state complexation) of **H** and **R**, because the $\Delta\lambda_{max}$ between the two dyes was as small as 3 nm. Similar results were obtained using Cy3: strong hypochromism occurred with **M** and **R** (Fig.s 4-2B(c) and 4-2B(d), respectively), although this hypochromism was smaller than that of **H** due to the larger $\Delta\lambda_{max}$ (37 nm for **R** and 70 nm for **M**). No spectral change was induced when Flu(**Y**) was combined with Qnt(**Z**), because the $\Delta\lambda_{max}$ was as large as 216 nm (note that the Flu(**Y**)/Qnt(**Z**) spectrum almost completely overlapped with that of the summation spectrum; Fig. 4-1B(a)). This spectroscopic behavior agreed with our previous results and above expectation based on the model shown in Scheme 4-2.

***Investigation of relationship between coherency and quenching efficiency***

Next, the quenching efficiency of this model Flu/Qnt duplex was evaluated. As shown in Fig.s 4-3a and 4-3b, all the quenchers that were tested dramatically quenched emission from **H** or **Y** in the Flu/Qnt duplex, demonstrating that close stacking of a

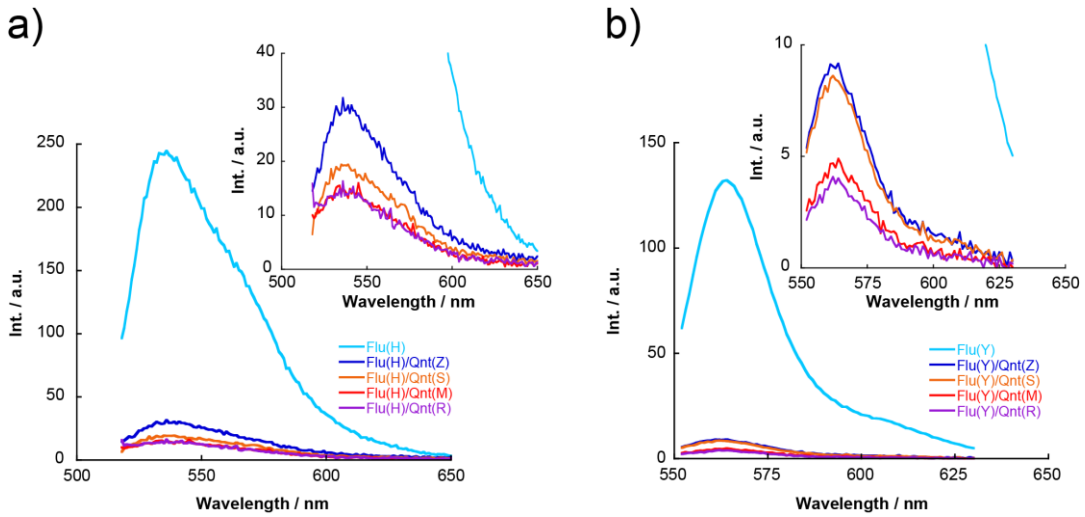


Figure 4-3. Fluorescence emission spectra of a) Flu(**H**) excited at 516 nm and b) Flu(**Y**) excited at 546 nm, and their duplexes with Qnt(**Q**). Solution conditions: [Flu(**F**)] = 0.2 μm, [Qnt(**Q**)] = 0.4 μm, [NaCl] = 100 mm, pH 7.0 (10 mm phosphate buffer); 20 $^{o}$C.

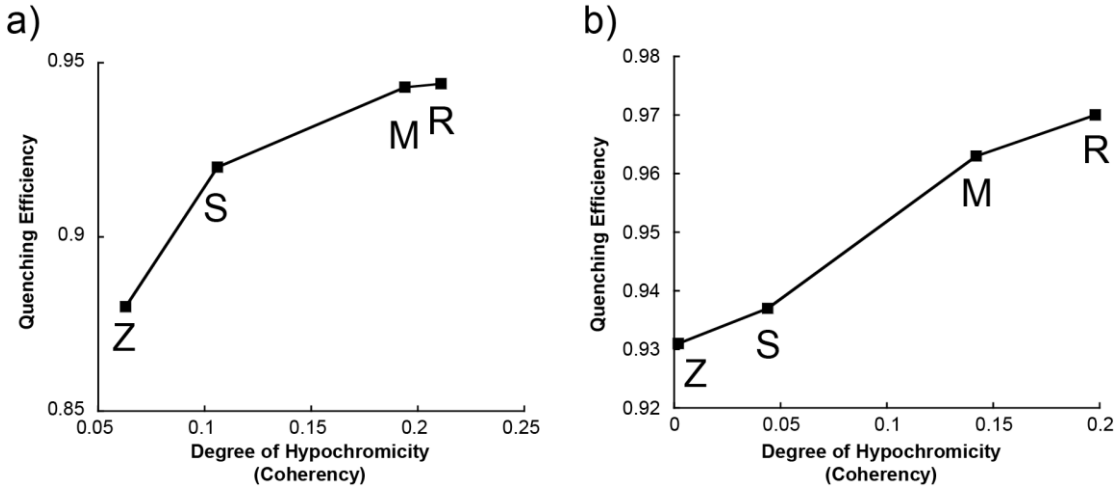


Figure 4-4. Relationship between the degree of hypochromicity based on the coherency (excitonic interaction) and quenching efficiency for (a) **H** and (b) **Y**. Quenching efficiency (vertical axis) was evaluated from the ratio of fluorescence intensity of **Flu(F)/Qnt(Q)** duplex with respect to that of single-stranded **Flu(F)** monitored at 546 (**F** = **H**, excited at 516 nm) or 564 nm (**F** = **Y**, excited at 546 nm). See Appendix Table 4-1 for the actual values.

fluorophore and a quencher on D-threoninols facilitates quenching. Compared with fluorescent intensity of the each dimer, the efficiency of **H** quenching was in the order: **R**>**M**>**S**>**Z**. Moreover, Cy3 was quenched by azo dyes in a similar order: **R**>**M**>**S**>**Z**. These results obviously demonstrate that the quenching efficiency depended on the type of quencher that was used. Herein, we plotted the quenching efficiency as a function of coherency in Fig. 4-4. The coherency (Degree of hypochromicity (abscissa axis)) was evaluated from the difference of absorbance (hypochromicity) between the simple sum of **Flu(F)** and **Qnt(Q)** (sum-spectrum, corresponding to orange line in Fig. 4-2) and **Flu(F)/Qnt(Q)** duplex (corresponding to black line in Fig. 4-2) at 516 nm (**F** = **H**) or 550 nm (**Q** = **Y**). The efficiency of both **H** and **Y** quenching followed the order of the coherency: **R**>**M**>**S**>**Z**. Therefore, the coherency positively correlated with quenching efficiency of the fluorophore.

### 4-3-3 Development of a highly sensitive In-Stem Molecular Beacon

Based on the above experiments, we chose **R** or **M** as a quencher of Cy3 to design an

ISMB (Scheme 4-1) targeting the survivin gene.[15] We designed the ISMB as sharing **R** or **M** strand of the stem region with the target **Surv**, a synthetic 18 nucleotide-long DNA (see Scheme 4-1b for the sequence), because sharing of **Y** or **H** strand (that is, intercalation of **Y** or **H**) reduced its fluorescence (data not shown). As the $T_m$ of $\mathbf{MB_R}$ was determined to be 63.1 °C,[16] $\mathbf{MB_R}$ was available below 60 °C, where the MB was closed in the absence of the target. Figure 4-5a depicts the fluorescence emission spectra of $\mathbf{MB_R}$ involving a **Y** and **R** pair at the stem region in the presence and absence of the target at 20 °C. The ratio of the fluorescence intensities of $\mathbf{MB_R}$ with and without the target ($I_{open}/I_{close}$) at 564 nm was as high as 70 under the conditions employed.[17] This high sensitivity was attributed to effective quenching of the **Y** emission. We also tested an $\mathbf{MB_M}$ bearing **M** (Dabcyl) that is used as a conventional quencher, and found that $I_{open}/I_{close}$ was as high as 30 (Fig. 4-5b). However, this value was still less than half that obtained with $\mathbf{MB_R}$. Undoubtedly, strong coherency (excitonic interaction) facilitated the quenching that strongly enhanced the sensitivity of the ISMB.[18]

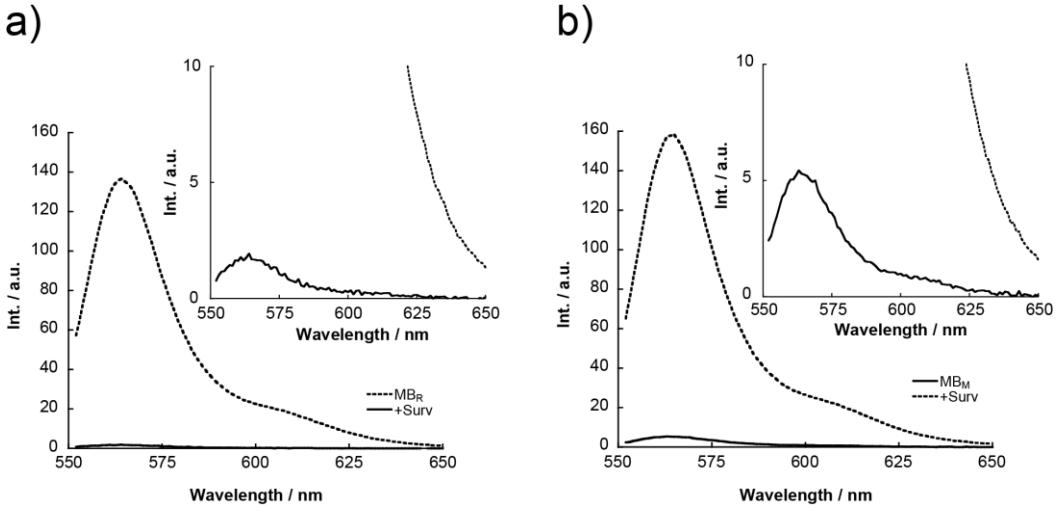


Figure 4-5. Fluorescence emission spectra of a) $\mathbf{MB_R}$ and b) $\mathbf{MB_M}$ excited at 546 nm with (a dotted line) and without (solid line) the presence of **Surv**. Solution conditions: [$\mathbf{MB_R}$] = [$\mathbf{MB_M}$] = 0.2 μm, [Surv] = 0.4 μm, [NaCl] = 100 mm, pH 7.0 (10 mm phosphate buffer); 20 °C.

## 4-4 Discussion

### 4-4-1 Effect of the duplex stabilities on quenching efficiency

To examine the effect of duplex stability on the quenching efficiency, relationship between the melting temperature and quenching efficiency of the Flu/Qnt duplex was investigated (Table 4-1). In the case of Flu(**H**)/Qnt(**Q**), the $T_m$ decreased with **Q** in the order **R**>**M**>**S**>**Z**, which coincided with the order of quenching efficiency. However, combination of these quenchers with Flu(**Y**) completely reversed the order of the $T_m$ decrease with **Q** to **Z**>**S**>**M**>**R**. Therefore, a contribution of the stability of the Flu/Qnt duplex to the quenching efficiency appears to be unlikely. These results strongly suggest that coherency between the fluorophore and the quencher and also direct contact of the fluorophore-quencher pair significantly contribute to effective quenching. Thus D-threoninol may be an ideal scaffold for the pairing of a fluorophore and a quencher because their close contact in the duplex facilitates ground state complexation (that is, coherency or excitonic interaction) to allow rapid electron (or hole) transfer to the quencher. It can now be concluded that to maximize the quenching efficiency $\Delta\lambda_{max}$, the difference in the absorption maxima between the fluorophore and the quencher should be minimized to enhance the coherency.[19]

### 4-4-2 Emitting and quenching elements

To investigate which elements contribute the emission or quenching, we measured the excitation spectra of the dimers and compared them with their absorption spectra as shown in Fig. 4-6. The excitation spectrum of the Flu(**H**)/Qnt(**R**) duplex was very similar in shape to the excitation and absorption spectra of Flu(**H**), demonstrating that the heterodimer did not emit fluorescence at all. Accordingly, this result indicates that

the emitting elements mainly derived from the monomer state of the fluorophore. On the other hand, the quenching can occur through various processes according to past reports, though we strongly believe that the excitonic interaction largely contributes quenching of the fluorophore. Then, effects of other factors on the quenching need to be investigated in order to exclude the effects. In the following sections, we discussed the effects on quenching of the fluorophore.

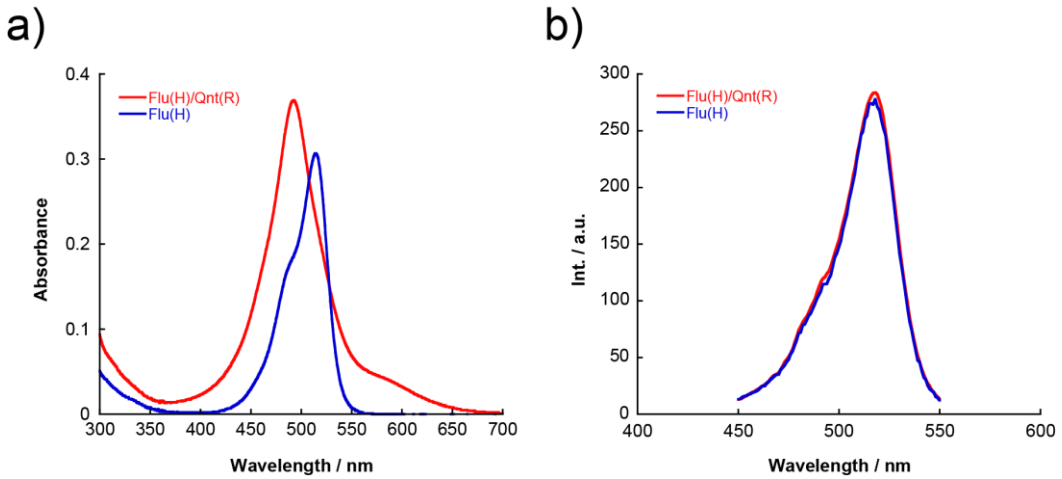


Figure 4-6. Absorption a) and fluorescence excitation b) spectra of the single-stranded **Flu(H)** (blue) and **Flu(H)/Qnt(R)** duplex (red). Conditions for the measurement of absorption spectra: [**Flu(H)**] = [**Qnt(R)**] = 4 μM, [NaCl] = 100 mM, pH 7.0 (10 mM phosphate buffer), 20 $^{o}$C. Conditions for the measurement of fluorescence excitation spectra: [**Flu(H)**] = 2 μM, [**Qnt(R)**] = 4 μM, [NaCl] = 100 mM, pH 7.0 (10 mM phosphate buffer), 20 $^{o}$C, Emission wavelength = 570 nm, Sensitivity mode: **Flu(H)** = medium, **Flu(H)/Qnt(R)** = high.

### *Effect of energy transfer*

In general, FRET (fluorescence resonance energy transfer) is one of the important factors for quenching of a fluorophore.[7, 20] When dyes contact with each other, relationship between energy levels of the fluorophore and quencher is significant for quenching of the fluorophore, because FRET mainly occurs through Dexter mechanism.[21] Because of this, we calculated the HOMO and LUMO energy levels of the dyes by Gaussian 09 as shown in Appendix Table 4-3.[22] If the quenching is mainly performed by Dexter mechanism, HOMO and LUMO energy levels of two dyes should

take following relationship: ${}^{f}E_{HOMO} < {}^{q}E_{HOMO} < {}^{q}E_{LUMO} < {}^{f}E_{LUMO}$. However, the relative relationship between the dyes which were used in this chapter was completely different: ${}^{f}E_{HOMO} < {}^{q}E_{HOMO} < {}^{f}E_{LUMO} < {}^{q}E_{LUMO}$. This difference suggests that electron exchange reaction between dyes is difficult and Dexter FRET gives only a minor contribution to quenching of the fluorophore in this case.

On the other hand, overlap area between a fluorescent spectrum of the fluorophore and an absorption spectrum of the quencher is also important for the quenching at the viewpoint of another mechanism (Förster mechanism). Figure 4-7 shows fluorescent spectra of the fluorophores and absorption spectra of the quenchers with monomer states. The overlap between **H** emission and **M** or **R** absorption was a little large while **H** emission and **Z** or **S** absorption was hardly overlapped. If the quenching is mainly performed by Förster FRET, quenching efficiencies of **H-R** pair should be much larger than those of **H-Z** and **H-S** pairs, which should be almost the same, while that of **H-M** pair should be medium value. Certainly, the efficiency of **H-R** pair was the largest in all combination of the quenchers. However, the quenching efficiency of **H-S** pair was much

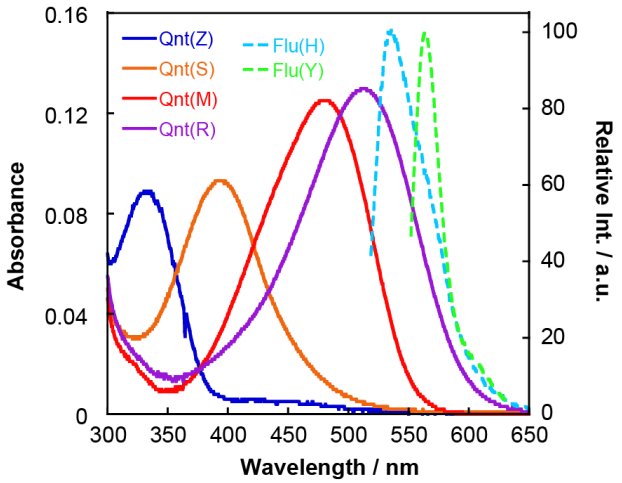


Figure 4-7. Absorption and fluorescence emission spectra of the single-stranded **Qnt(Q)** (solid lines) and **Flu(F)** (broken lines), respectively. Conditions for the measurement of absorption spectra: [**Qnt(Q)**] = 4 μM, [NaCl] = 100 mM, pH 7.0 (10 mM phosphate buffer), 20 °C. Conditions for the measurement of fluorescence emission spectra: [**Flu(F)**] = 2 μM, [NaCl] = 100 mM, pH 7.0 (10 mM phosphate buffer), 20 °C, Excitation wavelength = 510 nm (**Flu(H)**), 546 nm (**Flu(Y)**).

larger than that of **H-Z** pair and that of **H-M** pair was only a slight lower than that of **H-R** pair, obviously demonstrating that quenching efficiency largely depended on excitonic interaction. In addition, these facts indicate that effect of Förster FRET is relatively low than that of excitonic interaction. Moreover, the same tendency was observed in the case of using Cy3 as a fluorophore. Therefore, contribution of Förster FRET for quenching of the fluorophore might be low in these dimers.

***Effect of electron transfer***

Photo-induced electron transfer is known as one of the quenching mechanisms between different dyes.[21, 23] This quenching largely depends on distance between dyes and their combination. Thus, quenching by PET is one of the important factors in the case of hetero dye-clustering. According to energy diagram in Appendix Table 4-3, electron transfer in all Flu(**F**)/Qnt(**Q**) pairs should take a reductive way. Accordingly, HOMO energy levels of quenchers should be important for the quenching because an electron in HOMO of a quencher transfers to HOMO orbital with an excited fluorophore. To compare with energy level of each quencher, the order of HOMO energy levels was following: **M>R>S>Z**. This order does not coincide with the order of the quenching efficiency and a clear correlation was not observed between their HOMO energy levels and the quenching efficiency. Therefore, we can conclude effect of PET should slightly contribute to determination of the order of quenching efficiency between the quenchers.

## 4-5 Conclusions

In conclusion, we successfully developed a novel fluorophore-quencher design for

the efficient quenching by use of excitonic interaction. As a result, large excitonic interaction (coherency) was utilized to design a highly sensitive ISMB. Based on the results of a systematic study, we conclude that minimizing the $\Delta\lambda_{max}$ maximizes quenching efficiency due to maximization of coherency. This strategy can be used for any fluorescent probes based on fluorophore-quencher dimers and clusters.

## 4-6 Experimental Section

### 4-6-1 Materials

See 2-6-1 because the contents are the same.

### 4-6-2 Synthesis of DNA modified with **H**, **M**, **R**, **S**, **Y** or **Z**

All the modified DNAs were synthesized using an automated DNA synthesizer (ABI-3400 DNA synthesizer, Applied Biosystems) using conventional and dye-carrying phosphoramidite monomers. Azobenzene, 4'-methylthioazobenzene, Methyl Red, and 4'-dimethylamino-2-nitroazobenzene phosphoramidite monomers were synthesized according to chapter 3. The compounds thiazole orange and Cy3 synthesized according to the literature, were converted to phosphoramidite monomers as described in the section 4-6-6 (Scheme 4-3 and 4-4)[24,25]. The coupling efficiency of the monomers with modified residues was as high as that of the conventional monomers as judged from the intensity of the color of the released trityl cation. Modified **Flu(F)** and **Qnt(Q)** DNAs were purified by reversed-phase HPLC, whereas $\mathbf{MB_M}$ and $\mathbf{MB_R}$ were first purified by PAGE and were then further purified by reversed phase HPLC. All the modified DNAs were characterized by MALDI-TOF mass spectrometry (Autoflex II, Bruker Daltonics).

The MALDI-TOFMS data, observed (Obsd.) versus calculated (Calcd.), for the monomers were:

**Qnt(Z)**: Obsd. m/z 4019 (Calcd. for [**Qnt(Z)**+$H^+$]: m/z 4020); **Qnt(S)**: Obsd. m/z 4066 (Calcd. for [**Qnt(S)**+$H^+$]: m/z 4066); **Qnt(M)**: Obsd. m/z 4065 (Calcd. for [**Qnt(M)**+$H^+$]: m/z 4063); **Qnt(R)**: Obsd. m/z 4108 (Calcd. for [**Qnt(R)**+$H^+$]: m/z 4108); **Flu(H)**: Obsd. m/z 4141 (Calcd. for [**Flu(H)**+$H^+$]: m/z 4142); **Flu(Y)**: Obsd. m/z 4233 (Calcd. for [**Flu(Y)**+$H^+$]: m/z 4236); $\mathbf{MB_M}$: Obsd. m/z 8124 (Calcd. for [$\mathbf{MB_M}$ +$H^+$]: m/z 8121); $\mathbf{MB_R}$: Obsd. m/z 8165 (Calcd. for [$\mathbf{MB_R}$ +$H^+$]: m/z 8166).

4-6-3 Spectroscopic measurements

The UV-Vis were measured on a JASCO model V-550 spectrophotometer and and Shimadzu UV-1800 instruments with a 10 mm quartz cell. Fluorescent spectra were measured with a JASCO model FP-6500 with a microcell. The excitation wavelength was 510 nm for thiazole orange and 546 nm for Cy3. All models were equipped with programmable temperature controllers. The conditions of the sample solutions were as follows (unless otherwise noted): [NaCl] = 100 mM, pH 7.0 (10 mM phosphate buffer), [DNA] = 4 μM. All samples of DNA-dye conjugates were heated at 80 °C for 5 min in the dark to thermally isomerize the *cis*-form, which might be photo-isomerized by ambient light, to the *trans*-form before spectroscopic measurement.[26]

4-6-4 Measurement of melting temperature

See 2-6-1 because the procedures are the same. The conditions of the sample solutions were the same as those described for the above spectroscopic measurements.

4-6-5 Computer calculation

Calculation of HOMO and LUMO energy levels was performed with the Gaussian 09 software (Gaussian, Inc.) on PC with the operating system windows XP and TD-DFT method pbe1pbe/6-31g(d) was used for the calculations. Validity of the calculation results were investigated by checking each vibration level and comparing with UV/Vis spectra of single-stranded DNA-dye conjugates (corresponding monomer states).

4-6-6 Syntheses of phosphoramidite monomers

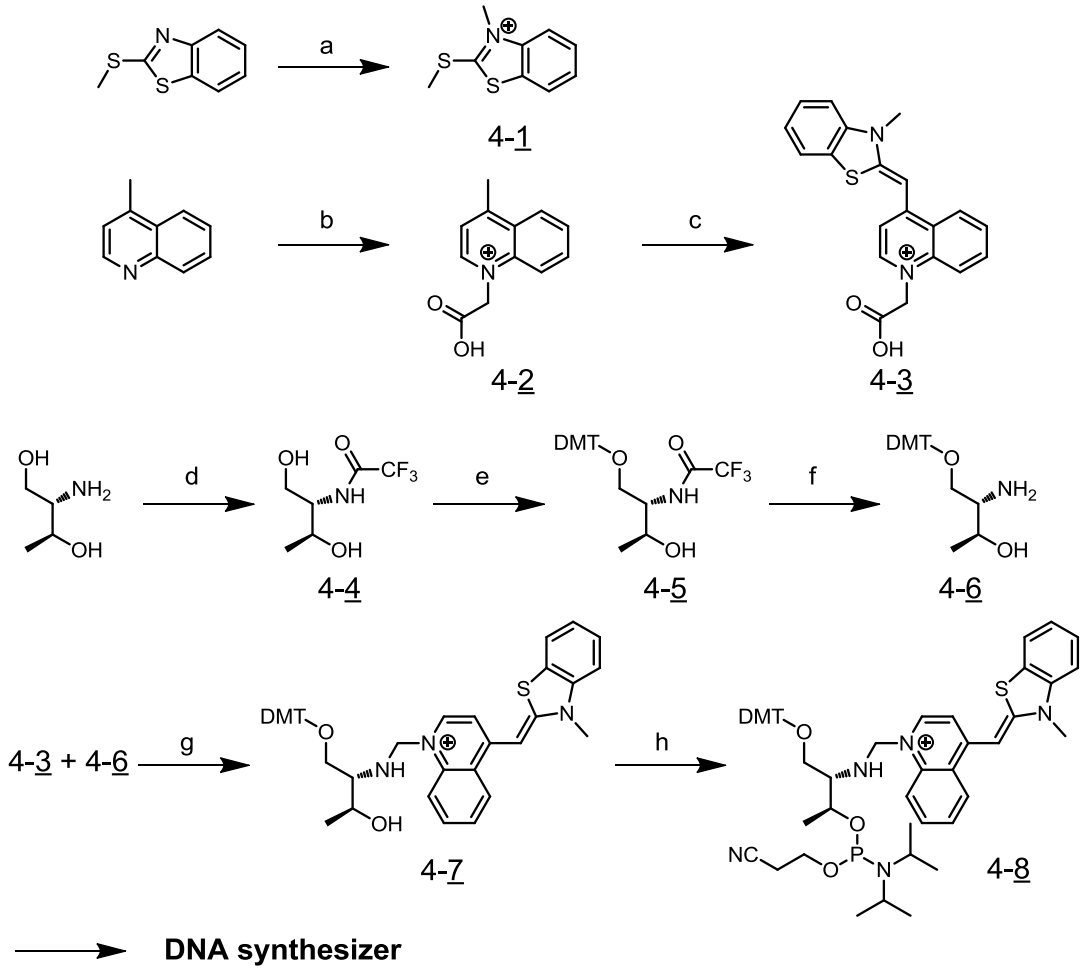


Scheme 4-3. Synthesis of modified DNAs tethering Thiazole Orange (**H**). Reagents and conditions: a) $CH_3I$, EtOH, 50 $^oC$, 5h, 40%; b) bromoacetic acid, EtOAc, DMF, r.t., 27%; c) Compound **1**, $Et_3N$, dry EtOH, NaI, under $N_2$, 60 $^oC$ →r.t., 78 %; d) $CF_3COOC_2H_5$, dry MeOH, 0→r.t., 92%; e) DMT-Cl, DIEA, DMAP, $CH_2Cl_2$, pyridine, 0→r.t., 82 %; f) $NH_3$, EtOH/$H_2O$, r.t. 3 days, 80%; g) PyBOP, DIPEA, DMF, r.t., overnight, 83%; h) $(i Pr_2N)_2PO(CH_2)_2CN$, 1*H*-tetrazole, $CH_3CN$, 0→r.t., 1.5h, 31 %

**Synthesis of Compound 3**

To ethanol solution (15 mL) of 2-(methylthio)benzothiazole (6.0 g, 33 mmol) was added iodomethane (4.1 mL, 67 mmol), followed by refluxing at 50 $^oC$ for 5 h to afford 4.3 g (22 mmol) of compound **1** (yield, 40 %) as precipitate.

To ethyl acetate solution (10 mL) of bromoacetic acid (6.1 g, 44 mmol) was added

4-methylquinoline (5.7 mL, 43 mmol), followed by stirring the reaction mixture for overnight to afford 3.3 g (12 mmol) of compound **2** (yield, 27%) as precipitate.

Compounds **1** (4.0 g, 12 mmol) and **2** (4.0, 14 mmol) were suspended in dry ethanol (10 mL) and stirred under nitrogen at 60 $^{o}$C, followed by the addition of triethylamine (5 mL). After the color of the reaction mixture turned deep red, sufficient amount of NaI was added. Then the solvent was removed by evaporation and the crude mixture was subjected silica gel column chromatography ($CHCl_3$: MeOH =5:1) to afford 4.6 g (9.7 mmol) of compound **3** (yield, 78%).

**Synthesis of Compound 6**

D-Threoninol (1.0 g, 9.5 mmol) was dissolved into dry methanol (15 mL) in an ice bath, followed by the dropwise addition of ethyl trifluoroacetate (1.3 mL, 1.5 g, 10.5 mmol). After stirring for 2h at 0 $^{o}$C, the solvent and excess ethyl trifluoroacetate was removed by evaporation to afford 1.8 g (8.8 mmol) of compound **4** (yield, 92%).

Dry pyridine (20 mL) solution containing compound **4** (1.8 g, 8.8 mmol) and diisopropylethylamine (1.7 mL, 1.4 g, 10.5 mmol) was cooled on ice under nitrogen, and 4,4'-dimethoxytrityl chloride (3.6 g, 10.5 mmol) and 4-dimethylaminopyridine (0.16 g, 1.3 mmol) in 15 mL of dry dichloromethane was added to the above mixture. After 2.5 h of stirring at room temperature, the solvent was removed, followed by silica gel column chromatography (Hexane : AcOEt : $Et_3N$= 80 : 20 : 3) to afford 3.6 g (7.2 mmol) of compound **5** (yield 82%).

To an ethanol solution (100 mL) containing compound **5** (3.6 g, 7.2 mmol) was added 28% aqueous ammonia (200 mL). After stirring the resulting reaction mixture for 3 days at room temperature, the solvent was removed by evaporation to afford crude oily compound **6** (yield ~80%), which was directly used for the next reaction.

**Synthesis of Compound 7**

To DMF solution (10 mL) containing compound **3** (0.86 g, 1.8 mmol), PyBOP (1.3 g, 2.5 mmol), and DIPEA (1 mL) was added DMF solution (5 mL) of compound **6** (1.0 g, 2.5 mmol). Then the resulting reaction mixture was stirred at room temperature for overnight. After the precipitate was removed by filtration, the filtrate was evaporated and the obtained solid was subjected to silica gel column chromatography ($CHCl_3$ : MeOH = 5:1) to afford 1.3 g (1.5 mmol) compound **7** (yield, 83%).

**Synthesis of Compound 8**

In dry acetonitrile (5 mL) under nitrogen, compound **7** (1.5 g, 1.73 mmol) and 2-cyanoethyl *N,N,N',N'*-tetraisopropylphosphordiamidite (0.78 mL, 2.4 mmol) were reacted with 170 mg (2.5 mmol) of 1*H*-tetrazole. Prior to the reaction, compound **7** and 1*H*-tetrazole were dried by coevaporation with dry acetonitrile (three times). After 1.5 h, the solvent was removed by evaporation and the crude mixture was subjected to silica gel column chromatography ($CHCl_3$ : MeOH = 10 : 1) to afford 0.57 g (0.54 mmol) of compound **8** (yield, 31%), which was immediately used for the DNA synthesis. The coupling efficiency of the compound **8** was not high (~50%) as judged from the coloration of the released trityl cation, even though it was purified by column chromatography.

**NMR assignments**

**Compound 1:** 1H-NMR [DMSO, 500 MHz] δ = 8.42-7.75 (m, 4H, aromatic protons), 4.15 (s, 3H, =N(C*H*$_3$)), 3.17 (s, 3H, -S(C*H*$_3$)

MS(FAB): m/z 196 (MH)+ (calcd. 196)

**Compound 3:** 1H-NMR [DMSO, 500 MHz] δ = 8.80-7.42 (m, 10H, aromatic protons), 6.94 (s, 1H, -C*H*=), 4.86 (s, 2H, -C*H*$_2$COOH), 4.02 (s, 3H, =$NCH_3$)

MS(FAB): m/z 349 (MH)+ (calcd. 349)

**Compound 4:** 1H-NMR [DMSO, 500 MHz] δ = 8.90 (d, 1H, *J* = 9.0 Hz, -N*H*CO-), 4.74 (d, 1H, *J* = 5.5, -O*H*), 4.73 (d, 1H, *J* = 5.5, -O*H*), 3.84 (m, 1H, -C*H*($CH_3$)OH), 3.75 (m, 1H, >C*H*NHCO-), 3.59-3.47 (m, 2H, -C$H_2$OH), 1.05 (d, 3H, *J* = 6.5 Hz, -CH(C$H_3$)OH)

MS(FAB): m/z 202 (M-H+) (calcd. 202)

**Compound 5:** 1H-NMR [DMSO, 500 MHz] δ = 9.30 (d, 1H, *J* = 8.5 Hz, -N*H*CO-), 7.40-6.91 (m, 13H, aromatic protons of DMT), 4.74 (d, 1H, *J* = 5.5, -O*H*), 3.92 (m, 2H, -C*H*($CH_3$)OH, >C*H*NHCO-), 3.77 (s, 6H, -OC$H_3$), 3.19 (dd, 1H, *J* = 9.5, 4.0 Hz, -C$H_2$ODMT), 2.99 (dd, 1H, *J* = 9.5, 6.5 Hz, -C$H_2$ODMT) 0.96 (d, 3H, *J* = 6.0 Hz, -CH(C$H_3$)OH)

MS(FAB): m/z 503 (M-H+) (calcd. 503)

**Compound 6:** 1H-NMR [DMSO, 500 MHz] δ = 7.76 (br, 2H, -N$H_2$), 7.46-6.93 (m, 13H, aromatic protons of DMT), 5.37 (br, 1H, -O*H*), 3.86 (m, 1H, -C*H*($CH_3$)OH), 3.78 (s, 6H, -OC$H_3$), 3.32 (dd, 1H, *J* = 10.0 Hz, 4.0 Hz, -C$H_2$ODMT), 3.02 (m, 2H, -C*H*2ODMT, >C*H*(NH2)) 0.94 (d, 3H, *J* = 6.5 Hz, -CH(C$H_3$)OH)

**Compound 7:** 1H-NMR [$CDCl_3$, 500 MHz] δ = 7.99 (d, 1H, *J* = 8.5 Hz, aromatic proton), 7.91 (d, 1H, *J* = 6.5 Hz, aromatic proton), 7.55-7.09 (m, 15H, aromatic protons, -N*H*CO), 7.05 (t, 1H, *J* = 8.5 Hz, aromatic proton), 6.72 (m, 4H, aromatic protons), 6.64 (d, 1H, *J* = 7.0 Hz, aromatic proton), 6.11 (s, 1H, >C*H*=), 5.14 (d, 1H, *J* = 16.0, >N-C$H_2$-CO-), 4.92 (d, 1H, *J* = 16.0, >N-C$H_2$-CO-), 4.10 (m, 1H, -C*H*($CH_3$)OH), 3.94 (m, 1H, -C*H*NHCO-), 3.69 (s, 6H, -OC$H_3$), 3.56 (s, 3H, >NC$H_3$), 3.27-3.13 (m, 2H, -C$H_2$ODMT), 1.02 (d, 2H, *J* =6.0 Hz, -CH(C$H_3$)OH)

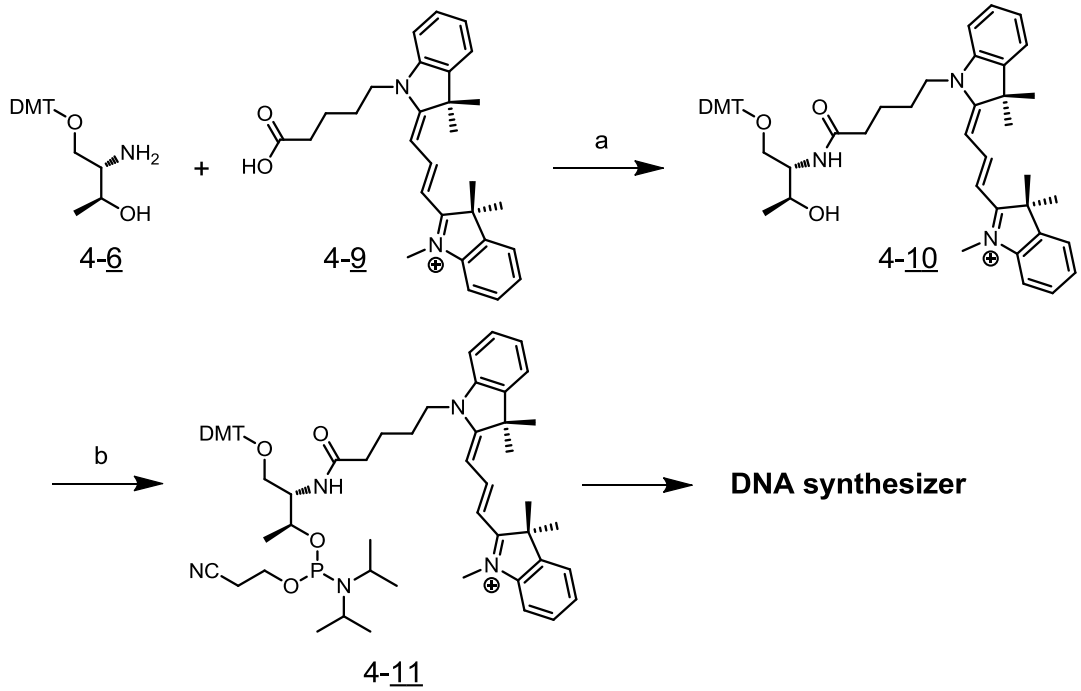


Scheme 4-4. Synthesis of modified DNAs tethering **Cy3**. Reagents and conditions: a) PyBOP, $Et_3N$, DMF, r.t., overnight; b) $(i Pr_2N)_2PO(CH_2)_2CN$, 1*H*-tetrazole, $CH_3CN$, 0→r.t., 1.5h, 56%

**Synthesis of Compound 10**

**Cy3** having carboxylate group (compound **9**) was synthesized by the same procedure reported previously.[27] To DMF solution (10 mL) containing compound **9** (0.57 g, 1.0 mmol), PyBOP (0.62 g, 1.2 mmol), and triethylamine (10 mL) was added DMF solution (5 mL) of compound **6** (0.41 g, 1.0 mmol) and the resulting reaction mixture was stirred at room temperature for overnight. After the precipitate was removed by filtration, the filtrate was evaporated and the obtained solid was subjected to silica gel column chromatography ($CHCl_3$ : MeOH = 1:0 → 30:1→ 10:1) to afford 1.0 g (1.0 mmol) compound **10** (yield, quant.).

**Synthesis of Compound 11**

In dry acetonitrile (5 mL) under nitrogen, compound **10** (8.0 g, 8.3 mmol) and 2-cyanoethyl *N*,*N*,*N'*,*N'*-tetraisopropylphosphordiamidite (4.6 mL, 14 mmol) were

reacted with 880 mg (12.5 mmol) of 1*H*-tetrazole. Prior to the reaction, compound **10** and 1*H*-tetrazole were dried by coevaporation with dry acetonitrile (three times). After 1.5 h, the solvent was removed by evaporation and the crude mixture was subjected to silica gel column chromatography ($CHCl_3$ : MeOH = 10 : 1) to afford 4.8 g (4.7 mmol) of compound **11** (yield, 56%), which was immediately used for the DNA synthesis. The coupling efficiency of the compound **11** was also not high (~50%) as judged from the coloration of the released trityl cation, even though it was purified by column chromatography.

**NMR assignments**

**Compound 9:** 1H-NMR [$CDCl_3$, 500 MHz] δ = 8.34 (t, 1H, *J* = 4.85 Hz, -CH=C*H*-CH=), 7.32-7.10 (m, 8H, aromatic protons), 6.94 (m, 2H, -C*H*=CH-C*H*=), 4.13 (m, 2H, >N-C$H_2$-), 3.67 (s, 3H, >N-C$H_3$), 2.40-1.82 (m, 6H, -(C$H_2$)$_3$-COOH), 1.62 (s, 6H, >C(C$H_3$)$_2$), 1.61 (s, 6H, >C(C$H_3$)$_2$)

MS(FAB): m/z 443 (MH)+ (calcd. 443)

**Compound 10:** 1H-NMR [$CDCl_3$, 500 MHz] δ = 8.42 (t, 1H, *J* = 4.85 Hz, -CH=C*H*-CH=), 7.48-6.81 (m, 22H, aromatic protons, -N*H*CO-), 4.25-4.12 (m, 3H, >N-C$H_2$-, -C*H*($CH_3$)OH)), 3.99 (m, 1H, -C*H*NHCO-), 3.76 (s (overlapped), 6H, >N-C$H_3$, -OC$H_3$), 3.74 (s, 3H, -OC$H_3$), 3.35 (dd, 1H, *J* = 4.5 Hz, *J* = 9 Hz, -C$H_2$-ODMT), 3.20 (dd, 1H, *J* = 4.5 Hz, 15.5 Hz, -C$H_2$-ODMT) 2.40-1.82 (m, 6H, -(C$H_2$)$_3$ –(C=O)-), 1.72 (s, 6H, >C(C$H_3$)$_2$), 1.71 (s, 6H, >(C$H_3$)$_2$), 1.15 (d, 3H, J = 6.5 Hz, -CH(C$H_3$)OH)

MS(FAB): m/z 349 (MH)+ (calcd. 349)

## 4-7 Notes and References


1. (a) E. T. Kool, *Acc. Chem. Res.*, 2002, **35**, 936; (b) A. A. Martí, S. Jockusch, N. Stevens, J. Ju and N. J. Turro, *Acc. Chem. Res.*, 2007, **40**, 402.
2. W. Tan, K. Wang and T. J. Drake, *Curr. Opin. Chem. Biol.*, 2004, **8**, 547.
3. S. Marras, *Mol. Biotechnol.*, 2008, **38**, 247.
4. S. Tyagi and F. R. Kramer, *Nat. Biotechnol.*, 1996, **14**, 303.
5. (a) O. Seitz, *Angew. Chem. Int. Ed*, 2000, **39**, 3249; (b) S. Tyagi, S. A. E. Marras and F. R. Kramer, *Nat. Biotechnol.*, 2000, **18**, 1191; (c) B. Dubertret, M. Calame and A. J. Libchaber, *Nat. Biotechnol.*, 2001, **19**, 365; (d) H. Du, M. D. Disney, B. L. Miller and T. D. Krauss, *J. Am. Chem. Soc.*, 2003, **125**, 4012; (e) C. J. Yang, H. Lin and W. Tan, *J. Am. Chem. Soc.*, 2005, **127**, 12772; (f) C. J. Yang, M. Pinto, K. Schanze and W. Tan, *Angew. Chem. Int. Ed*, 2005, **44**, 2572; (g) L. Wang, C. J. Yang, C. D. Medley, S. A. Benner and W. Tan, *J. Am. Chem. Soc.*, 2005, **127**, 15664; (h) C. Crey-Desbiolles, D.-R. Ahn and C. J. Leumann, *Nucleic Acids Res.*, **2005**, **33**, e77; (i) D. M. Kolpashchikov, *J. Am. Chem. Soc.*, 2006, **128**, 10625; (j) Y. Kim, C. J. Yang and W. Tan, *Nucleic Acids Res.*, 2007, **35**, 7279; (k) T. N. Grossmann, L. Röglin and O. Seitz, *Angew. Chem. Int. Ed*, 2007, **46**, 5223; (l) E. Socher, L. Bethge, A. Knoll, N. Jungnick, A. Herrmann and O. Seitz, *Angew. Chem. Int. Ed*, 2008, **47**, 9555; (m) S. Nakayama, L. Yan and H. O. Sintim, *J. Am. Chem. Soc.*, 2008, **130**, 12560; (n) E. Socher, D. V. Jarikote, A. Knoll, L. Röglin, J. Burmeister and O. Seitz, *Anal. Biochem.*, 2008, **375**, 318; (o) S. Berndl and H.-A. Wagenknecht, *Angew. Chem. Int. Ed*, 2009, **48**, 2418.
6. M. K. Johansson and R. M. Cook, *Chem. Eur. J.*, 2003, **9**, 3466.
7. T. Förster, *Ann. Phys.*, 1948, **2**, 55.
8. J. R. Lakowicz, *Principles of Fluorescence Spectroscopy*, 2nd edn., Springer, New York, 1999.
9. H. Kashida, T. Takatsu, T. Fujii, K. Sekiguchi, X. Liang, K. Niwa, T. Takase, Y. Yoshida and H. Asanuma, *Angew. Chem. Int. Ed*, 2009, **48**, 7044.
10. M. K. Johansson, H. Fidder, D. Dick and R. M. Cook, *J. Am. Chem. Soc.*, 2002, **124**, 6950.
11. (a) W. Algar, M. Massey and U. Krull, *J. Fluoresc.*, 2006, **16**, 555; (b) R. B. Mujumdar, L. A. Ernst, S. R. Mujumdar, C. J. Lewis and A. S. Waggoner, *Bioconjugate Chem.*, 1993, **4**, 105; (c) G. A. Korbel, G. Lalic and M. D. Shair, *J. Am. Chem. Soc.*, 2000, **123**, 361; (d) O. Seitz, F. Bergmann and D. Heindl, *Angew. Chem. Int. Ed*, 1999, **38**, 2203; (e) F. Menacher, M. Rubner, S. Berndl

and H.-A. Wagenknecht, *J. Org. Chem.*, 2008, **73**, 4263.

12. Quantitatively evaluated degree of hypochromicity (coherency) and quenching efficiency for the Flu(**F**)/Qnt(**Q**) duplex are summarized in Appendix Table 4-1.
13. This large spectral change is explained from the molecular exciton theory. In the case of the Flu(**H**)/Qnt(**R**) or Flu(**H**)/Qnt(**M**) combinations, strong excitonic interaction due to the small $\Delta\lambda_{max}$ induced large blue shift of **H** (in-phase) band and red shift of **R** (out-of-phase) band, which resulted in the appearance of new bands. However, as $\Delta\lambda_{max}$ of the Flu(**H**)/Qnt(**S**) or Flu(**H**)/Qnt(**Z**) combination was much larger, such large shift did not occur. See ref 14.
14. T. Kobayashi, *J-aggregates*, World Scientific, Singapore, 1996.
15. X.-H. Peng, Z.-H. Cao, J.-T. Xia, G. W. Carlson, M. M. Lewis, W. C. Wood and L. Yang, *Cancer Res.*, 2005, **65**, 1909.
16. Melting temperatures of $\mathbf{MB_M}$ and $\mathbf{MB_R}$ in the presence and absence of the target **Surv** are listed in AppendixTable 4-2.
17. MBR showed sufficient sequence-specificity; see Appendix Figure 4-1.
18. Note that $I_{open}/I_{close}$ of previous ISMB, composed of a single pair of perylene and anthraquinone, was 26 under similar conditions.
19. In other words, spectral overlap between the quencher and fluorophore should be maximized.
20. S. A. E. Marras, F. R. Kramer and S. Tyagi, *Nucleic Acids Res.*, 2002, **30**, e122.
21. B. Valeur, *Molecular Fluorescence: Principles and Applications*, Wiley-VHC, Weinheim, 2002.
22. 久保淳一　2009 年度修士学位論文　名古屋大学大学院工学研究科物質制御工学専攻　「会合体形成で誘起された軌道間相互作用による色素の励起エネルギー変化」
23. (a) 山崎巖, *有機量子化学と光化学*, 一麦出版社, 札幌, 2003; (b) Y. Urano, M. Kamiya, K. Kanda, T. Ueno, K. Hirose and T. Nagano, *J. Am. Chem. Soc.*, 2005, **127**, 4888.
24. 原雄一　2009 年度修士学位論文　名古屋大学大学院工学研究科物質制御工学専攻　「励起子相互作用を利用した高感度 In-Stem Molecular Beacon の開発」
25. These monomers (**H** and **Y**) were synthesized and provided by Yuichi Hara (an alumnus in Asanuma Lab.)
26. H. Nishioka, X. Liang, H. Kashida and H. Asanuma, *Chem. Commun.*, 2007, 4354.
27. E. Mayer-Enthart, C. Wagner, J. Barbaric and H.-A. Wagenknecht, *Tetrahedron*,

2007, **63**, 3434.

## 4-8 Appendixes

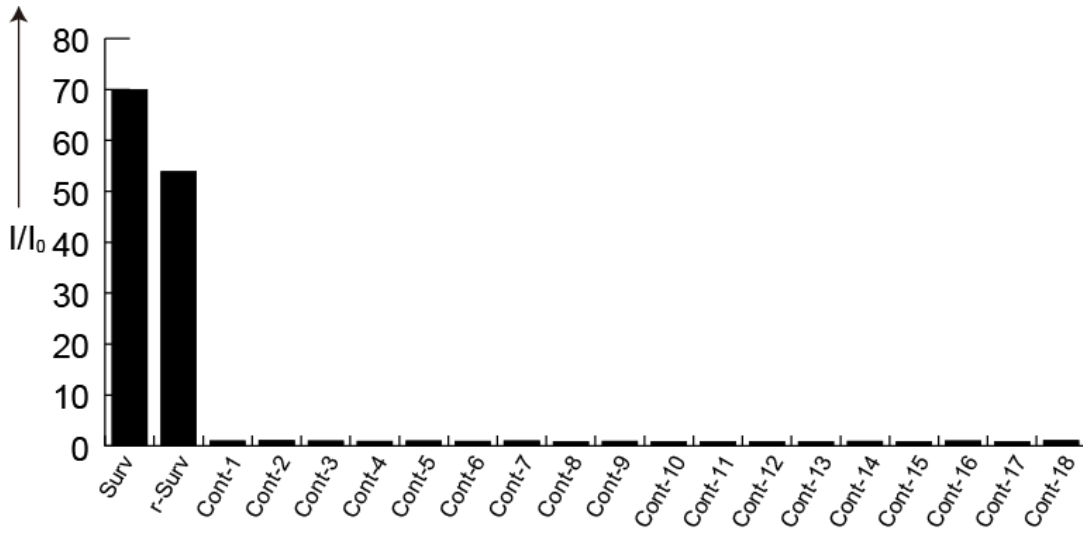


Appendix Figure 4-1. Change of fluorescence intensity of $\mathbf{MB_R}$ at 564 nm by the presence of DNA or RNA of various sequences with respect to that of closed one excited at 546 nm. Solution conditions were as follows: [$\mathbf{MR_R}$] = 0.2 μM, [DNA, or RNA] = 0.4 μM, [NaCl] = 100 mM, pH 7.0 (10 mM phosphate buffer), 20 $^{o}$C. Sequences of the added DNA or RNA are listed below. All these oligonucleotides are a part of survivin gene.

Surv: 5'-TGG-TCG-CCC-TTT-CTC-AAG-3'
r-Surv: 5'-UGG-UCG-CCC-UUU-CUC-AAG-3' (RNA)
Cont-1: 5'-CCG-CAT-CTC-TAC-ATT-CAA-3'
Cont-2: 5'-ACT-GGC-CCT-TCT-TGG-AGG-3'
Cont-3: 5'-TGC-GCC-TGC-ACC-CCG-GAG-3'
Cont-4: 5'-GAT-GGC-CGA-GGC-TGG-CTT-3'
Cont-5: 5'-GAG-CCA-GAC-TTG-GCC-CAG-3'
Cont-6: 5'-TTT-CTT-CTG-CTT-CAA-GGA-3'
Cont-7: 5'-TGG-AAG-GCT-GGG-AGC-CAG-3'
Cont-8: 5'-CAC-GGT-GGC-TTA-CGC-CTG-3'
Cont-9: 5'-ATA-CCA-GCA-CTT-TGG-GAG-3'
Cont-10: 5'-TTG-GCT-AAT-ACG-GTG-AAA-3'
Cont-11: 5'-CCG-TCT-CCA-CTA-AAA-ATA-3'
Cont-12: 5'-AGG-AGA-ATG-GCG-TGA-ACC-3'
Cont-13: 5'-GGA-GGC-GGA-GCT-TGC-AGT-3'
Cont-14: 5'-GCC-GAG-ATT-GCA-CCA-CTG-3'
Cont-15: 5'-AAT-GAG-ACT-CCG-TCT-CAA-3'
Cont-16: 5'-TTT-ACA-GTG-GAT-TAC-ATA-3'
Cont-17: 5'-AAT-TCC-AGT-GAA-ATG-AAA-3'
Cont-18: 5'-ACT-TCA-AAC-AGT-TCC-TTG-3'

Appendix Table 4-1. Quantitative evaluation of hypochromicity (coherency) and quenching efficiency with **Flu(F)/Qnt(Q)** model duplex.[a)]

| Qnt(**Q**) | Flu(**H**) (thiazole orange) (516 nm)[b)] | | | Flu(**Y**) (Cy3) (550 nm)[b)] | | |
|---|---|---|---|---|---|---|
| | $\Delta\lambda_{max}$ / nm[c)] | Hypochromicity (Coherency)[d)] | Quenching efficency[e)] | $\Delta\lambda_{max}$ / nm[c)] | Hypochromicity (Coherency)[d)] | Quenching efficency[e)] |
| **Z** (334 nm)[b)] | 182 | 0.063 | 0.88 | 216 | 0.002 | 0.931 |
| **S** (394 nm)[b)] | 122 | 0.106 | 0.92 | 156 | 0.044 | 0.937 |
| **M** (480 nm)[b)] | 36 | 0.194 | 0.943 | 70 | 0.142 | 0.963 |
| **R** (513 nm)[b)] | 3 | 0.211 | 0.944 | 37 | 0.198 | 0.97 |

a) Buffer conditions: [NaCl] = 100 mM, pH 7.0 (10 mM, phosphate buffer). Concentration of the DNA: for measuring the UV/Vis spectra, [**Flu(F)**] = [**Qnt(Q)**] = 4 μM, for measuring fluorescence spectra, [**Flu(F)**] = 0.2 μM, [**Qnt(Q)**] = 0.4 μM,
b) Absorption maximum of the dye in **Flu(F)** or **Qnt(Q)**.
c) Difference of the absorption maxima ($\lambda_{max}$) between the fluorophore (**H** or **Y**) in **Flu** and quencher in **Qnt**.
d) Difference of absorbance (hypochromicity) between the simple sum of **Flu(F)** and **Qnt(Q)** (sum-spectrum, corresponding to orange line in Fig. 4-2) and **Flu(F)/Qnt(Q)** duplex (corresponding to black line in Fig. 4-2) at 516 nm (**F** = **H**) or 550 nm (**F** = **Y**).
e) The ratio of fluorescence intensity of **Flu(F)/Qnt(Q)** duplex with respect to that of single-stranded **Flu(F)** monitored at 546 (**F** = **H**, excited at 516 nm) or 564 nm (**F** = **Y**, excited at 546 nm).

Appendix Table 4-2. Melting temperatures of molecular beacons. [a)]

| Sequence | $T_m$ (hairpin) / °C [b)] | $T_m$ (with Surv) / °C [c)] |
|---|---|---|
| **$MB_M$** | 65.8 | 63.5 |
| **$MB_R$** | 63.1 | 61.9 |

a) Melting curves were obtained by measuring the change of absorbance at 260 nm versus temperature. The melting temperature ($T_m$) was determined from the maximum in the first derivative of the melting curve.
b) [MB] = 2.0 μM, [NaCl] = 100 mM, pH 7.0 (10 mM phosphate buffer)
c) [MB] = 2.0 μM, [**Surv**] = 2.0 μM, [NaCl] = 100 mM, pH 7.0 (10 mM phosphate buffer)

Appendix Table 4-3. Energy levels of HOMO and LUMO with dye monomers[a)] by quantum calculation. TD-DFT calculation (pbe1pbe/6-31g(d)) was performed with the Gaussian 09.

| | | **Z** | **S** | **M** | **R** | **H(TO)** | **Y(Cy3)** |
|---|---|---|---|---|---|---|---|
| Energy /eV | HOMO | -6.83 | -6.15 | -5.63 | -5.89 | -8.68 | -8.27 |
| | LUMO | -2.61 | -2.55 | -2.17 | -2.60 | -5.37 | -5.18 |
| | ΔE | 4.23 | 3.60 | 3.46 | 3.29 | 3.31 | 3.09 |

a) N-Methylamided dye monomers were used for the calculation as a monomer state.

# Chapter 5. Maximizing Excitonic Interaction by Bulge Like Asymmetric Dye-clustering for Efficient Quenching of Background Emission

## 5-1 Abstract

For enhancement of excitonic interaction between dyes to quench fluorophores, we prepared asymmetric dye-clusters with a single fluorophore (Cy3) and multiple quenchers (4'-methylthioazobenzene, Methyl Red and 4'-dimethylamino -2-nitroazobenzene), which are tethered on D-threoninol (Threoninol Nucleotides) at the center of single-stranded DNAs. NMR analysis revealed that the clusters with a single fluorophore and two quenchers formed a sandwich like structure (antiparallel H-aggregates). The duplex stabilities of all asymmetric clusters were almost the same, although structural distortion should become larger with the number of the dyes. Excitonic interaction between the fluorophore and quencher, i.e., hypsochromicity of fluorophore (Cy3) band by clustering with quenchers, increased with the number quenchers and saturated at two quenchers. Asymmetric hetero-cluster of single fluorophore and two quenchers suppressed the background emission more efficiently than single pair of a fluorophore and a quencher due to the large exciton coupling between the dyes. However, further accumulation of quenchers did not enhanced quenching efficiency because of the saturation of exciton coupling among the fluorophore and quenchers. Finally, we introduced this asymmetric 2/1 hetero-cluster into the stem region of a molecular beacon (In-stem Molecular Beacon) targeting abnormal L6 *BCR-ABL* fusion genes. As the results, we could attain signal/background

ratio of as high as 68 by the efficient suppression of background emission due to the maximized excitonic interaction.

## 5-2 Introduction

Excitonic interaction is one of the static interactions among the closely stacked dye molecules,[1] and induces narrowing of the band and bathochromic or hypsochromic shift depending on its stacking manner.[2] H- and J-bands that show large hypsochromicity and bathochromicity due to vertical and stair-like stacking, respectively, are typical examples of excitonic interaction.[2-3] It is well-known that UV/Vis spectra depend on the size of the dyes as well as their mutual orientation. Notably, many experiments on the homo dye-clusters realized that exciton coupling among the cluster (spectroscopic aggregation number or coherence length) was saturated with more than 13 dye molecules on experiment.[4] On the other hand, relationship between the cluster size and excitonic interaction in hetero clusters of different dyes had been scarcely investigated due to the difficulty of their preparation.[5] So far, only a limited number has been reported on the exciton coupling which a "dye-A" receives by "dye-Bs".[6]

Recently, DNA and RNA have been regarded as a scaffold of dyes to prepare their organized assembly because number of the dyes and their mutual orientation are easily controllable.[7] Especially, in some of these methods, controlling the sequences and number of the dyes was realized by introduction of the dye residues as a artificial base.[8] For example, Kool et al. reported oligo-"fluorosides" composed of fully artificial base-surrogates tethering fluorophore on D-ribose to prepare various functional hetero clusters in the single-stranded state.[9] Häner et al. developed hetero clusters with diethinylpylene-perylenediimide pairs which were introduced into DNA as a linker and

dye moieties.[10] In this way, hetero-clustering base on DNA or RNA duplexes can realize flexible designs for regulation of the dye sequences and number.

From chapter 2 to 4, we have also developed a new methodology to prepare organized assemblies of homo and hetero dyes by using D-threoninol as a scaffold of a functional molecule (Threoninol Nucleotides). Introduction of base-surrogates consecutively into two complementary DNAs at their center allowed firmly stacked H-type dye cluster in the duplex in an antiparallel orientation. Moreover, our systematic investigations about spectroscopic behaviors of various hetero dimers revealed that exciton coupling strongly depended on difference of absorption maxima ($\Delta\lambda_{max}$) between dyes. Next, we applied our method to the design of highly sensitive molecular beacon (MB), in-stem molecular beacon (ISMB)[11], by introducing hetero-dimer of fluorophore and quencher into the stem region of MB to facilitate the quenching of emission in the closed state. Interestingly, as Johansson et al. proposed, our systematic studies on the spectroscopic behavior of fluorophore-quencher dimer revealed that stronger excitonic interaction between the dyes suppressed the background emission in the closed MB more efficiently, resulted in eminent signal/background (S/B) ratio.[12] Accordingly, further enhancement of excitonic interaction between the dyes should

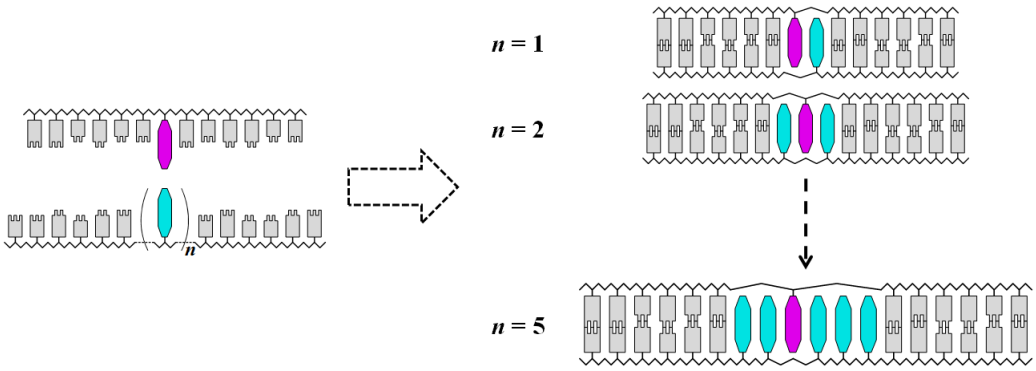


Scheme 5-1. Schematic illustration of the design of the asymmetric dye-clusters using threoninol-nucleotides as dye tethers. One strand with a fluorophore and the other strand with multiple quenchers (from 1-5 residues) hybridized for dye-clustering. In this illustration, ***n*** indicate the number of the quenchers.

raise quenching efficiency, leading to highly sensitive detection of DNAs. In this chapter, we combined single fluorophore (Cy3) and multiple quenchers (azo-dyes) on D-threoninols to form asymmetric dye cluster in the duplex (see Scheme 5-1) for further enhancement of excitonic interaction. We found that asymmetric hetero-cluster of single fluorophore and two quenchers suppressed the background emission more efficiently than single pair of a fluorophore and a quencher due to the larger exciton coupling. Based on this result, highly-sensitive ISMB was designed with asymmetric 2/1 hetero-cluster in the stem region.

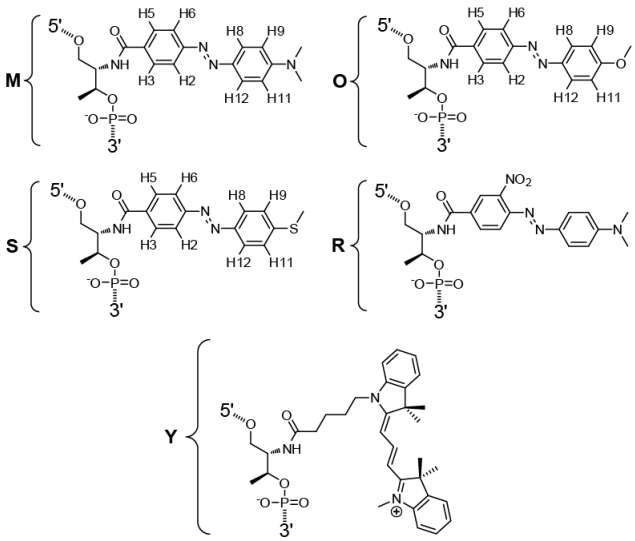

NMR-**MSa** : 5'-C$^{1}$G$^{2}$A$^{3}$-**MS**-G$^{4}$T$^{5}$C$^{6}$-3'
NMR-**Ob** : 3'-G$^{12}$C$^{11}$T$^{10}$-**O**-C$^{9}$A$^{8}$G$^{7}$-5'

**N** : 5'-GGT-ATC-GCA-ATC-3'
**C** : 3'-CCA-TAG-CGT-TAG-5'

**Y1a** : 5'-GGT-ATC-**Y**-GCA-ATC-3'
**R*n*b** : 3'-CCA-TAG-**R**$_n$-CGT-TAG-5'
**M*n*a** : 5'-GGT-ATC-**M**$_n$-GCA-ATC-3'  ***n*** = 1-5
**S*n*a** : 5'-GGT-ATC-**O**$_n$-GCA-ATC-3'
**Y1b** : 3'-CCA-TAG-**Y**-CGT-TAG-5'
**S2b** : 3'-CCA-TAG-**SS**-CGT-TAG-5'
**M1S1b** : 3'-CCA-TAG-**SM**-CGT-TAG-5'

**T-MB** : 5'-CA-GAG-TTC-AAA-AGC-CCT-TCA-3'
**MB1** : 5'-TG-**Y**-GTC-*TGA-AGG-GCT-TTT-GAA-CTC-TG*-GAC-**R**-CA-3'
**MB2** : 5'-TG-**Y**-GTC-*TGA-AGG-GCT-TTT-GAA-CTC-TG*-GAC-**RR**-CA-3'
**MB3** : 5'-TGG-**Y**-TC-*TGA-AGG-GCT-TTT-GAA-CTC-TG*-GA-**R**-CCA-3'
**MB4** : 5'-TGG-**Y**-TC-*TGA-AGG-GCT-TTT-GAA-CTC-TG*-GA-**RR**-CCA-3'

Scheme 5-2. Chemical structures and sequences of the ODNs synthesized in this chapter. In the MB sequences, the bases in the stem part are underlined and in loop part, which recognizes the target sequence, are italicized.

## 5-3 Results

### 5-3-1 Structural determination and evaluation of duplex stabilities of the asymmetric dye clusters

Scheme 5-1 shows a schematic illustration of *n*/1 asymmetric dye cluster formed in the middle of the duplex; each strand has single and consecutive dye residues at the center, respectively, and their hybridization affords *n*/1 asymmetric dye cluster on the assumption that dyes are stacked with each other. Actual sequences of the DNAs involving dyes synthesized in this chapter are outlined in Scheme 5-2. We first conducted NMR analysis of a 2/1 hetero cluster dyes to determine their alignment, and then evaluated the stabilities of *n*/1 clustered duplexes.

***NMR analysis of 2/1 the clusters***

In order to discriminate proton signals of all the dye molecules in the duplex, we introduced three different dyes; 4-dimethylaminoazobenzene-4'-carboxylate (Methyl Red, **M**), 4-methylthioazobenzene-4'-carboxylate (**S**), and 4-methoxyazobenzene

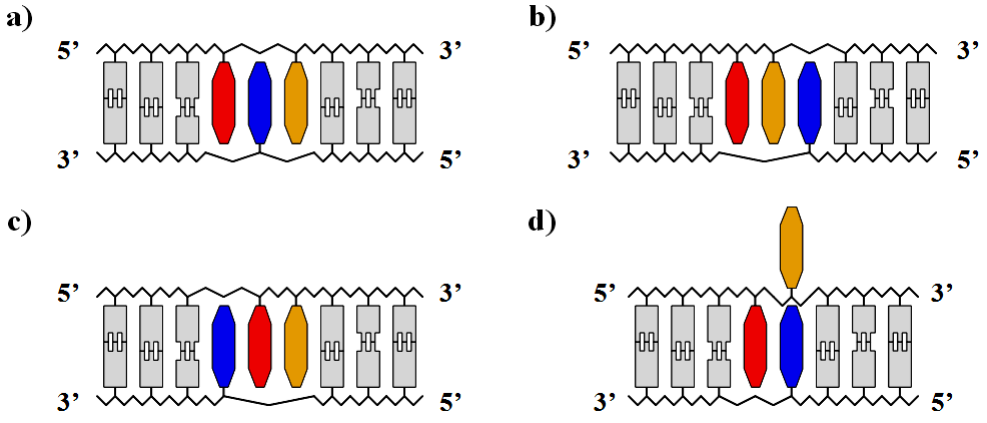


Scheme 5-3. Schematic illustration of alignments of the asymmetric dyes-clusters using threoninol-nucleotides as dye tethers. There are several possible dye locations: the dyes are located between the opposite two dyes (a) (corresponding to **MOS** orientation in NMR-**MSa**/NMR-**Ob**), adjacent to the 5'-side (b) (corresponding to **MS*O*** orientation), the 3'-side (c) of a natural nucleobase (corresponding to ***O*MS** orientation), or at least one of the dyes are flipped out from the duplexes (d).

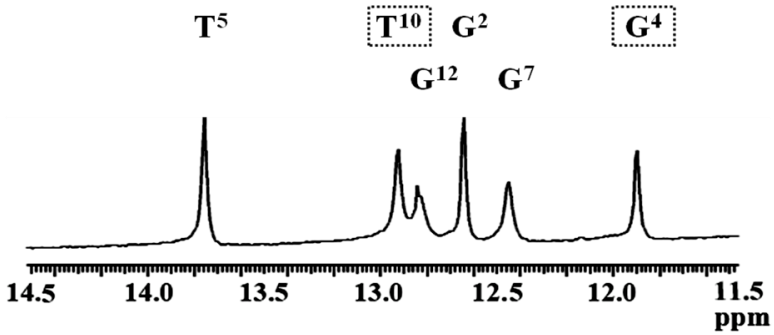


Figure 5-1. One-dimensional NMR spectrum of the NMR-**MSa**/NMR-**Ob** duplex at the imino region in $H_2O/D_2O$ 9:1 at 278 K (mixing time = 150 ms), pH 7.0 (20 mM phosphate buffer), in the presence of 200 mM NaCl. The concentration of NMR-**MSa**/NMR-**Ob** was 1.0 mM. Assignments of the imino-protons and the residue number are denoted at the top of the peak.

-4'-carboxylate (**O**). Two complementary strands NMR-**MSa** and NMR-**Ob** (see Scheme 5-2) involve both **M** and **S** residues consecutively and an **O** residue at the center, respectively. There are several possible alignments of the dyes as shown Scheme 5-3: the dyes are located between the opposite two dyes (corresponding to **M*O*S** orientation in NMR-**MSa**/NMR-**Ob**), adjacent to the 5'-side (corresponding to **MS*O***

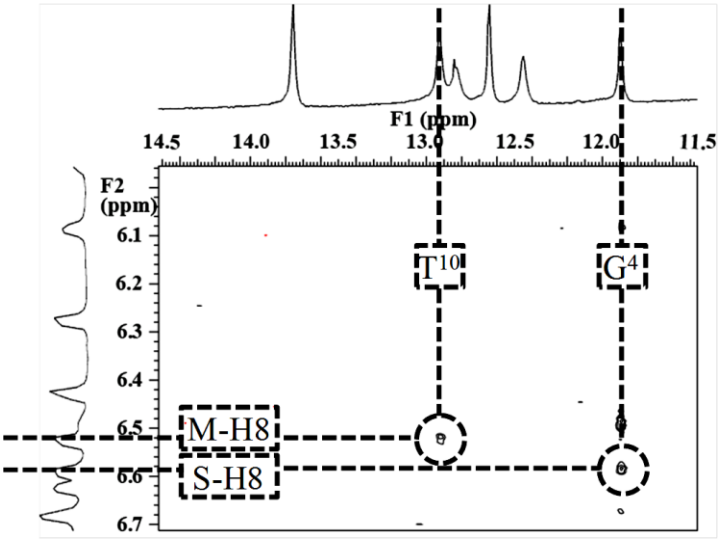


Figure 5-2. 2D NOESY spectrum (mixing time = 150 ms) between the imino-proton signal (11.5-14.5 ppm) and the aromatic-proton signal regions (6.0-6.7 ppm) for the NMR-**MSa**/NMR-**Ob** duplex in $H_2O/D_2O$ 9:1 at 278 K, pH 7.0 (20 mM phosphate buffer), in the presence of 200 mM NaCl. Assignments of the Methyl Red and 4'-methylthioazobenzene protons are denoted on the one-dimensional spectra (*F1* axis) using the numbers designated in Scheme 2. The NOE signals surrounded by broken circles demonstrate intercalation of the Methyl Red and 4'-methylthioazobenzene.

orientation), the 3'-side of a natural nucleobase (corresponding to ***O*MS** orientation), or at least one of the dyes are flipped out from the duplexes.

The one-dimensional NMR spectrum measured in $H_2O$ at the region of imino-protons (11.5-14.0 ppm) is depicted in Fig. 5-1.[13-14] NMR-**MSa**/NMR-**Ob** allowed six natural base-pairs ($C^1$-$G^{12}$, $G^2$-$C^{11}$, $A^3$-$T^{10}$, $G^4$-$C^9$, $T^5$-$A^8$ and $C^6$-$G^7$) and one tentative **MS**-**O** bulge (Scheme 5-2). As expected, there were six individual signals that could be assigned on the basis of the NOESY and chemical shift of each signal, indicating that the non-natural **M**, **S** and **O** did not interrupt the base-pairing (See Fig. 5-1).[15] Figure 5-2 depicts the NOEs between the imino-proton signal (11.5-14.0 ppm) and the aromatic-proton signal (6.0-6.7 ppm) regions. A distinct NOE signal was observed between the imino proton of $T^{10}$ and H8 (H12) of the **M** protons, indicating that the **M** residue was located at around $T^{10}$. On the contrary, imino proton of $G^4$ did not have NOE signal with **M** but with H8 (H12) of the **S** protons, indicating that **S**

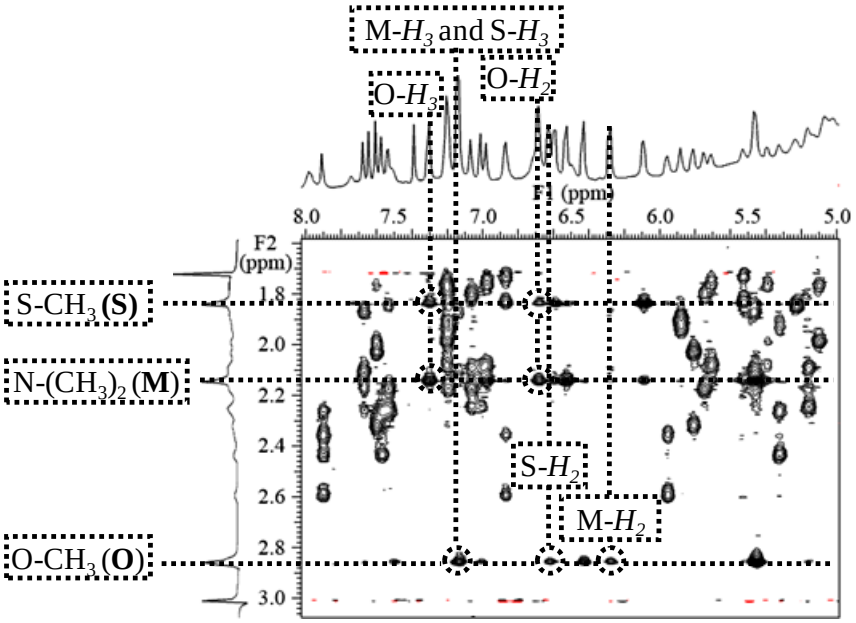


Figure 5-3. 2D NOESY spectrum (mixing time = 150 ms) between the regions of 5.0-8.0 ppm and 1.6-3.0 ppm for the NMR-**MSa**/NMR-**Ob** duplex in $H_2O/D_2O$ 9:1 at 278 K (20 mM phosphate buffer), in the presence of 200 mM NaCl.

residue was located in the vicinity of $G^4$. Thus, we could unambiguously exclude the possibilities of **MS*O*** or ***O*MS** alignment (see Scheme 5-3) and conclude **M*O*S** cluster formation, which was further evidenced as below.

Figure 5-3 shows the NOESY between the regions of 5.0-8.0 ppm and 1.6-3.0 ppm. Proton signals of **O** residue were correlated only with those of **M** and **S** residues, and no cross-peaks were observed between **M** and **S** residues as schematically shown in Fig.4a. We could observe cross-peaks between aromatic proton signals of **O**-H2 (**O**-H6) and **O**-H3 (**O**-H5) with those of both S-$CH_3$ of **S** and N-$CH_3$ of **M**. Moreover, relatively strong signals were also observed between O-$CH_3$ of **O** and aromatic protons of **M**-H2 (**M**-H6), **M**-H3 (**M**-H5), **S**-H2 (**S**-H6) and **S**-H3 (**S**-H5). These NOE signals indicate that **M**, **O** and **S** are stacked antiparallel to each other as depicted in Fig.4a, which

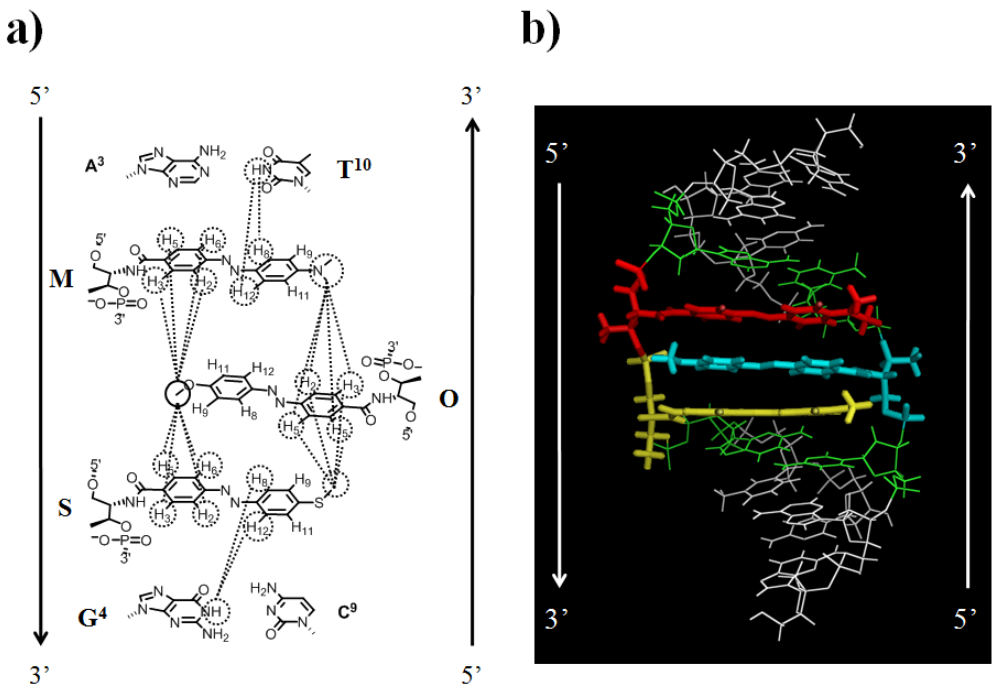


Figure 5-4. Stacking manner and orientation of **M**, **O** and **S** residues in the duplex determined from NOESY a), and energy-minimized structures of the NMR-**MSa**/NMR-**Ob** duplex b) calculated with InsightII/Discover3 from the initial structure determined by NMR analyses. Broken lines in a) show the observed NOE signals. The sticks in b) depict 4'-methyoxyazobenzene (cyan), 4'-methylthioazobenzene (yellow) and Methyl Red (red) in the duplex.

validates our design of asymmetric dye-clusters (**M*O*S** orientation in Scheme 5-3a) in which **O** residue was sandwiched between **M** and **S** residue in DNA duplex. Computer modeling of NMR-**MSa**/NMR-**Ob**, using the InsightII/discover3 software, was entirely consistent with these NMR analyses (Fig. 5-4b). Although actual fluorescent dye is not 4-methoxyazobenzene (**O** residue) but Cy3 (**Y** residue), we thought that similar sandwich-type cluster was formed.

***Duplex stabilities of the asymmetric dye clusters***

Further introduction of quencher dyes should induce severe distortion of the duplex structure due to the increased asymmetry of the strands, which should affect the stability of the duplex. Thus, we measured melting temperatures of the duplexes involving *n*/1 cluster by varying *n* from 1 to 5 as listed in Table 5-1. Insertion of single **R-Y** pair (**R1b/Y1a:** 44.5 $^{o}$C) slightly decreased the duplex stability from native duplex (**N/C:** 47.7 $^{o}$C). On the other hand, $T_m$ value of the cluster with a 2/1 bulge composed of single **Y** residue and double **R** residues (**R2b/Y1a:** 44.8 $^{o}$C) was almost same as that with a **R-Y** pair. Interestingly, further multiplication of the **R** residues did not much affect $T_m$s (46.1-47.1 $^{o}$C, see Table 5-1), in spite of increased distortion.[16-17] Similar results were

Table 5-1. Effect of the number and kinds of quencher dyes on the melting temperature ($T_m$). [a]

| | $T_m$ / $^{o}$C | | |
|---|---|---|---|
| | **Y1a/R*n*b** | **M*n*a/Y1b** | ***Sn*a/Y1b** |
| **N/C** | 47.7 | — | — |
| *n* = 1 | 44.5 | 45.3 | 46.2 |
| *n* = 2 | 44.8 | 46.0 | 48.2 |
| *n* = 3 | 46.1 | 47.5 | 49.2 |
| *n* = 4 | 47.1 | 48.2 | 50.0 |
| *n* = 5 | 47.1 | 49.3 | 49.1 |

[a] Measurement conditions were pH 7.0: [DNA] = 5 μM, [NaCl] = 100 mM (10 mM phosphate buffer).

observed when **M** or **S** residue was used as the quencher instead of **R** residue. It is likely that asymmetric *n*/1 combination did not much destabilize the duplex, probably due to the stacking of Cy3 with multiplied quenchers.

5-3-2 Effect of the number of quenchers on excitonic interaction among the dyes

We next investigated effect of the accumulation of quencher dyes on excitonic interaction. To estimate the strength of exciton coupling between a fluorophore and multiplied quenchers, hypochromicity of Cy3 absorption by the quencher(s) was quantified by the comparison of UV/Vis spectrum of Cy3 before and after hybridization of quencher strand. Figure 5-5a shows typical excitonic interaction between Cy3 in **Y1a** and 4'-dimethylamino-2-nitroazobenzene (**R** residue) in **R1b**.[6, 7c, 7e, 18] Each single-stranded **Y1a** (red line) and **R1b** (purple line) gave absorption maxima at 549 nm and 512 nm assigned to Cy3 and **R**, respectively, while hybridization of these two

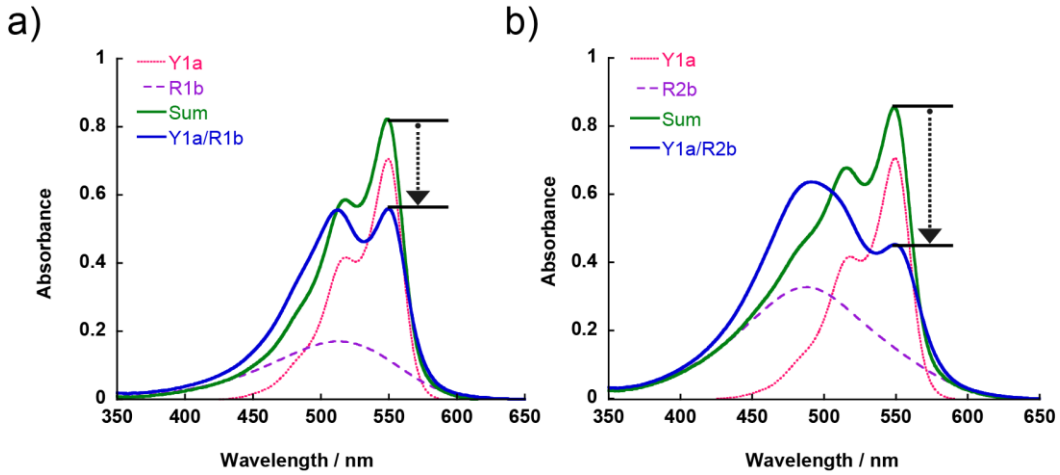


Figure 5-5. a) UV-Vis spectra of the **Y1a/R1b** duplex (blue line), single-stranded **Y1a** (pink dotted line), **R1b** (purple dashed line), and a simple sum of their spectra (sum-spectrum, **Y1a + R1b,** green line) at 20 °C. b) UV-Vis spectra of the **Y1a/R2b** duplex (blue line), single-stranded **Y1a** (pink dotted line), **R2b** (purple dashed line), and a simple sum of their spectra (sum-spectrum, **Y1a + R2b,** green line) at 20 °C. Hypochromicities (difference of absorbance) of Cy3 absorption before and after clustering were calculated as strength of the exciton couplings (The strengths were shown by dotted arrows). Solution conditions were as follows: [DNA] = 5 μM, [NaCl] = 100 mM, pH 7.0 (10mM phosphate buffer).

strands afforded decrease (hypsochromicity) in absorbance of Cy3 band (at 513 nm) and hypochromicity of **R** band (at 550 nm) as compared with the sum-spectrum (blue line) of **Y1a** and **R1b**. Here, decrease in the absorbance (black arrow in Fig. 5-5a) corresponds to the quantified strength of excitonic interaction, which was estimated as 0.32 (see Table 5-2). Increase in the excitonic interaction was observed with **R2b/Y1a** (strength of excitonic interaction; 0.47) involving 2/1 quenchers/fluorophore pair as shown in Fig. 5-5b and Table 5-2. However, further introduction of the quencher dyes did not change it (Table 5-2 and Appendix Fig. 5-1), indicating excitonic interaction between **R** and **Y** was saturated with two quenchers. Similarly, other quenchers such as Methyl Red or 4'-methylthioazobenzene showed the same saturation behavior (see Table 5-2, Appendix Fig.s 5-2 and 5-3), although attained strength of excitonic interaction depended on the kinds of quenchers. Based on these results, we conclude that introduction of two quenchers is enough for maximizing excitonic interaction between fluorophore and quencher.

Table 5-2. Effect of the number and kinds of quencher dyes on the exciton couplings of the quenchers to a fluorophore and the quenching efficiencies.

| | **Y1a/R*n*b** | | **M*n*a/Y1b** | | **S*n*a/Y1b** | |
|---|---|---|---|---|---|---|
| | $H$ [a,b] | $QE$ [c] / % | $H$ [a,b] | $QE$ [c] / % | $H$ [a,b] | $QE$ [c] / % |
| $n$ = 1 | 0.32 | 98.5 | 0.25 | 96.5 | 0.10 | 93.9 |
| $n$ = 2 | 0.47 | 99.0 | 0.36 | 97.3 | 0.15 | 96.8 |
| $n$ = 3 | 0.48 | 99.0 | 0.38 | 96.8 | 0.18 | 96.8 |
| $n$ = 4 | 0.47 | 99.3 | 0.36 | 96.4 | 0.17 | 97.3 |
| $n$ = 5 | 0.52 | 99.0 | 0.39 | 97.7 | 0.19 | 97.1 |

[a] Measurement conditions were pH 7.0: [DNA] = 5 μM, [NaCl] = 100 mM (10 mM phosphate buffer).
[b] Hypochromicity ($H$) was evaluated from difference of absorbance between the hetero clusters and the sum-spectrum of each single strand at Cy3 absorption region (**Y1a/R*n*b**; 549 nm, **M*n*a/Y1b**; 552 nm, **S*n*a/Y1b**; 552 nm).
[c] Quenching efficiencies ($QE$) were calculated by the difference of fluorescent intensity between the clusters and the single strand with a Cy3 residue. The emission spectra of **Y1a/R*n*b**, **M*n*a/Y1b**, and **S*n*a/Y1b** at 564 nm, 563 nm and 562 nm, respectively, were used for these calculations. Measurement conditions were pH 7.0: [**M*n*a**] = [**S*n*a**] = [**R*n*b**] = 0.4 μM, [**Y1a**] = [**Y1b**] = 0.2 μM, [NaCl] = 100 mM (10 mM phosphate buffer).

5-3-3 Quenching efficiency of a fluorophore by multiple quenchers.

In chapter 4, we revealed that larger excitonic interaction between a fluorophore and a quencher induced more efficient quenching of a fluorophore. In order to compare the quenching efficiency by multiplied quenchers with strength of excitonic interaction, quenching efficiency was evaluated with the same duplexes as we used in the above section. Emission spectra of **R*n*b/ Y1a** and **S*n*a/Y1b** are shown in Fig. 5-6. As shown in the insets, all clusters (**R*n*b/Y1a** and **S*n*a/Y1b**) exhibited quite low fluorescence compared with that of single-stranded **Y1a** and **Y1b**. We found that doubled quenchers (**S2a/Y1b**) quenched the emission more efficiently (93.9%) that single quencher (**S1a/Y1b**; 96.8%). However, further multiplication of **S** residues did not change their quenching efficiencies. 4'-Dimethylamino-2-nitroazobenzene (**R**) intrinsically quenched Cy3 more efficiently than **S** residue due to the stronger excitonic interaction (Compare blue line in Fig. 5-6b with that in Fig. 5-6a) as shown in chapter 4. However, multiplication of more than two **R** residues did not further improve the quenching efficiency (99.0-99.3% quenching by **R*n*b/Y1a**, see Table 5-2). Interestingly, the same

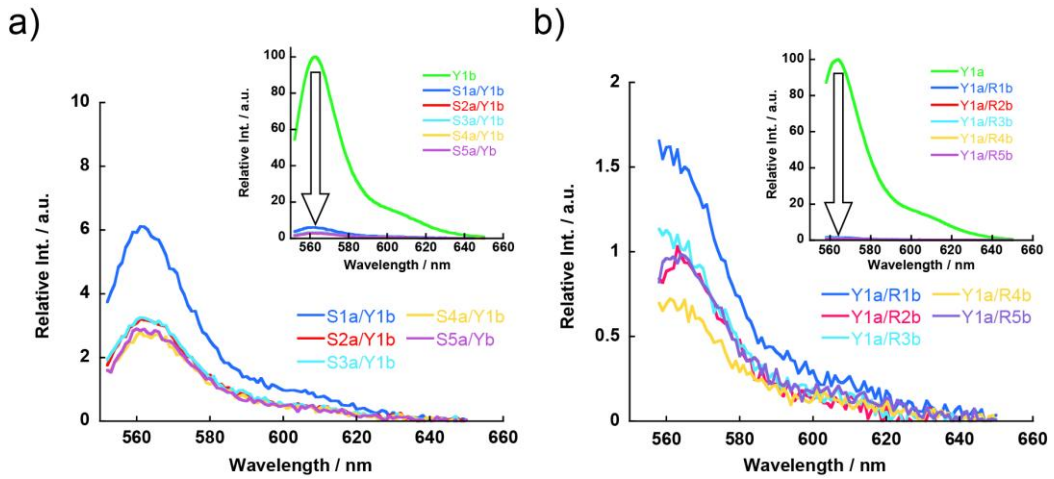


Figure 5-6. Fluorescence emission spectra of Cy3 (**Y**) excited at 546 nm and their duplexes with strands tethered a) 4'-methylthioazobenene and b) 4'-dimethylamino-2-nitroazobenzene as quenchers. Solution conditions were as follows: 20 °C, [**S*n*a**] = [**R*n*b**] = 0.4 μM, [**Y1a**] = [**Y1b**] = 0.2 μM, [NaCl] = 100 mM, pH 7.0 (10 mM phosphate buffer).

tendency was also observed with **M*n*a/Y1b** involving Methyl Red (Appendix Fig. 5-4). Note that excitonic interaction was saturated with two consecutive quenchers irrespective of the kinds of quenchers. Taken together, we concluded that two consecutive quenchers (double-quencher) were enough for maximizing the quenching of a fluorophore due to the saturated excitonic interaction.

5-3-4. Design of highly sensitive In-Stem Molecular Beacon by double-quencher

Based on the above quenching experiments, we designed In-Stem Molecular Beacons (ISMB) carrying two consecutive **R** residues as a quencher in the stem region, referred to as **MB2** and **MB4**, targeting abnormal L6 *BCR-ABL* fusion gene.[19] As a control ISMB having single quencher, **MB1** and **MB3** were also designed. As we designed, background emission of **MB2** with double quenchers was lower than that of **MB1** with single quencher in the absence of target as we designed; background emission from Cy3 in closed **MB2** was decreased by 56% as compared to that in**MB1**. Consequently, signal/background (S/B) ratio defined as the ratio of emission intensity of **MB2** in the presence and absence of the target attained as great as 68, while that of **MB1** was 27 (compare Fig.s 5-7b and 5-7c). This remarkable improvement of S/B ratio was also

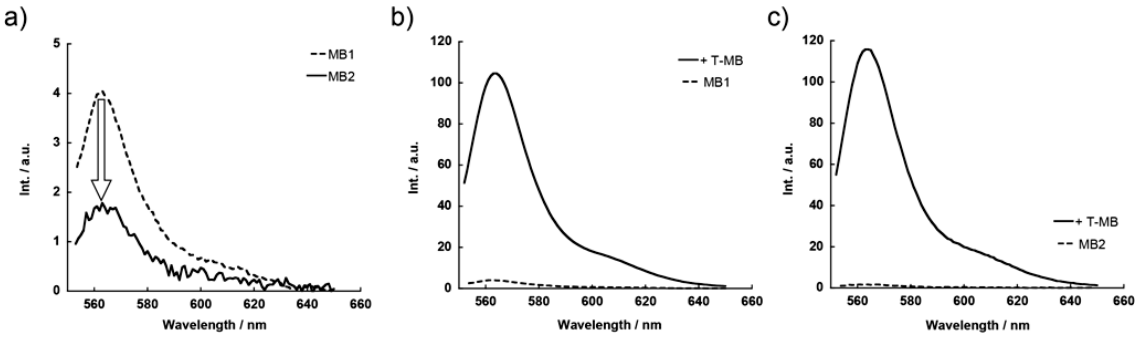


Figure 5-7. a) Comparison between the background emission of **MB1** and **MB2**. Fluorescence emission spectra of b) **MB1** and c) **MB2** excited at 546 nm with or without the presence of **T-MB**. Solution conditions were as follows: 20 °C, [**T-MB**] = 0.4 μM, [**MB1**] = [**MB2**] = 0.2 μM, [NaCl] = 100 mM, pH 7.0 (10 mM phosphate buffer).

observed for **MB3** and **MB4** having fluorophphore-quencher pair at different position (see Appendix Fig. 5-5). Thus, highly sensitive ISMBs were successfully prepared by double-quencher.

## 5-4 Discussion

### 5-4-1 Effect of multiple quenchers on stacked structures of the asymmetric dye-clusters

Our asymmetric design is based on clustering the dyes as a pseudo bulge part of threoninol-nucleotides incorporated at the center of a DNA. Increase in the bulge size of the clusters can distort the native parts of duplex structures or the stacking structures of the dyes.[20] In the case of the 2/1 cluster, NMR analysis revealed that dyes assembled antiparallel in **M*O*S** orientation and did not disturb the duplex and stacking structures. In addition, the $T_m$s of *2*/1 clusters, which were comparable to that of the native duplex, also support **M*O*S** orientation of the cluster. On the other hand, further insertion of the quenchers into the DNA duplexes did not destabilize the duplex and rather slightly stabilize that compared with the 2/1 cluster. These facts suggest that structural distortion occurred at either the native parts or the cluster parts, not both parts because of the same stabilities as native duplex. Here, to investigate which part structural disturbance occurred in, we focused on an excitonic interaction between identical dyes (quenchers). In this chapter, we evaluated the excitonic interaction contributed by quenchers to a fluorophore from hypochromicity of the fluorophore absorption (at longer wavelength). In contrast, hypsochromicity of the quencher absorption (at the shorter wavelength) shows a sum of the exciton couplings contributed by a fluorophore to quenchers and between the quenchers, and the result about the interaction contributed by quenchers to a fluorophore demonstrates that former interaction was saturated from introduction of

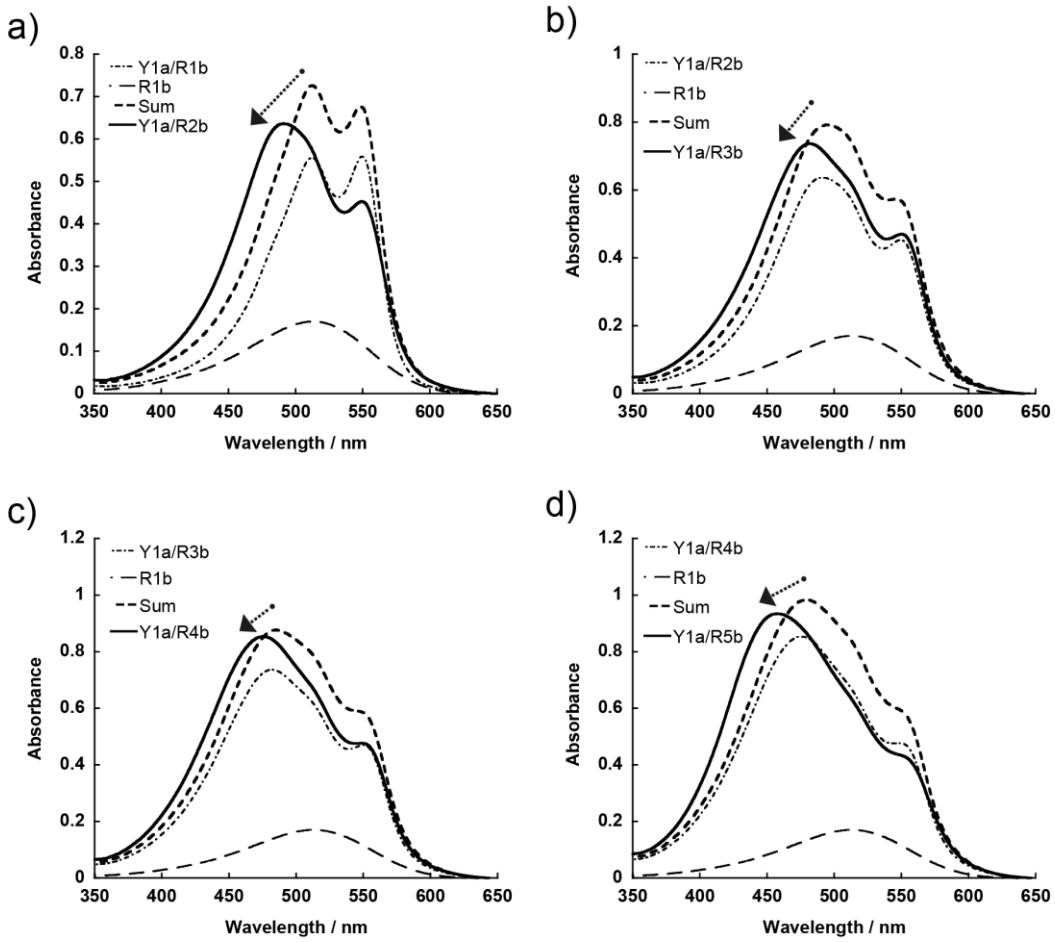


Figure 5-8. UV/Vis spectra of the **Y1a/R*n*b** duplex (solid line), the **Y1a/R(*n-1*)b** duplex (dashed and dotted line), single-stranded **R1b** (broken line), and a simple sum of their spectra (sum-spectrum, **Y1a/R(*n-1*)b + R1b,** dashed line) at 20 $^{o}$C (a); $n$ = 2, b); $n$ = 3, c); $n$ = 4, d); $n$ = 5). Dotted arrows show hypsochromicity of **R** residues associated with respect to each addition of the quencher. Solution conditions were as follows: [DNA] = 5 μM, [NaCl] = 100 mM, pH 7.0 (10mM phosphate buffer).

the over three quencher dyes. Therefore, the excitonic interactions between the quenchers were reflected by increase in the hypsochromicity associated with the expansion of the cluster size. Then, we compared the absorption spectrum of **Y1a/R*n*b** with the sum spectrum between **Y1a/R*(n-1)*b** and **R1b** to validate if the quenchers stack and interact each other ($n \geq 2$). As shown in Fig. 5-8, a blue shift of absorption spectra at shorter wavelength was observed with respect to each addition of the quencher. These clearly indicate that all the quenchers stacked each other and structural distortion occurred at only the native parts. Thus, stabilization should derive from stacking

interaction between the dyes neutralized the destabilization derived from structural strain at the native parts. Moreover, our conclusion of the relationship among the number of the quenchers, the coherency and quenching efficiency of a fluorophore should be reasonable from viewpoint of structural consistency.

5-4-2 Effect of alignment among the dyes on excitonic interaction.

At the main part, we have focused on the relationship between the excitonic interaction and the number of the quencher dyes. Although the number of the quenchers largely affected their spectroscopic behaviors, the alignment of the dyes is also one of the important factors to determine their behaviors. According to exciton theory, because each molecular orbital of the dyes, which assemble each other, cannot be identified, difference of their alignment such as **M*O*S** or ***O*MS** orientation should only give slight influence to their interaction.[1-2, 6] Then, we additionally investigated the influence of alignments on excitonic interaction by a use of model clusters. These clusters include one **M** residue and two **S** residues for observing strength of exciton couplings of **S**

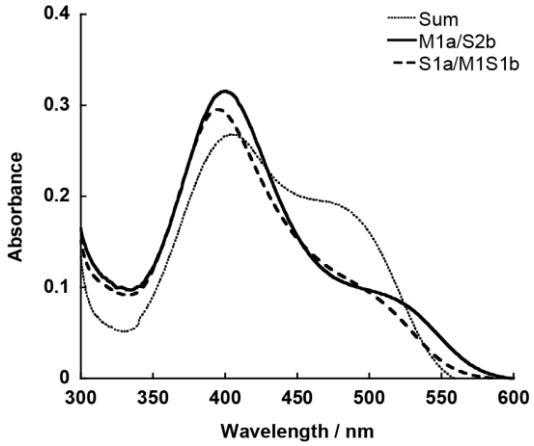


Figure 5-9. Effect of the alignment among dyes on the UV-Vis spectra of **M1a/S2b** (solid line) and **S1a/M1S1b** (broken line) combinations. To compare with their monomer spectra, the sum spectrum of **M1a** and twofold **S1b** (dotted line) are depicted at the same time. Solution conditions were as follows: 0 $^{o}$C, [DNA] = 5 μM, [NaCl] = 100 mM, pH 7.0 (10 mM phosphate buffer).

residues to **M** residue. UV/Vis spectra of **M1a/S2b** and **S1a/M1S1b** are shown in Fig. 5-9, and sum spectrum of **M1a** and twofold **S1b** is also calculated for their basis. Comparing to the sum spectrum, both spectra of **M1a/S2b** and **S1a/M1S1b** showed the same level of absorbance at shorter and longer wavelength, although amount of spectral shifts were slight different between each other. This result demonstrates that strengths of exciton couplings between two clusters are the almost same. Thus, we can conclude that the order among the dyes does not provide the large spectral difference as well as prediction based on exciton theory.

## 5-5 Conclusions

We have prepared asymmetric dye-clusters in DNA duplexes by using D-threoninol as a scaffold for the dyes (threoninol-nucleotide) for reduction of the background emission with the probe to detect the target DNA. Because of this, highly sensitive ISMB were realized by asymmetric clustering and we demonstrated that this design is one of the excellent ways to reduce the background emission of the probe. This probe can be utilized for high throughput detection on the DNA microarray and the imaging of wild-type and chimera mRNA *in vivo* directly associated with chronic myeloid leukemia. [19]

## 5-6 Experimental Section

### 5-6-1 Materials

See 2-6-1 because the contents are the same.

5-6-2 Synthesis of DNA modified with **M**, **O**, **R**, **S** or **Y**

All the modified DNAs were synthesized using an automated DNA synthesizer (ABI-3400 DNA synthesizer, Applied Biosystems) using conventional and dye-carrying phosphoramidite monomers. 4'-Methylthioazobenzene, Methyl Red, 4'-dimethylamino-2-nitroazobenzene and Cy3 phosphoramidite monomers were converted to phosphoramidite monomers as described in chapter 4.[21-22] The compound 4'-Methoxyazobenzene synthesized according to the literature,[23] was converted to a phosphoramidite monomer as described in the 5-6-7 (Scheme 5-4). The coupling efficiency of the monomers with modified residues was as high as that of the conventional monomers as judged from the intensity of the color of the released trityl cation. After the recommended work-up, the monomers were purified by reverse-phase HPLC and characterized by MALDI-TOFMS (Autoflex II, Bruker Daltonics).

The MALDI-TOFMS data, observed (Obsd.) versus calculated (Calcd.), for the monomers were:

**M1a**: Obsd. 4062 (Calcd. for [**M1a**+$H^+$]: 4063). **M2a**: Obsd. 4481 (Calcd. for [**M2a**+$H^+$]: 4481). **M3a**: Obsd. 4899 (Calcd. for [**M3a**+$H^+$]: 4899). **M4a**: Obsd. 5318 (Calcd. for [**M4a**+$H^+$]: 5317). **M5a**: Obsd. 5735 (Calcd. for [**M5a**+$H^+$]: 5735). **M1S1b**: Obsd. 4485 (Calcd. for [**M1S1b**+$H^+$]: 4484). **S1a**: Obsd. 4067 (Calcd. for [**S1a**+$H^+$]: 4066). **S2a**: Obsd. 4488 (Calcd. for [**S2a**+$H^+$]: 4487). **S3a**: Obsd. 4909 (Calcd. for [**S3a**+$H^+$]: 4908). **S4a**: Obsd. 5332 (Calcd. for [**S4a**+$H^+$]: 5329). **S5a**: Obsd. 5752 (Calcd. for [**S5a**+$H^+$]: 5750). **S2b**: Obsd. 4487 (Calcd. for [**S2b**+$H^+$]: 4487). **R1b**: Obsd. 4108 (Calcd. for [**R1b**+$H^+$]: 4108). **R2b**: Obsd. 4572 (Calcd. for [**R2b**+$H^+$]: 4571). **R3b**: Obsd. 5034 (Calcd. for [**R3b**+$H^+$]: 5034). **R4b**: Obsd. 5501 (Calcd. for [**R4b**+$H^+$]: 5497). **R5b**: Obsd. 5966 (Calcd. for [**R5b**+$H^+$]: 5960). **Y1a**: Obsd. 4234 (Calcd. for

[**Y1a**+$H^+$]: 4237). **Y1b**: Obsd. 4235 (Calcd. for [**Y1b**+$H^+$]: 4237). MMR-**MSa**: Obsd. 2630 (Calcd. for [MMR-**MSa**+$H^+$]: 2632). NMR-**Ob**: Obsd. 2198 (Calcd. for [NMR-**Ob**+$H^+$]: 2197). **MB1**: Obsd. 10300 (Calcd. for [**MB1**+$H^+$]: 10305). **MB2**: Obsd. 10772 (Calcd. for [**MB2**+$H^+$]: 10768). **MB3**: Obsd. 10302 (Calcd. for [**MB3**+$H^+$]: 10305). **MB4**: Obsd. 10769 (Calcd. for [**MB4**+$H^+$]: 10768).

5-6-3 Spectroscopic measurements

The UV/Vis were measured on a JASCO model V-550 spectrophotometer and and Shimadzu UV-1800 instruments with a 10 mm quartz cell. Fluorescent spectra were measured with a JASCO model FP-6500 with a microcell. The excitation wavelength was 546 nm for Cy3. All models were equipped with programmable temperature controllers. The conditions of the sample solutions were as follows (unless otherwise noted): [NaCl] = 100 mM, pH 7.0 (10 mM phosphate buffer), [DNA] = 5 μM. All samples of DNA-dye conjugates were heated at 80 °C for 5 min in the dark to thermally isomerize the *cis*-form, which might be photo-isomerized by ambient light, to the *trans*-form before spectroscopic measurement.[24]

5-6-4 Measurement of melting temperature

See 2-6-1 because the procedures are the same. The conditions of the sample solutions were the same as those described for the above spectroscopic measurements.

5-6-5 NMR measurements

See 3-6-5 because the procedures and conditions are the same.

5-6-6 Computer modeling

Molecular modeling by conformational energy minimization was performed with the InsightII/discover3 software (Molecular Simulation, Inc.) on a Silicon Graphics O2+ workstation with the operating system IRIX64 Release 6.5 and AMBER force field was used for the calculations. The results of the NMR analyses served as a starting point for the modeling. For the analysis a trimer of Methyl Red, 4'-methoxyazobenzene and 4'-methylthioazobenzene was prepared by positioning the three dye molecules in a cofacial orientation and replacing three native base-pairs.

5-6-7 Synthesis of a phosphoramidite monomer of 4'-Methoxyazobenzene

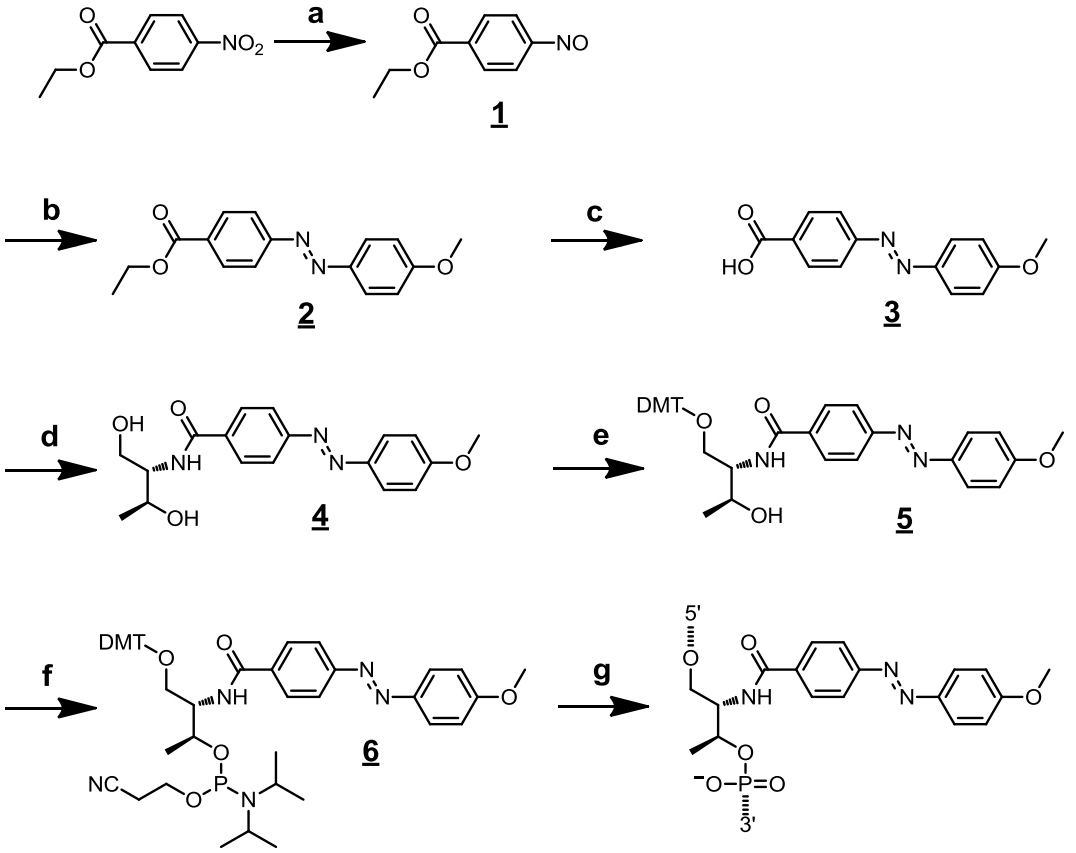


**Supplementary Scheme 1.** Synthetic procedures of 4'-methoxyazobenzene and corresponding phosphoramidite monomers. (a) 1) $NH_4Cl$, Zn, $CH_3OC_2H_5OH$, 20 $^oC$; 2) $FeCl_3$, $CH_3OH$, 0 $^oC$; (b) *p*-anisidine, AcOH; (c) 1) 2M NaOH, EtOH, 2) HCl; (d) D-threoninol, DCC, HOBt, DMF; (e) DMT-Cl, $CH_2Cl_2$, Pyridine, 0→25 $^oC$; (f) 2-cyanoethyl-*N*,*N*,*N'*,*N'*-tetraisopropylphosphorodiamidite, $CH_3CN$; (g) DNA synthesizer.

**Synthesis of 4'-methylthioazobenzene-4-carboxylic acid (Compound 1)**

Ethyl 4-nitrosobenzoate was synthesized according to the previous report.[24] This compound was used to next reaction without purification.

1.49 g (8.3 mmol) of ethyl 4-nitrosobenzoate and 1.43 g (11.7 mmol) of *p*-anisidine were dissolved in 33 mL of acetic acid. The mixture was stirred at room temperature overnight under dark. Then, the solution was poured into water and extracted with ethyl acetate. The organic layer was washed with distilled water, saturated solution of $NaHCO_3$ and NaCl, and then dried over $MgSO_4$. After the removal the solvent, the crude mixture was subjected to silica gel column chromatography (Hexane : AcOEt = 15 : 1) to afford 1.87 g (6.6 mmol) of compound **1** (yield 79.1%).

1.87 g (6.6 mmol) of compound **2** was dissolved in 200 mL of ethanol. Then 33 mL of aqueous NaOH solution (2M) was added and the mixture was stirred overnight under dark. After the hydrolysis was completed, aqueous HCl solution (1M) was added to mixture and pH of the solution was adjusted to around 5.0, followed by the extraction with ethyl acetate. The organic layer was washed with distilled water and saturated solution of NaCl and then dried over $MgSO_4$. After removal solvent, the crude product (compound **3**) was used in the next step without further purification (1.75 g (6.6 > mmol) yield > 99%).

**Synthesis of the phosphoramidite monomer**

0.40 g (3.8 mmol) of D-threoninol was coupled with 0.98 g (3.8 mmol) of compound **3** in the presence of dicyclohexylcarbodiimide (0.95 g, 4.6 mmol) and 1-hydroxybenzotriazole (0.62 g, 4.6 mmol) in 40 mL DMF. After the reaction mixture was stirred at room temperature for 11 h under dark, the solvent was removed and the

remained oil was subjected to silica gel column chromatography (Chloroform : MeOH = 10 : 1) to afford 1.53 g (3.8 > mmol) of compound **4** (yield > 99%)

Dry pyridine (20 mL) containing 1.53 g (3.8 > mmol) of compound **4** and 0.74 g (5.7 mmol) of diisopropylethylamine was cooled on ice under nitrogen, and 1.94 g (5.7 mmol) of 4,4'-dimethoxytrityl chloride and 58 mg (0.48 mmol) of 4-dimethylaminopyridine in 15 mL of dichloromethane was added to the above mixture. After 4 h of stirring, the solvent was removed, followed by silica gel column chromatography (Hexane : AcOEt : $Et_3N$= 50 : 50 : 3) to afford 1.61 g (2.49 mmol) of compound **5** (yield 65.3%).

In dry acetonitrile (9 mL) under nitrogen, 1.61 g (2.5 mmol) of compound **5** and 0.90 g (3.0 mmol) of 2-cyanoethyl *N,N,N',N'*-tetraisopropylphosphorodiamidite were reacted with 0.23 g (3.2 mmol) of 1*H*-tetrazole. Prior to the reaction, compound **5** and 1*H*-tetrazole were dried by coevaporation with dry acetonitrile (twice). After 2 h, the solvent was removed by evaporation and the crude mixture was dissolved in ethyl acetate. The solvent was washed with distilled water and saturated solution of $NaHCO_3$ and NaCl and dried over $MgSO_4$. After the removal the solvent, the crude mixture was subjected to silica gel column chromatography (Hexane : AcOEt : $Et_3N$= 60 : 40 : 3) to afford 1.52 g (1.8 mmol) of compound **6** (yield 72.2%).

**NMR and MS assignment**

**Compound 2 (Ethyl 4'-methoxyazobenzene-4-carboxylate)**

Silica gel column chromatography (Hexane : AcOEt = 15 : 1) (yield 79.1%): $^1$H NMR [DMSO-$d_6$, 500 MHz] δ = 8.19 ppm (d、2H、*J* = 8.5 Hz、aromatic protons), 8.00 ppm (d、4H、*J* = 8.0 Hz、aromatic protons), 7.21 ppm (d、2H、*J* = 9.0 Hz、

aromatic protons), 4.40 ppm (q、2H、$^{3}J$ = 7.0 Hz、$CH_3$-$CH_2$-O-CO-R), 3.93 ppm (s、3H、-O-$CH_3$), 1.40 ppm (t、3H、$^{3}J$ = 7.0 Hz、$CH_3$-$CH_2$-O-CO-R) ; $^{13}$C NMR [DMSO-$d_6$, 125 MHz] δ = 165.2 (1C), 162.7 (1C), 154.6 (1C), 146.2 (1C), 131.1 (1C), 130.4 (2C), 125.1 (2C), 122.4 (2C), 114.8 (2C), 61.0 (1C), 55.7 (1C), 14.1 (1C) ppm

FAB-HRMS: *m/z* calcd for $C_{16}H_{17}N_2O_3^+$: 285.1239 ($M^+$+H); found: 285.1227

**Compound 3 (4'-methoxyazobenzene-4-carboxylic acid, corresponding to O)**

(yield > 99%): $^{1}$H NMR [DMSO-$d_6$, 500 MHz] δ = 13.3 ppm (s、1H、R-CO-O*H*), 8.16 ppm (d、2H、*J* = 8.5 Hz、aromatic protons), 7.98 ppm (d、2H、*J* = 9.0 Hz、aromatic protons), 7.95 ppm (d、2H、*J* = 8.5 Hz、aromatic protons), 7.20 ppm (d、2H、*J* = 8.5 Hz、aromatic protons), 3.93 ppm (s、3H、-O- $CH_3$) ; $^{13}$C NMR [DMSO-$d_6$, 125 MHz] δ = 166.8 (1C), 162.6 (1C), 154.4 (1C), 146.2 (1C), 132.4 (1C), 130.6 (2C), 125.0 (2C), 122.2 (2C), 114.8 (2C), 55.7 (1C) ppm

FAB-HRMS: *m/z* calcd for $C_{14}H_{12}N_2O_3$: 256.0848 ($M^+$); found: 256.0864

**Compound 4 of O**

Silica gel column chromatography (Chloroform : MeOH = 10 : 1) (yield > 99%): $^{1}$H NMR [DMSO-$d_6$, 500 MHz] δ = 8.10 ppm (dd、2H、*J* = 9.0 Hz、aromatic protons), 7.95 ppm (m、5H、aromatic protons and –N*H*-CO-), 7.20 ppm (dd、2H、*J* = 9.0 Hz、aromatic protons), 4.66 ppm (m 、 2H 、 -O*H*), 3.96 ppm (m 、 2H 、 R-C*H*(NHR)-C*H*$CH_3$-OH), 3.92 ppm (s、3H、Azo-O- $CH_3$), 3.55 ppm (m、1H、HO-C$H_2$-CH(NHR)-), 3.65 ppm (m、1H、HO-C$H_2$-CH(NHR)-), 1.11 ppm (d、3H、$^{3}J$ = 6.0 Hz、R-CH(NHR)-CHC$H_3$-OH) ; $^{13}$C NMR [DMSO-$d_6$, 125 MHz] δ = 165.9 (1C), 162.4 (1C), 153.4 (1C), 146.2 (1C), 136.4 (1C), 128.6 (2C), 124.9 (2C), 122.0 (2C), 114.7 (2C), 64.9 (1C), 60.5 (1C), 56.9 (1C), 55.7 (1C), 20.2 (1C) ppm

FAB-HRMS: *m/z* calcd for $C_{18}H_{22}N_3O_4^+$: 344.1610 ($M^+$+H); found: 344.1618

**Compound 5 of O**

Silica gel column chromatography (Hexane : AcOEt : $Et_3N$= 50 : 50 : 3) (yield 65.3%): $^1$H NMR [DMSO-$d_6$, 500 MHz] δ = 8.25 (d, 1H, $^3J$ = 8.5 Hz, -N*H*-CO-), 8.14 (d, 2H, *J* = 8.5 Hz, aromatic protons), 7.98 (m, 4H, aromatic protons), 7.45 (d, 2H, *J* = 7.0 Hz, aromatic protons), 7.30 (m, 6H, aromatic protons), 7.26-7.18 (m, 3H, aromatic protons), 6.89 (m, 4H, aromatic protons), 4.66 (d, 1H, $^3J$ = 6.0 Hz, -O*H*), 4.20 (m, 1H, DMT-O-$CH_2$C*H*(NH-)-), 4.09 (m, 1H, -C*H*(OH)$CH_3$), 3.92 (s, 3H, -O-C$H_3$), 3.76 (s, 6H, -Ph-O-C$H_3$), 3.29 and 3.03 (m, 2H, DMT-O-C$H_2$CH(NH-)-), 1.08 ppm (d, 3H, $^3J$ = 6.5 Hz, -CH(OH)C$H_3$) ; $^{13}$C NMR [DMSO-$d_6$, 125 MHz] δ = 165.9 (1C), 162.4 (1C), 158.0 (2C), 153.2 (1C), 146.2 (1C), 145.2 (1C), 136.3 (1C), 135.9 (1C), 135.8 (1C), 129.7 (4C), 128.7 (2C), 127.7 (4C), 126.6 (1C), 124.9 (2C), 122.0 (2C), 114.7 (2C), 113.1 (4C), 85.1 (1C), 65.3 (1C), 63.0 (1C), 55.7 (1C), 55.4 (1C), 55.0 (2C), 20.4 (1C) ppm

FAB-HRMS: *m/z* calcd for $C_{39}H_{40}N_3O_6^+$: 646.2917 ($M^+$+H); found: 646.2936

**Compound 6 of O**

Silica gel column chromatography (Hexane : AcOEt : $Et_3N$= 60 : 40 : 3) (yield 72.2%): $^{31}$P NMR [$CDCl_3$, 121 MHz] δ = 149.1, 148.5 ppm; FAB-HRMS: *m/z* calcd for $C_{48}H_{57}N_5O_7P^+$: 846.3990 ($M^+$+H); found: 846.3975

## 5-7 Notes and References


1. A. S. Davydov, *Theory of molecular excitons*, Plenum, New York, 1971.
2. M. Kasha, *Radiat. Res.*, 1963, **20**, 55.
3. T. Kobayashi, *J-aggregates*, World Scientific, Singapore, 1996.
4. (a) A. H. Herz, *Adv. Colloid Interface Sci.*, 1977, **8**, 237; (b) E. W. Knapp, *Chem. Phys.*, 1984, **85**, 73; (c) J. R. Durrant, J. Knoester and D. A. Wiersma, *Chem. Phys. Lett.*, 1994, **222**, 450; (d) A. S. R. Koti and N. Periasamy, *J. Mater. Chem.*, 2002, **12**, 2312; (e) A. S. R. Koti, J. Taneja and N. Periasamy, *Chem. Phys. Lett.*, 2003, **375**, 171.
5. (a) K. Murata, S.-i. Kuroda and K. Saito, *Thin Solid Films*, 1997, **295**, 73; (b) F. D. Lewis, Y. Wu, L. Zhang, X. Zuo, R. T. Hayes and M. R. Wasielewski, *J. Am. Chem. Soc.*, 2004, **126**, 8206; (c) F. D. Lewis, L. Zhang, X. Liu, X. Zuo, D. M. Tiede, H. Long and G. C. Schatz, *J. Am. Chem. Soc.*, 2005, **127**, 14445; (d) A. Yamaguchi, N. Kometani and Y. Yonezawa, *Thin Solid Films*, 2006, **513**, 125; (e) A. L. Burin, M. E. Armbruster, M. Hariharan and F. D. Lewis, *Proc. Natl. Acad. Sci.*, 2009, **106**, 989.
6. Czikkely V., Dreizler G., Försterling H. D., Kuhn H., Sondermann J., Tillmann P. and Wiegand J. Z., *Z. Naturforsch.*, 1969, **24a**, 1821.
7. (a) J. L. Seifert, R. E. Connor, S. A. Kushon, M. Wang and B. A. Armitage, *J. Am. Chem. Soc.*, 1999, **121**, 2987; (b) M. Wang, G. L. Silva and B. A. Armitage, *J. Am. Chem. Soc.*, 2000, **122**, 9977; (c) S. Bernacchi and Y. Mély, *Nucleic Acids Res.*, 2001, **29**, e62; (d) R. A. Garoff, E. A. Litzinger, R. E. Connor, I. Fishman and B. A. Armitage, *Langmuir*, 2002, **18**, 6330; (e) S. Bernacchi, E. Piémont, N. Potier, A. v. Dorsselaer and Y. Mély, *Biophys. J.*, 2003, **84**, 643; (f) M. Hariharan, Y. Zheng, H. Long, T. A. Zeidan, G. C. Schatz, J. Vura-Weis, M. R. Wasielewski, X. Zuo, D. M. Tiede and F. D. Lewis, *J. Am. Chem. Soc.*, 2009, **131**, 5920; (g) T. M. Wilson, T. A. Zeidan, M. Hariharan, F. D. Lewis and M. R. Wasielewski, *Angew. Chem. Int. Ed*, 2010, **49**, 2385; (h) A. L. Stadler, B. R. Renikuntla, D. Yaron, A. S. Fang and B. A. Armitage, *Langmuir*, 2010, **27**, 1472.
8. (a) K. Yamana, R. Iwase, S. Furutani, H. Tsuchida, H. Zako, T. Yamaoka and A. Murakami, *Nucleic Acids Res.*, 1999, **27**, 2387; (b) A. Mahara, R. Iwase, T. Sakamoto, K. Yamana, T. Yamaoka and A. Murakami, *Angew. Chem. Int. Ed*, 2002, **41**, 3648; (c) C. Brotschi and C. J. Leumann, *Angew. Chem. Int. Ed*, 2003, **42**, 1655; (d) E. Mayer-Enthart and H.-A. Wagenknecht, *Angew. Chem. Int. Ed*, 2006, **45**, 3372; (e) D. Baumstark and H.-A. Wagenknecht, *Angew. Chem. Int. Ed*, 2008, **47**, 2612; (f) D. Baumstark and H.-A. Wagenknecht, *Chem. Eur. J.*,

2008, **14**, 6640; (g) M. Nakamura, Y. Murakami, K. Sasa, H. Hayashi and K. Yamana, *J. Am. Chem. Soc.*, 2008, **130**, 6904; (h) I. V. Astakhova, V. A. Korshun and J. Wengel, *Chem. Eur. J.*, 2008, **14**, 11010; (i) M. Fukuda, M. Nakamura, T. Takada and K. Yamana, *Tetrahedron Lett.*, 2010, **51**, 1732.

9. (a) T. J. Matray and E. T. Kool, *J. Am. Chem. Soc.*, 1998, **120**, 6191; (b) J. Gao, C. Strässler, D. Tahmassebi and E. T. Kool, *J. Am. Chem. Soc.*, 2002, **124**, 11590; (c) J. N. Wilson, Y. N. Teo and E. T. Kool, *J. Am. Chem. Soc.*, 2007, **129**, 15426; (d) S. S. Tan, S. J. Kim and E. T. Kool, *J. Am. Chem. Soc.*, 2011, **133**, 2664.
10. (a) V. L. Malinovskii, F. Samain and R. Häner, *Angew. Chem. Int. Ed*, 2007, **46**, 4464; (b) H. Bittermann, D. Siegemund, V. L. Malinovskii and R. Häner, *J. Am. Chem. Soc.*, 2008, **130**, 15285; (c) A. L. Nussbaumer, D. Studer, V. L. Malinovskii and R. Häner, *Angew. Chem. Int. Ed*, 2011, **50**, 5490.
11. H. Kashida, T. Takatsu, T. Fujii, K. Sekiguchi, X. Liang, K. Niwa, T. Takase, Y. Yoshida and H. Asanuma, *Angew. Chem. Int. Ed*, 2009, **48**, 7044.
12. M. K. Johansson, H. Fidder, D. Dick and R. M. Cook, *J. Am. Chem. Soc.*, 2002, **124**, 6950.
13. Because the melting temperature of the NMR-**MSa**/NMR-**Ob** duplex was determined to be 25.6 $^{o}$C, NMR measurements were performed at 5 $^{o}$C (278 K), at which temperature a stable duplex exists.
14. In order to monitor imino protons that are exchangeable with water molecules, NMR was measured in $H_2O$ ($H_2O/D_2O$, 9:1) with a 3-9-19 WATERGATE pulse sequence for $H_2O$ suppression. When these data were combined with the NOESY, DQF-COSY and TOCSY spectra obtained in $H_2O$, most of the signals of the duplex could be assigned.
15. The imino-proton signals of the terminal $G^7$ and $G^{12}$ were little broad because of the rapid exchange with water, whereas signals from the other residues remained sharp.
16. When **M5a** and **N** were hybridized, the duplex stabilities were remarkably destabilized ($T_m$ = 36.3). See ref. 17.
17. H. Asanuma, K. Shirasuka, T. Takarada, H. Kashida and M. Komiyama, *J. Am. Chem. Soc.*, 2003, **125**, 2217.
18. B. Z. Packard, D. D. Toptygin, A. Komoriya and L. Brand, *J. Phys. Chem. B*, 1998, **102**, 752.
19. (a) H. Döhner, S. Stilgenbauer, K. Fischer, M. Schröder, M. Bentz and P. Lichter, *Stem Cells*, 1995, **13**, 76; (b) C. Preudhomme, F. Révillion, A. Merlat, L. Hornez,

C. Roumier, N. Duflos-Grardel, J. P. Jouet, A. Cosson, J. P. Peyrat and P. Fenaux, *Leukemia.*, 1999, **13**, 957; (c) C. L. Sawyers, *N. Engl. J. Med.*, 1999, **340**, 1330; (d) P. Bolufer, G. F. Sanz, E. Barragan, M. A. Sanz, J. Cervera, E. Lerma, L. Senent, I. Moreno and M. D. Planelles, *Haematologica*, 2000, **85**, 1248.

20. C. Brotschi, G. Mathis and C. J. Leumann, *Chem. Eur. J.*, 2005, **11**, 1911.
21. a) 原雄一　2009年度修士学位論文　名古屋大学大学院工学研究科物質制御工学専攻　「励起子相互作用を利用した高感度 In-Stem Molecular Beacon の開発」; b) 大澤卓矢　2010年度卒業論文　名古屋大学工学部化学・生物工学科生物機能工学コース　「カチオン性グラフトポリマーとの併用による超高感度インステムモレキュラービーコンシステムの開発」
22. The monomers (**Y**) was synthesized and provided by Yuichi Hara (an alumnus in Asanuma Lab.) and Takuya Osawa (A master course student in Asanuma Lab.)
23. (a) W. H. Nutting, R. A. Jewell and H. Rapoport, *J. Org. Chem.*, 1970, **35**, 505; (b) M. A. Rahim, P. N. P. Rao and E. E. Knaus, *J. Heterocycl. Chem.*, 2002, **39**, 1309.
24. H. Nishioka, X. Liang, H. Kashida and H. Asanuma, *Chem. Commun.*, 2007, 4354.

## 5-8 Appendixes

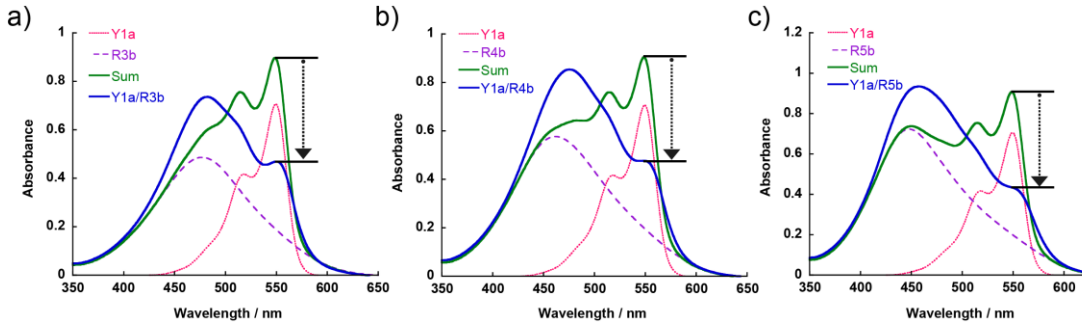


Appendix Figure 5-1. a) UV-Vis spectra of the **Y1a/R3b** duplex (blue line), single-stranded **Y1a** (pink dotted line), **R3b** (purple dashed line), and a simple sum of their spectra (sum-spectrum, **Y1a + R3b,** green line) at 20 $^{o}$C. b) UV-Vis spectra of the **Y1a/R4b** duplex (blue line), single-stranded **Y1a** (pink dotted line), **R4b** (purple dashed line), and a simple sum of their spectra (sum-spectrum, **Y1a + R4b,** green line) at 20 $^{o}$C. c) UV-Vis spectra of the **Y1a/R5b** duplex (blue line), single-stranded **Y1a** (pink dotted line), **R5b** (purple dashed line), and a simple sum of their spectra (sum-spectrum, **Y1a + R5b,** green line) at 20 $^{o}$C. Hypochromicities (difference of absorbance) of Cy3 absorption before and after clustering were calculated as strength of the exciton couplings (The strengths were shown by dotted arrows). Solution conditions were as follows: [DNA] = 5 μM, [NaCl] = 100 mM, pH 7.0 (10mM phosphate buffer).

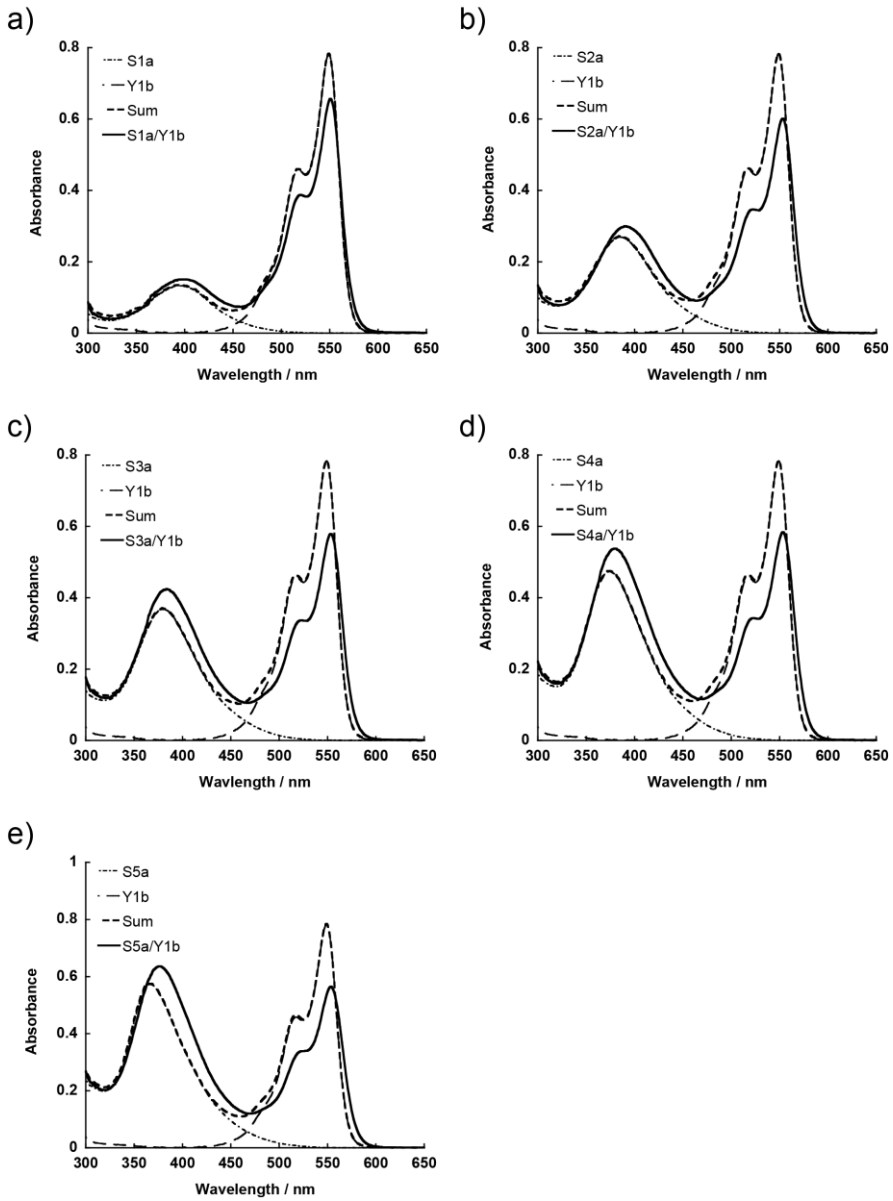


Appendix Figure 5-2. UV-Vis spectra of the **S*n*a/Y1b** duplex (solid line), single-stranded **S*n*a** (dashed and dotted line), **Y1b** (long broken line), and a simple sum of their spectra (sum-spectrum, **S*n*a + Y1b**, short broken line) at 20 $^{o}$C (a); $n$ = 1, b); $n$ = 2, c); $n$ = 3, d); $n$ = 4, e); $n$ = 5). Hypochromicities (difference of absorbance) of Cy3 absorption before and after clustering were calculated as strength of the exciton couplings. Solution conditions were as follows: [DNA] = 5 μM, [NaCl] = 100 mM, pH 7.0 (10mM phosphate buffer).

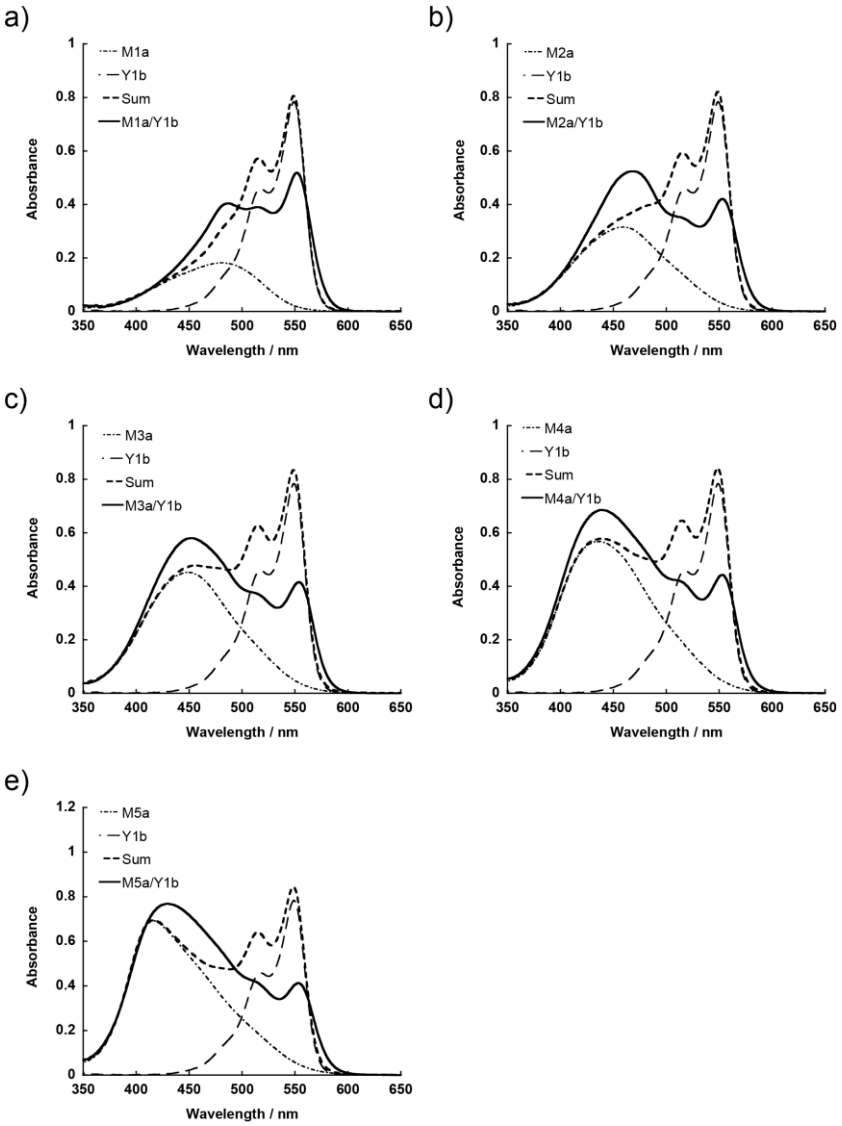


Appendix Figure 5-3. UV-Vis spectra of the **M*n*a/Y1b** duplex (solid line), single-stranded **M*n*a** (dashed and dotted line), **Y1b** (long broken line), and a simple sum of their spectra (sum-spectrum, **M*n*a + Y1b**, short broken line) at 20 $^{o}$C (a); $n$ = 1, b); $n$ = 2, c); $n$ = 3, d); $n$ = 4, e); $n$ = 5). Hypochromicities (difference of absorbance) of Cy3 absorption before and after clustering were calculated as strength of the exciton couplings. Solution conditions were as follows: [DNA] = 5 μM, [NaCl] = 100 mM, pH 7.0 (10mM phosphate buffer).

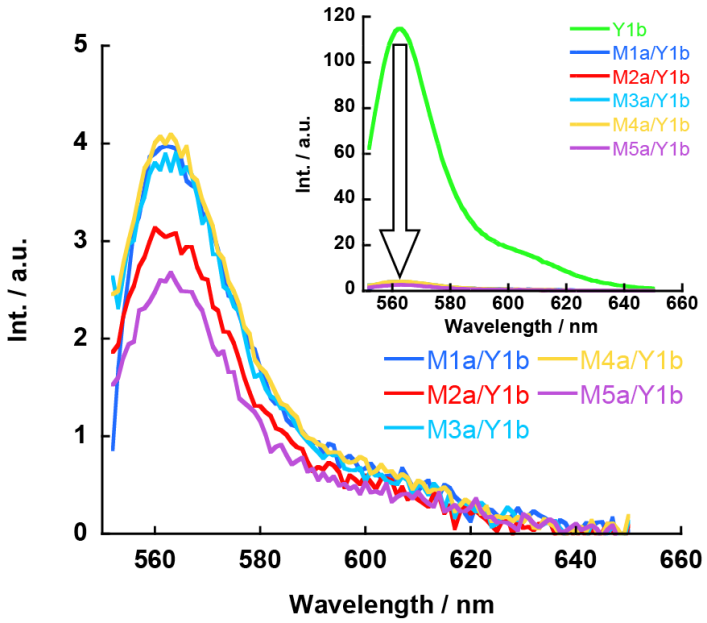


Appendix Figure 5-4. Fluorescence emission spectra of Cy3 (**Y**) excited at 546 nm and their duplexes with strands tethered Methyl Red as quenchers. Solution conditions were as follows: 20 °C, [**M*n*a**] = 0.4 μM, [**Y1b**] = 0.2 μM, [NaCl] = 100 mM, pH 7.0 (10 mM phosphate buffer).

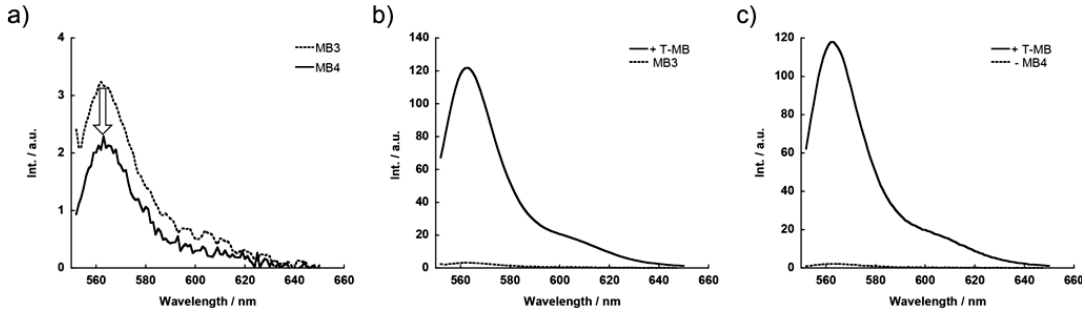


Appendix Figure 5-5. a) Comparison between the background emission of **MB3** and **MB4**. Fluorescence emission spectra of b) **MB3** and c) **MB4** excited at 546 nm with or without the presence of **T-MB**. Solution conditions were as follows: 20 °C, [**T-MB**] = 0.4 μM, [**MB3**] = [**MB4**] = 0.2 μM, [NaCl] = 100 mM, pH 7.0 (10 mM phosphate buffer).

# Chapter 6. Dye-clustering in RNA duplexes to apply for a fluorophore-quencher system

## 6-1 Abstract

We prepared reversed dye clusters by hybridizing two RNA oligomers, each of which tethered dyes (Methyl Red, 4'-methylthioazobenzene, and thiazole orange) on D-threoninols (threoninol-nucleotides) at the center of their strands. NMR analyses revealed that two dyes from each strand were axially stacked in an antiparallel manner to each other in the duplex, and were located adjacent to the 3'-side of a natural nucleobase. Interestingly, this positional relationship of the dyes was completely the opposite of that assembled in DNA that we showed in chapter 3: dyes in DNA were located adjacent to the 5'-side of a natural nucleobase. This observation was also consistent with the circular dichroism of dimerized dyes in which the Cotton effect of the dyes (i.e., the winding properties of two dyes) was inverted in RNA compared with that in DNA. Further spectroscopic analyses revealed that clustering of the dyes on RNA duplexes induced distinct hypsochromicity and narrowing of the band, demonstrating that the dyes were axially stacked (i.e., H-aggregates) even on an A-type helix. Based on these results, we also prepared heterodimers of a fluorophore (thiazole orange) and quencher (Methyl Red) in an RNA duplex. Fluorescence from thiazole orange was found to be strongly quenched by Methyl Red due to the excitonic interaction, so that the ratio of fluorescent intensities of the RNA-thiazole orange conjugate with and without its complementary strand carrying a quencher became as high as 27. We believe that these RNA-dye conjugates are potentially useful probes for

real-time monitoring of RNA interference (RNAi) mechanisms.

## 6-2 Introduction

Recently, RNA as well as DNA have attracted much attention because of new discoveries of various functional RNAs, such as ribozymes,[1] microRNAs (miRNA),[2] and short interfering RNAs (siRNA),[3] most of which are concerned with gene expression.[4] In particular, a huge number of studies have been conducted on RNA interference (RNAi) to clarify its strong silencing mechanism of gene expression through the RNA-induced silencing complex (RISC).[5] Since siRNA is potentially applicable as a nucleic acid drug to knockout specific genes, chemical modification of RNA is increasingly important in order to avoid off-target effects and provide enzymatic durability.[6] Furthermore, modified RNAs are also a powerful tool for investigating the role of functional small RNAs *in vivo* whose mechanisms have not yet been clarified in detail.[7]

From chapter 2 to chapter 5, we have developed new methodology for preparation of dye-clusters in DNA duplex based on threoninol nucleotides and proposed novel fluorophore-quencher system based on excitonic interaction. This system can be applicable to various scaffolds such as not only DNA duplex, but also RNA duplex. If the system is applied to RNA duplex, this modified RNA should provide various applications in biology, biotechnology and molecular diagnostics.[8] Then, we then applied the clustering and system to RNA duplexes for their functionalization. However, as mentioned in section 1-6, chapter 1 (general introduction of this chapter), functional molecules in RNA duplexes do not necessarily behave similar to those in DNA duplexes, although DNA and RNA have similar nucleotide structures. Accordingly,

prior to designing functional RNA for applications, we first investigated the structure of RNA duplexes involving base-surrogates in detail because the local structure around a base-surrogate in an RNA duplex, reflecting an A-form structure, should be different from that in a DNA duplex.

In this chapter, we prepared dye clusters tethered on D-threoninol in RNA duplexes, and investigated their structure and spectroscopic behavior in detail. In chapter 2 and 3, we prepared dye clusters in DNA duplexes by hybridization of two single-stranded DNAs, each of which tethered dyes through D-threoninols at the center of the strand. We found that dyes excitonically interacted with each other, and the duplex was highly stabilized due to stacking interactions between the dyes. NMR structural analysis revealed that the dyes were located adjacent to a natural nucleobase at the 5'-side in the DNA duplex (Scheme 6-1a). Here, we applied these designs to the preparation of dye clusters in RNA duplexes. We found that dyes from each strand are axially stacked, even in an A-form RNA duplex, as observed in DNA duplexes. But NMR and CD analyses revealed that the dyes are located adjacent to the 3'-side of a natural nucleobase, which was completely the reverse of that assembled in DNA. Based on this investigation, we next designed an RNA duplex involving a pair (dimer) of a fluorophore (thiazole orange) and quencher (Methyl Red). Fluorescence from thiazole orange is remarkably quenched by the stacked Methyl Red in the duplex, while

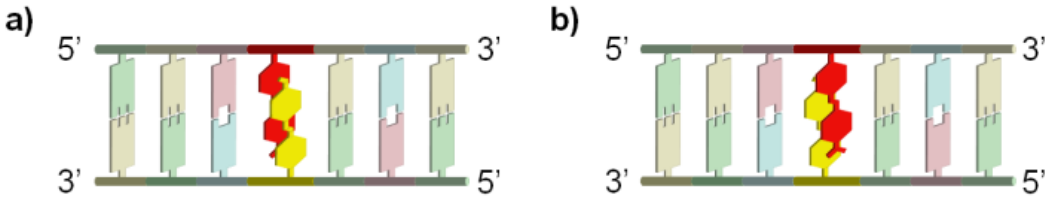


Scheme 6-1. Schematic illustration of the two possible stacking modes of the heterodimer. The dyes are located adjacent to a) the 5'-side corresponding to the **M/S** orientation or b) the 3'-side of a natural nucleobase corresponding to the **S/M** orientation in rNMR-**Ma**/rNMR-**Sb**.

single-stranded RNA with the fluorophore emits strongly. Since RISC forms mature complexes with the antisense strand from an siRNA duplex, this modified RNA duplex having a fluorophore-quencher pair can be a useful tool for tracing RISC in living cells.

rNMR-**Ma** : 5'-C$^{1}$G$^{2}$A$^{3}$-**M**-G$^{4}$U$^{5}$C$^{6}$-3'
rNMR-**Sb** : 3'-G$^{12}$C$^{11}$U$^{10}$-**S**-C$^{9}$A$^{8}$G$^{7}$-5'

r**M*n*a** : 5'-GGU-AUC-**M**$_n$-GCA-AUC-3'
r**M*n*b** : 3'-CCA-UAG-**M**$_n$-CGU-UAG-5' ***n*** = 1,2,3,6
r**S*n*b** : 3'-CCA-UAG-**S**$_n$-CGU-UAG-5'
r**H1b** : 3'-CCA-UAG-**H**-CGU-UAG-5'

r**N** : 5'-GGU-AUC-GCA-AUC-3'
r**C** : 3'-CCA-UAG-CGU-UAG-5'

d**M1a** : 5'-GGT-ATC-**M**-GCA-ATC-3'
d**H1a** : 5'-GGT-ATC-**H**-GCA-ATC-3'
d**M1b** : 3'-CCA-TAG-**M**-CGT-TAG-5'

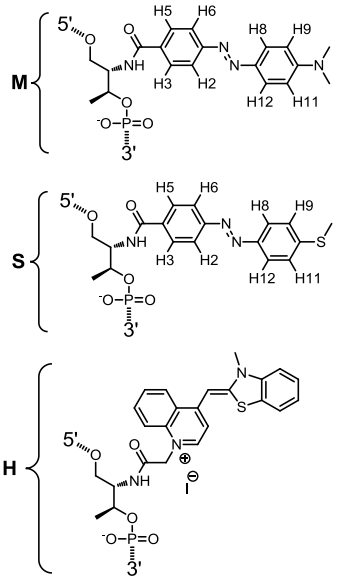


Scheme 6-2. Sequences of the (modified) RNAs and DNAs synthesized in this chapter.

## 6-3 Results

### 6-3-1 Structural determination of the dimer by NMR spectroscopy

The design of the dye clusters in RNA duplexes is illustrated in Scheme 6-1 (in dimer formation): the hybridization of two complementary RNAs, each of which tethers base-surrogates having dyes on D-threoninols, results in assembled dyes at the center of the duplex. Actual RNAs involving the surrogates synthesized in this chapter are shown in Scheme 6-2. First, we carried out NMR analysis of double-stranded RNA-dye conjugates involving Methyl Red and 4'-methylthioazobenzene (rNMR-**Ma**/rNMR-**Sb**, respectively), in order to clarify the stacked structures of **M** and **S** in the RNA duplex. Here, we focused on the mutual orientation of two dyes because there are two possible stacking patterns of the dyes as shown in Scheme 6-1: adjacent to the 5'-side (Scheme 6-1a, **M**/**S**) or to the 3'-side (Scheme 6-1b, **S**/**M**) of the natural nucleobase.

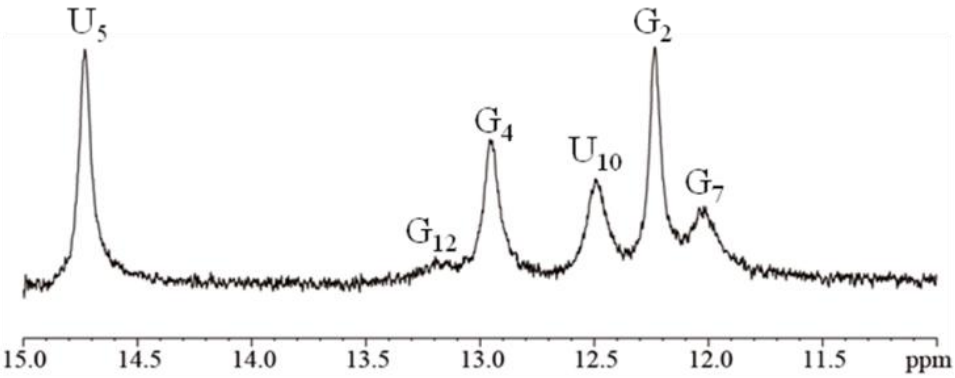


Figure 6-1. One-dimensional NMR spectrum of the rNMR-**Ma**/rNMR-**Sb** duplex at the imino region in $H_2O/D_2O$ 9:1 at 278 K, pH 7.0 (20 mM phosphate buffer) in the presence of 200 mM NaCl. The concentration of rNMR-**Ma**/rNMR-**Sb** was 1.0 mM. Assignments of the imino-protons and the residue numbers are denoted at the top of the peaks.

The one-dimensional NMR spectrum measured in $H_2O$ at the region of imino-protons (11-15 ppm) is depicted in Fig. 6-1.[9-10] rNMR-**Ma**/rNMR-**Sb** allows six natural base pairs ($C^1$-$G^{12}$, $G^2$-$C^{11}$, $A^3$-$U^{10}$, $G^4$-$C^9$, $U^5$-$A^8$, and $C^6$-$G^7$) and one tentative **M**-**S** pair Scheme 6-2). Corresponding to the six base pairs, we could observe five individual signals and one shoulder signal, all of which could be assigned on the basis of the NOE connectivities and chemical shifts of each signal. The imino-proton signals of the terminal $G^7$ and $G^{12}$ were rather broad because of the rapid exchange with water. In addition, the signal assignable to $U^{10}$, which was located adjacent to the incorporated surrogate, was slightly broad, probably due to the disturbed hydrogen bondings by the **M**-**S** pair. Figure 6-2 shows the NOEs between the imino-proton signal (11-15 ppm) and the methyl-proton signal (1.0-3.0 ppm) regions. A strong NOE signal was observed between the imino-proton of $G^4$ and N-$CH_3$ of **M**, demonstrating that the Methyl Red moiety was located near the $G^4$-$C^9$ pair. Concurrently, we also detected weak but distinct NOE between N-$CH_3$ of the **M** residue and the imino $U^5$ proton located next to the $G^4$-$C^9$ pair. On the other hand, we observed NOE only between S-$CH_3$ of the **S** residue and the imino-proton of $G^2$, which is one base ($A^3$) apart from the **S** residue, but not $U^{10}$ located more closely to it. Oddly, $U^{10}$ did not show NOE with S-$CH_3$ of the **S**

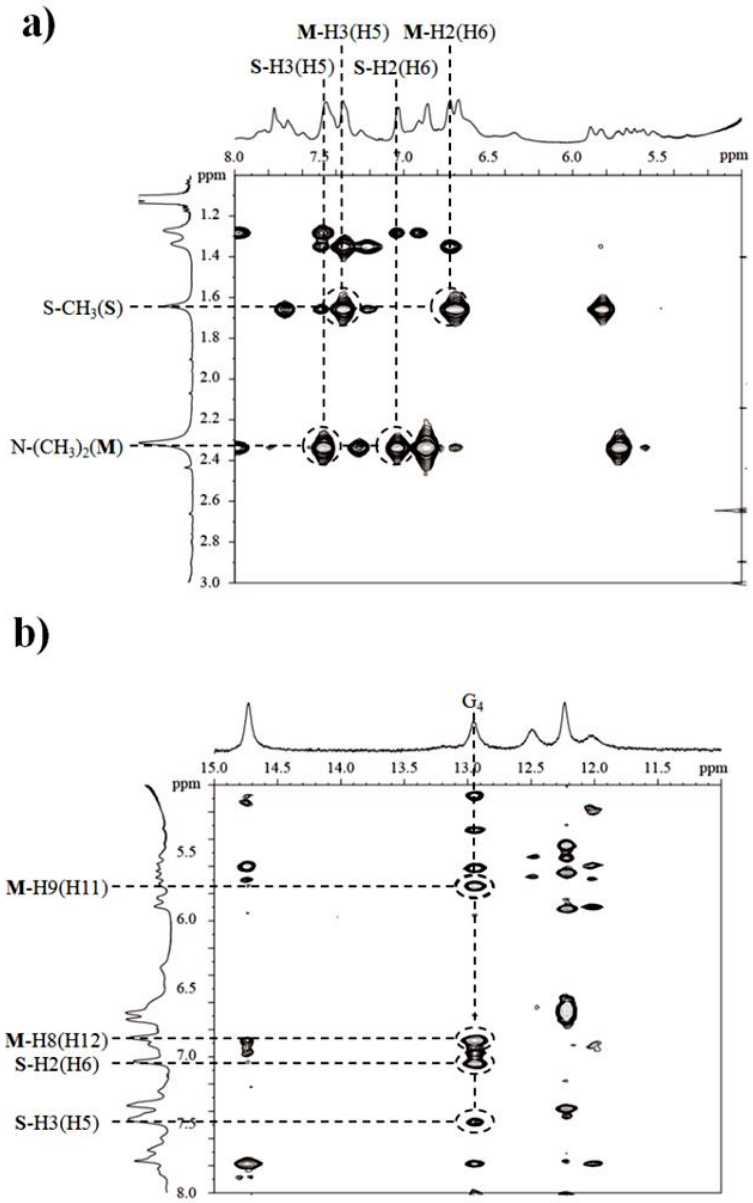


Figure 6-3. 2D NOESY spectrum (mixing time = 150 ms) a) between the regions of 5.0-8.0 ppm and 1.0-3.0 ppm, b) between the regions of 11-15 ppm and 5.0-8.0 ppm for the rNMR-**Ma**/rNMR-**Sb** duplex in $H_2O/D_2O$ 9:1 at 278 K (20 mM phosphate buffer) in the presence of 200 mM NaCl. Assignments of the Methyl Red and 4'-methylthioazobenzene protons are denoted on the one-dimensional spectra (*F1* axis or *F2* axis) using the numbers designated in Scheme 6-2.

residue, while $G^2$ did. However, since we could not see NOE between $U^{10}$ and most of the other protons around $U^{10}$, broadening of the imino-proton due to rapid exchange with water might be the reason for its absence. Based on these NOE results, we concluded that each dye was located adjacent to the 3'-side of the natural nucleobase as

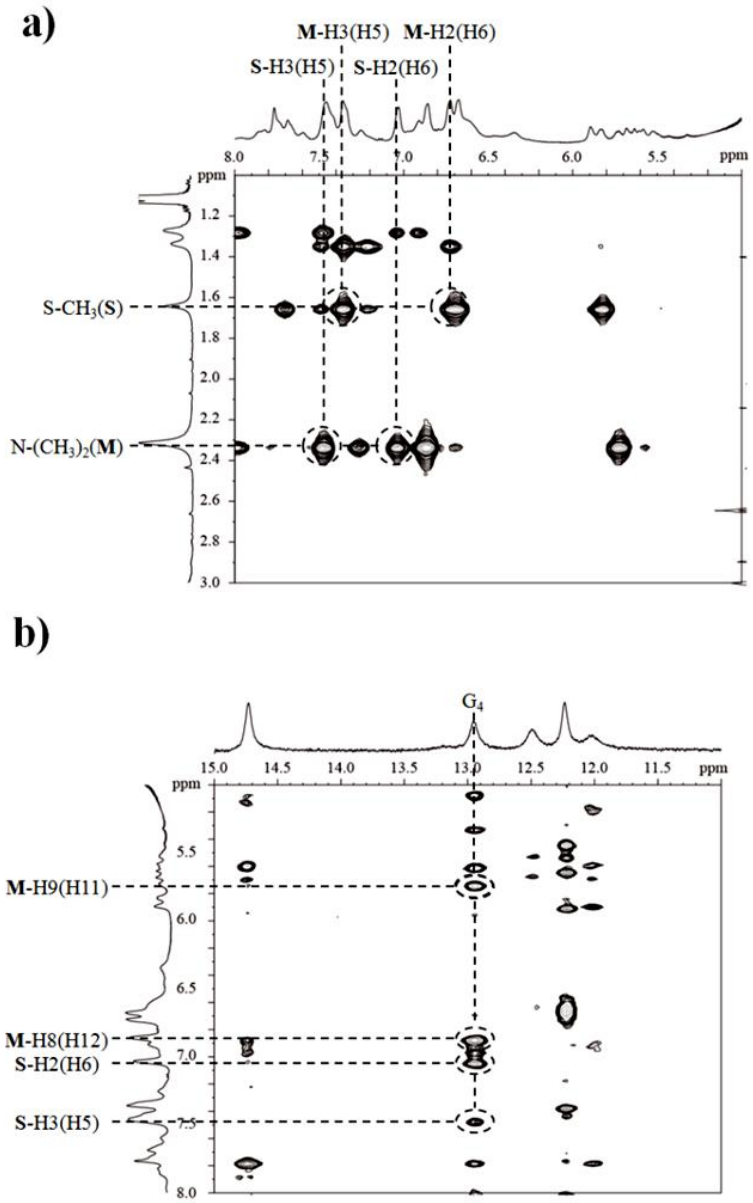


Figure 6-3. 2D NOESY spectrum (mixing time = 150 ms) a) between the regions of 5.0-8.0 ppm and 1.0-3.0 ppm, b) between the regions of 11-15 ppm and 5.0-8.0 ppm for the rNMR-**Ma**/rNMR-**Sb** duplex in $H_2O/D_2O$ 9:1 at 278 K (20 mM phosphate buffer) in the presence of 200 mM NaCl. Assignments of the Methyl Red and 4'-methylthioazobenzene protons are denoted on the one-dimensional spectra (*F1* axis or *F2* axis) using the numbers designated in Scheme 6-2.

depicted in Scheme 6-1b (**S**/**M** orientation). Interestingly, this orientation is totally the opposite of that in the DNA duplex (**M/S** orientation, corresponding to Scheme 6-1a) as we prepared in chapter 3. This structural difference is attributable to the difference of the 3D structure between RNA and DNA duplexes (*vide infra*).

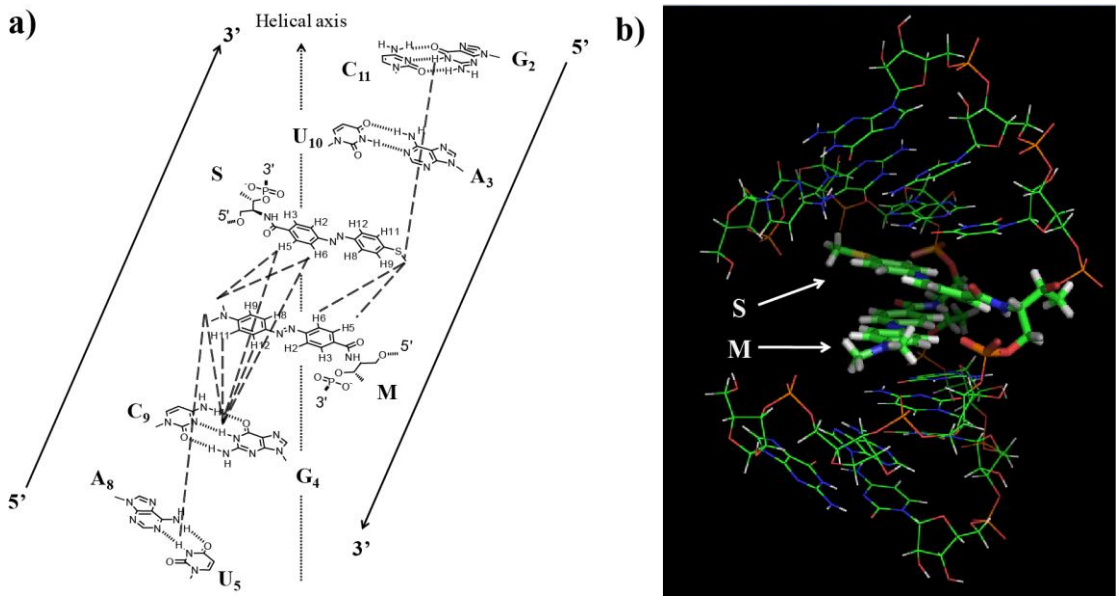


Figure 6-4. Stacking manner and orientation of **M** and **S** residues in the duplex as determined from NOESY a), and model structures of the rNMR-**Ma**/rNMR-**Sb** duplex that we propose based on the NOE signals b). Broken lines in a) show the observed NOE signals. The sticks in b) depict 4'-methylthioazobenzene and Methyl Red in the duplex.

The stacked structure of the two dyes in the RNA duplex was also determined from NOESY between 5.0-8.0 ppm and 1.0-3.0 ppm (Fig. 6-3a), and between 11.0-15.0 ppm and 5.0-8.0 ppm (Fig. 6-3b). We observed clear NOE between N-$CH_3$ of **M** and of each aromatic proton of **S**-H2 (H6) and **S**-H3 (H5), as well as between S-$CH_3$ of the **S** residue and each aromatic proton of **M**-H2 (H6) and **M**-H3 (H5), respectively, demonstrating a head-to-tail (antiparallel) orientation of **M** and **S** residues. As expected, strong NOEs were observed between the imino-proton of $G^4$ and each aromatic proton of **M**-H8 (H12) and **M**-H9 (H11), which is consistent with the **S/M** orientation concluded as above. However, medium NOE signals were also detected between $G^4$ and each aromatic proton of **S**-H2 (H6) and **S**-H3 (H5), respectively, although the **M** residue should be sandwiched between $G^4$ and **S**. These observations are presumably derived from the overall strain of the 3D structure at around the center of the dyes, and each proton is spatially located at a short distance as illustrated in Fig. 6-4. Therefore, we concluded that the two dyes are stacked in an **S/M** and head-to-tail orientation at the

center of the A-formed RNA duplex.

6-3-2 Clustering of the homo-dyes in RNA duplexes as a model system

***M-M homodimers*** Next, we investigated the spectroscopic properties of Methyl Red homo-clusters in RNA duplexes in comparison with DNA.[11] Figure 6-5 shows UV/Vis spectra of r**M1a**/r**M1b** and the simple sum of each r**M1a** and r**M1b** (sum- spectrum). Dimerized Methyl Reds in r**M1a**/r**M1b** showed an absorption maximum at 455 nm with a band slightly narrower than the corresponding sum-spectrum giving a maximum at 479 nm. Large hypsochromicity (24 nm) with a slight narrowing of the band is characteristic of the H-aggregates in which dyes are vertically stacked. These spectroscopic behaviors are similar to those of d**M1a**/d**M1b** in DNA duplexes giving $\lambda_{max}$ at 470 nm with a line-width of 3109 $cm^{-1}$ (compare Fig. 6-5 with Appendix Fig. 6-1a in the Appendixes).

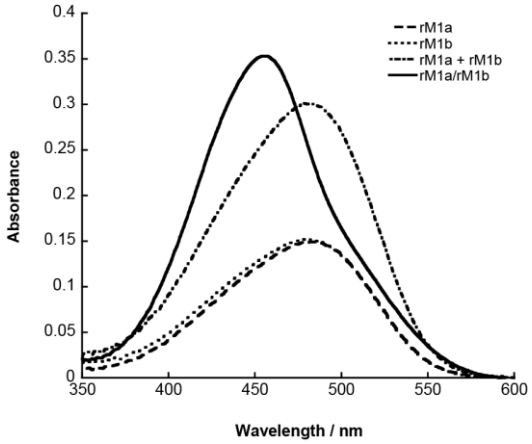


Figure 6-5. UV/Vis spectra of the **rM1a/rM1b** duplex (solid line), single-stranded **rM1a** (dashed line), **rM1b** (dotted line), and a simple sum of their spectra (sum-spectrum, **rM1a** + **rM1b**, dashed-dotted line) at 20 °C. Solution conditions were as follows: [RNA] = 5 μM, [NaCl] = 100 mM, pH 7.0 (10 mM phosphate buffer).

To compare the mutual orientation of the stacked dyes in RNA with DNA, circular dichroism (CD) spectra of r**M1a**/r**M1b** and d**M1a**/d**M1b** were measured at 20 °C where both dimers were stably formed ($T_m$s of r**M1a**/r**M1b** and d**M1a**/d**M1b** were 55.2 and

50.5 °C, respectively). As shown in Fig. 6-6, r**M1a**/r**M1b** and d**M1a**/d**M1b** exhibited typical induced CD (ICD) spectra of A- and B-forms, respectively, at around 250 nm, demonstrating that the native portion of these duplexes kept their intrinsic structures. Interestingly, however, the ICD of r**M1a**/r**M1b** displayed a positive-negative Cotton effect (clockwise winding, see Appendix Fig. 6-2a) at around 350-600 nm where dyes absorb, while that of d**M1a**/d**M1b** showed a negative-positive Cotton effect (counterclockwise winding, see Appendix Fig. 6-2b), indicating that the helical property of the dyes was inversed by changing the framework from DNA to RNA.

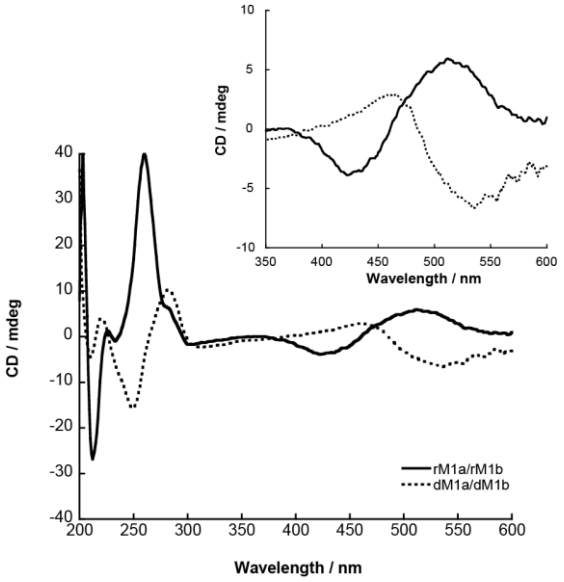


Figure 6-6. CD spectra of r**M1a**/r**M1b** (solid line) and d**M1a**/d**M1b** (dashed line) at the region of 200-600 nm. Solution conditions were as follows: 20 °C, [DNA] = [RNA] = 5 μM, [NaCl] = 100 mM, pH 7.0 (10 mM phosphate buffer).

***Effect of aggregate sizes on duplex stabilities and spectroscopic behavior.*** The $T_m$s of r**M*n*a**/r**M*n*b** determined from the change in absorbance at 260 nm are shown in Table 6-1. Incorporation of a single **M**-**M** pair (r**M1a**/r**M1b:** 55.2 °C) slightly lowered the $T_m$ compared with the native r**N**/r**C** duplex (57.6 °C), probably due to the distortion of the rigid RNA duplex. But the $T_m$ uniformly and remarkably increased with the number of **M**-**M** pairs from 55.2 to as high as 73.3 °C (for r**M6a**/r**M6b** involving three

Table 6-1. Effect of the number of dye-pairs on the melting temperature ($T_m$), and absorption maximum ($\lambda_{max}$), and half-line-width of π-π* transitions of Methyl Red.[a]

| Sequences | $T_m$ / °C | $\lambda_{max}$ / nm | Half-line-width / $cm^{-1}$ |
|---|---|---|---|
| r**N**/r**C** | 57.6 | — | — |
| r**M1a**/r**M1b** | 55.2 | 455 | 4105 |
| r**M2a**/r**M2b** | 61.2 | 431 | 4095 |
| r**M3a**/r**M3b** | 67.2 | 422 | 3636 |
| r**M6a**/r**M6b** | 73.3 | 410 | 3752 |
| d**M1a**/d**M1b**[b] | 50.5 | 470 | 3109 |

[a] Measurement conditions were pH 7.0: [DNA] = [RNA] = 5 μM, [NaCl] = 100 mM (10 mM phosphate buffer). For measurement of UV/Vis spectra, measurements were carried out at 20 °C. [b] Data from chapter 2

**M-M** pairs), because the structural distortion was overcompensated by the accumulated stacking interactions among the dyes. The same is true for clustering of Methyl Red in DNA that we developed in chapter 2, except for destabilization by a single **M-M** pair in the RNA duplex (see Appendix Fig. 6-3).

Next, the effect of the dye number on spectroscopic behavior was systematically examined. As depicted in Fig. 6-7 and summarized in Table 6-1, multiplication of the dyes induced a remarkable hypsochromic shift that is characteristic of H-aggregates: the r**M1a**/r**M1b** dimer gave $\lambda_{max}$ at 455 nm, which shifted to 431 and 422 nm by tetramer

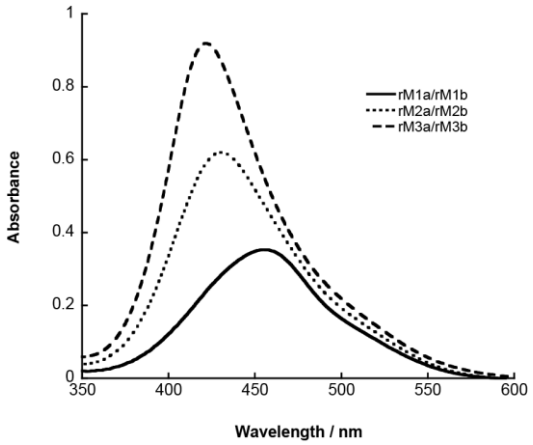


Figure 6-7. Effect of the number of dye pairs on the UV/Vis spectra of r**M*n*a**/r**M*n*b**. Solution conditions were as follows: 20 °C, [RNA] = 5 μM, [NaCl] = 100 mM, pH 7.0 (10 mM phosphate buffer).

(r**M2a**/r**M2b**) and hexamer (r**M3a**/r**M3b**) formation, respectively. We observed strong ICD at the π-π* transition region (350-600 nm) with a clear positive-negative Cotton effect irrespective of the number of dyes, demonstrating that they possessed similar helical properties (Fig. 6-8). As we reported previously, similar hypsochromicity of the Methyl Red cluster was also observed in DNA duplexes because dyes were axially stacked. However in contrast with the clusters in RNA duplexes that showed positive-negative Cotton effect, the ICDs of tetramers and hexamers were reversed in DNA duplexes (see Appendix Fig. 6-4). More specifically, the helical property of axially stacked dyes was inversed by embedding the clusters in RNA in place of DNA.

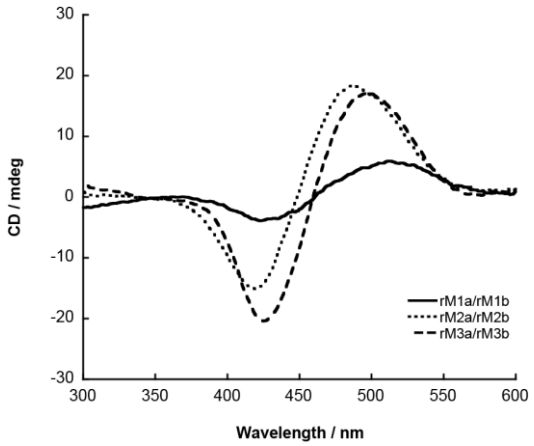


Figure 6-8. Effect of the number of dye pairs on the CD spectra of r**M*n*a**/r**M*n*b**. Solution conditions were as follows: 20 °C, [RNA] = 5 μM, [NaCl] = 100 mM, pH 7.0 (10 mM phosphate buffer).

### 6-3-3 Assembling a fluorophore-quencher heterodimer in RNA duplexes

By using Methyl Red, we verified that stacked homo-assemblies were stably formed in RNA duplexes. Dye assemblies are not only attractive as a novel cluster, but also as a monitoring tool or device for recognition of target oligonucleotides,[12] B-Z DNA transitions,[13] and so on.[14] Dye assembly on RNA as well as on DNA also has the potential to be a useful tool for artificial regulation of gene expression, and activation and fluorescence monitoring of functional RNA, for example. We therefore next

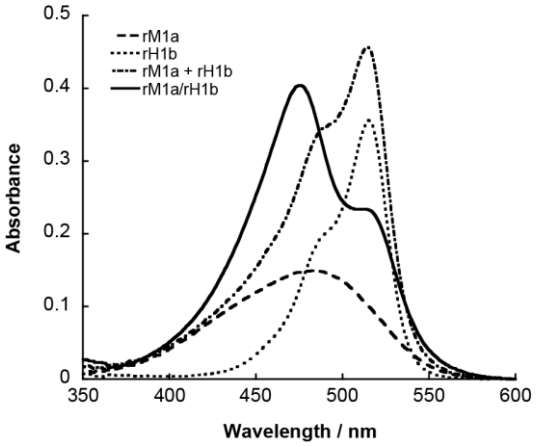


Figure 6-9. UV/Vis spectra of the r**M1a**/r**H1b** duplex (solid line), single-stranded r**M1a** (broken line), r**H1b** (dotted line), and the simple sum of their spectra (sum-spectrum, r**M1a** + r**H1b**, dashed-dotted line) at 20 °C. Solution conditions were as follows: [RNA] = 5 μM, [NaCl] = 100 mM, pH 7.0 (10 mM phosphate buffer).

designed a heterodimer of a fluorophore and a quencher in an RNA duplex aimed at fluorescent tracing of siRNA based on the fact that dyes are stably stacked even in RNA duplexes. It is well known that RISC involves single-stranded antisense RNA embedded in protein. Hence, duplexed siRNA involving a fluorophore-quencher pair does not emit fluorescence, whereas RISC formation should give bright emission by releasing the quencher strand, and enable real-time monitoring of RISC by fluorescence in living cells. For this purpose, we synthesized two modified RNAs (r**H1b** and r**M1a,** see Scheme 6-2), each of which contains a fluorophore and a quencher. Thiazole orange and Methyl Red were selected as the fluorophore and a quencher, respectively, because Methyl Red effectively quenches the emission of thiazole orange in a DNA duplex. First, UV/Vis spectra of r**M1a**/r**H1b**, r**M1a**, and r**H1b** were measured to analyze the heterodimerization of RNA duplexes at 20 °C where the duplex was firmly formed ($T_m$ of r**M1a**/r**H1b** was 53.3 °C). As depicted in Fig. 6-9, single-stranded r**M1a** and r**H1b** gave broad weak, bands at 484 nm, and a relatively intense band at 515 nm, respectively, and their sum-spectrum (dashed-dotted line in Fig. 6-9) showed one main band at 515

nm with shoulders at around 350-500 nm. However, the hybridization of these strands (r**M1a**/r**H1b**, solid line) afforded one main band at 475 nm and a shoulder band at around 510-570 nm; the absorbance of thiazole orange of r**M1a**/r**H1b** at 515 nm decreased by 49% as compared to the sum-spectrum of single-stranded r**M1a** and r**H1b**. The hyperchromism and hypochromism at the shorter and longer wavelengths, respectively, are characteristic of exciton coupling between the axially stacked heterodimer (i.e., hetero-H-aggregates). Note that almost the same exciton coupling has been observed for the d**M1b**/d**H1a** duplex involving thiazole orange/Methyl Red heterodimer in a DNA duplex as depicted in Appendix Fig. 6-1b, demonstrating that equally strong exciton coupling occurred in the RNA duplex. Then, we evaluated the quenching efficiency of the heterodimer in an RNA duplex. As shown by the solid line in Fig. 6-10, single-stranded r**H1b** excited at 510 nm gave strong fluorescence at around 533 nm, which was remarkably quenched when r**M1a** was hybridized with r**H1b**. The ratio of the emission intensity of single-stranded r**H1b** at 533 nm with respect to that of r**M1a**/r**H1b** was as great as 27 (i.e., signal/background (S/B) ratio = 27) due to the pseudo "base-pairing" of the fluorophore and quencher on D-threoninol; the close

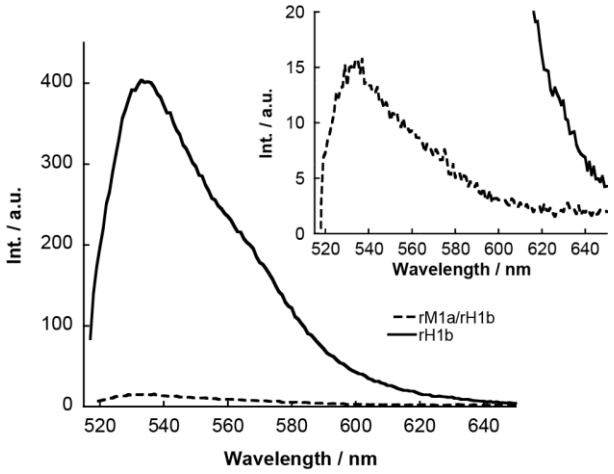


Figure 6-10. Fluorescence emission spectra of r**H1b** excited at 510 nm (solid line) and the duplex with r**M1b** (broken line). Solution conditions were as follows: 20 °C, [r**M1a**] = 0.4 μM, [r**H1b**] = 0.2 μM, [NaCl] = 100 mM, pH 7.0 (10 mM phosphate buffer).

stacking facilitates excitonic interactions between the dyes and electron (or hole) transfer to the quencher.[15] Accordingly, RNA duplexes as well as DNA duplexes are also suitable scaffolds for the pairing of a fluorophore and a quencher.

## 6-4 Discussion

### 6-4-1 Structural differences of the clusters in RNA and DNA duplexes

There are two possible stacked structures in which the dyes are located either adjacent to the 5'-side (**M**/**S**) or the 3'-side (**S**/**M**) of the natural nucleobase (see Scheme 6-1). NMR analyses of the rNMR-**Ma**/rNMR-**Sb** duplex revealed that the dyes were located adjacent to the 3'-side (**S**/**M**); this stacked structure was totally the opposite of that in DNA, which preferred the **M**/**S** orientation. The opposite orientation can be

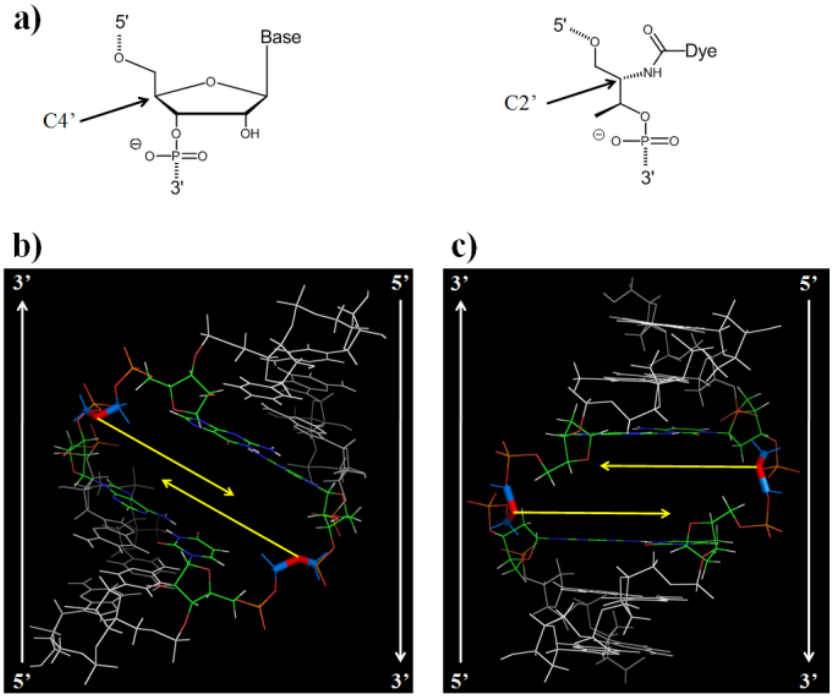


Figure 6-11. Chemical structure of D-ribose and D-threoninol a). Illustration of the stacking manner of the dyes from each strand based on native RNA b) and DNA c) duplexes. Base and D-ribose moieties of the base pair at the center of the duplex in the heptamer are hidden. The C4' atoms of D-ribose, which correspond to the C2' atoms of D-threoninol, are shown in red. Yellow arrows that show the relative location of the dye residues are depicted for each crotch, indicating that the **S**/**M** orientation suits the RNA backbone, whereas there is an **M**/**S** orientation for the DNA duplex.

explained from the relative location of the C4' atom of D-ribose, which corresponds to the C2' atom of D-threoninol conjugated with the dye moiety (Fig. 6-11a). As shown in Fig. 6-11b, the C4' atom (red) is closer to the 3'-side of the self-strand than the 5'-side because RNA base pairs tilt from the vertical plane to the helical axis due to the A-form duplex. Conversely, the C4' atom in a DNA duplex is closer to the 5'-side of the self-strand because DNA base pairs and vertical plane of the helical axis are parallel (Fig. 6-11c). As a result, the **S/M** orientation is suitable for RNA duplexes and gives less steric hindrance to an adjacent base pair than the **M/S** orientation, whereas dyes in DNA duplexes adopt the **M**/**S** orientation. Thus, the dyes in the RNA duplex are located adjacent to the 3'-side of the natural nucleobase. In other words, orientation of the clusters largely depends on their secondary structures (A- and B-type duplex).

The secondary structure also affected the melting temperatures of the dimeric dyes (d**M1a**/d**M1b** and r**M1a**/r**M1b**). Since the helicity of the RNA duplex is tighter than that of the DNA duplex due to its A-type geometry,[16] a small destabilization of the RNA duplex (a decrease of $T_m$) was induced by the introduction of a single **M**-**M** pair into the native duplex (r**M1a**/r**M1b**) as shown in Table 6-1. Steric hindrance between a dye residue and base pairs exceeded the stacking interaction between dye residues, and thus the duplex was destabilized. The destabilization of the RNA duplex is consistent with the fact that RNA duplex does not easily accommodate intercalators.[17] Moreover, the broadened imino-proton signal of $U^{10}$ also supported the disturbance caused by the insertion of a dye pair. On the other hand, further introduction of dye-pairs into the RNA duplex allowed remarkable stabilization of the duplex, which was very similar to clustering of the dyes in the DNA duplex that we reported in previous chapter (Appendix Fig. 6-3). Namely, dyes on D-threoninol were aligned orderly with each

other in RNA as well as in DNA duplexes (except for the mutual orientation of the dyes, *vide infra*), and thus the RNA duplex was remarkably stabilized because of the accumulated stacking interaction.

6-4-2 Difference of winding properties of the cluster between RNA and DNA

The CD behaviors of d**M1a**/d**M1b** and r**M1a**/r**M1b** are also closely related to **S/M** and **M/S** orientations in the duplex. Dyes in d**M1a**/d**M1b** showed a negative-positive Cotton effect, whereas those in r**M1a**/r**M1b** had a positive-negative Cotton effect. This reversed CD signal can be explained from the reversed arrangement of the dyes, i.e., the dyes take either an **S/M** or **M/S** orientation in the duplex. If the assembly order of the dyes is reversed without changing other properties as depicted in Appendix Fig. 6-2, the winding property of the dyes should be reversed accordingly. Since dyes of d**M1a**/d**M1b** in the DNA duplex wound counterclockwise, those of r**M1a**/r**M1b** in RNA took a clockwise conformation. The same was true for clustered dyes such as in r**M2a/**r**M2b** and r**M3a/**r**M3b** duplexes. The CD signal of dyes at around 500 nm assignable to dye absorption were reversed in DNA and RNA duplexes (see Appendix Fig. 6-4 for d**M2a**/d**M2b** and d**M3a**/d**M3b**). Note that other properties, such as the absorption maximum of the assembled dyes and the $T_m$ increase (see Appendix Fig. 6-3b) in RNA, were very similar to d**M2a**/d**M2b** and d**M3a**/d**M3b**, and only the CD signal was reversed. These results can be interpreted as stacked dyes in RNA and DNA also maintaining **S/M** and **M/S** orientations, respectively. In other words, the DNA or RNA scaffold mainly changed the assembly order of the stacked dyes with other properties essentially unchanged as illustrated in Appendix Fig. 6-6.

## 6-5 Conclusions

We have prepared dye clusters in RNA duplexes by using D-threoninol as a scaffold for the dyes (threoninol-nucleotide). NMR study revealed that the dyes incorporated at the center were stacked in an antiparallel manner to each other and were located adjacent to the 3'-side of a natural nucleobase, which was completely the opposite of that in DNA duplexes. This difference in orientation, derived from the structural differences between A- and B-form duplexes, changed the sign of the CD signal. On the other hand, the absorption spectra of the dyes in RNA duplexes were almost identical to those in DNA duplexes, indicating similar H-aggregation in RNA. In addition, the clustering of the dyes raised the melting temperature due to stacking interactions, with the exception of the first insertion of a dye-pair to a native RNA duplex. Thus, dye clusters also efficiently formed in RNA, and the major difference between DNA and RNA was the assembly order of the dyes: the **S/M** and **M/S** orientations in RNA and DNA, respectively. Based on these results, we prepared hetero-clusters of thiazole orange and Methyl Red for fluorescent monitoring of siRNAs. UV/Vis and fluorescence spectra of heterodimers showed that these dyes excitonically interacted, and accordingly, fluorescence from thiazole orange was efficiently quenched by Methyl Red due to the close stacking as we observed in DNA. Since dissociated RNA emits strong fluorescence from thiazole orange, this system has the potential to be utilized as a probe of RISC. We are now applying this heterodimer RNA to the monitoring of siRNA *in vivo*.

## 6-6 Experimental Section

### 6-6-1 Materials

See 2-6-1 because the contents are the same.

### 6-6-2 Synthesis of DNA and RNA modified with **M**, **H**, or **S**

All modified DNAs and RNAs were synthesized using an automated DNA synthesizer (ABI-3400 DNA synthesizer, Applied Biosystems) using conventional and dye-carrying phosphoramidite monomers. Methyl Red, 4'-Methylthioazobenzene, and thiazole orange phosphoramidite monomers synthesized according to previous chapters, were converted to phosphoramidite monomers as described in chapter 2, 3 and 4.[18] The coupling efficiency of the monomers with modified residues was as high as that of conventional monomers as judged by the intensity of the color of the released trityl cation. After the recommended work-up, the monomers were purified by reverse-phase HPLC and characterized by MALDI-TOFMS (Autoflex II, Bruker Daltonics).

The MALDI-TOFMS data, observed (Obsd.) versus calculated (Calcd.), were:

r**M1a**: Obsd. 4213 (Calcd. for [r**M1a**+$H^+$]: 4213). r**M2a**: Obsd. 4631 (Calcd. for [r**M2a**+$H^+$]: 4631). r**M3a**: Obsd. 5050 (Calcd. for [r**M3a**+$H^+$]: 5049). r**M6a**: Obsd. 6306 (Calcd. for [r**M6a**+$H^+$]: 6303). r**M1b**: Obsd. 4215 (Calcd. for [r**M1b**+$H^+$]: 4213). r**M2b**: Obsd. 4631 (Calcd. for [r**M2b**+$H^+$]: 4631). r**M3b**: Obsd. 5049 (Calcd. for [r**M3b**+$H^+$]: 5049). r**M6b**: Obsd. 6305 (Calcd. for [r**M6b**+$H^+$]: 6303). r**H1b**: Obsd. 4297 (Calcd. for [r**H1b**+$H^+$]: 4293). d**M1a**: Obsd. 4062 (Calcd. for [d**M1a**+$H^+$]: 4063). d**M1b**: Obsd. 4065 (Calcd. for [d**M1b**+$H^+$]: 4063). d**H1a**: Obsd. 4141 (Calcd. for [d**H1a**+$H^+$]: 4142). rNMR-**Ma**: Obsd. 2292 (Calcd. for [rNMR-**Ma**+$H^+$]: 2292). rNMR-**Sb**: Obsd. 2295 (Calcd. for [rNMR-**Sb** +$H^+$]: 2295).

6-6-3 Spectroscopic measurements

UV/Vis spectra were measured on a JASCO model V-550 spectrophotometer and Shimadzu UV-1800 instruments, and CD spectra were measured on a JASCO model J-820 spectropolarimeter with a 10 mm quartz cell. Fluorescent spectra were measured with a JASCO model FP-6500 with a microcell. The excitation wavelength was 510 nm for thiazole orange. All models were equipped with programmable temperature controllers. The conditions of the sample solutions were as follows (unless otherwise noted): [NaCl] = 100 mM, pH 7.0 (10 mM phosphate buffer), [DNA] = [RNA] = 5 μM. For measurements of fluorescent spectra, the concentration of RNA tethered with a fluorophore or quencher was 0.2 μM or 0.4 μM, respectively. All samples of RNA- and DNA-dye conjugates were heated at 80 °C for 5 min in the dark to thermally isomerize the *cis*-form, which might be photo-isomerized by ambient light, to the *trans*-form before spectroscopic measurement.[19]

6-6-4 Measurement of melting temperatures

See 2-6-1 because the procedures are the same. The conditions of the sample solutions were the same as those described for the above spectroscopic measurements.

6-6-5 NMR measurements

NMR samples were prepared by dissolving three-times-lyophilized RNA (modified and complementary RNA) in a $H_2O/D_2O$ 9:1 solution containing 20 mM sodium phosphate (pH 7.0) to give a duplex concentration of 1.0 mM. NaCl was added to give a final sodium concentration of 200 mM. NMR spectra were measured with a Bruker DMX-500 (500 MHz) equipped with a cryogenic probe at a probe temperature of 278 K.

Resonances were assigned by standard methods using a combination of 1D, TOCSY (60 ms of mixing time), DQF-COSY, and NOESY (150 ms of mixing time) experiments. All spectra in the $H_2O/D_2O$ 9:1 solution were recorded using the 3-9-19 WATERGATE pulse sequence for water suppression.[20]

## 6-7 Notes and References


1. (a) K. Kruger, P. J. Grabowski, A. J. Zaug, J. Sands, D. E. Gottschling and T. R. Cech, *Cell*, 1982, **31**, 147; (b) C. Guerrier-Takada, K. Gardiner, T. Marsh, N. Pace and S. Altman, *Cell*, 1983, **35**, 849; (c) T. R. Cech and B. L. Bass, *Annu. Rev. Biochem.*, 1986, **55**, 599; (d) J. A. Doudna and T. R. Cech, *Nature*, 2002, **418**, 222.
2. (a) R. C. Lee, R. L. Feinbaum and V. Ambros, *Cell*, 1993, **75**, 843; (b) D. P. Bartel, *Cell*, 2009, **136**, 215.
3. (a) A. Fire, S. Xu, M. K. Montgomery, S. A. Kostas, S. E. Driver and C. C. Mello, *Nature*, 1998, **391**, 806; (b) M. K. Montgomery and A. Fire, *Trends Genet.*, 1998, **14**, 255.
4. D. M. Dykxhoorn, C. D. Novina and P. A. Sharp, *Nat. Rev. Mol. Cell Biol.*, 2003, **4**, 457.
5. (a) S. M. Hammond, E. Bernstein, D. Beach and G. J. Hannon, *Nature*, 2000, **404**, 293; (b) M. A. Valencia-Sanchez, J. Liu, G. J. Hannon and R. Parker, *Genes Dev.*, 2006, **20**, 515; (c) L. Aagaard and J. J. Rossi, *Adv. Drug Deliv. Rev.*, 2007, **59**, 75; (d) R. W. Carthew and E. J. Sontheimer, *Cell*, 2009, **136**, 642; (e) T. Kawamata and Y. Tomari, *Trends Biochem. Sci.*, 2010, **35**, 368.
6. (a) M. Sano, M. Sierant, M. Miyagishi, M. Nakanishi, Y. Takagi and S. Sutou, *Nucleic Acids Res.*, 2008, **36**, 5812; (b) M. Gaglioneg and A. Messere, *Mini-Rev. Med. Chem.*, 2010, **10**, 578.
7. (a) A. Järve, J. Müller, I.-H. Kim, K. Rohr, C. MacLean, G. Fricker, U. Massing, F. Eberle, A. Dalpke, R. Fischer, M. F. Trendelenburg and M. Helm, *Nucleic Acids Res.*, 2007, **35**, e124; (b) J. Cheng, S. M. Sagan, Z. J. Jakubek and J. P. Pezacki, *Biochemistry*, 2008, **47**, 8130; (c) A. Jagannath and M. J. A. Wood, *Mol. Biol. Cell*, 2009, **20**, 521.
8. (a) E. Uhlmann and A. Peyman, *Chem. Rev.*, 1990, **90**, 543; (b) J. Kurreck, *Eur. J. Biochem.*, 2003, **270**, 1628; (c) C. Wilson and A. D. Keefe, *Curr. Opin. Chem. Biol.*, 2006, **10**, 607.
9. NMR measurements were performed at 5 $^{o}$C (278 K), because the melting temperature of the rNMR-**Ma**/rNMR-**Sb** duplex was determined to be 26.2 $^{o}$C.
10. In order to observe signals originating from the imino-protons, which are exchangeable with water molecules, NMR was measured in $H_2O$ ($H_2O/D_2O$, 9:1) with a 3-9-19 WATERGATE pulse sequence for $H_2O$ suppression. Furthermore, we also measured NMR in $D_2O$ so as to exclude the exchangeable protons (data not shown). By combining the NOESY, COSY, and TOCSY

spectral data obtained in $H_2O$ and $D_2O$, most of the signals of the duplex could be assigned.

11. H. Asanuma, K. Shirasuka and M. Komiyama, *Chem. Lett.*, 2002, **31**, 490.
12. (a) S. Tyagi and F. R. Kramer, *Nat. Biotechnol.*, 1996, **14**, 303; (b) M. K. Johansson, H. Fidder, D. Dick and R. M. Cook, *J. Am. Chem. Soc.*, 2002, **124**, 6950; (c) E. Socher, L. Bethge, A. Knoll, N. Jungnick, A. Herrmann and O. Seitz, *Angew. Chem. Int. Ed*, 2008, **47**, 9555.
13. A. Okamoto, Y. Ochi and I. Saito, *Chem. Commun.*, 2005, 1128.
14. (a) B. Z. Packard, D. D. Toptygin, A. Komoriya and L. Brand, *J. Phys. Chem. B*, 1998, **102**, 752; (b) D. Baumstark and H.-A. Wagenknecht, *Angew. Chem. Int. Ed*, 2008, **47**, 2612; (c) M. Hariharan, Y. Zheng, H. Long, T. A. Zeidan, G. C. Schatz, J. Vura-Weis, M. R. Wasielewski, X. Zuo, D. M. Tiede and F. D. Lewis, *J. Am. Chem. Soc.*, 2009, **131**, 5920; (d) H. Kashida, T. Hayashi, T. Fujii and H. Asanuma, *Chem. Eur. J.*, 2011, **17**, 2614.
15. H. Kashida, T. Takatsu, T. Fujii, K. Sekiguchi, X. Liang, K. Niwa, T. Takase, Y. Yoshida and H. Asanuma, *Angew. Chem. Int. Ed*, 2009, **48**, 7044.
16. G. Mayer, *The Chemical Biology of Nucleic Acids*, Wiley, Chichester, UK 2010.
17. (a) R. Sinha, M. M. Islam, K. Bhadra, G. S. Kumar, A. Banerjee and M. Maiti, *Bioorg. Med. Chem.*, 2006, **14**, 800; (b) M. M. Islam and G. Suresh Kumar, *DNA Cell Biol.*, 2009, **28**, 637; (c) R. Pei, J. Rothman, Y. Xie and M. N. Stojanovic, *Nucleic Acids Res.*, 2009, **37**, e59.
18. The monomers (**H**) was synthesized and provided by Masaaki Urushihara (A master course student in Asanuma Lab.)
19. H. Nishioka, X. Liang, H. Kashida and H. Asanuma, *Chem. Commun.*, 2007, 4354.
20. (a) K. Wüthrich, *NMR of proteins and nucleic acids*, Wiley, New York, 1986; (b) M. Liu, X.-a. Mao, C. Ye, H. Huang, J. K. Nicholson and J. C. Lindon, *J. Magn. Reson.*, 1998, **132**, 125.

## 6-8 Appendixes

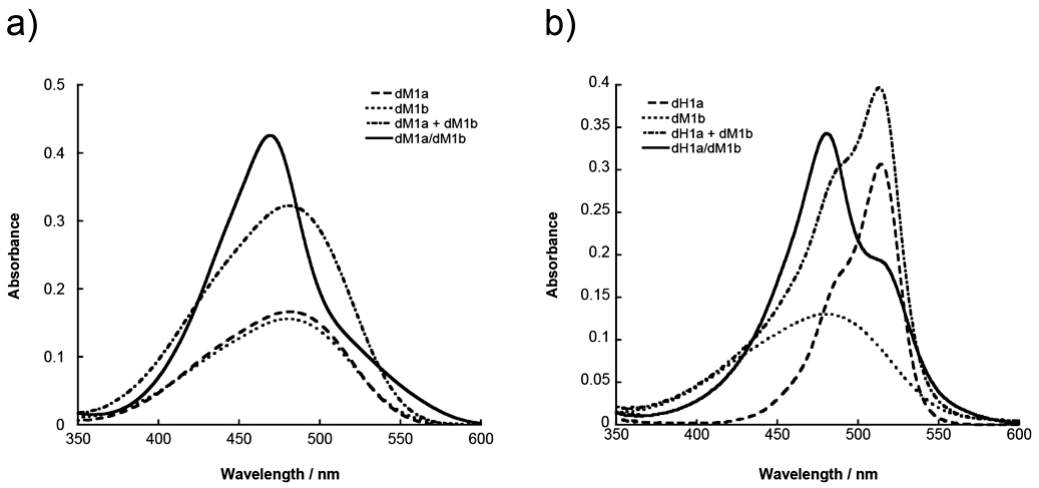


Appendix Figure 6-1. a) UV/Vis spectra of the d**M1a**/d**M1b** duplex (solid line), single-stranded d**M1a** (dashed line), d**M1b** (dotted line), and a simple sum of their spectra (sum-spectrum, d**M1a** + d**M1b,** dashed-dotted line) at 20 °C. Solution conditions were as follows: [DNA] = 5 µM, [NaCl] = 100 mM, pH 7.0 (10 mM phosphate buffer). Half-line-width of the spectrum with d**M1a**/d**M1b** is 3109 $cm^{-1}$.b) UV/Vis spectra of the d**M1b**/d**H1a** duplex (solid line), single-stranded d**H1a** (dashed line), d**M1b** (dotted line), and a simple sum of their spectra (sum-spectrum, d**H1a** + d**M1b**, dashed-dotted line) at 20 °C. Solution conditions were as follows: [DNA] = 4 µM, [NaCl] = 100 mM, pH 7.0 (10 mM phosphate buffer).

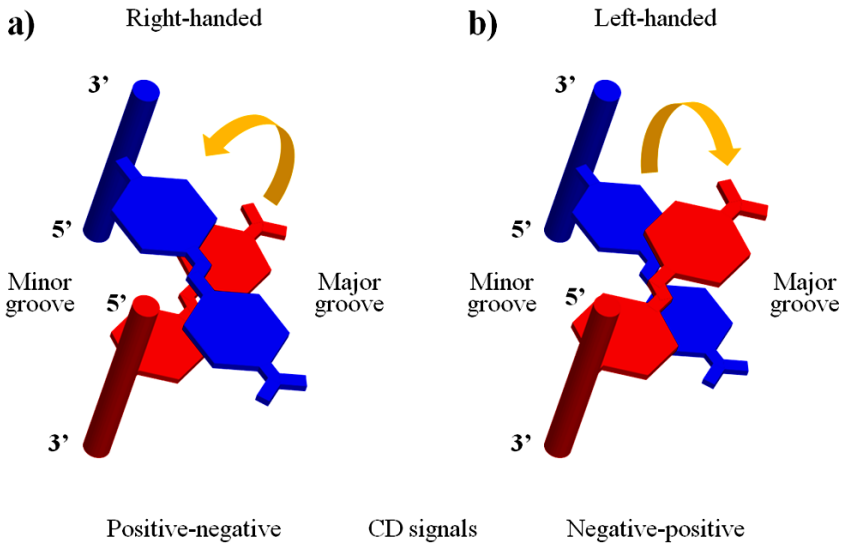


Appendix Figure 6-2. Illustration of relative orientation and prospective CD signals of the dye residues including winding properties. The dyes are a) located adjacent to the 3'-side of a natural nucleobase and assemble dextrorsely (**S/M** orientation), or b) located adjacent to the 5'-side of a natural nucleobase and assemble sinistrorsely (**M/S** orientation).

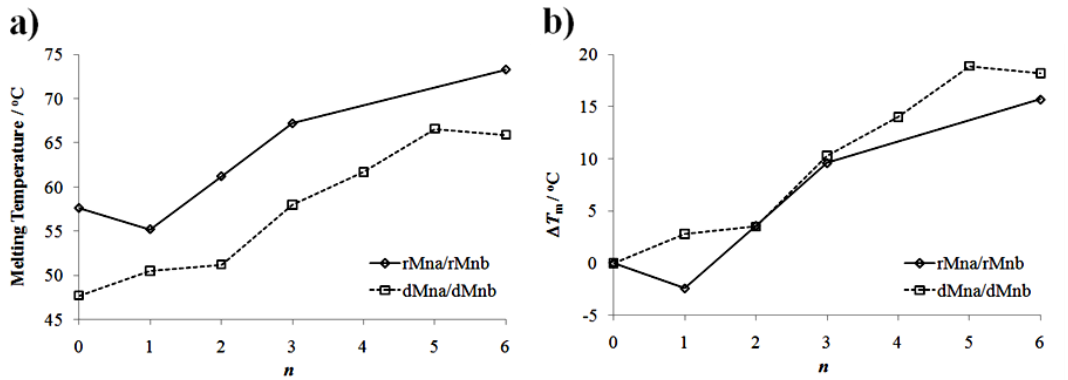


Appendix Figure 6-3. Comparison of duplex stability either on RNA or DNA. a) Melting temperatures of r**M*n*a**/r**M*n*b** involving a Methyl Red homo-cluster on RNA duplex (solid line) and d**M*n*a**/d**M*n*b** involving a Methyl Red homo-cluster on DNA duplex (dotted line). b) Difference of $T_m$ between each duplex ($n$ = 0-6) and corresponding native duplex ($n$ = 0) ($\Delta T_m$) on RNA (solid line) or DNA (dotted line) duplex. Solution conditions are as follows: [RNA] = [DNA] = 5 μM, [NaCl] = 100 mM, pH 7.0 (10 mM phosphate buffer)
d**M*n*a** : 5'-GGT-ATC-**M**$_n$-GCA-ATC-3'
d**M*n*b** : 3'-CCA-TAG-**M**$_n$-CGT-TAG-5'

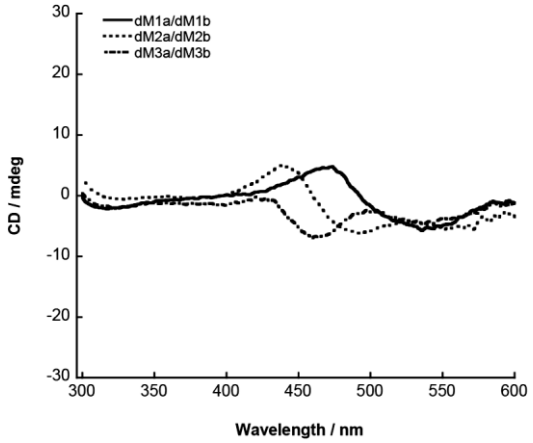


Appendix Figure 6-4. Effect of the number of dye pairs on the CD spectra of d**M*n*a**/d**M*n*b**. Solution conditions were as follows: 0 °C, [DNA] = 5 μM, [NaCl] = 100 mM, pH 7.0 (10 mM phosphate buffer).

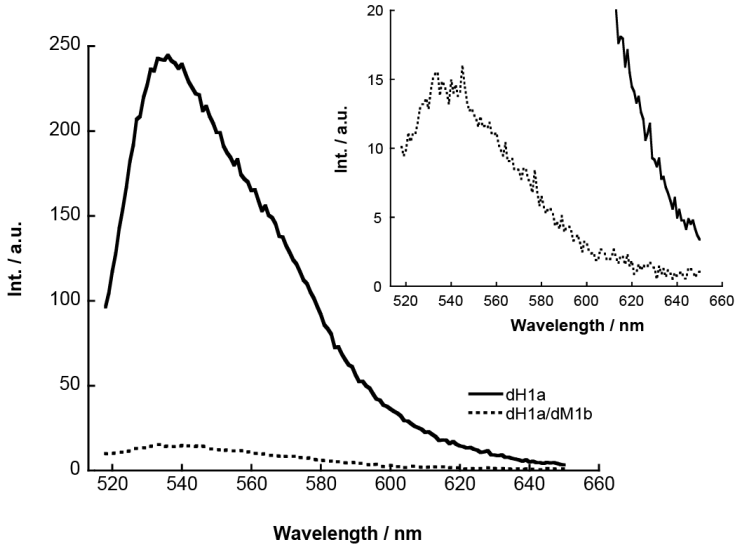


Appendix Figure 6-5. Fluorescence emission spectra of d**H1a** excited at 510 nm (solid line) and the duplex with d**M1a** (dotted line). Solution conditions were as follows: 20 °C, [d**M1b**] = 0.4 μM, [d**H1a**] = 0.2 μM, [NaCl] = 100 mM, pH 7.0 (10 mM phosphate buffer).

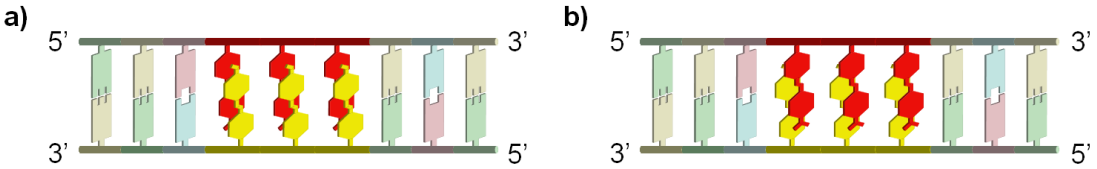


Appendix Figure 6-6. Illustration of the dye cluster on a) DNA with **M/S** orientation and b) RNA with **S/M** orientation.

# Publication List

1. "A polycation-chaperoned in-stem molecular beacon system"
   H. Asanuma, T. Osawa, H. Kashida, T. Fujii, X. G. Liang, K. Niwa, Y. Yoshida, N. Shimada, A. Maruyama, *Chem. Commun.*, *accepted*.

2. "Femtosecond photoisomerization of azobenzene-derivative binding to DNA."
   T. Chen, K. Igarashi, N. Nakagawa, K. Yamane, T. Fujii, H. Asanuma, M. Yamashita, *J. Photochem. Photobiol. A*, **2011**, *223*, 119-123.

3. "A Cationic Dye Triplet as a Unique "Glue" That Can Connect Fully Matched Termini of DNA Duplexes."
   H. Kashida, T. Hayashi, T. Fujii, H. Asanuma, *Chem. Eur. J.*, **2011**, *17*, 2614-2622.

4. "Design of a Functional Nanomaterial with Recognition Ability for Constructing Light-Driven Nanodevices."
   X.G. Liang, T. Mochizuki, T. Fujii, H. Kashida, H. Asanuma, *LNCS* **2011**, *6518*, 112-122.

5. "Coherent Quenching of a Fluorophore for the Design of a Highly Sensitive In-Stem Molecular Beacon."
   Y. Hara, T. Fujii, H. Kashida, K. Sekiguchi, X. G. Liang, K. Niwa, T. Takase, Y. Yoshida, H. Asanuma, *Angew. Chem. Int. Ed.*, **2010**, *49*, 5502-5506.

6. "Analysis of Coherent Heteroclustering of Different Dyes by Use of Threoninol-Nucleotides for Comparison with the Molecular Exciton Theory."
   T. Fujii, H. Kashida, H. Asanuma, *Chem. Eur. J.*, **2009**, *15*, 10092-10102.

7. "Positively Charged Base Surrogate for Highly Stable "Base Pairing" through Electrostatic and Stacking Interactions."
   H. Kashida, H. Itoh, T. Fujii, T. Hayashi, H. Asanuma, *J. Am. Chem. Soc.*, **2009**, *131*, 9928-9930.

8. "In-Stem Molecular Beacon Containing a Pseudo Base Pair of Threoninol Nucleotides for Removal of Background Emission."
   H. Kashida, T. Takatsu, T. Fujii, K. Sekiguchi, X. G. Liang, K. Niwa, T.

Takase, Y. Yoshida, H. Asanuma, *Angew. Chem. Int. Ed.*, **2009**, *48*, 7044-7047.

9. "Incorporation of cationic dyes into DNA for distinct stabilization of duplex"
   H. Kashida, H. Itoh, T. Fujii, H. Asanuma, *Nucleic Acids Symp. Ser.*, **2008**, *52*, 701-702.

10. "Preparation of coherent hetero clusters with threoninol scaffold."
    T. Fujii, H. Kashida, H. Asanuma, *Nucleic Acids Symp. Ser.*, **2008**, *52*, 699-700.

11. "Threoninol as a scaffold of dyes (threoninol-nucleotide) and their stable interstrand clustering in duplexes."
    H. Kashida, T. Fujii, H. Asanuma,*Org. Biomol. Chem.*, **2008**, *6*, 2892-2899.

12. "Construction of novel dye aggregates based on "comb-type" sequence."
    H. Kashida, T. Fujii, H. Asanuma, *Nucleic Acids Symp. Ser.*, **2007**, *51*, 11-12.

13. "Preparation of "comb-type" hetero aggregates by DNA-dye conjugation."
    T. Fujii, H. Kashida, H. Asanuma, *Nucleic Acids Symp. Ser.*, **2007**, *51*, 277-278.

# List of Oral Presentations

1. “Enhancement of excitonic interaction by asymmetric hetero dye-clustering in DNA duplexes for the efficient quenching of a fluorophore”

   T. Fujii, Y. Hara, T. Osawa, H. Kashida, X. G. Liang, Y. Yoshida, H. Asanuma

   The 38th International Symposium on Nucleic Acid Chemistry, *Sapporo*, November, 2011.

2. “Development of highly sensitive In-Stem Molecular Beacon by using asymmetric dye-cluster”

   T. Fujii, Y. Hara, Y. Yoshida, X. G. Liang, H. Kashida, H. Asanuma

   The 59th Symposium on Macromolecules, *Sapporo*, September, 2010.

3. “Preparation of coherent hetero clusters by DNA-dye conjugation”

   T. Fujii, H. Kashida, H. Asanuma

   The 57th Symposium on Macromolecules, *Osaka*, September, 2008.

# Acknowledgment

The present study was carried out at the Department of Molecular Design and Engineering, Graduate School of Engineering, Nagoya University, from April 2006 to March 2012.

I wish to express his grateful acknowledgment to Professor Hiroyuki Asanuma whose encouragement and helpful suggestions have been indispensable to the completion of the present thesis. I also especially thank Associate Professor Hiromu Kashida for his advice and valuable discussion to lead this study. Moreover, I really appreciate giving his advice from Professor Xingguo Liang. In addition, I would like to express thanks to co-worker Mr. Atsuro Yamada, Dr. Hidenori Nishioka, Mr. Hiroshi Ito, Mr. Tomohiko Takatsu, Mr. Tomohiro Kato, Mr. Yuichi Hara, Mr. Hidehiro Ito, Mr. Koji Sekiguchi, Mr. Takamitsu Hayashi, Mr. Masaaki Urushihara, Mr. Takuya Osawa, Mr. Tetsuya Doi and other members of Asanuma Laboratory for their contribution and advice for this study.

I am deeply grateful to Associate Professor Kyoichi Sawabe and Mr. Junichi Kubo for valuable suggestions about exciton model of hetero dimers and supply of quantum calculation data of the absorption spectra. I also express special thanks to Professor Koichi Kato and Dr. Maho Yagi-Utsumi for NMR measurement of the cluster in RNA. Moreover, I appreciate their help in the X-ray diffraction measurements from Professors Takashi Yamane, Associate Professor Atsuo Suzuki, and Mr. Tatsuo Hikage.

I am also greatly indebted to “Japan Society for Promotion of Science” for their financial support to me.

Finally, I would like to give special thanks to Professor Takahiro Seki and Professor Kentarou Tanaka for giving many helpful comments and suggestions on accomplishing this thesis.